

Understanding the role of abiotic stress in biosphere-atmosphere exchange of reactive trace gases

Frederick Otu-Larbi

BSc, MSc.

May 2021

Lancaster Environment Centre
Faculty of Science and Technology
Lancaster University

This thesis is submitted in fulfilment of the requirements for the degree of
Doctor of Philosophy.

This thesis is the work of the author, except where otherwise stated. It has not
been submitted for the award of a higher degree at this or any other institution.
Excerpts of this thesis have been published in journals, as indicated within.

Abstract

The terrestrial biosphere removes carbon dioxide (CO₂) from the atmosphere through photosynthesis and is a major sink for atmospheric pollutants like ozone (O₃). It is also the main source of biogenic volatile organic compounds (BVOCs) in the atmosphere. In turn, atmospheric conditions such as temperature, precipitation and photosynthetically active radiation regulate the growth and functioning of plants. The role of some environmental factors like temperature and solar radiation in regulating plant physiological processes are well understood and parameterised in land surface models (LSMs) but others like drought stress and ozone damage are poorly understood and hence poorly represented in LSMs. Yet, these LSMs are integral to climate modelling and climate change mitigation measures as they provide estimates of carbon stored in forests currently and how this will change in future. This thesis seeks to bridge the gap between the latest scientific knowledge about the effects of drought stress and ozone damage on plant physiological processes, and how these stressors are currently modelled. The response of plant isoprene emissions and gas exchange to drought stress and ozone damage was investigated using various model parametrisations, and long-term measurements of isoprene mixing ratios and fluxes, carbon dioxide and water fluxes made in a broad range of forest ecosystems. We find that current isoprene emission models are unable to account for stress-induced isoprene emissions during mild or moderate drought stress leading to underestimation of observed isoprene mixing ratios and fluxes. New methods for modelling isoprene emissions during moderate drought were developed and shown to improve model reproduction of observations. Further, it is shown that both drought stress and ozone damage act to reduce plant productivity and gas exchange. However, the impact of drought stress on vegetation was found to outweigh that of ozone damage at individual forest sites in both present day and future climate scenarios but accounting for the impact of both stress factors provided the best model-observation fit. As global climate changes, abiotic stress factors will become increasingly important in regulating biosphere-atmosphere interactions with potentially negative impacts on plant productivity and hence climate mitigation efforts. These findings highlight the need for more observations, especially in remote and data-sparse regions of the world such as the tropics, to improve understanding of how plants will respond to future stress, and how to better model the impacts.

Dedication

This work is dedicated to all my teachers, family and friends who have helped in my education career. Special dedication to Geraldine, Wendy, Emily, and Myles.

Acknowledgement

I would like to express my profound gratitude to my supervisors, Dr. Kirsti Ashworth and Prof. Oliver Wild, for the excellent supervision and guidance they have provided over the course of my studentship. I am eternally grateful to them.

I am also grateful to the Faculty of Science and Technology (FST) and Lancaster Environment Centre (LEC) at Lancaster University for funding my studentship. My PhD studies wouldn't have been possible without this funding.

This research has also been made possible through assistance of collaborators at various organisations who have provided data, training, or technical support to ensure a successful completion of my studies. These include Adriano Conte, who taught me that VPD is not measured but calculated, Silvano Fares, Valerio Ferracci, Conor Bolas, and Karina Williams. I am thankful for your support.

Prof. Emily Black advised me to apply for this studentship when I saw the advert and discussed it with her. She together with Prof. Keith Shine wrote references letters which were instrumental in my successful application, leading to all the research work described in this thesis. Thank you, Emily, and Keith.

To my thesis appraisal committee members, especially Dr. Andy Jarvis, I am grateful for your guidance and support. To the members of the Ashworth Lab group I am grateful for making my PhD journey an enjoyable one.

Above all else, I want to thank God for his guidance, protection and grace that have seen me through these past three and half years.

Table of Contents

Table of Contents	v
List of Figures	vii
List of Tables	xiv
Chapter 1: Introduction	1
1.1 Motivation and Rationale	1
1.2 Aims and Objectives.....	3
1.3 Structure of the thesis	4
Chapter 2: Modelling Biosphere-Atmosphere Interactions	6
2.1 Biosphere-atmosphere Interactions	6
2.2 Stress factors affecting biosphere-atmosphere interactions.....	10
2.3 Land Surface Models.....	22
2.4 Observations	25
Chapter 3: Modelling the effect of the 2018 summer heatwave and drought on isoprene emissions in a UK woodland	30
3.1 Introduction	33
3.2 Materials and Methods	36
3.3 Results	42
3.4 Discussion.....	52
3.5 Supplementary Information for chapter 3	56
Chapter 4: FORCAsT-gs: Importance of stomatal conductance parameterization to estimated ozone deposition velocity.....	66
4.1 Introduction	69
4.2 Methods	72
4.3 Results	84
4.4 Discussion and Conclusion.....	96
4.5 Supplementary material for Chapter 4.....	100
Chapter 5: Current and future impacts of drought and ozone stress on Northern Hemisphere forests.....	113
5.1 Introduction	116
5.2 Methods	118
5.3 Results	128
5.4 Discussion.....	136
5.5 Supplementary Information for Chapter 5.....	141
Chapter 6: Process-based approach to modelling isoprene fluxes during drought	154
6.1 Introduction	155
6.2 Materials and methods.....	157
6.3 Results and discussion	164

6.4 Conclusions	174
Chapter 7: Conclusions	177
7.1 Summary of findings	178
7.2 Limitations and Future Works	182
References	186

List of Figures

- Figure 1.1: Simplified schematic of biosphere-atmosphere interactions. 1
- Figure 2.1: Responses of leaf isoprene emission rate (I) to variation in temperature (T , °C) and incident quantum flux density (PPFD, $\mu\text{mol m}^{-2} \text{s}^{-1}$) according to isoprene emission model of Guenther et al. (1995). PPFD is a measure of PAR intensity. 7
- Figure 2.2: schematic of how the soil moisture stress response factor, β , depends on the value of q . The red and blue dashed lines show the shape of the response curve when $q < 1$ and $q > 1$ respectively. The black line indicates the linear response of β when $q = 1$. SWC values of $0.20\text{m}^3\text{m}^{-3}$ and $0.50\text{m}^3\text{m}^{-3}$ were used θ_w and θ_c respectively. 14
- Figure 2.3: Conceptual model of the response of ecosystem isoprene emission and photosynthesis to drought stress. The orange vertical line denotes the initiation of drought stress (i.e. at the critical threshold), and the red vertical line the onset of severe drought. The grey dashed line represents changes in photosynthesis in response to drought. The red dashed line show isoprene emissions expected if isoprene synthesis continues to follow photosynthesis. The black dashed line shows isoprene emissions modelled on the assumption that mild drought stress increases leaf temperature and/or C_i , stimulating isoprene emissions under mild drought. During the severe phase of drought stress, isoprene emissions again decline in relation to declining photosynthesis. 17
- Figure 2.4:(a) A schematic of the FORCAsT column model. Each level within the column is a box model (b) incorporating the processes involved in canopy–atmosphere exchange of energy and mass appropriate for that level. (Source: Ashworth et al., 2015) 23
- Figure 2.5: A schematic showing the different processes and surface types included in the JULES model (Source: <https://jules.jchmr.org/content/about> last accessed 23/04/2021). 24
- Figure 2.6: A sample of the 212 sites included in the FLUXNET2015 dataset. The size of the circle indicates the length of the data record. The colour of the circles represents the ecosystem type based on the International Geosphere–Biosphere Programme (IGBP) definition. When overlapping, locations are offset slightly to improve readability. Numbers in parentheses indicate the number of sites in each IGBP group. The inset (bar chart) shows the distribution of data record lengths. (Source: Pastorello et al., 2020) 26
- Figure 2.7: Locations of forest sites used for model development and evaluation in this thesis. 29
- Figure 3.1: Meteorological data taken from the Wytham Woods Automatic Environmental Change Network station: (a) Photosynthetically active radiation (PAR), (b) 2 m air temperature, (c) soil water content (SWC; black) and total daily rainfall (blue). The grey shaded area indicates the start and end of the heatwave–drought while the white dashed line indicates the start of the rewetting period (20 July–8 August)..... 43
- Figure 3.2: Observed (black) and modelled (BASE; orange) isoprene mixing ratios at the WIsDOM site at (a) the top of the canopy (~15.6 m), (b) mid canopy (~13.5 m), (c) trunk height (~7.1 m) and (d) near the surface (~0.8 m). Observations of isoprene mixing ratios at the trunk and near-surface levels started on 6 July..... 44
- Figure 3.3: (a) Difference (in ppb) between model (BASE) and observed (OBS) isoprene mixing ratio at the top of the canopy for the BASE simulation for the entire season (1 June–30

September 2018). Note that negative values indicate periods when the model underestimates concentrations while positive values indicate an overestimation. (b) Diurnal profiles of isoprene mixing ratios at the top of the canopy before heatwave–drought (black), during the heatwave–drought (orange) and after the heatwave–drought (red). Model values are solid lines while observed values are dashed lines. Scatter plots of difference in mixing ratio versus (c) soil water content (SWC) coloured by temperature and (d) leaf temperature coloured by SWC 45

Figure 3.4: Observed (OBS) and modelled (MOD) isoprene mixing ratios at the top (15.6 m; a–c) and middle (13.5 m; d–f) of the canopy. Observations are shown in black and model results in red (BASE+LFT), green (BASE+SWT) and blue (BASE+RWT). Figure 3.9 in the Supplementary Information shows similar results for the trunk and near-surface levels ... 47

Figure 3.5: Scatter plots of model (MOD) and observed (OBS) isoprene (C_5H_8) mixing ratios for (a and e) BASE coloured by SWC, (b and f) BASE+LFT coloured by SWC, (c and g) BASE+SWT coloured by temperature, (d and h) BASE+RWT coloured by temperature. Panels (a–d) show the top of the canopy (15.6 m) and panels (e–h) the middle of the canopy (13.5 m). Figure 3.10 in the Supplementary Information reproduces these scatter plots for the trunk and near-surface levels. 48

Figure 3.6: Taylor diagram showing model output statistics from the four simulations for (a) top of canopy (15.6 m), (b) middle of canopy (13.5 m), (c) trunk level (7.1 m) and (d) near surface (0.8 m). Dashed black and brown curves and solid blue lines show normalized standard deviation, centred root mean squared error (RMS error) and correlation coefficients, respectively, against observations. The observed isoprene mixing ratios are summarized by the purple circle with a normalized standard deviation of 1.0, RMS error of 0.0 and correlation of 1.0. The summary statistics for the four model simulations are shown by orange (BASE), red (BASE+LFT), green (BASE+SWT) and blue (BASE+RWT) circles. Note the change in scale of standard deviation on panel (c) 49

Figure 3.7: (a–d) Time series of isoprene mixing ratios for a selected period during the heatwave–drought (22–27 July 2018) and (e–h) average diurnal profiles of isoprene mixing ratios for the same period. Black dashed lines are observations while the models are coloured orange (BASE), red (BASE+LFT), green (BASE+SWT) and blue (BASE+RWT). The grey shading indicates the uncertainty limits ($\pm 11\%$) around the observations. (a) and (e), (b) and (f), (c) and (g) and (d) and (h) are top of canopy, middle of canopy, trunk and near-surface levels, respectively. 51

Figure 3.8: Time series of modelled leaf temperature (red) and observed air temperature (black). Shaded region indicates heatwave-drought period. s 57

Figure 3.9: Observed (OBS) and modelled (MOD) isoprene mixing ratios at the trunk (a–c) (7.1m) and near surface (d–f) (0.8m) levels. Observations are shown in black and model results are red (BASE+LFT), green (BASE+SWT), and blue (BASE+RWT). 57

Figure 3.10: Scatter plots of model (MOD) and observed (OBS) isoprene (C_5H_8) mixing ratios for (a, e) BASE coloured by SWC, (b, f) BASE+LFT coloured by SWC, (c, g) BASE+SWT coloured by temperature, (d, h) BASE+RWT coloured by temperature. Panels a–d show the trunk level and panels e–h near surface level. 58

Figure 3.11: Scatter plot of observed isoprene mixing ratio vs GPP coloured by SWC, (a) before and after the heatwave-drought and (b) heatwave-drought. 58

- Figure 3.12: Observed (OBS) and modelled (MOD) isoprene mixing ratios at the top (a,e;15.6 m), middle (b,f; 13.5m), trunk (c,g; 7.1m) and near surface (d,h; 0.8m) levels. (a-d) are results of BASE+T experiment and (e-f) are results of BASE+VPD experiment. Note that observations are shown in black and model results are red (BASE+T) and green (BASE+VPD)..... 60
- Figure 3.13: Scatter plots of modelled (MOD) vs observed (OBS) isoprene (C_5H_8) mixing ratios for top (a,e 15.6 m), middle (b,f 13.5m), trunk (c,g 7.1m) and near surface (d,h 0.8m) levels. (a-d) show BASE+T coloured by temperature and (e-f) show BASE+VPD coloured by VPD. 61
- Figure 3.14: Taylor Diagrams showing model output statistics from BASE+T and BASE+VPD simulations for (a) top of canopy, (b) middle of canopy, (c) trunk level and (d) near surface. Dashed black and brown curves and solid blue lines show normalised standard deviation, centred root mean squared error (RMS error) and correlation coefficients respectively against observations. The observed isoprene mixing ratios are summarised by the purple circle with a normalised standard deviation of 1.0, RMS error of 0.0 and correlation of 1.0. The summary statistic for the model simulations are shown by orange (BASE), red (BASE+T), green (BASE+VPD) and blue (BASE+RWT). BASE and BASE+RWT (the experiment giving the best model-observation fit) have been added for ease of comparison. Note the change in scale of standard deviation on panel d..... 62
- Figure 3.15: (a-d) Time series of isoprene mixing ratios for a selected period during the heatwave-drought (22nd-27th July 2018) and (e-h) average diurnal profiles of isoprene mixing ratios for the same period. Black dashed lines are observations while the models are coloured orange (BASE), red (BASE+T), green (BASE+VPD) and blue (BASE+RWT). Grey shaded area around the observations indicate the uncertainty limits ($\pm 11\%$) within the observations. a and e are top of canopy, b and f are middle of the canopy, c and g are trunk level and d and h are near the surface. 63
- Figure 4.1: Site conditions and meteorology showing (a) soil moisture (volumetric soil water content, SWC; $m^3 m^{-3}$); (b) cumulative precipitation (mm); (c) 2-m air temperature ($^{\circ}C$) and (d) photosynthetically active radiation (PAR) at the top of the canopy ($W m^{-2}$) for an average year at BR_Sa1 (yellow), FI_Hyy (blue), IT_Cp2 (red), US_Blo (black) and US_Ha1 (grey) 79
- Figure 4.2: Net photosynthesis for an average year at each of the five FLUXNET sites, from top to bottom: BR_Sa1, FI_Hyy, IT_Cp2, US_Blo, US_Ha1. The first column shows average annual and the second average diel profiles of Gross Primary Productivity (GPP, a measure of photosynthesis rate) estimated from the Jarvis multiplicative (gold), Ball-Berry coupled (red) and Medlyn stomatal optimisation coupled (blue) stomatal conductance-photosynthesis models. The black dashed lines show observed GPP..... 86
- Figure 4.3: Taylor Diagram summarising model output statistics from FORCAsT sensitivity tests. Observed GPP has $SD=1.0$, $RMSE=0.0$ and $r=1.0$ (purple circle). Black and brown dashed curves and blue lines show normalised standard deviation (SD), centred root mean squared error (RMSE) and correlation coefficients (r) respectively against observations for each model on each diagram. The summary statistics for each JV simulation are shown by gold symbols, BB by red, MD simulation by blue. BASE simulations are denoted by circles, lower bounds (TEST-) by triangles, and upper bounds (TEST+) by diamonds. Note that JV, MD

and BB in these plots are the BASE simulations described in sections 2.5.1 and 3.1, and Figure 4.2.....	87
Figure 4.4: Gas exchange for an average year at each of the five FLUXNET sites, from top to bottom: BR_Sa1, FI_Hyy, IT_Cp2, US_Blo, US_Ha1, for, from left to right, the Jarvis, Ball-Berry and Medlyn stomatal conductance model sensitivity tests. Solid lines denote the unperturbed (BASE) simulation as shown in Figure 4.2 for each model, with dashed paler line for TEST- and dashed darker line for TEST+ simulations respectively. The black dashed lines show observed GPP at each site.....	90
Figure 4.5: Stomatal conductance and ozone deposition rates for an average year and day at each of the five FLUXNET sites, from top to bottom: BR_Sa1, FI_Hyy, IT_Cp2, US_Blo, and US_Ha1. Solid lines black lines denote the output from the model that best reproduced GPP at each site as shown in Figure 4.3 and 4. The shaded regions indicate the spread in stomatal conductance and deposition rates across all the model sensitivity tests.....	95
Figure 4.6: Locations of forest sites used in this study.....	107
Figure 4.7: Graphs showing the response of stomatal conductance in the Jarvis model to (a) photosynthetic flux density (f_{light}), (b) Temperature (f_{temp}) (c) vapour pressure deficit (f_{VPD}) and (d) soil water content (f_{SWC}).....	107
Figure 4.8: Taylor Diagram summarising model output statistics from FORCAsT BASE model configurations. The black and brown dashed curves and blue lines show normalised standard deviation (SD), centred root mean squared error (RMSE) and correlation coefficients (r) respectively against observations for each model on each diagram. The summary statistics for each JV simulation are shown by gold circles, BB by red, MD simulation by blue. ..	108
Figure 4.9: Stomatal conductance for an average year at each of the five FLUXNET sites, from top to bottom: BR-Sa1, FI-Hyy, IT-Cp2, US-Blo, US-Ha1. The first column shows average annual and the second average diel profiles of stomatal conductance estimated from the Jarvis multiplicative (gold), Ball-Berry coupled (red) and Medlyn stomatal optimisation coupled (blue) stomatal conductance-photosynthesis models.....	109
Figure 4.10: Stomatal conductance for an average year at each of the five FLUXNET sites, from top to bottom: BR-Sa1, FI-Hyy, IT-Cp2, US-Blo, US-Ha1, for, from left to right, the Jarvis, Ball-Berry and Medlyn stomatal conductance model sensitivity tests. Solid lines denote the unperturbed (BASE) simulation for each model, with dashed paler line for TEST- and dashed darker line for TEST+ simulations respectively.....	110
Figure 4.11: Ozone deposition velocity for an average year and day at each of the five FLUXNET sites, from top to bottom: BR-Sa1, FI-Hyy, IT-Cp2, US-Blo, and US-Ha1. Solid lines black lines denote the output from the model that best reproduced GPP at each site. The shaded regions indicate the spread in stomatal conductance and deposition rates across all of the model sensitivity tests.....	111
Figure 4.12: Concentration of ozone for an average year and day at each of the five FLUXNET sites, from top to bottom: BR-Sa1, FI-Hyy, IT-Cp2, US-Blo, and US-Ha1.	112
Figure 5.1: Average annual profiles of observed (a) volumetric soil water content (SWC), (b) O_3 mixing ratios, (c) air temperature and (d) photosynthetically active radiation at: Castelporziano (CPZ; red lines), Hyytiälä (HYT; blue lines) and Blodgett (BLO; black lines). The coloured backgrounds denote meteorological seasons: winter (grey), spring (white), summer (orange) and autumn (cyan)	125

- Figure 5.2: Annual mean gross primary productivity (GPP) (a–c) and latent heat flux (LE) (d–f) for Castelporziano (CPZ), Blodgett (BLO) and Hyytiälä (HYY). Observed (OBS) values are shown with black bars while model results are coloured as follows: orange (CTR and CTR + Dr), blue (AVD and AVD + Dr) and grey (TLR and TLR + Dr), with striped bars indicating drought stress. The percentage difference between modelled and observed values for each simulation is shown at the top of the bars. Positive values indicate model overestimation 130
- Figure 5.3: Taylor diagram showing model output statistics from FORCAsT simulations. Panels a, b and c show output statistics for gross primary productivity (GPP) at CPZ, BLO and HYY respectively while panels d, e and f show output statistics for latent heat flux (LE) at the same sites. Black and orange dashed curves and blue lines show normalized standard deviation (SD), centred root mean squared error (RMSE) and correlation coefficients (r) respectively against observations. Observed GPP and LE have $SD = 1.0$, $RMSE = 0.0$ and $r = 1.0$ (purple circle). The summary statistics for each model simulation are shown by orange (CTR and CTR + Dr), blue (AVD and AVD + Dr), and grey (TLR and TLR + Dr). Triangles represent simulations without drought stress and circles those with. Note the difference in scale of standard deviation on panel (a) 131
- Figure 5.4: Estimates of gross primary productivity (GPP; a–f) and latent heat flux (LE; d–e) at CPZ, BLO and HYY respectively using bias-corrected historical (1996–2005) general circulation model (GCM) output data compared with estimates from observed driving data. Ensemble mean is indicated by red dashed lines while present-day estimates are shown in black dashed lines. Individual GCM estimates are shown by grey lines 132
- Figure 5.5: Ensemble mean estimates of average yearly gross primary productivity (GPP) (a–c) and latent heat flux (LE) (d–f) compared with present-day estimates using observed driving data for CPZ, BLO and HYY respectively. Ensemble means for 2041–2050 and 2091–2100 are indicated by blue and red lines respectively while present-day estimates are shown by grey lines (historical general circulation model driving data) and black dashed lines (observed driving data)..... 133
- Figure 5.6: CMIP5 ensemble mean estimates of gross primary productivity (GPP) and latent heat flux (LE) for the period 2041–2050 (plain bars) and 2091–2100 (striped bars). Panels (a–c) show GPP and (d–f) LE for Castelporziano (CPZ), Blodgett (BLO) and Hyytiälä (HYY) respectively. Red, brown, blue and grey bars represent FUT, FUT + Dr, FUT + O₃ and FUT + DrO₃ model simulations respectively 135
- Figure 5.7: Comparison between non bias-corrected historical (1996–2005) CMIP5 model outputs and observations (black dashed lines) at CPZ (left column), BLO (middle column) and HYY (right column). Model output are shown in green (GFDL), violet (GFDL2), grey (GISS), cyan (IPSL), red (IPSL2), yellow (CSIRO) and orange (BNU) while observed (OBS) values are shown in black dashed lines..... 147
- Figure 5.8: Annual profile of bias-corrected historical (1996–2005) CMIP5 GCM data at CPZ (left column), BLO (middle column) and HYY (right column). Model output are shown in green (GFDL), violet (GFDL2), grey (GISS), cyan (IPSL), red (IPSL2), yellow (CSIRO) and orange (BNU) while observed (OBS) values are shown in black dashed lines..... 148
- Figure 5.9: Annual profile of bias-corrected mid-century (2041–2050) CMIP5 GCM data at CPZ (left column), BLO (middle column) and HYY (right column). Model output are shown in

green (GFDL), violet (GFDL2), grey (GISS), cyan (IPSL), red (IPSL2), yellow (CSIRO) and orange (BNU) while observed (OBS) values are shown in black dashed lines..... 149

Figure 5.10: Annual profile of bias-corrected end of century (2091-2100) GCM data at CPZ (left column), BLO (middle column) and HYY (right column). Model output are shown in green (GFDL), violet (GFDL2), grey (GISS), cyan (IPSL), red (IPSL2), yellow (CSIRO) and orange (BNU) while observed (OBS) values are shown in black dashed lines. 150

Figure 5.11: 1997-2014 annual average GPP (top) and LE flux (bottom) for HYY. Observed (OBS) values are shown by black bars while model output are: orange (CTR and CTR+Dr), blue (AVD and AVD+Dr), grey (TLR and TLR+Dr) with striped bars indicating drought stress. Percentage differences between modelled and observed values are shown at the top of the bars. Positive values indicate model overestimation while negative values indicate model underestimation. 150

Figure 5.12: Taylor Diagram showing model output statistics from FORCAsT simulations using historical GCM driving data. Black and orange dashed curves and blue lines show normalised standard deviation (SD), centred root mean squared error (RMSE) and correlation coefficients (r) respectively against model estimates made with observed driving data. Observed GPP and LE are summarised by the purple circle with SD=1.0, RMSE=0.0 and r =1.0. The summary statistics for ensemble mean (ENS MEAN) is shown by red circles, while individual GCMs are shown by green (GFDL), violet (GFDL2), grey (GISS), cyan (IPSL), pink ((IPSL2), yellow (CSIRO), and orange (BNU). Note the change in scale on panel (f)..... 151

Figure 5.13: Estimate GPP and LE for 2041-2050 grouped by CMIP5 GCM ensemble member. ssssPanels a- c show GPP while d-f show LE at CPZ, BLO and HYY respectively. Orange, brown, blue and grey bars represent FUT, FUT+Dr, FUT+O₃ and FUT+DrO₃ model configurations respectively..... 152

Figure 5.14: Estimate GPP and LE for 2091-2100 grouped by CMIP5 GCM ensemble member. Panels a-c show GPP while d-f show LE for CPZ, BLO and HYY respectively. Orange, brown, blue and grey bars represent FUT, FUT+Dr, FUT+O₃ and FUT+DrO₃ model configurations respectively..... 152

Figure 5.15: Best estimates of GPP and LE based on using different GCM model output data to drive FORCAsT for the period 2041-2050 compared with present-day estimates using observed driving data. Ensemble mean is indicated by red dashed lines and present-day estimates by black dashed lines. Estimates for each GCM are shown by green (GFDL), violet (GFDL2), grey (GISS), cyan (IPSL), pink (IPSL2), yellow (CSIRO), and orange (BNU). 153

Figure 5.16: Best estimates of GPP and LE based on using different GCM model out to drive FORCAsT for the period 2091-2100 compared with present-day estimates using observed driving data. Ensemble mean is indicated by red dashed lines and present-day by black dashed lines. Estimates for each GCM are shown by green (GFDL), violet (GFDL2), grey (GISS), cyan (IPSL), pink (IPSL2), yellow (CSIRO), and orange (BNU). 153

Figure 6.1: Observations of meteorology and soil conditions at each site. (a, c) SWC (brown) and rainfall (blue) and (b, d) Temperature (red) and PAR (black) at Wytham Woods (UK_Wyt) and MOFLUX site (US_Moz)..... 166

Figure 6.2: Scatter plots of isoprene fluxes against SWC coloured by temperature (left column) and temperature coloured by SWC (right column) at UK_Wyt and US_Moz. The top two rows present observations at UK_Wyt for 2018 and 2019 respectively. The bottom two rows present observations at US_Moz for 2011 and 2012 respectively. The isoprene vs SWC plots are coloured by temperature while the isoprene vs temperature plots are coloured by SWC..... 167

Figure 6.3: Timeseries of observed and modelled isoprene fluxes at UK_Wyt (a-d) and US_Moz (e-h). Observed isoprene is shown in black while model estimates (CTR) are shown in blue. Areas highlighted in grey are moderate drought periods as defined by Eqn. 8 and shown indicated by the orange lines. Dashed red lines indicate the upper and lower bounds of the moderate drought severity definition..... 169

Figure 6.4: Timeseries of observed and modelled isoprene fluxes at UK_Wyt (a-c) and US_Moz (d-f). Observed isoprene is shown in black while model estimates are shown in blue (CTR) and red (CTR+Dr). Areas highlighted in grey are moderate drought periods as explained in Figure 6.3..... 171

Figure 6.5: Percentage of assimilated carbon that is re-emitted as isoprene at UK_Wyt (a-b) and US_Moz (c-d). Areas highlighted in grey are moderate drought periods as explained in Figure 6.3..... 173

List of Tables

Table 3.1: Isoprene mixing ratios and model performance statistics for observations and model simulations at the top of the canopy (15.6m). Mixing ratios are shown for the entire season (June 1 st – September 30 th , 2018) and selected periods. Numbers in brackets show the percentage difference between observed and modelled values; negative percentages indicate model underestimation while positive values indicate model overestimation. Model performance statistics are provided for the entire season only.	64
Table 3.2: As Table 3.1 for middle of the canopy (13.5m).....	64
Table 3.3: As Table 3.1 for trunk level	65
Table 3.4: As Table 3.1 for near surface level (0.5m).....	65
Table 4.1: : Summary of the five FLUXNET2015 datasets used to evaluate modelled canopy-top CO ₂ and latent heat fluxes. IGBP ecosystems are described as: EBF – Evergreen Broadleaf Forests, ENF – Evergreen Needleleaf Forests, DBF - Deciduous Broadleaf Forests according to dominant vegetation type, canopy height and time of foliage cover.....	103
Table 4.2: Summary of the site- and species-specific parameter values used in model parameterisation at the five sites. N/A denotes not applicable. Where applicable, references for each value are indicated by superscripts and listed below.....	104
Table 4.3: Perturbed parameter values for each model simulation at each of the five FLUXNET2015 data sites. The first column indicates the stomatal conductance or coupled conductance-photosynthesis model applied, with – denoting lower bound and + upper. Those with no symbol represent the baseline simulation for each model. The values used in baseline simulations are highlighted in bold fonts.	105
Table 4.4: Summary statistics for an average year at each site for each test, showing number of data (n), centred Root Mean Square Error (cRMSE), coefficient of correlation (r^2), normalised standard deviation (relative to the observations; normSD) used to create the Taylor plots (Fig. 6). The summary for GPP for each model at each site shows the product of cRMSE, $1-r^2$ and the absolute value of normSD-1.....	105
Table 5.1: Summary of observed and modelled annual cumulative gross primary productivity (GPP) and latent heat fluxes (LE) in present-day simulations. Observations (OBS) and best-fit model simulations are highlighted in bold	128

ss: Details of study sites and parameter values used in estimating drought and ozone stress.
References for each value are indicated by superscripts and listed below 144

Table 5.3: Details of general circulation models (GCMs) used in future impact studies.. 145

Table 5.4a: Model performance statistics for FORCAsT compared to observation at CPZ.
Bold numbers indicate the best performing model configuration in each category. . 145

Table 6.1: Drought severity defined using soil moisture stress (β) 161

Table 6.2: Summary of site characteristics and datasets used in parameterising and driving
JULES. Abbreviations are explained below the table..... 163

Chapter 1: Introduction

1.1 Motivation and Rationale

The exchange of reactive gases between the terrestrial biosphere and atmosphere plays a crucial role in determining atmospheric composition and air quality and is an important driver of global and regional climate. Such interactions between the biosphere and atmosphere are the result of the complex systems of processes linking the Earth's vegetation and soil surface and the atmosphere above it.

The terrestrial biosphere covers approximately 30% of the Earth's surface. As depicted in Figure 1.1, plants release oxygen, volatile organic compounds, and water vapour into the atmosphere. The terrestrial biosphere also removes carbon dioxide (CO_2) from the atmosphere through photosynthesis and is a major sink for atmospheric pollutants like ozone (O_3). These processes are crucial as they regulate global climate and precipitation patterns, and atmospheric chemistry, as well as sustaining life on Earth. The biosphere can also be considered as a living and dynamic component of the Earth system which responds to its surrounding environment. Environmental conditions such as temperature and solar radiation regulate the growth and functioning of plants. This system of processes between biosphere and atmosphere is termed as biosphere-atmosphere interactions.

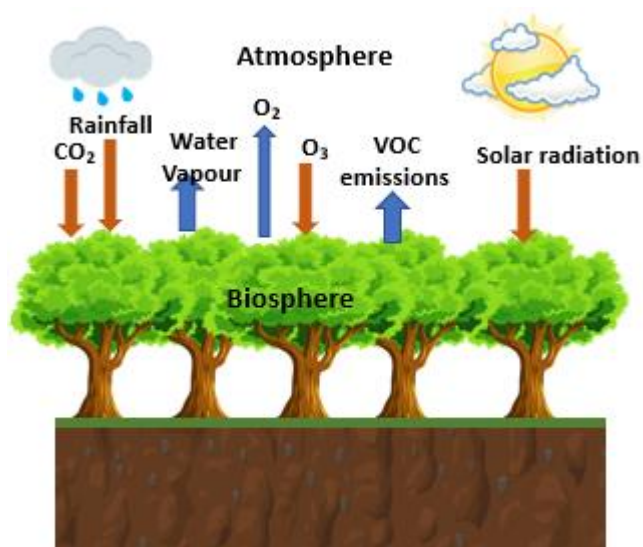


Figure 1.1: Simplified schematic of biosphere-atmosphere interactions.

To understand and quantify these biosphere-atmosphere interactions, a network of ground-based (in situ) and remote sensing instruments have been deployed to provide observations of climatic conditions as well as monitor the exchanges between the various components of the global climate system. These observations have been of immense help in improving our understanding of the underlying processes governing biosphere-interactions and how such interactions change in space and time. However, observations have their limitations. Large portions of the globe are not covered by any observation network. Where they exist, equipment failure and other problems often lead to gaps in the data collected. Measurements made near each other can vary widely depending on instruments used and local conditions. Perhaps the biggest limitation of observation in the context of global climate system is that it cannot provide information about the future.

Land surface models (LSMs) have been developed to fill in the observation gaps, improve understanding of the underlying processes governing the global climate system, and provide information about potential changes in the future. Our understanding of important land surface and plant physiological processes such as stomatal conductance, the uptake of carbon dioxide (CO₂) from the atmosphere through photosynthesis, the release of water vapour into the atmosphere through transpiration, and the emissions of biogenic volatile organic compounds (BVOCs), have been greatly enhanced with the use of LSMs. Indeed, LSMs are the only tools capable of providing such crucial information at the regional and global scale. As a result, LSMs play an important role in climate change mitigation strategies. For example, information about the amount of carbon stored in the ocean, biosphere and atmosphere and how these will change in the future are all based on estimates by general circulation models in which LSMs are central.

However, there still exist gaps in our understanding of some of the factors that drive biosphere-atmosphere exchange, particularly in forested environments, leading to crude assumptions and uncertainties in their parameterisation in models. For instance, BVOCs play vital roles in governing atmospheric composition, air quality and climate. The total amount of isoprene, the most abundant BVOC emitted by plants, is comparable to methane emissions. However, uncertainties around isoprene emissions and hence mixing ratios, makes it difficult to properly parameterise and fully account for its impact in the global climate system. As explained in Chapter 2, the impact of stress from different sources on plant productivity and gas exchange remain one of the main sources of uncertainty in models.

This work seeks to understand the role of two specific abiotic stresses: drought and ozone damage in modifying biosphere-atmosphere exchange of trace gases and how well

these processes are represented in current models. It is motivated by the need to improve parameterisations of plant physiological processes and determine which are of sufficient relative importance to warrant inclusion in regional-global LSMs and hence GCMs.

The research described in this thesis addresses three main thematic areas: model development, model evaluation and model deployment. Model development, which is central to this work, involves improvement in drought and ozone stress parameterisations in the 1-Dimensional (vertical column) FORest Canopy Atmosphere Transfer (FORCA_sT) model and the Joint UK Land Environment Simulator (JULES) model (Ashworth et al., 2015; Best et al., 2011; Clark et al., 2011). New parameterisations, based on the latest understanding of the mechanisms involved in drought and ozone stress responses (e.g. Hoshika et al., 2013; Keenan et al., 2010; Pleijel et al., 2004; Sitch et al., 2007), are incorporated into coupled stomatal conductance and photosynthesis modules within these models to study the relationship between these stress factors and plant gas exchange, including often overlooked trace gases.

1.2 Aims and Objectives

This thesis seeks to bridge the gap between the latest scientific knowledge about the role of drought stress and ozone damage in controlling or regulating plant processes that are central to biosphere-atmosphere interactions, and how these stressors are currently modelled. By combining long-term measurements with vegetation models, this work attempts to unravel how drought stress and exposure to ozone affects isoprene emissions, plant productivity and gas exchange at different timescales ranging from hours to decades in present day as well as future climates. Ultimately, this thesis aims to improve how these processes are parameterised in models since models are fundamental to climate change mitigation efforts.

The aims of this work are to:

- investigate how drought severity affects isoprene emissions and determine how well current emission models account for this impact
- investigate the effect of soil moisture stress on ecosystem-scale plant gas exchange and the effect on the global terrestrial carbon sink in future climates
- determine the effect of O₃ uptake and damage on photosynthesis and stomatal conductance, and hence transpiration.
- investigate how plant gas exchange and ozone deposition rates are affected by variations in model parameterisations.

1.3 Structure of the thesis

In Chapter 2, the current state of knowledge on biosphere-atmosphere interactions and how these interactions change during periods of stress is explored. The key areas of uncertainty in modelling of isoprene emissions under drought conditions are also identified. Similarly, the impact of drought stress and ozone damage on photosynthesis, plant productivity and latent heat fluxes, and how these are currently modelled are explored.

Chapter 3 delves into how drought severity affects isoprene emissions and how effectively such impacts are currently modelled. The FORCAsT 1-Dimensional canopy model is applied to explore the capability of current emission algorithms to reproduce observed changes in isoprene emissions (and, hence, mixing ratios) during the WISDOM campaign at Wytham Woods in 2018. This study reveals that current emissions models struggle to account for stress-induced emissions and recommends the inclusion of parameterisations based on soil water content and re-wetting in LSMs to improve model estimates of isoprene emissions during moderate drought events.

Several stomatal conductance and photosynthesis models have been developed and are currently in use – each with specific input requirements and uncertainties. In Chapter 4, uncertainties associated with choice of key model parameters and the effect of changes in those parameters on simulated photosynthesis rates and ozone deposition are investigated. The stomatal conductance model developed by Jarvis, the coupled stomatal conductance-photosynthesis model of Ball-Berry and the Medlyn stomatal optimisation models are incorporated into the plant physiology module of FORCAsT to calculate photosynthesis rate and stomatal conductance. Model performance is evaluated against observations of gross primary productivity from Mediterranean, Boreal, temperate and tropical forest sites in the FLUXNET network. Sensitivity tests are conducted to determine the values of key stomatal conductance parameters that provide the best model-observation fit for each forest ecosystem. The impact of variations in stomatal conductance parameters on ozone deposition velocity and deposition rates is also explored in this chapter.

Chapter 5 explores the effect of ozone damage and soil water stress on canopy gas exchange, specifically CO₂ and water vapour fluxes, and how this may be affected by future climate change. By using empirical formulations that account for the impact of water stress and ozone damage on photosynthesis rates and stomatal conductance with present day and CMIP5 climate and surface ozone data, this study shows that drought stress far outweighs the impacts of ozone pollution under current and future climates. The results also suggest

that these two stress factors may, to a minor extent, counteract the effect of each other. This chapter also provides insights into how future changes in droughts and ozone concentrations, as projected by CMIP5 models under the RCP8.5 scenario, will affect the magnitude of the CO₂ sink of global forests, and hence the capacity of forests to sequester carbon from the atmosphere in the future.

Chapter 6 investigates the relationship between gross primary productivity and isoprene emissions and how this ratio changes during periods of low soil water content. A new drought stress algorithm is proposed for a process-based isoprene emission scheme and incorporated into the JULES LSM to investigate how drought severity (indicated by changes in soil water content) and increasing temperature affect isoprene emissions and fluxes above the forest canopy. Here, the percentage of carbon uptake that is re-emitted as isoprene under stressed and non-stressed conditions is quantified, and the implications for current estimates of the capacity of the terrestrial carbon sink are explored.

Chapters 3-5 are presented in the form of submitted papers. Each is prefaced by a short statement outlining my contribution to the research, the status of each publication, and its relevance to the overall aims of this thesis.

The concluding chapter of this thesis discusses the role of environmental stress on forest productivity and isoprene emissions, and the implications this has for terrestrial carbon uptake and storage in light of my findings. Finally, the sources and magnitude of uncertainties in the stress algorithms applied here are identified and recommendations made to guide future work in this area.

Chapter 2: Modelling Biosphere-Atmosphere Interactions

The atmosphere and biosphere behave as a coupled system and the exchange of heat, energy, and momentum between them control the global carbon, hydrological and nutrient cycles, governing climate, atmospheric composition, and air quality. This chapter discusses the key biosphere-atmosphere processes that are of primary concern in studying the global climate system. Here we focus on the role of trace gases in the climate system and how the atmosphere influences emissions rates and mixing ratios of isoprene, the bVOC emitted in largest quantities by plants. The role of abiotic stress factors like droughts and ozone damage on plants, and how they are currently modelled, is also explored in this chapter. The chapter concludes with a description of the datasets used in evaluating the models applied in this research and the requirements for improving our understanding of biosphere-atmosphere interactions.

2.1 Biosphere-atmosphere Interactions

The terrestrial biosphere influences the atmosphere through many processes amongst the most important of which, in the context of the Earth system, are the exchange of carbon dioxide (CO₂) and the partitioning of surface energy into latent and sensible heat fluxes. The terrestrial biosphere constitutes the largest of the three main reservoirs of carbon on Earth exceeding those of each of the atmosphere and oceans. Forests cover an estimated 4.06 billion hectares, ~31% of Earth's total land area (FAO, 2020). Tropical forests (45%) make up the largest proportion of the world's forests followed by Boreal (28%), temperate (16%) and subtropical (11%) (FAO, 2020). It is estimated that the total carbon stored in forests alone is 861 PgC (Pan et al., 2011), higher than in either the atmosphere (760 PgC) or oceans (800 PgC) (NASA, 2020). Forest carbon storage can further be divided into tropical (471 PgC: 54%), Boreal (272 PgC: 32%) and temperate (119 PgC: 14%) (Pan et al., 2011).

The biosphere's role in the carbon cycle consists of two main parts: fluxes (photosynthesis, plant respiration, soil respiration, litter fall) and reservoirs (soils and vegetation) (Lenton and Huntingford, 2003). CO₂ is taken up from the atmosphere through photosynthesis and lost via plant and soil respiration. Litter fall converts atmospheric CO₂ into soil carbon. Soils hold about two-thirds of terrestrial carbon with the remaining one-third in land surface vegetation: forests, crops, grasslands, and other plant ecosystems (Dixon and Turner, 1991). The biosphere therefore plays a crucial role in the global carbon cycle. It

also is a key component in the climate system, and will play a significant role in future climate change; forests absorb large quantities of CO₂ from the atmosphere but deforestation, especially in the tropical region is a major source of CO₂ emissions (Mitchard, 2018).

Vegetation also emits large quantities of other compounds such as biogenic volatile organic compounds (BVOCs) into the atmosphere which play a crucial role in atmospheric chemistry at regional and global scales (Fehsenfeld et al 1992; Fuentes et al., 2000; Laothawornkitkul et al., 2009). Thousands of BVOCs have been identified and there are suggestions that many others remain unidentified and even undetected (Goldstein and Galbally, 2007). BVOC emissions account for an estimated 5-10% of total net carbon exchange, especially under stress conditions, making them an important source of carbon in the atmosphere (Peñuelas and Llusà, 2003). An estimated 1 Pg of BVOCs, approximately twice the total annual global methane emissions, are emitted into the atmosphere annually. This total comprises isoprene (50%), with other BVOCs making up the remainder (Guenther et al., 2012). Isoprene (C₅H₈; 2-methyl-1,3-butadiene) is the most important BVOC emitted by terrestrial vegetation in terms of quantity and impacts on atmospheric composition (Guenther et al., 2012).

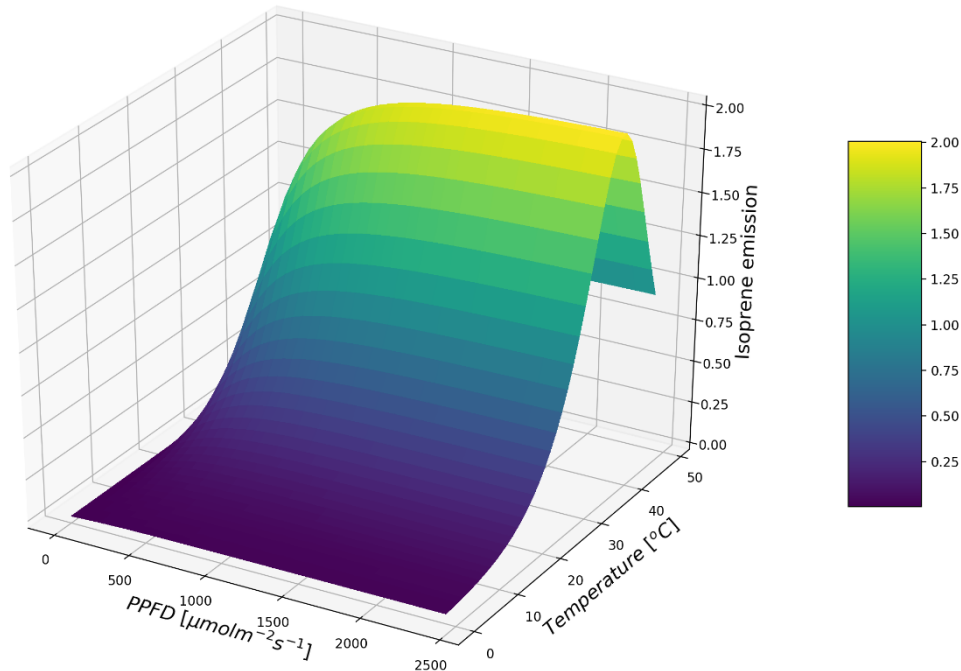


Figure 2.1: Responses of leaf isoprene emission rate (I) to variation in temperature (T , °C) and incident quantum flux density (PPFD, $\mu\text{mol m}^{-2} \text{s}^{-1}$) according to isoprene emission model of Guenther et al. (1995). PPFD is a measure of PAR intensity.

Isoprene emissions are strongly dependent on climatic conditions particularly solar radiation, temperature, atmospheric CO₂ concentrations and plant water status. The response of isoprene emissions to light (specifically photosynthetically active radiation, PAR) and temperature has been extensively studied in the laboratory and field (Monson et al., 1994; Tingey et al., 1981) and used as the basis of the first emission models (e.g. Guenther et al., 1991, 1993; Monson et al., 1994). Figure 2.1 shows the response of normalised leaf isoprene emissions to variation in temperature (T) and PAR based on the emission algorithm of Guenther et al. (1995). Isoprene emissions increase from zero in the absence of PAR (at night) and rise steadily in response to increasing temperature and PAR. Emissions peak at high levels PAR and at species-specific optimum temperatures.

Isoprene reacts with other atmospheric gases and can affect climate at local, regional, and global scales. This creates a strong feedback between environmental conditions and isoprene emissions. For instance, isoprene affects tropospheric ozone, hydroxyl radical OH (the main tropospheric oxidant), and aerosol budgets through its reactions with other atmospheric constituents. It has a lifetime of about an hour against oxidation by OH and therefore could reduce atmospheric oxidation capacity and enhance the atmospheric lifetime of climate forcers like methane (e.g. see Atkinson and Arey, 2003; Folberth et al., 2006; Pike & Young, 2009).

Isoprene chemistry also leads to production or depletion of tropospheric ozone, an effective greenhouse gas and air pollutant. Ozone is formed by photochemically-driven reactions between nitrogen oxides ($\text{NO}_x \equiv \text{NO} + \text{NO}_2$) and VOCs (including BVOCs like isoprene) (Fehsenfeld et al., 1992; Fuentes et al., 2000). However, the amount of ozone produced is strongly dependent on the ratio between VOCs and NO_x (VOC/NO_x) as well as the O₃ forming potential (OFP) of the VOC. Ozone formation is VOC-limited when $\text{VOC}/\text{NO}_x < 4$, optimum when $4 < \text{VOC}/\text{NO}_x < 15$, and NO_x -limited when $\text{VOC}/\text{NO}_x > 15$ (Calfapietra et al., 2013). VOC-limited conditions, in which O₃ production is limited by a high concentration of NO_x , are often observed in urban areas. By contrast, O₃ production is NO_x -limited in rural areas where anthropogenic NO_x sources are few. Optimum conditions for ozone production are found in transition zones between rural and urban areas (Calfapietra et al., 2013; Royal society, 2008).

Reactions between isoprene and OH produce peroxy radicals (Mao et al., 2013). In the presence of NO_x , these peroxy radicals react with NO leading to the production of organic nitrates (Royal Society, 2008). These nitrates may act as a sink for both NO_x and HO_x radicals ($\text{HO}_x \equiv \text{OH} + \text{peroxy radicals}$) which are ozone precursors and therefore affect

global and regional ozone budgets (Brown et al., 2009; Horowitz et al., 2007; Ito et al., 2009; Paulot et al., 2012; Royal Society, 2008; Wu et al., 2007; Xie et al., 2013).

Isoprene is also important in the formation and growth of secondary organic aerosols which could grow and serve as cloud condensation nuclei (Carlton et al., 2009; Hallquist et al., 2009; Jimenez, et al et al., 2009; Surratt et al., 2007). Clouds can reflect incoming solar radiation and thus have a cooling effect on Earth's climate. However, clouds can also absorb outgoing longwave radiation leading to global warming. Whether clouds have a cooling or heating effect depends on the absorption, reflection, and transmission characteristics of the cloud (Kokhanovsky, 2004). Secondary organic aerosols formed from isoprene reactions could affect these cloud optical properties. Isoprene could therefore have an indirect climate impact through the formation of secondary organic aerosols (Carslaw et al., 2010; Unger, 2014).

Changing atmospheric CO₂ changes stomatal conductance which can affect emissions of some BVOC. For example, increasing CO₂ has been shown to suppress isoprene synthesis leading to a decline in emission rates (Possell and Hewitt, 2011). In future climates, CO₂ levels are projected to reach ~900 ppm (Riahi et al., 2011) depending on the emissions scenario used. Any decline in isoprene emissions due to increasing atmospheric CO₂ could however be offset by increased emissions due to increasing global temperatures (Arneeth et al., 2008; Heald et al., 2009).

Modelling studies indicate that such an increase in CO₂ could increase global gross primary productivity by 20-60% (Anav et al., 2013; Piao et al., 2013) as plant photosynthesis rates increase leading to more carbon assimilation – often referred to as the CO₂ fertilisation effect (Lewis et al., 2004; Melillo et al., 1993). However, the CO₂ fertilisation effect appears to diminish with time as trees mature and the additional carbon uptake during photosynthesis is re-emitted back into the atmosphere (Feeley et al., 2007; Holtum and Winter, 2010; Jiang et al., 2020). The magnitude of any CO₂ fertilisation effect is dependent on the availability of micro-nutrients such as nitrogen, phosphorus, and sulphur from the soil (Jiang et al., 2020; Norby et al., 2010).

The impacts of other environmental factors like soil moisture stress and air pollution on BVOC emissions and mixing ratios are poorly understood and represented in emission models. Understanding how BVOC emissions respond to changes in environmental conditions in present and future climates is crucial for predicting important feedbacks in the biosphere-atmosphere-climate system.

Soil properties such as water and nutrient content, and temperature can limit plant photosynthesis rates, although PAR and temperature are the primary factors controlling plant productivity (Atkinson, 1973; Nemani et al., 2003; Passioura, 2002; Pemadasa and Lovell 1974). Higher productivity results in increased uptake of atmospheric gases such as CO₂ and O₃ and thus soils can indirectly impact atmospheric composition and chemistry. Soils can also have direct impacts on atmospheric composition by either emitting gases such as oxides of nitrogen (Slemr and Seiler 1984) and BVOCs (see e.g. Bourtsoukidis et al., 2018; Hellén et al., 2006; Tang et al., 2019) or acting as sinks for these and other trace gases and particles. Depending on the type of ecosystem, season, and age of litter, the contribution of soil BVOC emissions to the total ecosystem BVOC budget could range from less than one to tens of percent (Asensio et al., 2007; Schade and Goldstein, 2001). Under drought conditions, soil moisture also regulates the rate of canopy photosynthesis and emissions of BVOCs from foliage. The precise mechanism of this process and how it can be parameterized in emissions models is an active area of scientific investigation (e.g. see Jiang et al., 2018; Pegoraro et al., 2004; Seco et al., 2015).

2.2 Stress factors affecting biosphere-atmosphere interactions

The soil-biosphere-atmosphere system contains a variety of positive and negative feedbacks. For example, increased atmospheric CO₂ concentration could lead to greater CO₂ uptake by plants and hence increased productivity. However, any positive climate impacts from this increased carbon sequestration by plants could be offset by reduced land albedo, which increases solar energy absorption and warms the climate. Each component of this coupled system can create non-optimal conditions with negative impacts on the others. These non-optimal conditions are referred to as stresses and are categorized as biotic or abiotic depending on origin. Biotic stress is a result of the impacts of living organisms such as insects and micro-organisms on plants. These biological agents cause various diseases, infections, and damage to plants, affecting productivity, and in extreme cases, resulting in the death of the host plant. While well-documented to affect BVOC synthesis and emission, biotic stresses are not the subject of this thesis.

By contrast, abiotic stress is caused by environmental factors. Plant growth, development, productivity, and yield are strongly dependent on external environmental conditions (Verma et al., 2013) and thus, abiotic stress again reduces growth and causes mortality. Multiple biotic and abiotic stresses often occur simultaneously, e.g. drought and

heatwave, or drought and herbivory, and may act synergistically or antagonistically. Global climate change has led to an increase in the frequency and intensity of extreme weather event (IPCC, 2013; Zhang et al., 2013). Extreme weather events like heatwaves and droughts, are projected to further increase in severity, frequency, and extent with potentially substantial impacts on physiological and canopy processes (Burke et al., 2006; IPCC, 2013; Warren et al., 2009). Geographical location determines the external environment in which plants live, and hence the biotic and abiotic stresses to which they are most likely to be exposed. It also determines the adaptations different plant species have developed to combat those stresses (Levitt, 1980).

Plants are sessile organisms and have developed complex defence mechanisms that enable them to either tolerate or avoid stress. These strategies are tailored towards individual stressors and vary between plant types and different species of the same type of plants. For example, plant response to drought stress can be categorised into four: avoidance, tolerance, drought escape and recovery (Fang et al., 2015). Drought avoidance strategies adopted by plants include increased stomatal and cuticular resistance and changes in leaf area and anatomy (Jones and Corlett 1992; Morgan 1984; Touchette et al, 2007; Zlatev 2005). Reduced transpiration and increased emissions of biogenic volatile organic compounds are some of the strategies used by plants to tolerate drought stress (Calfapietra et al., 2009; Paoletti, 2006). In climates with seasonal droughts such as the Mediterranean, plants have evolved to regulate their growth period to avoid soil moisture stress, a process known as drought escape (Manavalan et al., 2009). The ability of plants to continue growing after exposure to drought stress is referred to as drought recovery. It has been suggested that such recovery from drought is dependent on tree hydraulics and is enhanced at slower leaf hydraulic conductance (Blackman et al., 2009).

Future changes in climate and extreme weather pose a threat to plant productivity, especially for plants currently surviving at the edge of their climatic hardiness or in geographical locations where such stresses are unusual. This thesis mainly focuses on two specific abiotic stresses likely to change under changing global weather patterns and atmospheric composition: drought and ozone exposure. It also to a lesser extent explores the role of thermal stress on isoprene emissions and mixing ratios via increase in leaf temperature. We explore how the response of vegetation to each stress is parameterised in vegetation models, and how these environmental factors affect plant productivity and isoprene emissions.

2.2.1 Drought impact on plant productivity and gas exchange

Although light and temperature are the main drivers controlling plant productivity rates, water stress is the main limiting environmental factor to global plant photosynthesis and productivity (Nemani et al., 2003; Zeppel et al., 2014). Water availability is critical for plant physiological processes with diminished productivity and growth, and mortality all observed in plants and crops exposed to water stress (Jamieson et al., 1995). In response to drought, plants avoid oxidative and dehydrative damage to their cells by decreasing stomatal conductance to limit transpiration and conserve water (Anjum et al., 2011; Wilkinson and Davies, 2010; Qaderi et al., 2006). Reduced gross primary productivity (GPP) or carbon assimilation is an unintended consequence of this strategy (Bréda et al., 1993; Clenciala et al., 1998; Irvine et al., 1998). Drought can also impact plant productivity through early leaf senescence (Wehner et al., 2016), structural changes in canopy characteristics such as leaf area and leaf angle distribution and reduced leaf expansion (Fisher et al., 2007), further reducing gas exchange and growth.

With climate change already altering patterns of precipitation (Dore, 2005; Trenberth, 2011), and the extent, severity and duration of drought projected to rise further (Zhao and Dai, 2017), water stress is becoming an increasingly important factor in ecosystem carbon exchange and hence the global carbon cycle (Anderegg et al., 2015; Ciais et al., 2005; Yu et al., 2017). An increase in anomalous events such as the 2003 and 2018 European heatwaves and droughts (Toreti et al., 2019) would also increase the abiotic stress experienced in forest ecosystems that are unused to such conditions. It is therefore critical that we better understand the impact of drought stress on vegetation and how to improve its parameterisation in physiological modules of land-atmosphere and Earth system models.

The first biochemical model for photosynthesis rates, the Farquhar model, was developed about four decades ago (Farquhar et al., 1980). The model estimates net photosynthesis (A) as the minimum of two limiting rates of CO_2 assimilation: the Rubisco-limited rate (A_c) and the electron transport-limited rate (A_j). Since then, this model has been progressively developed as our understanding of plant physiological processes has improved. Ball et al. (1987) for instance integrated the effects of environmental factors such as relative humidity into the Farquhar biochemical model to produce a coupled relationship between stomatal conductance and the rate of photosynthesis (the Ball Woodrow Berry: BWB model). The BWB model has subsequently been modified by Medlyn et al. (2011) using optimal stomatal behaviour theory in which leaf gas exchange is internally controlled

via stomatal aperture to maximize carbon gain while simultaneously minimizing water loss. The underlying assumptions in these models have been applied to develop other models to estimate photosynthesis rates and stomatal conductance for a variety of ecosystems (e.g. Katul et al., 2010, Pe and Yu, 2008).

These photosynthesis models are incorporated into vegetation and land surface models to provide estimates of terrestrial carbon uptake and storage under different climate scenarios - crucial for climate change mitigation strategies. However, several modelling studies have highlighted the lack of model skill at reproducing observed plant photosynthesis rates at the ecosystem scale during periods of low soil water availability (Keenan et al., 2010 and references therein). This is especially true for Mediterranean ecosystems where models underestimate observed GPP during seasonal water stress (Harper et al., 2020; Jung et al., 2007; Morales et al., 2005).

This model underperformance is in part due to the challenge of accounting for drought stress impacts on plants in LSMs (McDowell et al., 2011) because the response depends on sub-gridscale variations and interactions between soil characteristics, ecosystem type, climatic conditions, and plant species. For example, soil moisture content that causes severe drought stress to plants in one ecosystem may only trigger mild or even negligible stress in another (Knapp and Smith, 2001). Several alternative metrics for plant water status have been developed in an attempt to more accurately define what constitutes drought stress in a consistent manner across ecosystems (eg. De Kauwe et al., 2015b; Egea et al., 2011; Keenan et al., 2010; Zhou et al., 2014): volumetric soil water content (SWC), soil water potential and predawn leaf water potential. The latter two are more physiologically relevant but require detailed and often difficult measurements at the leaf or plant level (Zhou et al., 2014). As SWC can be measured at the landscape-scale and, increasingly, through remote sensing, it is still more widely used in model parameterisations.

A common approach has therefore been to calculate an empirical soil water stress function, β (ranging between one and zero), from SWC (e.g. Porporato et al., 2001; Keenan et al., 2010):

$$\beta = \begin{cases} 1 & \text{for } \theta \geq \theta_c \\ \left[\frac{(\theta - \theta_w)}{(\theta_c - \theta_w)} \right]^q & \text{for } \theta_w < \theta < \theta_c \\ 0 & \text{for } \theta < \theta_w \end{cases} \quad 2.1$$

where θ is the measured SWC, θ_w the wilting point of that PFT or ecosystem and θ_c the critical value of SWC below which drought impacts occur. The wilting point is defined as the soil moisture at which a plant cannot further extract water from soil. It generally occurs at a suction of -1.50 MPa but varies with soil texture. A β value of one indicates water stress is not a limiting factor for stomatal conductance or plant productivity; below the wilting point the plant is non-productive and β is set to zero. Between these two limits, productivity declines with decreasing SWC. Here, q is a site-specific empirical factor estimated using in situ observations, which describes the non-linearity of the downregulation of stomatal function with decreasing SWC, i.e. increasing soil moisture stress.

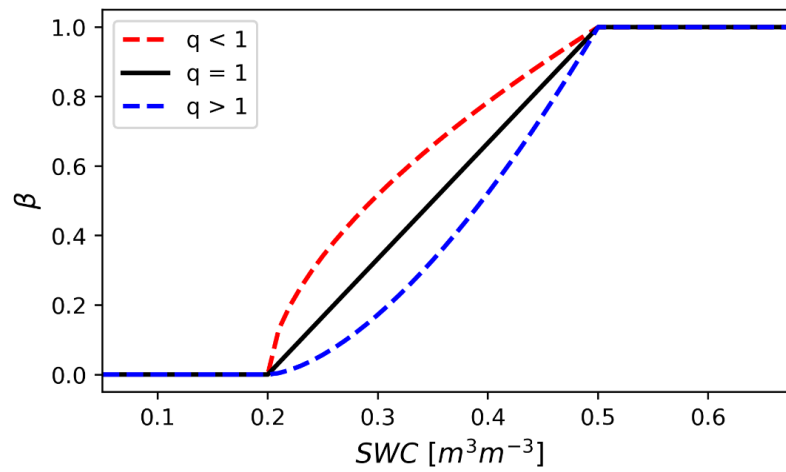


Figure 2.2: schematic of how the soil moisture stress response factor, β , depends on the value of q . The red and blue dashed lines show the shape of the response curve when $q < 1$ and $q > 1$ respectively. The black line indicates the linear response of β when $q = 1$. SWC values of $0.20\text{m}^3\text{m}^{-3}$ and $0.50\text{m}^3\text{m}^{-3}$ were used for θ_w and θ_c respectively.

As shown in Figure 2.2, β can either vary linearly or non-linearly between these values, depending on the value of q . For a specific value of SWC, soil moisture at sites where $q > 1$ will exert greater stress on trees and hence lead to a bigger reduction in plant physiological processes (e.g. stomatal conductance) than those for which $q < 1$. This is associated with a greater tolerance to drought for the plant species with $q < 1$ than the species with $q > 1$. The value assumed for q , and thus the shape of β , is a determinant of model performance during periods of low SWC (Egea et al., 2011). As a result, there is a need to determine q for as wide a range of PFTs and ecosystems as possible to improve understanding of how SWC affects plant physiology, and hence to enable more accurate modelling of plant productivity and gas exchange under drought conditions. One of the focal

themes in this thesis is how well vegetation models reproduce changes in stomatal conductance and photosynthesis during periods of drought stress and, hence, how plant-atmosphere gas exchange may be affected by drought in the future.

2.2.2 Drought Impacts on Isoprene Emissions

Isoprene synthesis and emission play many crucial roles in plants. Isoprene synthesis is believed to protect plants from oxidative, heat and drought stress (Loreto and Schnitzler, 2010) allowing plant photosynthetic apparatus to function normally under such conditions. The impact of oxidative stress on isoprene emissions is covered extensively elsewhere (e.g. Guenther et al., 1993; Sharkey et al., 2008; Velikova et al., 2008; Velikova and Loreto, 2005; Vickers et al., 2009) and will not be the focus of this thesis. Instead, we focus on drought stress which is expected to increase in frequency as global precipitation and temperature patterns change due to climate change.

Our understanding of the effect of drought stress on isoprene emissions has mostly emanated from laboratory-based experiments. The findings from these studies show that the effects of drought on isoprene emissions depend on the severity of drought (Niinimets, 2010). While there is consensus that severe drought substantially decreases emissions (Llusà and Peñuelas, 1998; Pegoraro et al., 2005), mild and moderate drought stress has been observed to either increase (Pegoraro et al., 2004) or have no effect on emissions (Brilli et al., 2007, Lavoit et al., 2009; Sharkey and Loreto, 1993). Emissions have also been observed to increase after re-watering following a period of drought stress in laboratory experiments (Penuelas et al., 2009). However, there is little evidence of this phenomena in natural environments due to the absence of observations of emissions following soil re-watering after a period of drought.

Laboratory or enclosure measurements usually involve seedlings or young plants (e.g. Brilli et al., 2007; Pegoraro et al., 2004) and variables such as light and temperature are controlled, allowing for the impact of drought only or the combined impact of drought and heatwave to be studied in isolation. By contrast, plants in the field or natural environment like forests are usually mature and are often subjected to multiple stressors simultaneously. For example, a tree experiencing drought stress may also be exposed to other abiotic stresses such as high temperatures or air pollution, and to biotic stresses such as herbivory or pathogen attacks which could modify BVOC emission rates and patterns (Baldwin, 2010; Loreto et al., 2014). For these reasons, forest trees can be expected to respond differently to

environmental stress in comparison to seedlings and saplings used in laboratory studies. It is therefore not surprising that observations in forest environments often show different emission responses to stress compared to lab experiments (e.g. Seco et al., 2015; Ferracci et al., 2020). However, laboratory-based experiments remain a vital tool for improving our understanding of the mechanisms underlying the impact of drought on BVOC emissions.

Isoprene emissions from vegetation are modelled using either process-based models which link isoprene production to carbon assimilation in a mechanistic way or empirical models which account for the effect of individual environmental factors based on observed statistical relationships (Arneth et al., 2007a; 2007b; Guenther et al., 1995). In either case, as previously discussed, isoprene synthesis and emissions are driven by light and temperature in the same way as photosynthesis.

Empirical models are the most widely used algorithms to describe isoprene emissions from leaves. Laboratory experiments by e.g. Guenther et al. (1991; 1993) showed strong relationships between light and temperature and isoprene emissions, similar to those of photosynthesis, as shown in Figure 2.1. Guenther et al. (1995) developed the earlier single-species models of Guenther et al. (1991; 1993) into a global emissions algorithm for a full range of global ecosystems in which isoprene emissions varied non-linearly in response to changing leaf temperature and radiation at the leaf surface - often referred to as the G95 emission model. It is this isoprene emissions scheme that is included in the FORCAST canopy exchange model.

Process-based models determine isoprene production rates based on enzyme activity and the supply of precursors from photosynthesis. They link emissions of isoprene to biochemical processes occurring within plants such as the electron requirement for isoprene synthesis, the supply of carbon for isoprene synthesis, and the role of CO₂ in stimulating or inhibiting isoprene synthesis and emissions (e.g. see Arneth et al., 2007b; Back et al., 2005; Martin et al., 2000; Niinemets et al., 1999; Zimmer et al. 2000). Arneth et al. (2007b) identified four types of process based isoprene emission models, and went on to develop the Niinemets et al. (1999) model into a global emissions model which has been applied within land surface models (e.g. see Arneth et al., 2011; Pacifico et al., 2011). The Niinemets et al. (1999) model proposes that isoprene emissions are directly related to the electron transport rate, a theoretical parameter linking isoprene synthesis and the fraction of electrons available for isoprene production. This is the approach adopted by the isoprene emissions module in JULES.

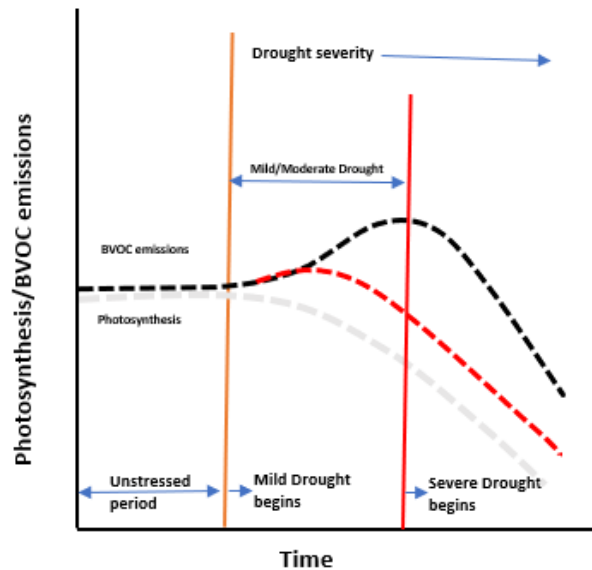


Figure 2.3: Conceptual model of the response of ecosystem isoprene emission and photosynthesis to drought stress. The orange vertical line denotes the initiation of drought stress (i.e. at the critical threshold), and the red vertical line the onset of severe drought. The grey dashed line represents changes in photosynthesis in response to drought. The red dashed line show isoprene emissions expected if isoprene synthesis continues to follow photosynthesis. The black dashed line shows isoprene emissions modelled on the assumption that mild drought stress increases leaf temperature and/or C_i , stimulating isoprene emissions under mild drought. During the severe phase of drought stress, isoprene emissions again decline in relation to declining photosynthesis.

It is generally understood that isoprene synthesis and emissions are closely correlated with photosynthesis rates (Brilli et al., 2007; Harley et al. 1994; Litvak et al. 1996; Schnitzler et al., 2004) and there is strong evidence that both isoprene and photosynthesis rates change during periods of drought stress (Ferracci et al., 2020; Pegoraro et al., 2004; Potosnak et al., 2014; Seco et al., 2015; Sharkey and Loreto, 1993). While foliage emission rates of isoprene are closely coupled with photosynthesis when soil moisture is above a critical threshold, and during severe droughts (Pegoraro et al., 2004a), recent studies have shown this relationship breaks down under moderate drought stress (Brilli et al., 2007; Seco et al., 2015).

Figure 2.3 shows a conceptual model of how isoprene emissions and photosynthesis rates respond to reduction in soil water availability. It was developed based on the hypothesis of Niinemets (2010) that there are two phases to the leaf-level response of isoprene emissions to drought stress. It would be expected that reductions in plant photosynthetic capacity as a result of water stress would lead to a corresponding decline in isoprene emissions as indicated by the red dashed line on Figure 2.3. However, observations have shown that

during moderate drought emissions of isoprene are enhanced. Niinemets (2010) and Potosnak et al. (2015) postulated that, under such conditions, isoprene synthesis is stimulated by increases in leaf temperature due to the decrease in stomatal conductance and transpiration associated with the physiological response of plants to drought stress. This increase in synthesis leads to an increase in isoprene emission rates proportionate to the increase in leaf temperature as indicated by the black dashed line. However, as drought stress becomes more severe, isoprene emissions decline due to a reduction in the supply of carbon available for its synthesis (e.g. Brill et al., 2007; Brüggemann and Schnitzler, 2002; Lerdau et al., 1997; Pegoraro et al., 2004a). In Chapter 3, the G95 model, and the associated representation of emissions under drought stress are explained and applied. In Chapter 6, we propose a method for including drought impacts into the process-based emission model described above.

Decreasing internal CO₂ concentration in leaves (C_i) can also stimulate leaf-level isoprene emissions (Rosenstiel et al., 2003). As drought stress reduces stomatal conductance which in turn reduces C_i , this provides another possible mechanism behind the increase in isoprene emission (Grote and Niinemets, 2007; Pegoraro et al., 2007) observed under mild and moderate drought.

The Model of Emissions of Gases and Aerosols from Nature (MEGAN) was developed from the G95 global emission model to account more fully for the effect of environmental conditions on isoprene emissions. MEGAN incorporates an activity factor that explicitly accounts for the reduction in emissions observed under severe and extreme drought. The response of isoprene emissions to soil moisture stress is calculated as:

$$\gamma_{SM} = \begin{cases} 1 & \text{for } \theta > \theta_1 \\ \frac{(\theta - \theta_w)}{\Delta\theta_1} & \text{for } \theta_w < \theta < \theta_1 \\ 0 & \text{for } \theta < \theta_w \end{cases} \quad 2.2$$

where θ is soil moisture (volumetric water content, m³ m⁻³), θ_w is wilting point (m³ m⁻³), $\Delta\theta_1$ (=0.06 m³ m⁻³) is an empirical parameter such that θ_1 is defined as $\theta_w + \Delta\theta_1$ which represents the soil moisture value below which drought stress affects isoprene emissions.

The formulation of γ_{SM} was based on observations of Pegoraro et al. (2004) who used Live oak (*Quercus virginiana* Mill) seedlings to study the impact of drought on isoprene emissions. Recent observations (e.g. Ferracci et al., 2020; Seco et al., 2015) and modelling studies (e.g. Jiang et al., 2019; Potosnak et al., 2015) have shown that this form of γ_{SM} does

not accurately reflect the effect of drought stress on isoprene emissions from mature forest environments, especially during mild or moderate phases of drought. As shown in Figure 2.3, isoprene emissions modelled using γ_{SM} recreate an emissions profile that follows photosynthesis, i.e. emissions decline, tracking photosynthesis (red dashed line), once the critical threshold for reductions in photosynthesis is passed (orange vertical line), although recent observations show that in fact the ecosystem response is an initial stimulation in emissions (black dashed line).

The process-based model of isoprene emissions does not include a specific parameterisation of the response of isoprene emissions to drought stress. Instead, similar to the Pegoraro formulation of γ_{SM} , it is implicitly assumed to follow photosynthesis under all environmental conditions.

As indicated in Section 2.1 and Figure 2.1, isoprene emissions are dependent on PAR and temperature. As global climate changes, heatwaves have increased in frequency and climate models predict further increases in the future (Deryng *et al.*, 2014; Perkins-Kirkpatrick and Gibson, 2017; IPCC, 2013). High temperatures associated with heatwaves can cause thermal stress to plants leading to irreversible damage like wilting and death, and reducing plant growth and productivity (Wahid *et al.*, 2007). Studies have shown that isoprene synthesis and emissions increase thermotolerance and helps plants to maintain photosynthesis at high temperature (Sharkey *et al.*, 2001; Singaas *et al.*, 1997). Isoprene synthesis reduces the levels of reactive oxygen species which cause damage to plant photosynthetic apparatus (Affek and Yakir, 2002; Loreto and Fares, 2007; Sharkey *et al.*, 2008). Sharkey and Loreto (1993) showed that an increase in leaf temperature from 30 to 40°C led to an 8-fold increase in isoprene emissions in kudzu plant (*Pueraria lobata*). However, each isoprene-emitting plant species has an optimal temperature range below or above which temperature becomes a stress factor that could inhibit isoprene synthesis and emissions (e.g. Monson *et al.*, 1992). Emissions models such as G95 and the process-based models described in Section 2.2.2 both include formulations to account for the effect of temperature on isoprene emissions within the optimal temperature range. However, the simultaneous impact of drought stress and high temperature could lead to increases in leaf temperatures beyond the optimum range due to stomatal closure thus stimulating isoprene emission rates beyond what is currently assumed in models (Niinemets *et al.*, 2010; Ferracci *et al.*, 2020). Using observations of isoprene mixing ratios and fluxes during heatwaves and drought event, this thesis provides novel insights into how best to model isoprene emissions during periods of combined thermal and water stress. In Chapter 3 algorithms based on leaf

temperature were incorporated into the G95 model to investigate the role of thermal stress in unusually high isoprene mixing ratios observed in a UK woodland during the heatwave and drought of 2018.

2.2.3 Impacts of ozone damage on plant productivity and gas exchange

O₃ is a secondary pollutant produced by the photochemical oxidation of other agents, called O₃ precursors, specifically volatile organic compounds (VOCs), in the presence of nitrogen oxides (NO_x=NO+NO₂). Tropospheric O₃ is a powerful greenhouse gas, with radiative forcing estimated to be between ~0.30 and 0.40 W m⁻² (Checa-Garcia et al., 2018; Yeung et al., 2019), and therefore has a direct effect on global warming and climate change, indirectly affecting plant growth and development. O₃ is also a phytotoxin. Following uptake through the stomata, and to a lesser extent the cuticles, O₃ initiates oxidative damage to plant tissue, reducing photosynthesis and growth. Thus, O₃ also indirectly affects global climate by reducing plant productivity and CO₂ sequestration capacity (Talhelm et al., 2014; Wittig et al., 2009).

O₃-Free-Air Concentration Enrichment (O₃-FACE) experiments are increasingly being used to study the potential impact of elevated O₃ on crops and trees (e.g. see Feng et al., 2018; Hoshika et al., 2015; Long et al., 2005; Matyssek et al., 2010; Zak et al., 2011). Results from O₃-FACE experiments are used to understand the effect of ozone on plant physiology, biochemistry, and growth. These experiments have shown that exposure to O₃ concentrations of 50% and 100% respectively above ambient levels could reduce aspen biomass by up to 23% (Karnosky et al., 2003) and stem-growth in adult beech by 44% (Matyssek et al., 2010). The insights gained from O₃-FACE studies have been applied to parameterise the loss of plant biomass or carbon sequestration capacity because of O₃ exposure in vegetation models.

The parameterisations developed to model ozone damage to plants take one of two forms. The first use dose-response calculations based on mean O₃ concentration (Emberson et al., 2000) or accumulated ozone concentrations above a threshold X (AOT_x: Mills et al., 2007).

Open-Top Chamber (OTC) experiments demonstrated that wheat yield was highly correlated with accumulated ozone concentration above 40 ppb during daylight hours leading to the widely used AOT₄₀ metric (Fuhrer et al., 1997). However, there are several conceptual flaws to the application of AOT₄₀ and other concentration-based metrics used to

assess ozone damage. The first is that only ozone concentrations during daylight hours are accumulated, but reductions in whole-plant biomass production have been reported due to night-time exposure to ozone (Matyssek et al., 1995). Second, the use of a fixed threshold does not account for the tolerance level of different vegetation and ecosystems to ozone exposure although this has been observed to be a key determinant of occurrence and severity of damage (Matyssek and Innes, 1999; Vanderheyden et al., 2001). Third, AOT40 is based on ambient ozone concentration (usually at the top of the vegetation canopy) rather than on the stomatal uptake of ozone (Mills et al., 2011; Pleijel et al., 2000) which is necessary for damage to the photosynthetic apparatus and stomatal guard cells to occur (e.g. Matyssek et al., 2007; Musselman et al., 2006).

The alternative parameterisations, such as the Phytotoxic Ozone Dose above a flux threshold of Y (PODy) (Ashmore et al., 2004, Lombardozzi et al., 2012;2015; Mills et al., 2011; Pleijel et al., 2004) therefore use actual flux or uptake of O₃ into the leaves, to estimate ozone impacts on plants. The PODy metric is based on the accumulated stomatal O₃ flux over the growing season and directly down-regulates plant photosynthesis rate and/or stomatal conductance in response to O₃ exposure (Ashmore et al., 2004; Hoshika et al., 2013; Pleijel et al., 2004; Sitch et al., 2007). As this approach is based on actual uptake through the stomata, it better accounts for the environmental and physiological conditions of the vegetation, making it suitable for use across a range of environmental conditions (Paoletti, 2006; Paoletti and Manning, 2007).

Although physiologically more realistic, the PODy approach is not without its uncertainties. For example, the role of plant development stage and leaf age in regulating the severity of damage for a given dose is not well represented in models, yet recent studies suggest this could be important (Bernacchi et al., 2006; Uddling et al., 2009). Further research is also needed to elucidate the combined impact of O₃ and other abiotic stresses, particularly drought, on stomatal conductance (Ainsworth et al., 2012).

Plants have also been observed to reduce their stomatal conductance in response to oxidative stress, including that resulting from ozone (Hoshika et al., 2015; Neill et al., 2008). A parameterisation of the impact of ozone exposure resulting from this stomatal closure has been developed and applied to study the impact of ozone damage in Siebold's beech (*Fagus crenata*) grown in an O₃-FACE facility (Hoshika et al., 2013). However, this parameterisation has not been tested in other plant species or in different climates. Ozone exposure can also cause stomatal sluggishness; a process in which ozone damages a plant's ability to regulate stomatal aperture causing stomata to remain open (Hoshika et al., 2015;

Huntingford et al, 2018; Sun et al., 2012). Stomatal sluggishness could exacerbate the impacts of drought stress as plants continue to transpire.

In Chapter 5, strategies adopted by plants to tolerate or avoid ozone stress and how they are parametrised in models to account for O₃ damage is investigated. This chapter also explores the uncertainties around the choice of parameterisation and the interaction of O₃ exposure with drought.

2.3 Land Surface Models

Land surface models (LSMs) provide estimates of land surface and plant physiological processes such as stomatal conductance, gross and net primary productivity, and latent and sensible heat fluxes. LSMs incorporate dynamic vegetation models which allows them to model natural changes in land cover over time. Additionally, LSMs include physical representation of the exchange of heat, moisture and momentum between the atmosphere and land surface. As a result, they provide insights into key climate processes such as uptake of carbon dioxide (CO₂) by plants through photosynthesis and the release of water vapour into the atmosphere through transpiration. LSMs also provide the lower boundary conditions for global climate models (GCMs) and weather models by simulating the surface energy and water balance as well as carbon and water fluxes. In addition to offering critical understanding of the importance of individual processes at a range of scales on the current global carbon budget, they enable exploration of future changes in the carbon budget and its implications for global warming. For example, LSMs are often applied in Earth system models to explore how global carbon sinks may change in future in response to changes in climate and land surface cover (e.g. see Albani et al., 2006; Fatichi et al., 2019).

As indicated in Section 2.2, models struggle to reproduce observed plant gas exchange during periods of abiotic stress, particularly drought. The key reasons for the poor performance of models in water-stressed environments are reported as being difficulties reproducing the volumetric soil water content, its availability to plants (soil water potential), and poor parameterisations of drought response (Keenan et al., 2010). In this thesis, two land-atmosphere models are used to investigate how soil moisture stress parameterisations currently used in LSMs affect model reproduction of GPP, latent heat fluxes, and isoprene mixing ratios and fluxes in drought-stressed environments and the uncertainties associated with such parameterisations. These models are described extensively in Chapters 3-6 but a brief overview of each is provided here.

2.3.1 FORCAsT 1-Dimensional Model

FORest Canopy Atmosphere Transfer (FORCAsT) is a 1-Dimensional (vertical column) model of biosphere–atmosphere exchange designed to simulate in- and above-canopy concentrations and vertical fluxes of carbon, water, heat and trace gases (Ashworth et al., 2015; Bryan et al., 2015). Processes like foliar emissions of BVOCs, vertical mixing, advection, chemical production and loss, and deposition within and above the canopy are explicitly modelled in FORCAsT. As shown in Figure 2.4, the 40 vertical model levels are subdivided into 10 between the ground surface and trunk height, a further 10 within the crown space with the remaining 20 levels in the mixed layer of the atmosphere above the canopy (usually up to ~3-5 km).

Isoprene emissions from foliage in the crown space are modelled using the G95 parameterisation (Guenther et al., 1995). Isoprene is lost through oxidation reactions initiated by the OH and NO₃ radicals and O₃ (Fan and Zhang, 2004; Wennberg et al., 2018), through deposition to the soil following Stroud et al. (2005), and through vertical transport out of the canopy.

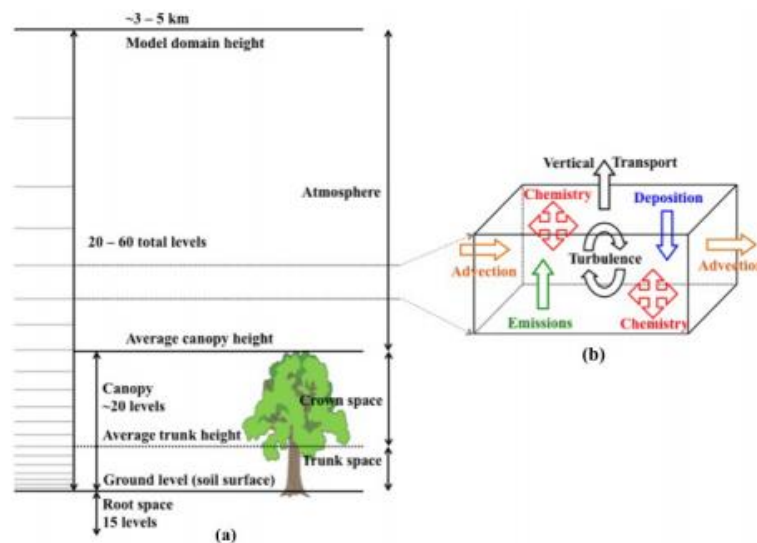


Figure 2.4:(a) A schematic of the FORCAsT column model. Each level within the column is a box model (b) incorporating the processes involved in canopy–atmosphere exchange of energy and mass appropriate for that level. (Source: Ashworth et al., 2015)

As part of this thesis, three methods of estimating photosynthesis and stomatal conductance based on the Jarvis multiplicative model (Jarvis, 1976), the Ball-Berry coupled stomatal conductance-photosynthesis model (Baldocchi et al., 1994), and the Medlyn stomatal optimisation model (Medlyn et al., 2011) were incorporated into FORCAsT.

Estimates of leaf-level emissions and gas exchange in each layer of the canopy are scaled by leaf area index over each crown space model level and summed over the full crown space to obtain canopy-scale estimates. These can then be compared with measured GPP, latent heat and isoprene fluxes at the top of the canopy.

2.3.2 JULES land surface model

The Joint UK Land Environment Simulator (JULES) model is the land surface component of the UK Met Office (UKMO) Unified Model (UM). It is the successor to the Met Office Surface Exchange Scheme (MOSES) land surface scheme (Cox et al., 1999; Essery et al., 2003), incorporating the dynamic vegetation model TRIFFID. JULES is a community process-based model that simulates the fluxes of carbon, water, energy and momentum between the land surface and the atmosphere (Best et al., 2011; Clark et al., 2011). In addition to being applied as part of the UM, it can be used offline for simulation of gas exchange at the global, regional and point scale. Leaf level photosynthesis in JULES is modelled using the C3 and C4 photosynthesis models of Collatz et al. (1991; 1992) respectively. Stomatal conductance is then calculated from the photosynthesis rate following the formulations of Jacobs (1994).

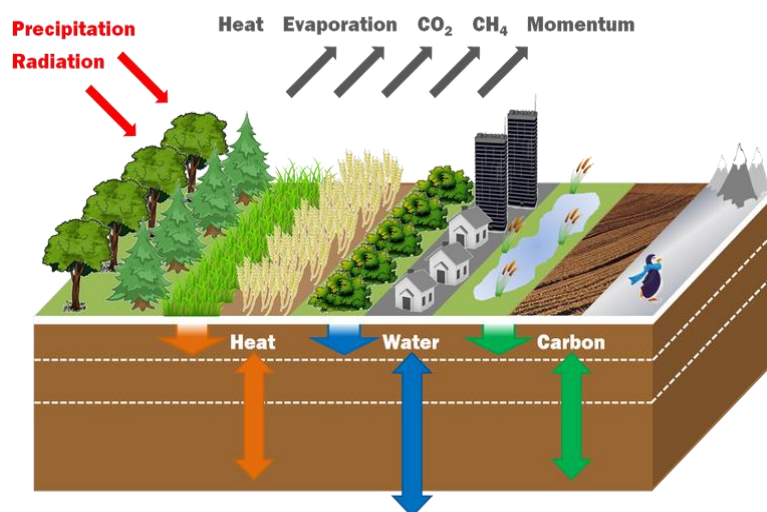


Figure 2.5: A schematic showing the different processes and surface types included in the JULES model (Source: <https://jules.jchmr.org/content/about> last accessed 23/04/2021).

Isoprene emissions in JULES are estimated using gross primary productivity (GPP), leaf internal carbon and leaf temperature as a proxy for the electron requirement for isoprene synthesis while emissions of other BVOCs are based on G95-based temperature-dependent empirical approaches (Pacifico et al., 2011). This scheme has been shown to reproduce

observed diurnal and seasonal variability of isoprene mixing ratios at six broadleaf forest sites with significant correlation between model and observation at 95% confidence level (Pacífico et al., 2011) but the performance is sensitive to the choice of reference emission potential and plant functional type.

JULES can be run as a big-leaf model, in which case leaf level estimates are summed to obtain canopy scale estimates, or as a multi-layer canopy model in which configuration leaf level estimates are scaled by leaf area distributions and summed over all model layers to obtain canopy-scale estimates of plant gas exchange. Here, JULES is used as a big leaf model. JULES does not include parameterisations for chemical production and loss, vertical mixing, or deposition.

2.4 Observations

The performance of LSMs under current and future climate conditions are critically dependent on the availability and quality of observations used to parameterise and evaluate them. Models require detailed observational data such as species-specific physiological parameters, emission factors, and vegetation characteristics such as leaf area distribution which may be obtained through in-situ observations, laboratory and chamber experiments, and remote sensing retrievals. Measurement campaigns, open-top chamber (OTC) experiments, and Free-Air Carbon dioxide Enrichment (FACE) experiments have all been employed as part of efforts to better understand biosphere-atmosphere interactions and have been the main source of data used in parameterising and evaluating LSMs. Here, we describe the techniques used in acquiring these observations and the available datasets that are relevant to this thesis.

2.4.1 Flux observations and data

Measurements of the exchanges of carbon, water and energy between the land surface and the atmosphere at the ecosystem level have been conducted at flux sites across the globe using eddy covariance techniques (Aubinet et al., 2012) over the past two decades. These measurements provide ecosystem-scale data on CO₂, water vapour, and energy fluxes. Additionally, meteorological data like air temperature and pressure, wind speed and direction, and precipitation are routinely measured at these sites. Soil water content and vegetation characteristics like leaf area index are also monitored at some sites. Together,

these datasets provide an invaluable resource for improving our understanding of biosphere-atmosphere interactions (Vuichard and Papale, 2015).

Flux measurement sites in different geographical regions have been organised into networks that allow for data-sharing, comparison of methodologies and cross-site validation; examples include Ameriflux (North and South America), Euroflux (Europe), Asiaflux (Asia). Flux Network (FLUXNET) is a global network of these regional networks which bring together observations from over 500 sites worldwide (Pastorello et al., 2020; Vuichard and Papale, 2015).

With data coming from different sites and using different instruments, there was the need for harmonisation and standardization of the datasets to allow for easy comparison of ecosystem gas exchange (Pastorello et al., 2020; Vuichard and Papale, 2015). The FLUXNET2015 dataset is the latest in a series of efforts to achieve this goal. More than 200 flux sites from around the world contributed flux, meteorological, environmental, and soil data at half-hourly or hourly resolutions to this dataset (Figure 2.6; Pastorello et al., 2020). Contributed data underwent a uniform data quality control process and gaps in meteorological data were filled using downscaled data based on the ERA-Interim global reanalysis data set (Vuichard and Papale, 2015).

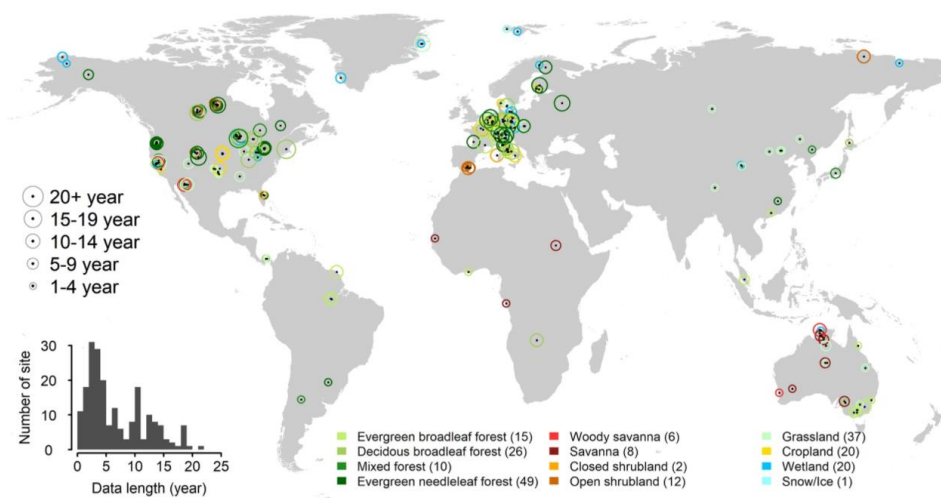


Figure 2.6: A sample of the 212 sites included in the FLUXNET2015 dataset. The size of the circle indicates the length of the data record. The colour of the circles represents the ecosystem type based on the International Geosphere–Biosphere Programme (IGBP) definition. When overlapping, locations are offset slightly to improve readability. Numbers in parentheses indicate the number of sites in each IGBP group. The inset (bar chart) shows the distribution of data record lengths. (Source: Pastorello et al., 2020)

Due to the availability of longer time series and data from different geographical regions, FLUXNET2015 has become the principal dataset for understanding biosphere-atmosphere interactions, especially for the land surface modelling community. These data have already been used in studies focusing on the role of drought stress on latent heat fluxes and GPP (e.g. Harper et al., 2020; Otu-Larbi et al., 2020). North America and Europe have the highest density of flux sites as shown on Figure 2.6. By contrast, the network of flux measurement sites in tropical regions and the Southern Hemisphere is sparse.

2.4.2 Isoprene observations and data

Measurements of plant volatile emissions may be grouped under two broad categories: laboratory and enclosure based, and field campaigns. Laboratory and enclosure measurements are the more common of these as they can easily be monitored and maintained, and the safety of personnel and equipment can be guaranteed. Isoprene measurements ranging in duration from a few days to several weeks have been made in such settings (e.g. Brillì et al., 2007; Harley et al., 1994; Pegoraro et al., 2004, 2007; Sharkey and Loreto, 1993). These have greatly enhanced understanding of how isoprene emissions vary under different environmental conditions.

Numerous field campaigns have been conducted to measure BVOCs in various ecosystems and locations in recent decades from ground level using soil chamber techniques (e.g. Bourtsoukidis et al., 2018) up to the top of the boundary layer and above using tethered balloons and aircrafts (e.g. Crutzen et al., 1985; Ganzeveld et al., 2008). Data from these campaigns have enabled the development of models currently used in simulating canopy exchange processes (e.g. GABRIEL campaign: Ganzeveld et al., 2008). They have also helped to improve our understanding of the role BVOCs play in atmospheric chemistry (e.g. INTEX-A: Stavrou et al., 2010) and aerosol cloud interactions (e.g. HIPPO: Wofsy, 2011). In addition to these short campaigns, a few FLUXNET sites also measure BVOCs routinely e.g. Hyytiälä (Hari and Kulmala, 2005) or periodically e.g. Castelporziano (Fares et al., 2019 and references therein) and Harvard Forest (McKinney et al., 2011).

Intensive field campaigns are typically of short duration due to the costs involved as well as logistical constraints in remote regions, and as result long-term field measurements of BVOCs are rare. This was especially true for isoprene measurements in drought stressed ecosystems until recently. Campaigns at MOFLUX site during the summer of 2011 and 2012 (Potosnak et al., 2014; Seco et al., 2015) and Wytham Woods during the summer of 2018

and 2019 (WISDOM campaign: Ferracci et al., 2020) have provided continuous datasets of isoprene, meteorology, and soil data at times when each forest experienced prolonged heatwave and drought conditions. MOFLUX measurements were made using proton transfer reaction quadrupole mass spectrometer (PTR-Quad-MS; Karl et al., 2001) while an iDirac (Bolas et al., 2020) was used in the WISDOM campaign. The PTR has been extensively described elsewhere but a brief description of the iDirac is provided here as its development and deployment at Wytham were pivotal in guiding the direction of this thesis.

The iDirac is a portable gas chromatograph equipped with a photoionisation detector (GC-PID). It allows for isoprene in an air sample to be separated on chromatographic columns and then sequentially detected by the PID. It has four inlets for gas sampling with a detection limit of ~38 ppt and an instrument precision of $\pm 10\%$ (Bolas et al., 2020). This allows for measurements at 4 different heights in the canopy at temporal resolution of ~15 minutes. The iDirac has been designed as a low power, low gas consumption device that can be deployed autonomously making it suitable for long-term measurements of isoprene in remote locations. It has previously been tested in laboratory evaluations, and in a tropical forest in Sabah, Malaysia, (Bolas et al., 2020), and its deployment during the WISDOM campaign at Wytham Woods (Ferracci et al., 2020).

This thesis aims to understand the role of drought and ozone stress in regulating plant BVOC emissions, productivity, and gas exchange. The work presented here also investigates how these stress factors affect biosphere-atmosphere exchange of trace gases within forest ecosystems through model experiments designed to test how isoprene emissions and plant productivity respond to drought stress and ozone damage. This chapter has provided an overview of biosphere-atmosphere interactions and some of the more relevant feedbacks that occur in this coupled system. It has also highlighted the impacts of drought, thermal and ozone stress on isoprene emissions and plant gas exchange, and how they are currently parameterised in land surface models. The observational datasets and models used in understanding these processes have also been introduced in this chapter. The next four chapters describe model development and application studies that combine model experiments and long-term observations to test the responses of isoprene emissions and mixing ratios as well as plant gas exchange to these stressors.

These model studies are underpinned by long-term observations of CO₂ and water vapour fluxes, and isoprene fluxes and mixing ratios from 7 forest sites (Figure 2.7) covering a range of climate zones and plant functional types (PFTs). These sites are described in detail in Chapters 3-6, but namely they are: (1) an oak-dominated temperate mixed deciduous

forest, Wytham Woods, located in Oxford, UK; (2) a Mediterranean flux measurement site, in the Castelporziano Estate, Rome, Italy which is dominated by evergreen Holm Oak; (3) a Boreal coniferous forest at Hyytiälä, Finland which is dominated by Scots pine; (4) Blodgett Forest, a Mediterranean evergreen Ponderosa pine forest located in California, USA; (5) Harvard Forest, a temperate mixed deciduous woodland located in the northeast USA which is dominated by red oak; (6) an oak-hickory mixed broadleaf deciduous forest located in central Missouri, USA; (7) Santarém-Km67-Primary Forest, a tropical evergreen broadleaf forest situated within the Tapajós National Forest in the Brazilian Amazon, comprising a wide range of tree species of various ages.

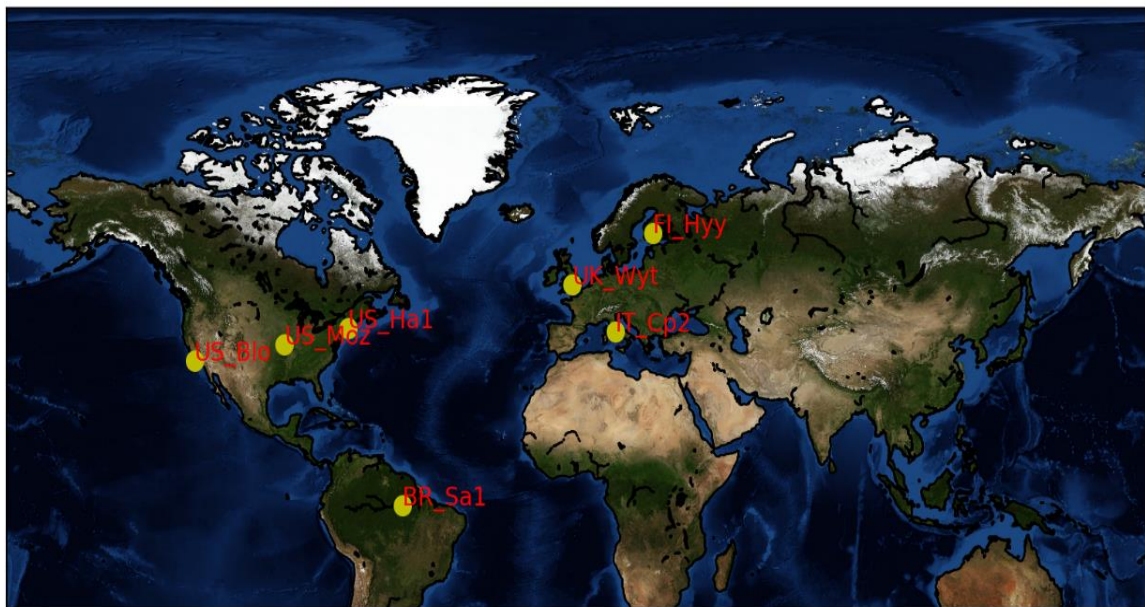


Figure 2.7: Locations of forest sites used for model development and evaluation in this thesis

Chapter 3: Modelling the effect of the 2018 summer heatwave and drought on isoprene emissions in a UK woodland

Isoprene is considered the most important biogenic volatile organic compound due to the amount that is emitted by vegetation and its role in atmospheric chemistry and climate. Although drought stress is an important factor in regulating isoprene emission rates, the exact effect remains uncertain. Increasing and decreasing emission rates have both been previously reported in response to drought stress (e.g. Brilli et al., 2007; Pegoraro et al., 2004; Potosnak et al., 2014). This uncertainty makes it difficult to properly parameterise the impact of drought stress in current emissions model leading to failure of models to reproduce observed isoprene emission rates and fluxes (Jiang et al., 2019; Potosnak et al., 2014) with implications for global climate and air quality monitoring. The effect of soil rewetting after drought stress on emissions and hence atmospheric mixing ratios is another source of uncertainty in emissions modelling.

Long term isoprene and meteorological measurements made during a heatwave and drought event in the summer of 2018 in a UK woodland are used to test the ability of current emissions models to reproduce observed isoprene mixing ratios during a prolonged heatwave and drought (Ferracci et al., 2020). Through a series of modelling experiments, the roles of leaf temperature, soil moisture stress, and soil rewetting in stimulating isoprene emissions was explored. We show that a combination of leaf temperature stimulation due to a decrease in soil moisture and soil rewetting emission bursts were responsible for a 400% increase in isoprene mixing ratios observed during the heatwave drought period. By accounting for the effect of drought stress and soil re-wetting, we improve model-observation fit, overcoming an initial 40% model underestimation of isoprene mixing ratios during the heatwave and drought period.

This work has been published in Global Change Biology, 26(4) on 13 December 2019 (citation: Otu-Larbi et al., 2020; <https://doi.org/10.1111/gcb.14963>). The authors and their contributions are listed below

Frederick Otu-Larbi: Devised research methodology and conducted model simulations. Processed FORCAST output and observations and performed model-observation comparisons and analysis. Compiled manuscript.

Conor G. Bolas: Processed and supplied meteorological and isoprene data for model simulations. Participated in research design and manuscript preparation.

Valerio Ferracci: Processed and supplied meteorological and isoprene data for model simulations. Participated in research design and manuscript preparation.

Zosia Staniaszek: Processed and supplied meteorological and isoprene data for model simulations. Participated in research design and manuscript preparation.

Roderic L. Jones: Participated in research design and manuscript preparation.

Yadvinder Malhi: Participated in research design and manuscript preparation.

Neil R.P. Harris: Supplied isoprene data for model simulations. Participated in research design and manuscript preparation.

Oliver Wild: Devised research methodology and model simulations. Participated in interpretation of results, manuscript preparation.

Kirsti Ashworth: Devised research methodology and model simulations. Performed model-observation comparisons and results analysis. Participated in manuscript preparation.

Abstract

Projected future climatic extremes such as heatwaves and droughts are expected to have major impacts on emissions and concentrations of biogenic volatile organic compounds (BVOCs) with potential implications for air quality, climate and human health. While the effects of changing temperature and photosynthetically active radiation (PAR) on the synthesis and emission of isoprene, the most abundant of these BVOCs, are well known, the role of other environmental factors such as soil moisture stress are not fully understood and are therefore poorly represented in land surface models. As part of the Wytham Isoprene iDirac Oak Tree Measurements campaign, continuous measurements of isoprene mixing ratio were made throughout the summer of 2018 in Wytham Woods, a mixed deciduous woodland in southern England. During this time, the United Kingdom experienced a prolonged heatwave and drought, and isoprene mixing ratios were observed to increase by more than 400% at Wytham Woods under these conditions. We applied the state-of-the-art FORest Canopy-Atmosphere Transfer canopy exchange model to investigate the processes leading to these elevated concentrations. We found that although current isoprene emissions algorithms reproduced observed mixing ratios in the canopy before and after the heatwave, the model underestimated observations by ~40% during the heatwave–drought period implying that models may substantially underestimate the release of isoprene to the atmosphere in future cases of mild or moderate drought. Stress-induced emissions of isoprene based on leaf temperature and soil water content (SWC) were incorporated into current emissions algorithms leading to significant improvements in model output. A combination of SWC, leaf temperature and rewetting emission bursts provided the best model-measurement fit with a 50% improvement compared to the baseline model. Our results highlight the need for more long-term ecosystem-scale observations to enable improved model representation of atmosphere–biosphere interactions in a changing global climate.

3.1 Introduction

The biogenic volatile organic compound (BVOC), isoprene (C₅H₈), has important impacts on atmospheric composition and chemistry due to its relative abundance and high reactivity (e.g. Fuentes et al., 2000; Laothawornkitkul et al., 2009). Chemical reactions involving isoprene lead to the production of secondary pollutants, for example, ozone (O₃) and secondary organic aerosol (SOA), which are also short-lived climate forcers. Isoprene also indirectly affects climate by reducing the oxidative capacity of the atmosphere, hence enhancing the atmospheric lifetime of climate active gases such as methane (CH₄; see e.g. Pike and Young, 2009). Increased isoprene emissions could potentially lead to up to a 50% change in surface ozone concentrations (Pike and Young, 2009) but the sign of change depends on geographical location and atmospheric composition, in particular on the concentrations of the oxides of nitrogen (NO_x = NO + NO₂). The large quantities of isoprene emitted into the atmosphere make it a major source of SOA, although aerosol yield from isoprene depends on a number of factors including levels of organic aerosol loading and NO_x concentrations (Carlton et al., 2009). SOA has an indirect impact on climate through changing cloud optical properties (Carslaw et al., 2010; Unger, 2014). Isoprene and other BVOCs have been estimated to have a net negative radiative forcing which offsets the positive radiative forcing of anthropogenic volatile organic compounds (Unger, 2014). Isoprene could therefore play an important role in future climates through its regulation of atmospheric chemistry and formation of secondary pollutants, although its overall climate impact is minor compared to greenhouse gases such as CO₂, and remains uncertain (Arneeth et al., 2010).

More than 90% of global isoprene is emitted by terrestrial vegetation (Guenther et al., 2006) at a rate primarily dependent on vegetation type (with forests contributing ~80% of global annual emissions) but also on environmental conditions such as temperature, solar radiation, atmospheric CO₂ concentration and soil moisture (Guenther et al., 2006 and references therein; Laothawornkitkul et al., 2009). Several hypotheses have been proposed to explain why some plants synthesize and emit isoprene, the best supported being that it prevents cellular damage caused by heat and oxidative stress (e.g. Sharkey, 2000; Vickers et al., 2009). Hence, emissions increase under high temperature and insolation.

During periods of water stress, however, physiological processes such as stomatal conductance, photosynthesis rate and respiration are reduced, resulting in a decrease in plant productivity (Keenan et al., 2010). Isoprene emissions are closely coupled with

photosynthesis and so reductions in plant photosynthetic capacity as a result of water stress would be expected to lead to a decrease in isoprene emissions by reducing the supply of carbon available for its synthesis. Indeed, studies have observed decreases in isoprene emission rates of between 40% and 60% under severe drought conditions (e.g. Brillì et al., 2007; Brüggemann and Schnitzler, 2002; Lerdau and Keller, 1997; Pegoraro et al., 2004).

However, an increase in emissions under drought has also been reported (Brillì et al., 2007; Loreto and Schnitzler, 2010; Rennenberg et al., 2006; Sharkey and Loreto, 1993) suggesting that water stress can decouple isoprene emission from photosynthesis, possibly because isoprene emissions are unaffected by decreasing stomatal conductance (Centritto et al., 2011; Pegoraro et al., 2004; Tingey et al., 1981). Experiments using ^{13}C labelling have shown that isoprene can be produced from older pools of stored carbon when photosynthetic gas exchange is reduced by drought (e.g. Brillì et al., 2007).

The net impact of soil water stress on isoprene emissions remains uncertain due to these competing effects. It is likely that the apparently contradictory responses observed in laboratory experiments are due to differences in the severity of the applied drought and the tolerance of different plant species to water stress, with severe drought, in which the soil water content (SWC) falls below the permanent wilting point, leading to a decline in isoprene emissions and mild-to-moderate drought having either no impact or leading to an increase. Niinemets (2010) developed a conceptual model in which the initial increase in leaf temperature that occurs as stomata close in response to a decline in soil moisture stimulates isoprene synthesis and emissions, leading to the observed decoupling of emissions from gas exchange rates. Evidence for this model was later provided by Potosnak et al. (2014) who observed this behaviour at the onset of a prolonged drought in the Ozarks, an oak-dominated mid-latitude forest.

An additional complexity is the response of isoprene emission rates to rewetting. Sharkey and Loreto (1993) and Penuelas et al. (2009) observed a substantial increase in isoprene emissions from seedlings after rewetting but this effect has not been observed in all experiments. Pegoraro et al. (2004) reported a lag of about a week between declining soil moisture and changes in isoprene emission rates most likely the result of plants having to adjust to the restoration of the photosynthetic carbon source for isoprene synthesis and emission.

The effect of temperature and solar radiation on isoprene emissions are relatively well understood and emissions estimates from land surface models have been shown to

capture observed diurnal variations in fluxes and concentrations reasonably effectively across a range of ecosystems (e.g. Guenther et al., 2012; Zimmer et al., 2000). Unlike temperature and solar radiation, there is no direct impact of soil water deficit and soil rewetting on isoprene emissions and these are therefore not well represented in coupled land surface-atmosphere models although numerous studies have shown their importance to emission rates and atmospheric composition (e.g. Emmerson et al., 2019; Guenther et al., 2006; Jiang et al., 2018; Sindelarova et al., 2014).

Rising levels of CO₂ and future changes in climate, such as increasing temperature and altered patterns of precipitation, can thus be expected to change isoprene emissions from the current estimated 450–600 Tg C/year (Arneth et al., 2008; Guenther et al., 2006, 2012). Heald et al. (2009) projected increases of as much as ~190 Tg C/year in global isoprene emissions due to a temperature increase of 2.3°C by 2100 but also showed that a decrease in isoprene emissions due to increasing CO₂ concentrations could off-set this temperature effect almost entirely.

Most studies to understand the effect of combined heatwaves and drought on isoprene emissions have been laboratory-based experiments which permit close control of environmental factors such as temperature, photosynthetically active radiation (PAR) and soil moisture but make use of saplings (e.g. Brillì et al., 2007), seedlings or young plants (e.g. Pegoraro et al., 2005) and are thus not representative of real-world forest environments. There are limited observations of isoprene emissions during drought in natural ecosystems (e.g. Emmerson et al., 2019; Potosnak et al., 2014; Seco et al., 2015) which are necessary to enable the development of robust parameterizations in emission models.

In the summer of 2018, the United Kingdom (UK), in common with most of northern and central Europe, experienced a prolonged drought and heatwave event. The UK Met Office officially declared heatwave conditions starting on June 22 which persisted to August 8 in southern England. Records from the UK Met Office show that the 2018 summer mean temperature over the UK as a whole was ~2.0°C above the 1961–1990 average, making the summer of 2018 the joint warmest on record (Regional Values, 2019). The mean temperature over southern England was 17.7°C, ~2.4°C warmer than the 1961–1990 average.

Under future climate scenarios, droughts and heatwaves that are currently thought of as anomalous (such as the one that occurred in 2018) are expected to increase in frequency (IPCC, 2013; Thornton et al., 2014) with the UK Met Office predicting that the UK may experience such conditions every other year by 2050 (e.g. UK Extreme Events—Heatwaves, 2019). Given the role of isoprene and other BVOCs in the formation of short-

lived climate forcers and SOAs, the potential impacts of these changes in climate on isoprene emission rates and therefore on atmospheric composition, air quality and climate (Pacífico et al., 2009; Sanderson et al., 2003) must be better understood.

The combined heatwave and drought (heatwave–drought) and rewetting episodes, which occurred during the Wytham Isoprene iDirac Oak Tree Measurements (WIsDOM) campaign in Wytham Woods in 2018, offered a unique opportunity to quantify the potential effect of future climate change on isoprene emissions in a natural environment. This study uses a state-of-the-art canopy model to explore the observed effects of heat and drought stress, and soil rewetting on isoprene emissions and mixing ratios in a temperate mixed deciduous woodland.

3.2 Materials and Methods

3.2.1 Site description

The WIsDOM campaign took place at Wytham Woods (51°46'23.3"N 1°20'19.0"W, 160 m a.s.l.), located ~5 km NW of the centre of Oxford in SW England, between May and October 2018. The forest has been owned and maintained by the University of Oxford as a site of special scientific interest since 1942 and has been part of the UK Environmental Change Network (ECN) since 1992. The forested area is made up of patches of ancient semi-natural woodland, secondary woodland, and modern plantations and is dominated by European Ash (*Fraxinus excelsior*—26%), Sycamore (*Acer pseudoplatanus*—18%), European Beech (*Fagus sylvatica*—11%) and English Oak (*Quercus robur*—7%; Kirby et al., 2014). The remainder of the forest comprises other broadleaf trees and shrubs. *Q. robur* (~95%) and *A. pseudoplatanus* (~5%) are the main contributors to the isoprene budget at Wytham Woods (Bolas, 2020). The forest has largely been undisturbed over the last 40–100 years (Morecroft et al., 2008; Thomas et al., 2011) and as a consequence the age range of mature trees in Wytham Woods is large—from 40 to >150 years. The climate in Oxfordshire can be classified as warm temperate with rainfall occurring all year round. The 1981–2010 average summer temperature ranges between 18 and 20°C and average rainfall is ~600–700 mm/year.

3.2.2 Measurement campaign

Continuous measurements of isoprene mixing ratios were made approximately every 20 min at four heights in the forest canopy between June and October 2018 during the

WISDOM campaign. Inlets to two dual-channel iDiracs (see Bolas et al., 2019 for a full description of the instrument design and deployment) were located at 15.55m (top of canopy), 13.17 m (mid-canopy), 7.26 m (trunk height) and 0.53 m (near surface) alongside a mature *Q. robur* of ~16 m height. Measurements at the trunk and near-surface levels did not start until July. The iDirac has a detection limit of ~38 ppt with an instrument precision of $\pm 11\%$ (Bolas et al., 2019).

Hourly measurements of temperature, PAR, relative humidity, soil moisture at a depth of 20 cm, wind speed and direction, and atmospheric pressure were obtained from the Upper Seeds automatic weather station located in a small clearing ~480 m from the site of the isoprene observations. We used 30 min averages of the measurements made between 1 June and 30 September in our model analysis. This covers the full extent of peak growth with roughly equal periods before, during and after the heatwave–drought. For full details of the WISDOM campaign, readers are referred to Ferracci et al. (2020).

3.2.3 Model description

We applied the FORest Canopy-Atmosphere Transfer (FORCAsT) 1D model of biosphere–atmosphere exchange to simulate the processes of biogenic emissions, chemical production and loss, vertical mixing, advection and deposition within and above the canopy at Wytham Woods. A detailed description of the FORCAsT model can be found in Ashworth et al. (2015), so here we focus only on those elements of the model configuration relevant to this study. We subdivided the 40 model levels into 10 between the ground surface and trunk height, and a further 10 within the crown space to ensure that observation heights aligned as closely as possible with the mid-point of a model level.

Vertical transport in FORCAsT is based on a modified k-theory of vertical turbulent diffusion (Blackadar, 1979; Raupach, 1989). In-canopy and above canopy mixing are simulated following Baldocchi (1988) and Gao et al. (1993), respectively. The simulated exchange of heat and trace gases is further improved by constraining the friction velocity (u^*) and the standard deviation of the vertical wind component (σ_w) following Bryan et al. (2012). As u^* and σ_w were not measured at Wytham, we estimated each from the horizontal wind speed (u) following Makar et al. (2017), Equation 3.1, and Shuttleworth and Wallace (1985), Equation 3.2, respectively:

$$u^* = \frac{u \times K}{\ln\left(\frac{h_c}{Z_o}\right)} \quad 3.1$$

$$\sigma_w\left(\frac{z}{h_c}\right) = \begin{cases} 1.25u^* & \text{and for } \frac{z}{h_c} > 1.0 \\ u^* \left[0.75 + 0.5 \times \cos\left(\pi\left(1 - \frac{z}{h_c}\right)\right) \right] & \text{and for } \frac{z}{h_c} < 1.0 \end{cases} \quad 3.2$$

where h_c is the height of top of canopy (18 m), Z_o is the roughness length (assumed $0.1 \cdot h_c$), u is the mean horizontal wind speed at height z and K is von Karman's constant (0.4).

In FORCAsT, isoprene is produced through emissions from foliage in the crown space and lost through oxidation reactions initiated by the OH and NO₃ radicals and O₃, and through deposition to the soil (following Stroud et al., 2005). The concentration of isoprene at each level in the canopy depends on these production and loss processes as well as fluxes into and out of that layer. Previous studies (e.g. Bryan et al., 2012; Guenther et al., 2006 and references therein) have shown that for moderate height canopies such as that at Wytham Woods, canopy residence times are sufficiently short that little isoprene is lost through oxidation within the canopy. Hence, concentrations are primarily dependent on emission rates when considered over periods greater than turbulent timescales (≤ 1 s to min). FORCAsT employs a half-hourly timestep. Our simulations therefore focused on the emissions of isoprene, which are calculated in FORCAsT by summing the contributions from 10 leaf angle classes in each crown-space model level, following the algorithms of Guenther et al. (1995):

$$ER = LAI \cdot \varepsilon \cdot \gamma_{iso} \quad 3.3$$

where ER is the total emission rate ($\text{mg m}^{-2} \text{hr}^{-1}$), LAI (m^2/m^2) is the leaf area index and ε is a site- and species-specific emission factor ($1.20 \text{ mg m}^{-2} \text{hr}^{-1}$ for *Q. robur*; Visakorpi et al., 2018) which represents the emission rate of isoprene into the canopy at standard conditions of 30°C and $1,000 \mu\text{mol m}^{-2} \text{s}^{-1}$. LAI was taken as the maximum reported for the site ($3.6 \text{ m}^2/\text{m}^2$; Herbst et al., 2008) throughout this study which coincides

with the period of peak growth. γ_{iso} is a dimensionless emission activity factor that accounts for changes in emission rates due to deviations from these standard conditions, with:

$$\gamma_{iso} = C_L C_T \quad 3.4$$

where C_L and C_T are the light and temperature dependence of isoprene emission rates respectively and are given by:

$$C_L = \frac{\alpha C_{LI} PAR}{\sqrt{1 + \alpha^2 PAR^2}} \quad 3.5$$

where α (= 0.0027) and C_{LI} (= 1.066) are empirical coefficients from Guenther et al. (1995).

$$C_T = \frac{\exp\left(\frac{C_{T1}(T-T_s)}{RT_s T}\right)}{1 + \exp\left(\frac{C_{T2}(T-T_m)}{RT_s T}\right)} \quad 3.6$$

where T is the leaf temperature (K), T_s is the temperature at standard conditions (i.e. 303 K), R is the ideal gas constant (=8.314 J K⁻¹ mol⁻¹), C_{T1} (=95,000 J/mol), C_{T2} (=230,000 J/mol) and T_m (=314 K) are empirical coefficients determined by Guenther et al. (1995). Leaf temperature is calculated from measured air temperature in FORCAsT using a canopy energy balance.

Equations (3.3) – (3.6) describe the default model set-up (hereafter referred to as BASE). We conducted a series of experiments introducing stress-induced emissions, achieved by further modifying the activity factor to account for extreme temperature and drought conditions. In these experiments, described below, γ_{iso} was calculated as follows:

$$\gamma_{iso} = C_L C_T \gamma_X \quad 3.7$$

where γ_X is an additional environmental activity factor and X denotes the environmental condition affecting isoprene emission rates in each experiment explained in detail below.

3.2.4 Model experiments

3.2.4.1 BASE

FORest Canopy-Atmosphere Transfer was configured using site-specific canopy parameters and isoprene emission factors and driven with meteorology measured at Wytham Woods during the WIsDOM campaign. Isoprene emission rates for each model level were calculated within the model using Equations 3.3-3.6. Comparison of modelled isoprene mixing ratios against observations from the iDirac instruments at four heights within the canopy showed good agreement in both diurnal profile and magnitude before and after the heatwave–drought. However, during the heatwave–drought period, the model substantially underestimated isoprene mixing ratios. The results from this simulation are described in more detail later.

We therefore performed three subsequent experiments, introducing γ_X , to explore the possible environmental factors driving the sharp increase in observed isoprene concentrations that the model was unable to account for using the standard emissions algorithms. In all three experiments, model configuration and driving meteorology remained unchanged from BASE; the only difference was the change to the isoprene activity factor described below.

3.2.4.2 BASE+LFT

During periods of drought stress, there is an increase in leaf temperature due to a reduction in transpiration rate as the plants attempt to conserve water (Zandalinas et al., 2018). Niinemets (2010) and Potosnak et al. (2014) hypothesized that this increase in leaf temperature is the cause of observed increases in isoprene emissions during mild-to-moderate drought stress. Here we test whether increases in leaf temperature explain the observed changes in isoprene mixing ratios observed during WisDOM by modifying γ_X against leaf temperature (hereafter referred to as LFT) with γ_{LFT} defined as follows:

$$\gamma_{LFT} = \begin{cases} 1 & T < T_{95} \\ \frac{T - T_S}{T_{95} - T_S} & T \geq T_{95} \end{cases} \quad 3.8$$

where T (K) is the leaf temperature, T_S (297 K) represents the standard conditions for leaf temperature (Guenther et al., 2006) and T_{95} is the 95th percentile of the seasonal leaf temperature which represents the threshold temperature above which we assume heat-induced emissions occur.

3.2.4.3 BASE+SWT

Under heatwave–drought conditions, it would be expected that reduced SWC and unusually high temperatures affect emissions rates simultaneously. This experiment therefore combines the effect of soil water deficit and leaf temperature on isoprene emissions into a single environmental activity factor, γ_{SWT} calculated as follows:

$$\gamma_{SWT} = \begin{cases} 1 & \text{for } \theta > \theta_c \\ \left[\frac{(\theta - \theta_w)}{\theta_c - \theta_w} \right]^{(-q)} \times [\gamma_{LFT}] & \text{for } \theta_w < \theta \leq \theta_c \end{cases} \quad 3.9^*$$

where θ (m³/m³) is the volumetric soil moisture, θ_w is the wilting point (0.15 m³/m³ following Jiang et al., 2018), θ_c (0.22 m³/m³) is a critical soil moisture content above which we observe no effect of water stress on isoprene emissions and q is a site-specific empirical factor describing the non-linearity of the effects of soil water stress on tree physiological processes. A range of q values have been tested for different plant functional types (e.g. see Egea, Verhoef, and Vidale, 2011). Here a value of 0.40 provided the best fit to observations. γ_{LFT} is defined in Equation 3.8.

**there was an error in the published version of equation 3.9 which has been corrected here.*

3.2.4.4 BASE+RWT

This experiment investigates whether the burst of isoprene emissions observed following rewetting after drought in laboratory studies is seen at the ecosystem scale. The environmental activity factor, γ_{RWT} , is a modification of Equation 3.9 such that during periods defined as rewetting (days within the heatwave–drought period for which SWC exceeds that of the previous 10 days), γ_{RWT} is given by:

$$\gamma_{RWT} = \gamma_{SWT} \times 1.30 \quad 3.10$$

that is, a 30% increase in isoprene emissions following soil rewetting.

3.3 Results

Here we present a comparison of continuous measurements of isoprene mixing ratios at all four iDirac inlet levels against the output from the nearest model level. For the top and middle of the canopy, we use half-hourly averages of both modelled and observed data covering the period June 1 to September 30 for this comparison; measurements are only available for the trunk and near-surface levels between July 6 and September 30. Statistical values reported in this section were restricted to isoprene mixing ratios between 0600 LT and 1900 LT coinciding with daylight hours when isoprene emissions occur, in keeping with previous studies (e.g. Potosnak et al., 2014; Seco et al., 2015). The data are presented in full as time series, and then summarized to show goodness of fit using scatter plots and a Taylor diagram (Taylor, 2001). The Taylor diagram provides a way to demonstrate the simultaneous variation of three model performance statistics: correlation coefficient (r^2), normalized standard deviation (SD) and centred root-mean-square error (RMSE). Output from an ideal model would show the same r^2 , SD and RMSE as the observations. Therefore, the closer a model's summary statistics are to that of the observations on the Taylor diagram, the better its performance. Results are first presented for the BASE simulation (i.e. the default model set-up) and then for each experiment. Model performance statistics for the top of the canopy is presented here while those for the other levels can be found in the Supplementary Information. The grey shaded region on all figures indicates the heatwave–drought period as defined by the UK Met Office for southern England and the dashed white line the start of rewetting.

3.3.1 Meteorological conditions

Figure 3.1a-c shows PAR, temperature, volumetric SWC and precipitation measured at the ECN station in Wytham Woods for the study period. Following a wet April in which rainfall was ~120% of the 1981–2010 mean (Monthly, seasonal and annual summaries 2018, 2019), SWC declined steadily from near field capacity (at $0.46 \text{ m}^3/\text{m}^3$) at the start of June to $0.16 \text{ m}^3/\text{m}^3$ (just above the wilting point of $0.15 \text{ m}^3/\text{m}^3$ for this site) at the peak of the heatwave–drought in July. A few low-intensity rainfall events (total precipitation $<0.2 \text{ mm}$) with negligible effect on SWC were recorded prior to the heatwave–drought. Rainfall during the heatwave–drought, on July 20 (3 mm) and July 27 (11.1 mm), led to increases in soil moisture and the ‘rewetting period’ extended from 20 July to 8 August as a result. The Standardized Precipitation Index (McKee et al., 1993), used to characterize the

severity of meteorological droughts, indicates Wytham Woods experienced a moderate drought in July (<https://eip.ceh.ac.uk/apps/droughts/>), consistent with in-situ SWC measurements. After 8 August (the official end of the heatwave period), rainfall frequency and intensity increased with a corresponding increase in soil moisture.

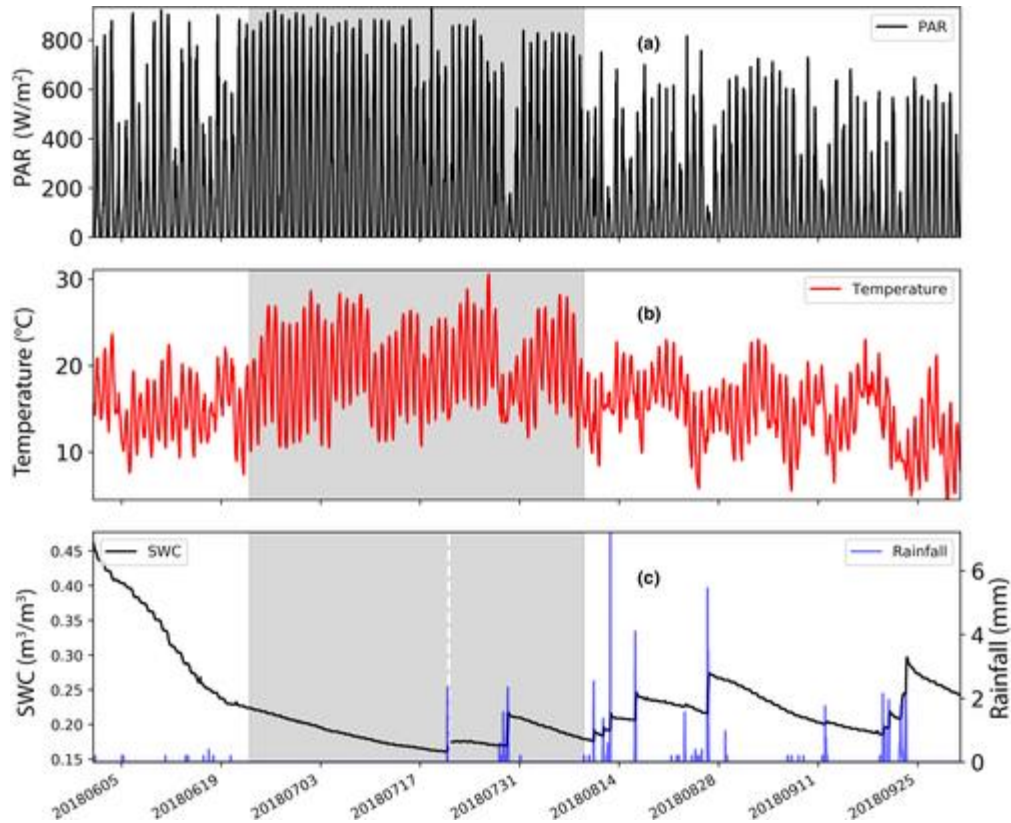


Figure 3.1: Meteorological data taken from the Wytham Woods Automatic Environmental Change Network station: (a) Photosynthetically active radiation (PAR), (b) 2 m air temperature, (c) soil water content (SWC; black) and total daily rainfall (blue). The grey shaded area indicates the start and end of the heatwave–drought while the white dashed line indicates the start of the rewetting period (20 July–8 August)

The average temperature recorded at Wytham Woods was $17.5^{\circ}C$ for the entire measurement period (1 June–30 September), but $19.6^{\circ}C$ during the heatwave (22 June–8 August). The diurnal temperature ranged from an average of $11.8^{\circ}C$ at night to $21.3^{\circ}C$ during the day for the whole season but increased sharply during the heatwave, with mean night-time and daytime temperatures of 13.5 and $25.2^{\circ}C$, respectively. For the same June to September period, climatological (1993–2015) temperature averaged $15.8^{\circ}C$ with a diurnal range of 10.2 – $18.9^{\circ}C$. Compared to the long-term average, the 2018 summer at Wytham Woods was $1.7^{\circ}C$ warmer mainly due to a $3.0^{\circ}C$ increase in temperature during the heatwave–drought. The maximum temperature recorded at Wytham Woods during the 2018 heatwave–drought ($30.6^{\circ}C$) was, however, lower than the climatological maximum

(32.2°C). Average PAR increased from 781 W/m² before the heatwave–drought to 1,277 W/m² during it, reflecting longer and more intense periods of sunshine associated with the underlying high-pressure conditions of the heatwave period.

3.3.2 Base model simulation

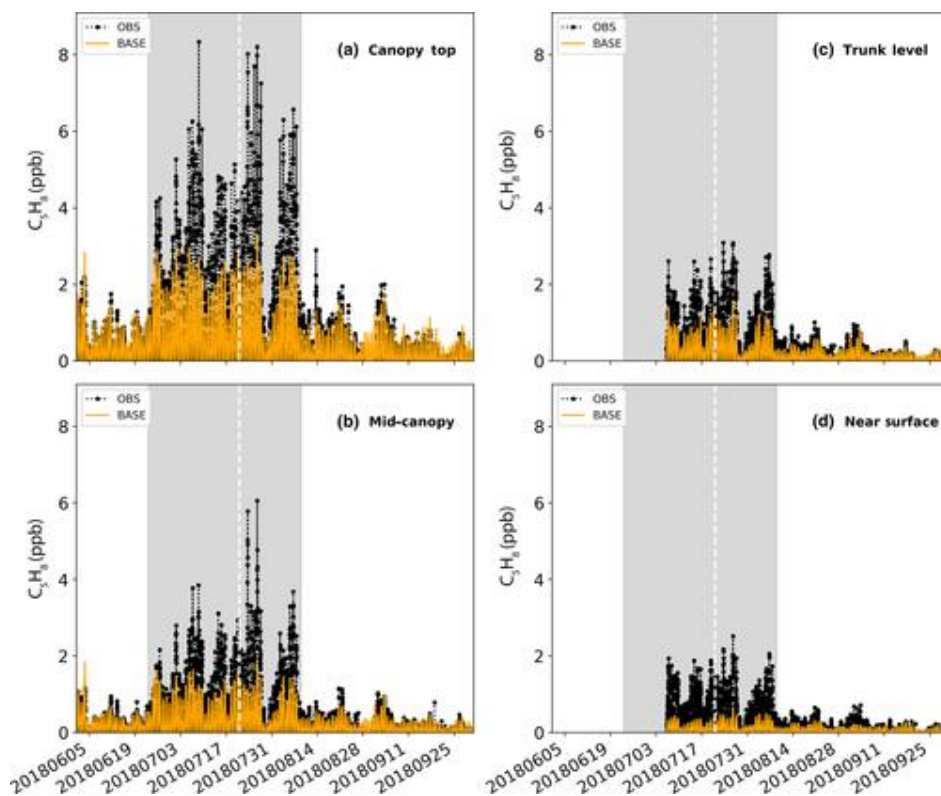


Figure 3.2: Observed (black) and modelled (BASE; orange) isoprene mixing ratios at the WIsDOM site at (a) the top of the canopy (~15.6 m), (b) mid canopy (~13.5 m), (c) trunk height (~7.1 m) and (d) near the surface (~0.8 m). Observations of isoprene mixing ratios at the trunk and near-surface levels started on 6 July

As isoprene emission rates are predominantly determined by light and temperature, BASE reliably reproduces the diurnal cycle of isoprene concentrations at each of the inlet levels (Figure 3.2a-d). Average modelled mixing ratios outside of the heatwave–drought are in good agreement with those observed (0.44 ppb vs. 0.37 ppb at the top of the canopy, 0.24 ppb vs. 0.18 ppb at mid-canopy level, 0.17 ppb vs. 0.15 ppb at trunk level and 0.09 ppb vs. 0.11 ppb near the surface), with no apparent systematic bias, suggesting that the emission factor, ϵ , is appropriate for the site. However, FORCAsT underestimates concentrations at all levels during the heatwave–drought by an average of 40% leading to a total underestimation of ~25% over the entire season. During the heatwave–drought, the average

isoprene mixing ratio measured at the top of the canopy was 1.97 ppb (i.e. >4 times that outside the heatwave period) but only 1.12 ppb in BASE. Similar results were obtained at the other levels for model versus observations (1.01 ppb vs. 0.60 ppb at mid-canopy level, 0.84 ppb vs. 0.49 ppb at trunk level and 0.58 ppb vs. 0.15 ppb near the surface). Following the two rewetting episodes in July, average observed isoprene mixing ratios increased to 2.05 ppb, while modelled isoprene was nearly a factor of 2 lower at 1.12 ppb for that period. There was a 48%, 44% and 70% underestimation in the model at the mid-canopy, trunk and near-surface levels, respectively, following the rewetting events. These systematic discrepancies show that the emission burst observed following rewetting is unaccounted for in current emissions algorithms.

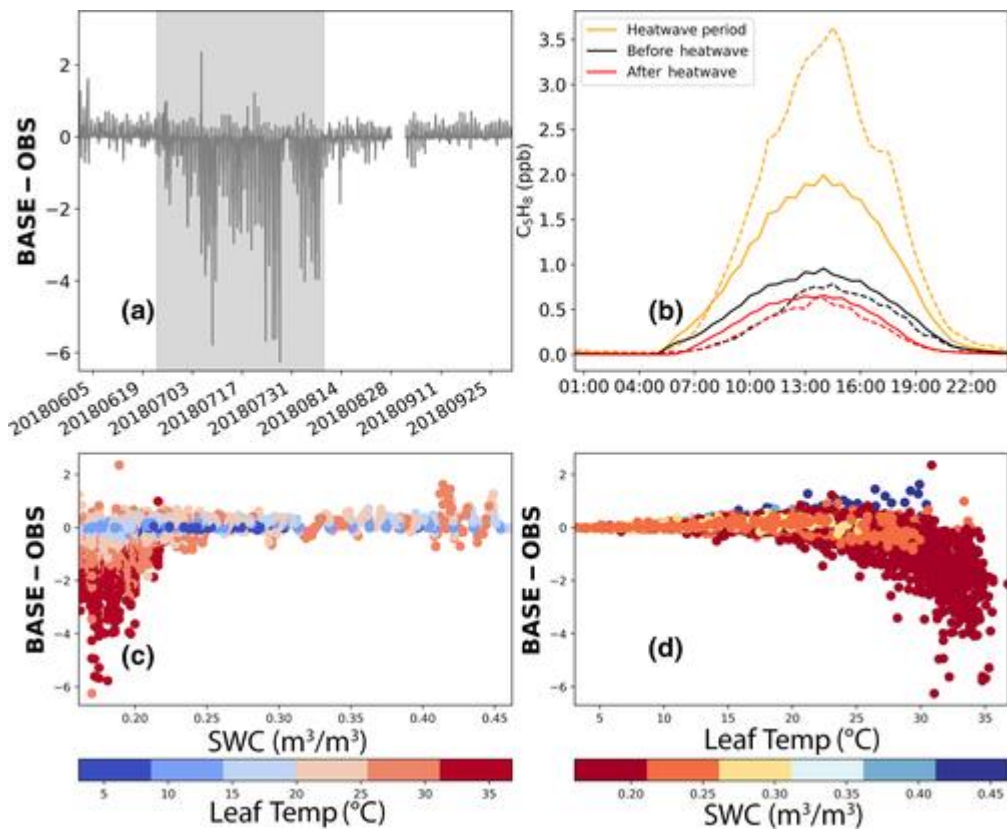


Figure 3.3: (a) Difference (in ppb) between model (BASE) and observed (OBS) isoprene mixing ratio at the top of the canopy for the BASE simulation for the entire season (1 June–30 September 2018). Note that negative values indicate periods when the model underestimates concentrations while positive values indicate an overestimation. (b) Diurnal profiles of isoprene mixing ratios at the top of the canopy before heatwave–drought (black), during the heatwave–drought (orange) and after the heatwave–drought (red). Model values are solid lines while observed values are dashed lines. Scatter plots of difference in mixing ratio versus (c) soil water content (SWC) coloured by temperature and (d) leaf temperature coloured by SWC

The time series of the difference between modelled and observed isoprene mixing ratios at the top of the canopy for BASE (Figure 3.3a) highlights the relatively poor skill of the standard emissions algorithms throughout the 7 week heatwave–drought (shaded region). The average diurnal profiles of isoprene mixing ratios before, during and after the heatwave–drought presented in Figure 3.3b further confirm the good performance of BASE before and after the heatwave and the substantial underestimation during the heatwave. Figure 3.3c,d, explores the relationship between these differences and the possible environmental drivers: SWC and temperature. Figure 3.3c points to a soil moisture threshold with isoprene mixing ratios (and therefore emissions) independent of SWC above $\sim 0.22 \text{ m}^3/\text{m}^3$ but increasing rapidly as SWC drops further. This is in keeping with the concept of a critical SWC used in modelling both photosynthesis and isoprene emissions in previous work (e.g. Emmerson et al., 2019; Guenther et al., 2006; Keenan et al., 2010), although we see an increase rather than decrease as SWC declines below this threshold, similar to that reported under moderate drought stress by Potosnak et al. (2014). Figure 3.3d suggests a similar but less pronounced response to high temperatures ($>20^\circ\text{C}$). We found no significant relationship between PAR and the difference between modelled and measured isoprene mixing ratios and conclude that high temperature and low SWC are the key drivers of the apparent stress-induced enhancement in isoprene emissions.

3.3.3 Results of modelling experiments

Figure 3.2 and Figure 3.3 show clearly that BASE underestimated isoprene concentrations during the heatwave–drought and at other times when isoprene levels in the canopy were high. In this section, we present the results of our model experiments exploring the addition of stress-induced emissions and compare them to the performance of BASE over the entire season. As for BASE, model performance statistics are similar for all levels for each experiment. We therefore present only statistics for top of the canopy here; statistics for the other levels are given in Table 3.1 in the Supplementary Information.

3.3.3.1 BASE+LFT

Modifying the isoprene activity factor when leaf temperature exceeds the 95th percentile (γ_{LFT}) reduces the net underestimation during the heatwave–drought but, as shown in Figure 3.4a,e, FORCAsT still substantially underestimates observed mixing ratios throughout this period. The average modelled isoprene mixing ratio is 1.26 ppb during the

heatwave–drought (~35% lower than observed) and 0.76 ppb (25% too low) over the entire season. This tendency towards underestimation can be seen clearly in Figure 3.5b,f (most of the points lie below the 1:1 line) as can the improvement over the performance of BASE (shown in Figure 3.5a,e). Figure 3.6 further confirms that the use of a temperature-induced enhancement (γ_{LFT}) in isoprene emissions improves the overall fit to measurements. The RMSE of modelled mixing ratio is reduced (from 0.60 in BASE to 0.57 in BASE+LFT), reflecting a slightly improved accuracy during the heatwave–drought. The normalized standard deviation (0.61 in BASE vs. 0.66 in BASE+LFT) indicates that the model is also better able to reproduce the variability seen in the observed concentrations although still tending to underestimate. It should be noted that the correlation between modelled and observed isoprene is very good (>0.9) for all simulations as the strong dependency of isoprene emissions on temperature and PAR is well captured by the standard emissions algorithms (Equations 3.3–3.6) included in BASE. Figure 3.6 shows that although BASE+LFT improves model reproduction of isoprene mixing ratios, it is still unable to account for the high concentrations during the heatwave–drought and suggests that other factors are responsible for the increase in isoprene concentration during this period.

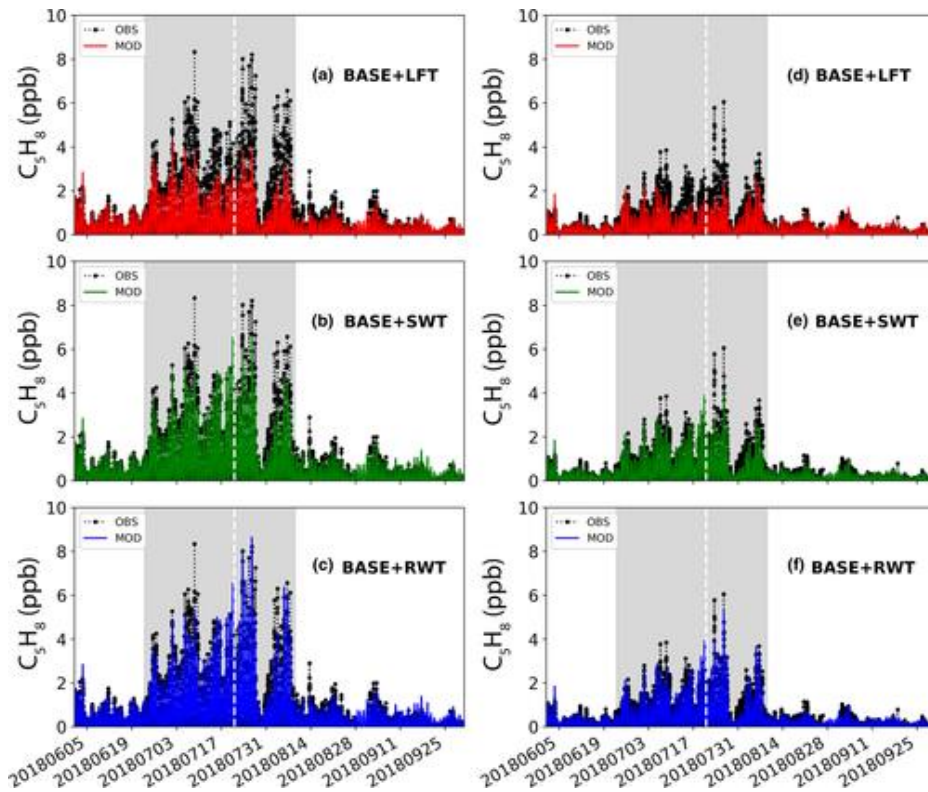


Figure 3.4: Observed (OBS) and modelled (MOD) isoprene mixing ratios at the top (15.6 m; a–c) and middle (13.5 m; d–f) of the canopy. Observations are shown in black and model results in red (BASE+LFT), green (BASE+SWT) and blue (BASE+RWT). Figure 3.9 in the Supplementary Information shows similar results for the trunk and near-surface levels

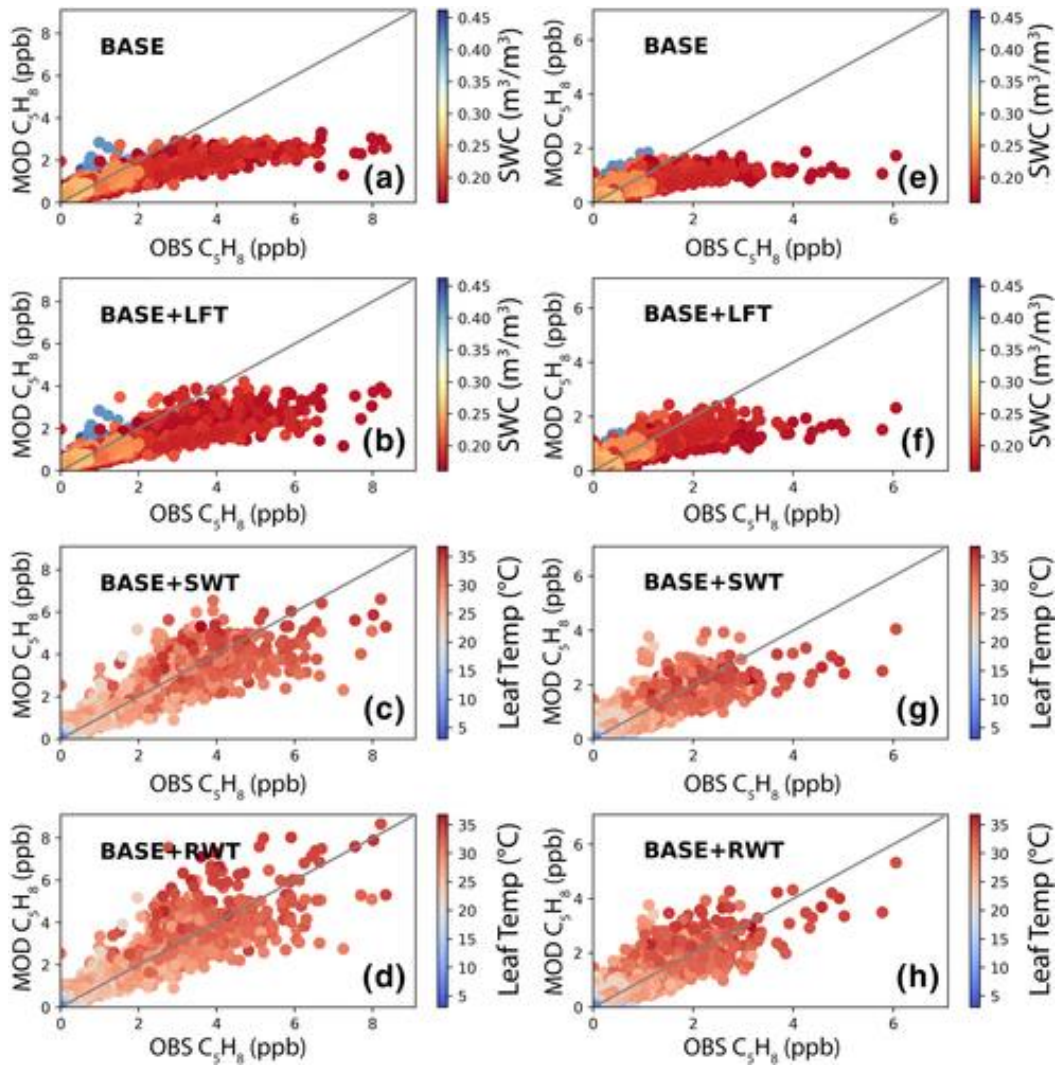


Figure 3.5: Scatter plots of model (MOD) and observed (OBS) isoprene (C_5H_8) mixing ratios for (a and e) BASE coloured by SWC, (b and f) BASE+LFT coloured by SWC, (c and g) BASE+SWT coloured by temperature, (d and h) BASE+RWT coloured by temperature. Panels (a–d) show the top of the canopy (15.6 m) and panels (e–h) the middle of the canopy (13.5 m). Figure 3.10 in the Supplementary Information reproduces these scatter plots for the trunk and near-surface levels.

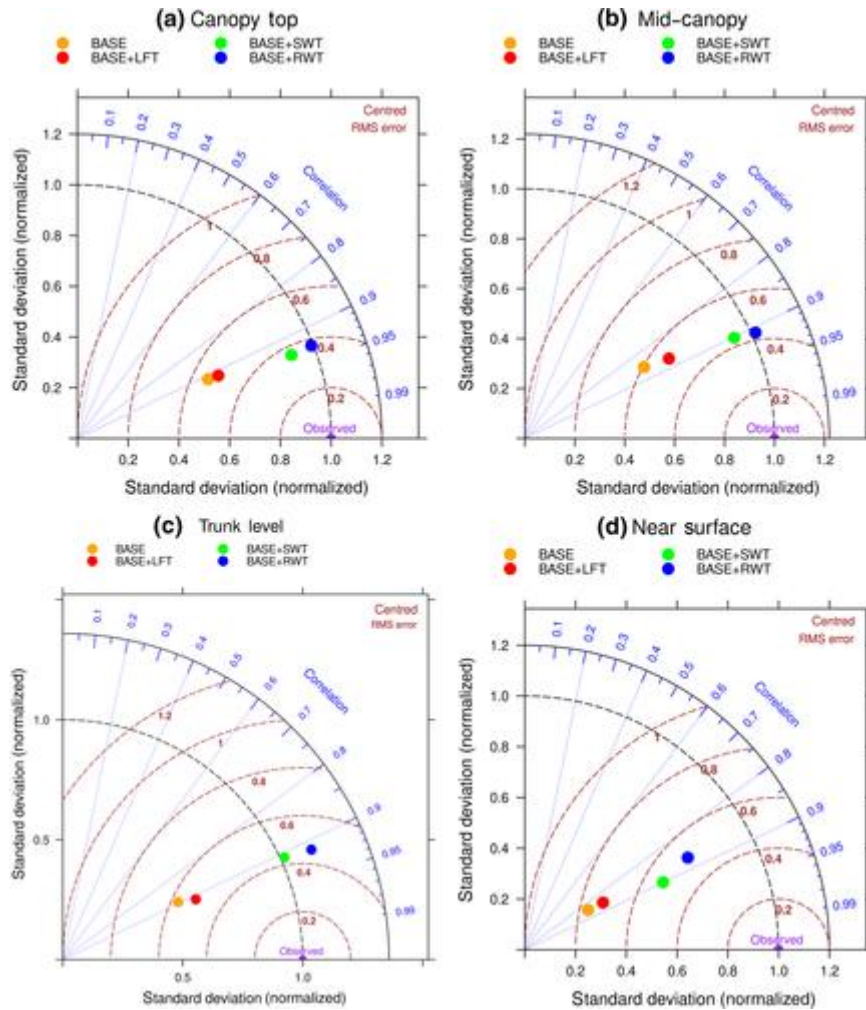


Figure 3.6: Taylor diagram showing model output statistics from the four simulations for (a) top of canopy (15.6 m), (b) middle of canopy (13.5 m), (c) trunk level (7.1 m) and (d) near surface (0.8 m). Dashed black and brown curves and solid blue lines show normalized standard deviation, centred root mean squared error (RMS error) and correlation coefficients, respectively, against observations. The observed isoprene mixing ratios are summarized by the purple circle with a normalized standard deviation of 1.0, RMS error of 0.0 and correlation of 1.0. The summary statistics for the four model simulations are shown by orange (BASE), red (BASE+LFT), green (BASE+SWT) and blue (BASE+RWT) circles. Note the change in scale of standard deviation on panel (c)

3.3.3.2 BASE+SWT

This experiment accounted for the simultaneous effect of heat and water stress. As shown in Figure 3.4b,e, there is a clear improvement in the model's estimation of isoprene mixing ratios during the heatwave–drought period compared to both BASE and BASE+LFT and this is further confirmed by Figure 3.5c,g, in which most points lie along or close to the 1:1 line. Figure 3.5c,g, also shows that BASE+SWT consistently underestimates when observed mixing ratios are high (>5 and >3 ppb at the top and middle of the canopy,

respectively). The mean modelled isoprene mixing ratio at the top of the canopy is 1.87 ppb, just ~5% lower than the observed value of 1.97 ppb. There are no periods of consistent model bias, rather FORCAsT underestimates isoprene concentrations periodically through the heatwave period, resulting in the standard deviation <1.0 in Figure 3.6. Referring to Figure 3.1b, it can be seen that these periods of underestimation correspond to rewetting periods following rainfall events. The average modelled mixing ratio during the rewetting period was 1.73 ppb compared to the observed value of 2.05 ppb. This constitutes ~15% underestimation compared to observed values but ~35% increase (improvement) over the 1.12 and 1.11 ppb estimated in BASE and BASE+LFT, respectively.

3.3.3.3 BASE+RWT

The final experiment included an additional 30% enhancement of the environmental activity factor following soil rewetting (γ_{RWT}) and, as shown in Figure 3.4c,f, further improves the model performance during the heatwave–drought. Mean isoprene mixing ratios during this period increase from 1.87 ppb in BASE+SWT to 1.98 ppb in BASE+RWT, equal to the average of observed values. Figure 3.5d,h indicates no systematic model bias and the use of a rewetting-enhanced soil moisture activity factor enables the model to capture the higher observed concentrations following rewetting episodes which all previous simulations failed to reproduce. The average isoprene mixing ratio during these rewetting periods is 1.98 ppb compared to 2.05 ppb in the observations, that is, an underestimation of only ~3%. The overall model performance statistics are depicted in Figure 3.6. While there is no significant difference between the overall correlation and RMSE values in BASE+SWT and BASE+RWT, there is a clear improvement in the model's ability to match the variability shown by the observations with a normalized standard deviation of 0.97 in BASE+RWT compared to 0.89 in BASE+SWT. Compared to BASE, there is ~80% and ~50% improvement in *SD* (0.97 in BASE+RWT vs. 0.61 in BASE) and RMSE (0.41 in BASE+RWT vs. 0.60 in BASE), respectively.

3.3.4 Time series of results

Figure 3.7 shows the isoprene mixing ratios for the period July 22–27 2018, selected as it falls within the heatwave–drought and includes the first of the rainfall events. These plots provide further evidence that all model configurations reproduce the observed diurnal patterns of isoprene concentrations at Wytham Woods at the top 3 levels, as expected given the strong dependency of isoprene emissions on temperature and PAR but confirm the earlier

results from Figure 3.2 and Figure 3.4 that BASE and BASE+LFT models systematically and substantially underestimate isoprene mixing ratios during this period. All three experiments improve model estimations of isoprene concentrations over BASE especially during the middle of the day when observed concentrations peak. Figure 3.7a-d shows clearly the effect of adding a rewetting-induced enhancement in isoprene emissions (Equation 3.10). For 22 July, when the rewetting effect is not active, the BASE+SWT and BASE+RWT lines overlap but they diverge between 23 and 27 July following rewetting. Figure 3.7h shows that all the simulations underestimate observed concentrations near the surface in the early part of the morning (before mid-day), which we ascribe to more light reaching the lower levels in the canopy than is currently accounted for in the model. Figure 3.7 confirms that BASE+RWT provides the overall best fit when compared to the observations at all levels.

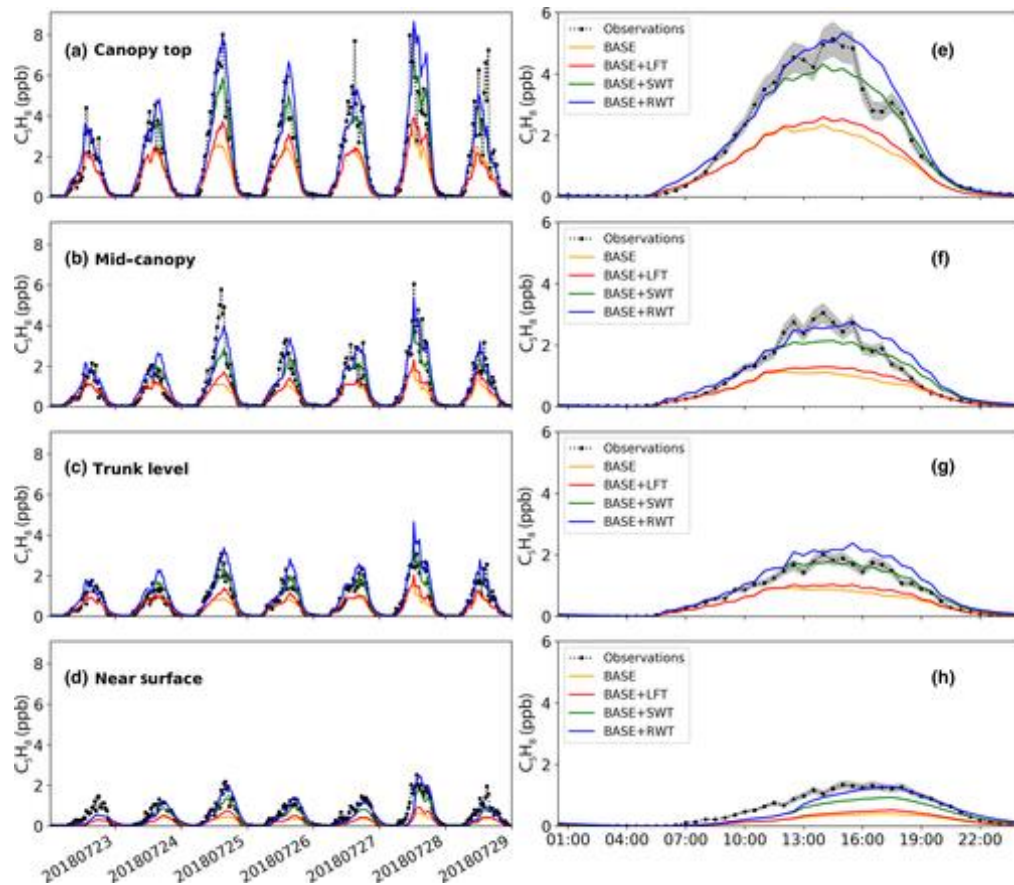


Figure 3.7: (a–d) Time series of isoprene mixing ratios for a selected period during the heatwave–drought (22–27 July 2018) and (e–h) average diurnal profiles of isoprene mixing ratios for the same period. Black dashed lines are observations while the models are coloured orange (BASE), red (BASE+LFT), green (BASE+SWT) and blue (BASE+RWT). The grey shading indicates the uncertainty limits ($\pm 11\%$) around the observations. (a) and (e), (b) and (f), (c) and (g) and (d) and (h) are top of canopy, middle of canopy, trunk and near-surface levels, respectively.

3.4 Discussion

Wytham Woods experienced a heatwave and moderate drought (heatwave–drought) during a 7 week period in the summer of 2018 during which time the soil moisture at the site decreased from $0.46 \text{ m}^3/\text{m}^3$ (just below field capacity) to $0.16 \text{ m}^3/\text{m}^3$ (just above wilting point). Continuous measurements of isoprene mixing ratios were made at the site during the WIsDOM campaign which was conducted in May–October 2018. The aims of our study were to determine how well a 1D canopy exchange model (FORCAsT) could capture the observed changes in isoprene concentrations during the heatwave–drought and to use the model to explore the environmental factors driving these changes. Modelled isoprene mixing ratios did increase substantially during the heatwave–drought in response to large increases in foliage emissions, driven by high temperature and PAR, but not to the extent observed. We conclude that the algorithms currently used in emissions models are unable to account for the actual increase in emission rate under such conditions. We hypothesize that the increase in emission rates during the heatwave–drought was most likely a mechanism to cope with abiotic stress as previously suggested by Holopainen (2004), Loreto and Velikova (2001), Peñuelas and Llusà (2002), Sharkey (1996), and in particular due to low soil moisture.

Many previous studies of the effect of soil water deficit on isoprene emissions have shown a decrease in emission rates with increasing severity of drought (e.g. Pegoraro et al., 2005; Seco et al., 2015) leading to the development of algorithms that decrease the isoprene activity factor (γ_{iso}) in response to decreasing SWC (Guenther et al., 2006). This approach has been used in emission models (e.g. Emmerson et al., 2019; Guenther et al., 2006; Jiang et al., 2018) with good results for severely drought-impacted sites. However, other studies have reported that isoprene emissions are enhanced during periods of mild or moderate drought and Potosnak et al. (2014) demonstrated that the ecosystem-scale response is dependent on drought severity. Some studies have also reported an increase in isoprene after rewetting (e.g. Brillì et al., 2007; Penuelas et al., 2009; Sharkey and Loreto, 1993). The isoprene measurements made during the WIsDOM campaign (Ferracci et al., 2020) together with the findings from our model simulations support the observation that isoprene emissions can increase under moderate drought conditions and after rewetting resulting in strong enhancements in canopy concentrations. Our model results (Figure 3.11) also provide evidence in support of the previous observations that isoprene emissions and photosynthesis

(often quantified as gross primary production, at an ecosystem scale; e.g. Brilli et al., 2007; Pegoraro et al., 2004) are uncoupled during periods of drought stress.

Emissions models have been shown to perform well in both the unstressed and severe drought phases (e.g. Emmerson et al., 2019; Guenther et al., 2012; Jiang et al., 2019) but underestimate observed concentrations during the mild-to-moderate drought phase (Potosnak et al., 2014; Seco et al., 2015). Conceptual models (Niinemets, 2010; Potosnak et al., 2014) have been developed to explain the impacts of mild droughts on isoprene emissions but these have not been tested until now. We hypothesize that drought severity is the main determinant of changes in isoprene emission rates at the ecosystem scale as well as in the laboratory and that the previous field campaigns used to develop and verify the Guenther soil moisture activity factor (see Pegoraro et al., 2004; Seco et al., 2015) encountered soil water deficits that were more severe than those at Wytham Woods in 2018. Indeed, the Ozark site (described in Gu et al., 2006) which has been used in parameterizing the Guenther soil moisture activity factor experienced two consecutive years of drought in 2011 (mild) and 2012 (severe). 2012 experienced the lowest rainfall in that decade and isoprene emissions decreased significantly (Seco et al., 2015). However, similar to Wytham Woods, isoprene fluxes were observed to increase at the Ozarks during the mild phase of the drought in 2011 (Potosnak et al., 2014).

Potosnak et al. (2014) hypothesized that an increase in leaf temperature due to reductions in transpiration during drought stress is responsible for the increase in isoprene emissions as emission rates depend on leaf rather than air temperature. We found that using a leaf temperature-based isoprene emission activity factor did improve model reproduction of observed isoprene mixing ratios, but a substantial underestimation remained. We therefore incorporated a soil moisture activity factor, based on the parameterization of Keenan et al. (2010) for changes in photosynthesis, that increases isoprene emissions under moderate drought conditions, that is, when SWC is close to but slightly above the critical value for the soil at which the standard (severe drought) soil moisture activity factor can be applied. We found that using this new activity factor to account for soil moisture stress when estimating isoprene emission rates improved model reproduction of observed isoprene mixing ratios during the moderate drought without compromising model performance during the rest of the season. However, this was not in itself sufficient to capture the enhancement in isoprene concentrations observed after rainfall events, when soil moisture increased substantially. We found it necessary to further modify our activity factor to account for these episodes, on the hypothesis that these rewetting events were of sufficient intensity to provide near-surface

roots access to water, leading to increased foliar activity and isoprene synthesis. Using this soil water and rewetting-based modifying factor that increased isoprene emission rates, a further 30% improved the model fit to observations by 50% based on the root mean squared error. In comparison, Brilli et al. (2007) observed a 20%–60% increase in isoprene emissions from saplings following soil rewetting. These experimental modelling results provide evidence that previous laboratory-based observations of the effect of mild-to-moderate drought stress and soil rewetting on BVOC emissions (e.g. Brilli et al., 2007; Centritto et al., 2011; Loreto and Schnitzler, 2010; Pegoraro et al., 2004) are also observable at the ecosystem scale.

Many field sites do not routinely measure either soil moisture or leaf temperature; our parameterizations are therefore only appropriate for model frameworks with a detailed land surface module. We performed two further experiments using air temperature and vapour pressure deficit (VPD), both readily available data products, as a proxy for the effects of leaf temperature and SWC. VPD, which can be readily calculated from standard meteorological measurements, increases with increasing temperatures and declining soil moisture. Although VPD is not a physiologically robust metric for assessing soil and foliar water availability, we found that an isoprene emission activity factor based on VPD improved modelled isoprene mixing ratios compared to the base case. Our air temperature and VPD parameterization and results are shown in Equations (3.5) and (3.8), Figure 3.9 - Figure 3.12 and Table 3.1. Although not as successful as the rewetting simulations (e.g. there is a ~10% and ~15% improvement on BASE RMSE in BASE+T and BASE+VPD, respectively, compared to ~50% in BASE+RWT), our results show that VPD in particular could be used to improve simulated emissions at sites where soil moisture or leaf temperature measurements are not available and in models without a detailed land surface parameterization.

The Guenther et al.'s (2006, 2012) algorithms reproduce observed isoprene concentrations or fluxes well in unstressed environments and in cases of severe drought. The methods developed in this paper are intended to be used in cases of mild-to-moderate drought which until now has remained a modelling challenge.

Prior to the summer of 2018, Wytham Woods experienced only infrequent moderate-to-severe droughts (in 1976, 1995–1997 and 2003; Mihók et al., 2009). It is projected that the incidence of droughts in southern England will increase in frequency, duration and severity under future climate change (e.g. Milly et al., 2005; Schär et al., 2004; Vidale et al., 2007). The summer of 2018 could therefore be viewed as a ‘natural experiment’ that

allowed us to investigate possible future biogenic emissions from Wytham Woods and similar temperate mixed woodlands. We found that the emissions algorithms currently included in global emissions and chemistry-climate models underestimated total isoprene emissions during the heatwave–drought by ~40% and by ~20% over the entire June–September period. While the findings of this single experiment should not be extrapolated to a global scale, if these are representative of the wider picture, the magnitude of the modelled change in emissions would have a major impact on local- to regional-scale emissions and hence atmospheric chemistry and composition in many world regions.

The main advantage of our natural experiment is that we were able to observe the impacts on mature trees in a real-world (uncontrolled) environment. Such conditions are impossible to reproduce in laboratory-based experiments that investigate potential impacts of global climate change on tree physiology and BVOC emissions. Saplings and young plants, the preferred options in laboratory experiments, do provide useful information about the general behaviour of trees under various environmental stressors, but cannot replicate the combinatorial stresses and symbioses experienced by mature trees and full ecosystems. The results from WISDOM and previous measurement campaigns carried out on mature trees (e.g. Genard-Zielinski et al., 2018; Llusia et al., 2016; Potosnak et al., 2014) show that emissions characteristics under heatwave–droughts in the natural environment differ from those observed in many laboratory experiments. However, it can be expected for the response to be dependent on tree species, with some adapted to withstand periods of water limitation, and on soil properties. It is clear therefore that more ecosystem-scale observations are required under mild, moderate and severe drought conditions if we are to understand how future changes in precipitation and ground-water levels are to affect isoprene emissions.

3.5 Supplementary Information for chapter 3

This supplementary material presents figures and explains additional experiments that were conducted as part of this study. Figure 3.8 compares leaf temperature estimated using FORCAsT to observed air temperature at Wytham woods. Leaf temperature was an average of 2.1°C above air temperature throughout the summer (JJA) and an average of 2.9°C higher during the heatwave-drought. Figure 3.9 and 3.10 presents observed and modelled isoprene mixing ratios at the trunk and near-surface levels for BASE+LFT, BASE+SWT and BASE+RWT experiments. Figure 3.9 shows a timeseries of mixing ratios while 3.10 presents the data as a scatter plot of observations versus model output. Figures 3.4 and 3.5 in the main paper shows an equivalent plot for the top and mid-canopy levels. Figure 3.11 shows a scatter plot of isoprene and GPP in the unstressed (a) and drought stressed periods (b). GPP was calculated based on Medlyn et al. (2011) and is used here as a proxy for photosynthesis rate. Panel A shows a positive correlation between SWC and GPP. However, as soil moisture is reduced (orange and red circles on panel (a) the relationship appears to break down. This is shown more clearly in panel (b) which focuses on periods of drought conditions only (SWC<0.22) which demonstrates that isoprene concentrations are decoupled from GPP as SWC is reduced.

Sections 3.5.1 and 3.5.2 explores the possibility of using air temperature and VPD instead of leaf temperature and SWC to model isoprene emissions under drought stress conditions. These are intended for use in situations where modelled or measured leaf temperature and SWC are unavailable. These experiments also improve model reproduction of observed isoprene mixing ratios but not to the extent observed when using leaf temperature and SWC. The results from these experiments are presented in section 3.5.3 and in Figures 3.12-3.15. Model output statistics from all experiments conducted in this study are presented in Tables 3.1 -3.4.

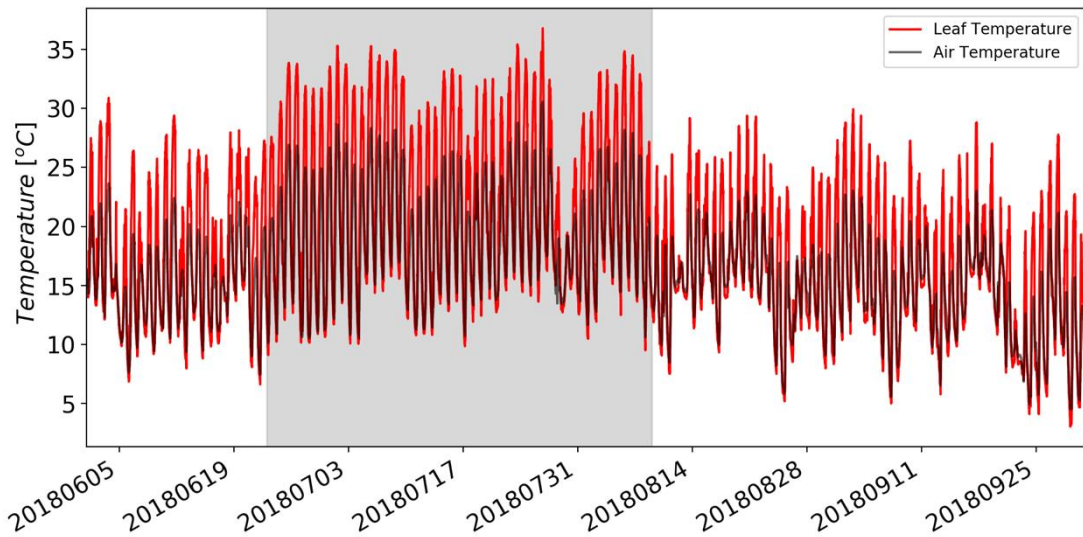


Figure 3.8: Time series of modelled leaf temperature (red) and observed air temperature (black). Shaded region indicates heatwave-drought period. *s*

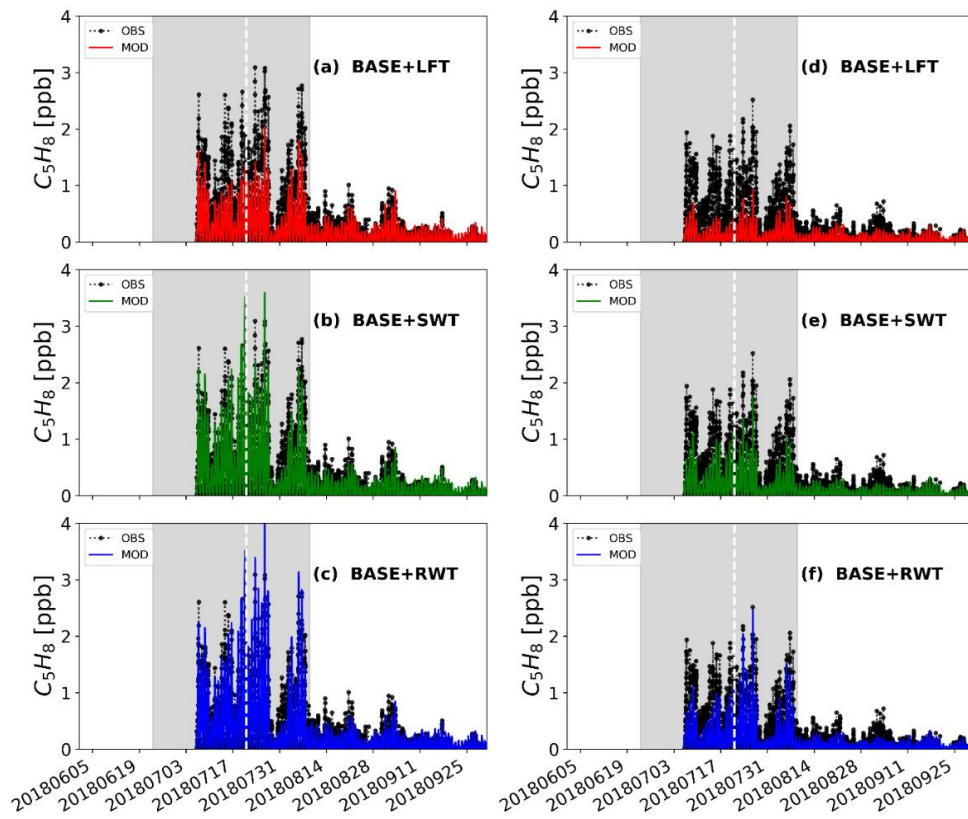


Figure 3.9: Observed (OBS) and modelled (MOD) isoprene mixing ratios at the trunk (a- c) (7.1m) and near surface (d-f) (0.8m) levels. Observations are shown in black and model results are red (BASE+LFT), green (BASE+SWT), and blue (BASE+RWT).

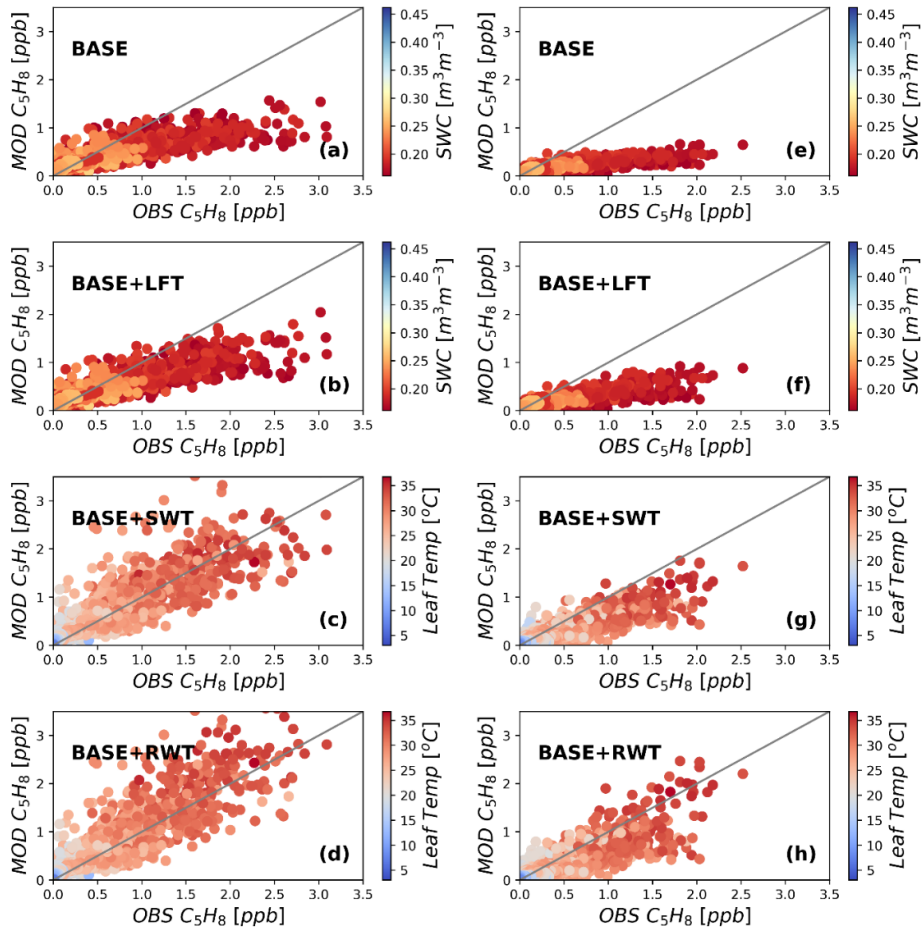


Figure 3.10: Scatter plots of model (MOD) and observed (OBS) isoprene (C_5H_8) mixing ratios for (a, e) BASE coloured by SWC, (b, f) BASE+LFT coloured by SWC, (c, g) BASE+SWT coloured by temperature, (d, h) BASE+RWT coloured by temperature. Panels a-d show the trunk level and panels e-h near surface level.

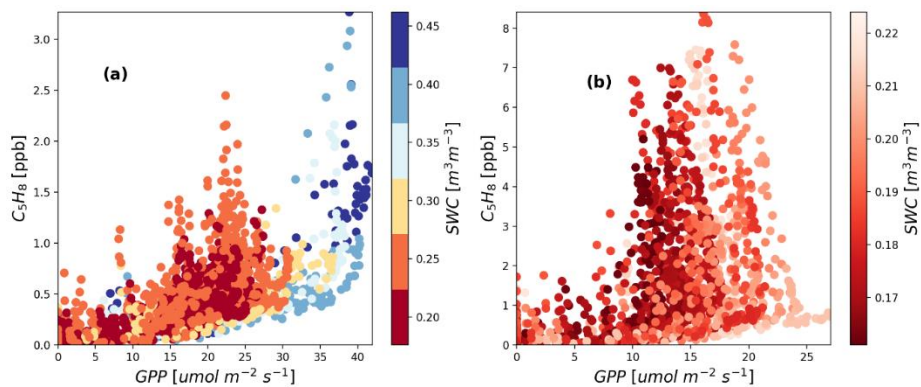


Figure 3.11: Scatter plot of observed isoprene mixing ratio vs GPP coloured by SWC, (a) before and after the heatwave-drought and (b) heatwave-drought.

3.5.1 BASE+T (Air temperature) Experiment

This experiment investigates whether air temperature can be used to model the effect of extreme temperature on isoprene emissions for situations where leaf temperature is unavailable. We define the environmental activity factor γ_T , as:

$$\gamma_T = \begin{cases} 1 & \text{for } T < T_x \\ \frac{(T - T_{mean})}{(T_x - T_{mean})} & \text{for } T \geq T_x \end{cases} \quad 3.11$$

where T ($^{\circ}\text{C}$) is the air temperature, T_{mean} (20.5°C) is the mean summer (JJA) daily maximum temperature at Wytham Woods and T_x (25.5°C) represents the threshold temperature above which a heatwave occurs as defined by the World Meteorological Organisation (WMO): that is five or more consecutive days during which the daily maximum temperature surpasses the average maximum temperature by 5°C or more. This threshold, T_x , ensures that γ_T will only be non-unity, i.e. will only effect isoprene emission rates, during extreme temperature events.

3.5.2 BASE+VPD Experiment

This final experiment explored the use of vapour pressure deficit (VPD) as a proxy to account for the effect of SWC and temperature stress on isoprene emission and concentration. VPD increases with increasing air temperature and declining soil moisture and can be readily calculated from standard meteorological measurements:

$$VPD = (1 - (RH/100)) * SVP \quad 3.12$$

where RH (%) is relative humidity and SVP (kPa) is saturation vapour pressure calculated as:

$$SVP = 0.6108 * 10^{(7.5*T/(237.3+T))} \quad 3.13$$

where T ($^{\circ}\text{C}$) is air temperature

The environmental isoprene activity factor, γ_{VPD} is then:

$$\gamma_{VPD} = \begin{cases} 1 & \text{for } VPD \leq 1 \\ VPD & \text{for } VPD > 1 \end{cases} \quad 3.14$$

3.5.3 Results of BASE+VPD and BASE+T Experiment

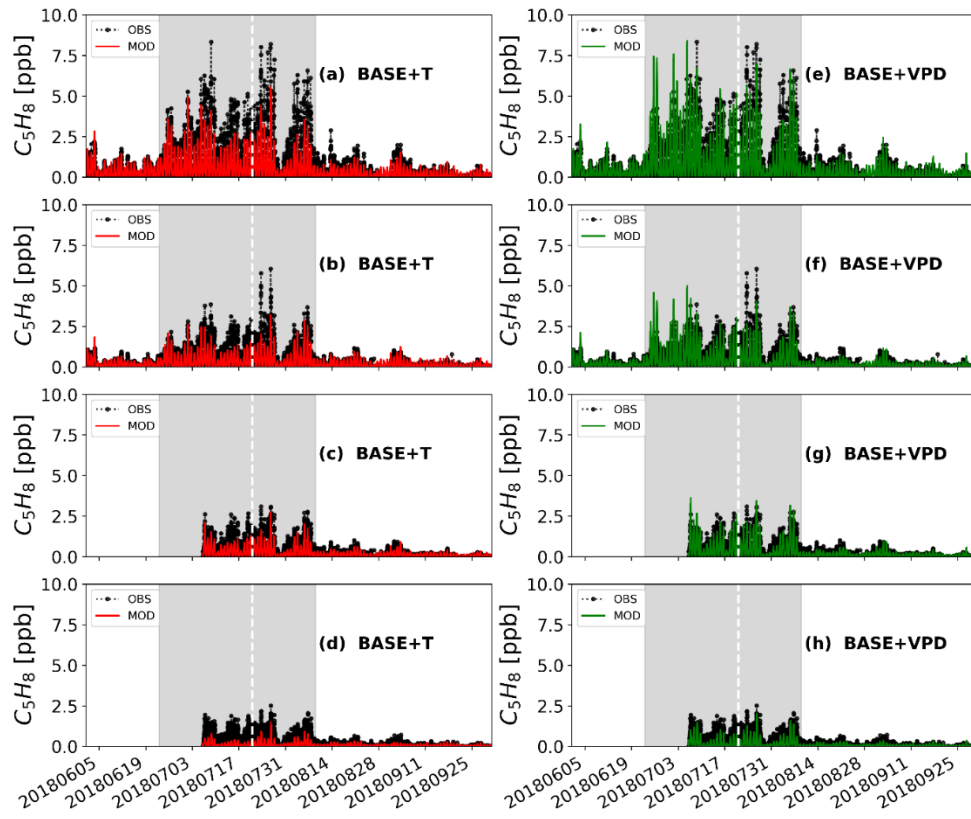


Figure 3.12: Observed (OBS) and modelled (MOD) isoprene mixing ratios at the top (a,e; 15.6 m), middle (b,f; 13.5m), trunk (c,g; 7.1m) and near surface (d,h; 0.8m) levels. (a-d) are results of BASE+T experiment and (e-f) are results of BASE+VPD experiment. Note that observations are shown in black and model results are red (BASE+T) and green (BASE+VPD)

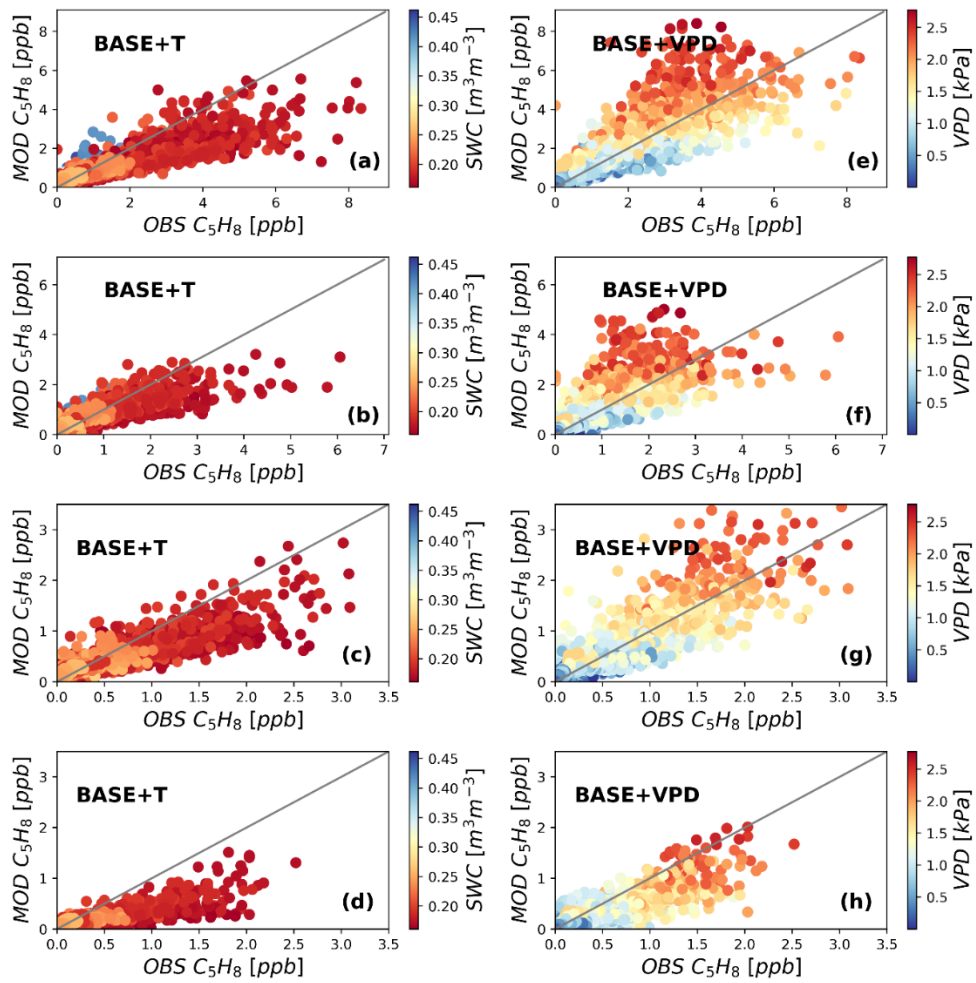


Figure 3.13: Scatter plots of modelled (MOD) vs observed (OBS) isoprene (C_5H_8) mixing ratios for top (a,e 15.6 m), middle (b,f 13.5m), trunk (c,g 7.1m) and near surface (d,h 0.8m) levels. (a-d) show BASE+T coloured by temperature and (e-h) show BASE+VPD coloured by VPD.

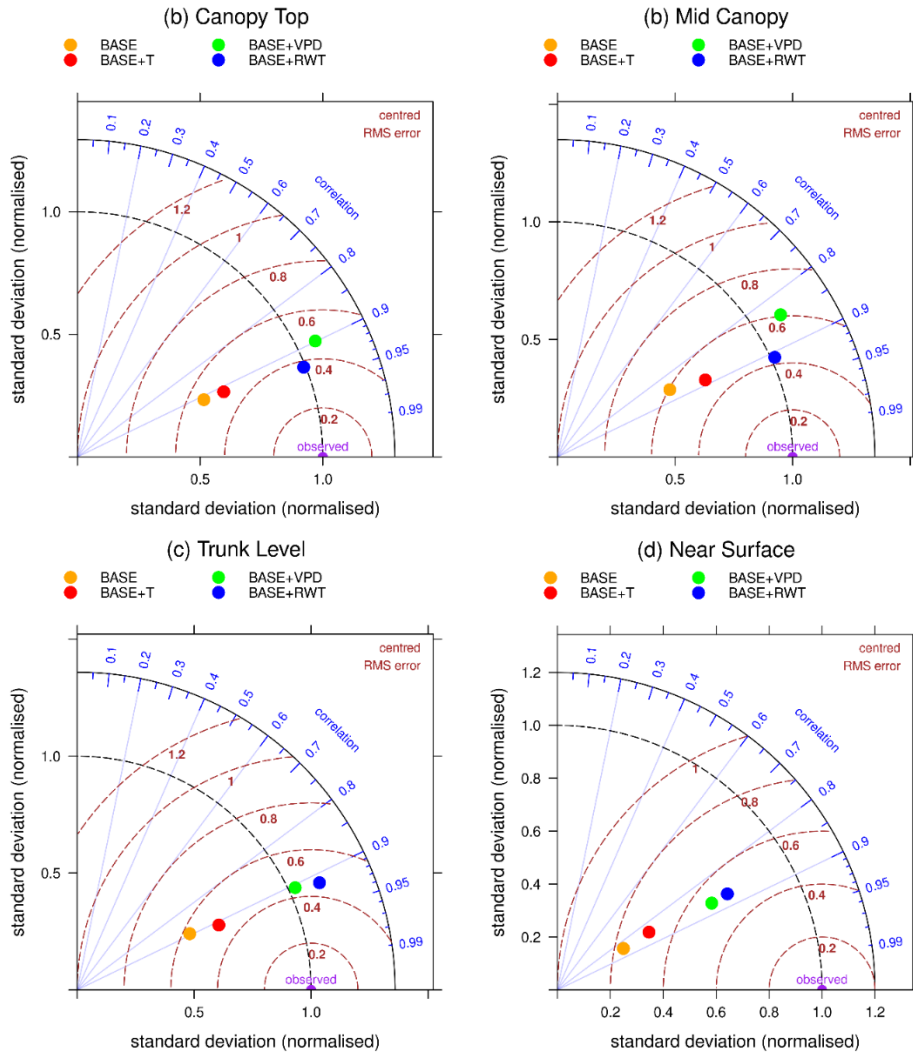


Figure 3.14: Taylor Diagrams showing model output statistics from BASE+T and BASE+VPD simulations for (a) top of canopy, (b) middle of canopy, (c) trunk level and (d) near surface. Dashed black and brown curves and solid blue lines show normalised standard deviation, centred root mean squared error (RMS error) and correlation coefficients respectively against observations. The observed isoprene mixing ratios are summarised by the purple circle with a normalised standard deviation of 1.0, RMS error of 0.0 and correlation of 1.0. The summary statistic for the model simulations are shown by orange (BASE), red (BASE+T), green (BASE+VPD) and blue (BASE+RWT). BASE and BASE+RWT (the experiment giving the best model-observation fit) have been added for ease of comparison. Note the change in scale of standard deviation on panel d.

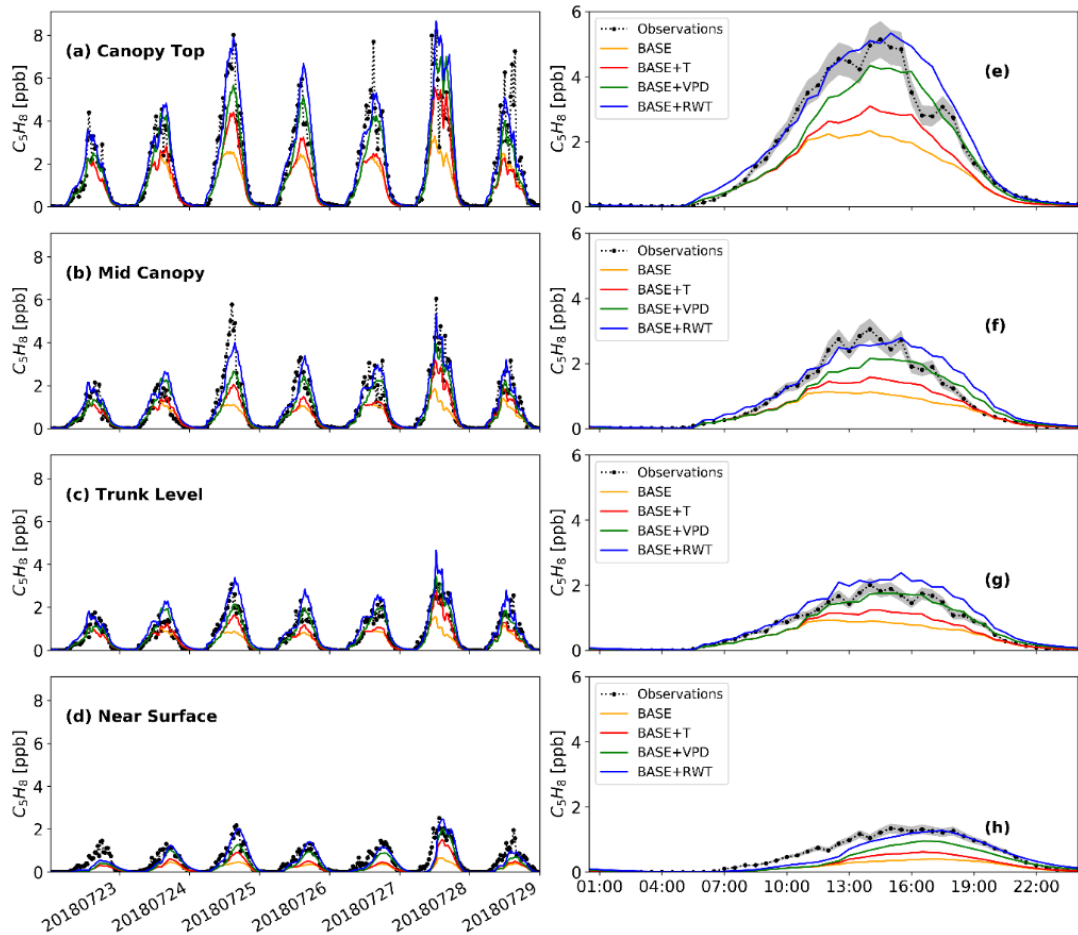


Figure 3.15: (a-d) Time series of isoprene mixing ratios for a selected period during the heatwave-drought (22nd-27th July 2018) and (e-h) average diurnal profiles of isoprene mixing ratios for the same period. Black dashed lines are observations while the models are coloured orange (BASE), red (BASE+T), green (BASE+VPD) and blue (BASE+RWT). Grey shaded area around the observations indicate the uncertainty limits ($\pm 11\%$) within the observations. a and e are top of canopy, b and f are middle of the canopy, c and g are trunk level and d and h are near the surface.

Table 3.1: Isoprene mixing ratios and model performance statistics for observations and model simulations at the top of the canopy (15.6m). Mixing ratios are shown for the entire season (June 1st – September 30th, 2018) and selected periods. Numbers in brackets show the percentage difference between observed and modelled values; negative percentages indicate model underestimation while positive values indicate model overestimation. Model performance statistics are provided for the entire season only.

	Isoprene Mixing Ratios at Canopy Top			Model Performance Statistics		
	Entire Season	Heatwave-Drought	Rewetting Events	R ²	Normalised SD	RMSE
OBS	1.01	1.97	2.05	-	-	-
BASE	0.76 (-25%)	1.22 (-38%)	1.12 (-45%)	0.91	0.56	0.60
BASE+LFT	0.76 (-25%)	1.26 (-36%)	1.11 (-46%)	0.91	0.60	0.57
BASE+SWT	1.03 (+2%)	1.87 (-5%)	1.73 (-16%)	0.93	0.89	0.40
BASE+RWT	1.07 (+6%)	1.98 (1%)	1.98 (-3%)	0.93	0.97	0.41
BASE+T	0.78 (-23%)	1.31 (-34%)	1.19 (-42%)	0.91	0.64	0.54
BASE+VPD	1.08 (+7%)	1.99 (1%)	1.70 (-17%)	0.89	1.06	0.52

Table 3.2: As Table 3.1 for middle of the canopy (13.5m)

	Isoprene Mixing Ratios at Mid Canopy			Model Performance Statistics		
	Entire Season	Heatwave-Drought	Rewetting Events	R ²	Normalised SD	RMSE
OBS	0.51	1.01	1.07	-	-	-
BASE	0.38 (-25%)	0.60 (-41%)	0.56 (-48%)	0.85	0.55	0.35
BASE+LFT	0.45 (-12%)	0.70 (-31%)	0.72 (-33%)	0.87	0.65	0.30
BASE+SWT	0.53 (+4%)	0.97 (-4%)	0.89 (-17%)	0.90	0.91	0.25
BASE+RWT	0.55 (+8%)	1.02 (1%)	1.02 (-5%)	0.91	1.00	0.25
BASE+T	0.46 (-10%)	0.73 (-28%)	0.76 (-29%)	0.89	0.70	0.28
BASE+VPD	0.56 (+10%)	1.03 (+2%)	0.85 (-21%)	0.84	1.11	0.35

Table 3.3: As Table 3.1 for trunk level

	Isoprene Mixing Ratios at Trunk Level			Model Performance Statistics		
	Entire Season	Heatwave-Drought	Rewetting Events	R ²	Normalised SD	RMSE
OBS	0.42	0.84	0.82	-	-	-
BASE	0.32 (-24%)	0.49 (-42%)	0.46 (-44%)	0.89	0.54	0.28
BASE+LFT	0.34 (-19%)	0.54 (-36%)	0.52 (-37%)	0.91	0.61	0.25
BASE+SWT	0.44 (+5%)	0.70 (-17%)	0.73 (-11%)	0.91	0.91	0.21
BASE+RWT	0.46 (+10%)	0.85 (+1%)	0.85 (+4%)	0.91	1.01	0.23
BASE+T	0.35 (-17%)	0.57 (-32%)	0.55 (-33%)	0.91	0.63	0.23
BASE+VPD	0.46 (+10%)	0.85 (+1%)	0.70 (-15%)	0.90	1.12	0.21

Table 3.4: As Table 3.1 for near surface level (0.5m).

	Isoprene Mixing Ratios Near Surface			Model Performance Statistics		
	Entire Season	Heatwave-Drought	Rewetting Events	R ²	Normalised SD	RMSE
OBS	0.29	0.58	0.54	-	-	-
BASE	0.12 (-59%)	0.15 (-74%)	0.16 (-70%)	0.81	0.28	0.30
BASE+LFT	0.13 (-55%)	0.20 (-66%)	0.20 (-63%)	0.87	0.34	0.27
BASE+SWT	0.16 (-45%)	0.28 (-52%)	0.28 (-48%)	0.91	0.53	0.18
BASE+RWT	0.17 (-41%)	0.34 (-41%)	0.34 (-37%)	0.88	0.63	0.18
BASE+T	0.13 (-55%)	0.19 (-67%)	0.22 (-59%)	0.84	0.38	0.27
BASE+VPD	0.17 (-41%)	0.29 (-50%)	0.28 (-48%)	0.87	0.68	0.20

Chapter 4: FORCAsT-gs: Importance of stomatal conductance parameterization to estimated ozone deposition velocity

Plant physiology and adaptation to changing environmental conditions is highly dependent on stomatal aperture (Damour et al., 2010) as it controls water losses and CO₂ uptake for photosynthesis. Modelling of stomatal conductance is of particular importance in models like FORCAsT because it controls key processes like deposition rates which in turn affects atmospheric composition and chemistry within and above forest canopies. Coupled stomatal conductance-photosynthesis (g_s - A_n) models allow for an exploration of biosphere-atmosphere processes such as carbon assimilation by plants and the release of water vapour into the atmosphere. Three of the most widely used of these models are the Jarvis (JV: Jarvis, 1976; UNECE, 2004), Ball-Berry (BB: Ball et al., 1987; Baldocchi, 1994) and Medlyn (MD: Medlyn et al., 2011). Each model has its own underlying assumptions and hence strengths and weaknesses, and data requirements. This chapter presents the results of model development work to incorporate parameterisations of these three g_s - A_n models into the plant physiology module of FORCAsT to estimate photosynthesis rate (net carbon assimilation) and stomatal conductance. Each model's performance is evaluated against observations of gross primary productivity from FLUXNET Mediterranean (US_Blo and IT_Cp2), Boreal (FI_Hyy), Temperate (US_Ha1) and Tropical (BR_Sa1) forest sites. Stomatal conductance simulated by the best and worst performing models at each site are used to estimate ozone deposition rates. The range of these estimates are compared to show the uncertainties in ozone deposition due to stomatal conductance model parameterisation can be as high as 10%

The study has been submitted to Journal of Advances in Modeling Earth Systems (manuscript 2021MS002581) and is undergoing peer review.

Frederick Otu-Larbi: Devised research, performed model simulations with FORCAsT, processed model output and performed model-observation comparison. Interpreted results and compiled manuscript together with co-authors.

Adriano Conte: Supplied and processed model input and evaluation datasets, participated in research conceptualisation and interpretation of results, and helped in compilation of manuscript.

Silvano Fares: Designed and conducted observations, supplied observed data for model parameterisations and evaluation, participated in research conceptualisation and interpretation of results, and helped in compilation of manuscript.

Oliver Wild: Participated in research conceptualisation, interpretation of results and helped in compilation of manuscript.

Kirsti Ashworth: Devised research, provided guidelines on FORCAsT simulations, interpreted results and compiled manuscripts.

Abstract

The role of stomata in regulating photosynthesis and transpiration, and hence governing global biogeochemical cycles and climate, is well-known. Less well-understood, however, is the importance of stomatal control to the exchange of other trace gases between terrestrial vegetation and the atmosphere. Yet these gases determine atmospheric composition, and hence air quality and climate, on scales ranging from local to global, and seconds to decades. Vegetation is a major sink for ground-level ozone via the process of dry deposition and the primary source of many biogenic volatile organic compounds (BVOCs). The rate of dry deposition is largely controlled by the rate of diffusion of a gas through the stomata, and this also governs the emission rate of some key BVOCs. It is critical therefore that canopy-atmosphere exchange models capture the physiological processes controlling stomatal conductance and the transfer of trace gases other than carbon dioxide and water vapour. We incorporate three of the most widely used coupled stomatal conductance-photosynthesis models into the one-dimensional multi-layer FORest Canopy-Atmosphere Transfer (FORCAsT1.0) model to assess the importance of choice of parameterisation on simulated ozone deposition rates. Modelled GPP and stomatal conductance across a broad range of ecosystems differ by up to a factor of 3 between the best and worst performing model configurations. This leads to divergences in seasonal and diel profiles of ozone deposition velocity of 1-30% and deposition rate of up to 10%, demonstrating that the choice of stomatal conductance parameterisation is critical in understanding ozone deposition.

4.1 Introduction

Photosynthesis and transpiration of the world's forests drive the carbon, hydrological and nutrient cycles, governing climate, ecosystem health and productivity, and biodiversity. Forests also serve as a sink for trace gases which are deposited onto plant surfaces and taken up through the stomata. Dry deposition of ozone is of particular importance as it represents a major sink of this tropospheric pollutant. It is also of particular concern because ozone can damage photosynthetic apparatus limiting growth and productivity. The rates of photosynthesis and uptake of ozone are both dependent on the degree of stomatal opening, referred to as stomatal conductance. Plants open and close the stomata to maintain a balance between photosynthesis (CO₂ uptake) and leaf transpiration (water loss), thereby regulating the exchange of CO₂ and water vapour between vegetation and the atmosphere (Hetherington & Woodward, 2003).

Gases and particles deposited on leaf surfaces may be taken up through the stomata or cuticle into the leaf tissue. Stomatal uptake is the dominant of these routes for most reactive trace gases like ozone (Royal Society, 2008). As gases diffuse through the stomata, their concentrations are reduced at the leaf surface, increasing the concentration gradient between the leaf and the atmosphere above it. This concentration gradient drives deposition and has the net effect of increasing the speed at which the gas reaches the plant surface, known as the deposition velocity. The rate of stomatal diffusion and uptake is dependent on both the diffusivity of the gas and the size of the stomata. Deposition velocities are therefore dependent on stomatal conductance: the wider the stomatal aperture the lower the resistance to diffusion through the stomata.

It is critical that models that couple the land surface and the atmosphere are able to accurately reproduce stomatal conductance in order to account fully for the processes driving photosynthesis and trace gas deposition rates. Many empirical and semi-empirical approaches have been developed to simulate stomatal conductance. One of the earliest and most widely used is a multiplicative model (Jarvis, 1976) which reduces stomatal conductance from its potential maximum according to observed responses to changing environmental conditions. Each environmental influence is assumed independent of the others (Damour et al., 2010) and does not consider physiological interactions or feedbacks that could alter stomatal movement (Yu et al., 2004).

Subsequent research demonstrated that stomatal aperture was also directly regulated by current photosynthesis rate (Wong et al., 1979) leading to the development of semi-

empirical coupled models that assume a linear relationship between photosynthesis (A_n) and g_s , and iterate to simultaneously solve for both (e.g. Ball et al., 1987). More recently, optimisation theory has been applied to these coupled photosynthesis-stomatal conductance models to replicate the ‘regulatory’ role of stomata, i.e. that plants control stomatal aperture to maximize carbon gain while minimizing water loss (Medlyn et al., 2011; Cowan and Farquhar, 1977).

The multi-layer canopy-atmosphere model FORCAsT1.0 (FORest Canopy-Atmosphere Transfer) was initially developed as an atmospheric chemistry tool for upscaling leaf-level biogenic emissions to the canopy scale and interpreting measurement data from intensive field campaigns at forest sites (CACHE; Forkel et al., 2006). It has since been modified to better capture observed dynamics and turbulent transport (CACHE; Bryan et al., 2012) and to reflect our improved understanding of the atmospheric chemistry of biogenic volatiles, particularly in low-NO_x environments (FORCAsT1.0; Ashworth et al., 2015). Parameterisations of the response of isoprene emissions to water stress and re-wetting have also been incorporated into the model and demonstrated to improve model reproduction of changes in isoprene concentrations at a temperate deciduous woodland during an extended heatwave-drought (Otu-Larbi et al., 2020a).

FORCAsT1.0 contains explicit representations of canopy structure and leaf distribution to directly calculate photosynthetically active radiation (PAR) extinction through the canopy layers, and hence perform a full canopy energy balance, at every timestep. The resulting vertical temperature gradient drives turbulence and mixing within the canopy, and transport of energy, momentum, and mass across the canopy sub-layer into the atmospheric boundary layer above, but physiology is limited to a simple parameterisation of stomatal conductance (Ashworth et al., 2015). The model has demonstrated considerable skill in reproducing observed concentrations and fluxes of short-lived biogenic reactive trace gases and their products over short time periods at a number of Northern Hemisphere forest sites (Forkel et al., 2006; Bryan et al., 2012; 2015; Ashworth et al., 2015). However, production outweighs loss processes for some gaseous species, suggesting that either deposition rates or vertical transport out of the canopy are too slow, or foliage emissions overestimated. These processes are dependent on the rate of gas exchange through the stomata, and hence the skill of the model in capturing stomatal conductance over time periods from minutes, to hours, to seasons.

Explicit inclusion of physiological processes in FORCAsT1.0 has the additional benefit of enabling model performance to be evaluated against canopy-scale photosynthesis

and transpiration (canopy-top fluxes of CO₂ and water vapour) which are routinely measured and readily available over long time periods across a wide range of ecosystems. This allows a more thorough exploration and constraint of the physical and dynamical processes occurring within the canopy than is possible from concentration and flux measurements of short-lived reactive species made during short intensive field campaigns. Constraining these processes would allow us to focus more closely on the mechanisms of the production and loss of short-lived atmospherically relevant biogenic trace gases.

We incorporate three parameterisations of stomatal conductance and photosynthesis into FORCAsT1.0 to assess:

- 1) the ability of different coupled stomatal conductance-photosynthesis models to reproduce observed CO₂ fluxes across a range of different forest ecosystems and climate regions

- 2) the divergence of simulated ozone deposition velocities and deposition rates due to differences in stomatal conductance modelling approach and parameterisation

We use data from five forest sites within the FLUXNET2015 dataset (Pastorello et al., 2020), the most comprehensive high-quality data available from worldwide flux networks, to evaluate the performance of each of the three stomatal conductance-photosynthesis models. The sites cover three different forest ecosystems classified by IGBP as Evergreen Broadleaf Forests (EBF), Evergreen Needleleaf Forests (ENF) and Deciduous Broadleaf Forests (DBF); and three climate regions: boreal, temperate and tropical, with two of the temperate sites further sub-classified as Mediterranean. Our ultimate goal is to understand and quantify the uncertainties in modelled gross primary productivity and ozone deposition rates due to choice of stomatal conductance model, and model parameters.

4.2 Methods

4.2.1 FORCAsT-gs

The 1-D (vertical column) model, FORest Canopy-Atmosphere Transfer (FORCAsT1.0), was developed to simulate exchanges of reactive biogenic volatiles between a forest site and the atmospheric boundary layer. Previous versions (CACHE: Forkel et al., 2006; Bryan et al, 2012; 2015; and FORCAsT1.0: Ashworth et al., 2015; Otu-Larbi et al., 2020a) have focused on the atmospheric processes governing the concentration and distribution of these volatiles and their oxidation products within and above the canopy. FORCAsT uses 40 vertical levels as a default, 20 of which are in the vegetation canopy space, with the remainder of the levels representing the planetary boundary layer above. The thickness of the layers increases with height, permitting greater resolution in the canopy levels, which are further sub-divided into a trunk space (10 levels) and crown space (10 levels). More details about how vegetation is treated in the model can be found in Ashworth et al. (2015).

Heat and mass fluxes are calculated at each model level by solving the continuity equations, shown here for (gas-phase) mass:

$$\frac{\partial c}{\partial t} = \frac{\partial}{\partial z} \left(K \frac{\partial c}{\partial z} \right) + S_c, \quad 4.1$$

where c is the concentration or mixing ratio of a chemical species, z is the height of the layer, K is the turbulent exchange coefficient and S_c represents all sources and sinks (i.e. emissions, deposition, chemical production and loss, and advection) of water vapour or chemical compounds. All are explicitly parameterised within the model and have been fully described by Bryan et al. (2012) and Ashworth et al. (2015). We briefly re-cap those that remain unchanged from FORCAsT1.0 (Ashworth et al., 2015) before fully describing the coupled stomatal conductance-photosynthesis models we have now incorporated into FORCAsT-gs.

Leaf-level volatile emissions are calculated for each foliated canopy layer in FORCAsT-gs following the light- and temperature-dependent emission algorithms developed by Guenther et al. (1995):

$$F = \text{LAI} \cdot \varepsilon \cdot \gamma_{\text{TS}} \cdot \gamma_{\text{LS}}, \quad 4.2$$

where LAI is the leaf area index in each leaf-angle class and layer, ε is the emission factor or base emission rate (i.e. at standard conditions of 30 °C and 1000 $\mu\text{mol m}^{-2} \text{s}^{-1}$ photosynthetically active radiation, PAR) and γ_{TS} and γ_{LS} are activity factors that scale the base emission rate according to actual temperature and PAR. For temperature-dependent-only emissions from specialised storage pools, γ_{TS} and γ_{LS} in Equation 4.2 is replaced by γ_{TP} based on Steinbrecher et al. (1999). Further details of the activity factors and parameters are presented in Ashworth et al. (2015).

The chemistry in FORCAsT-gs is unchanged from that described by Ashworth et al. (2015). Users can use either the Regional Atmospheric Chemistry Mechanism (RACM; Stockwell et al., 1997; Geiger et al., 2003) or the Caltech Atmospheric Chemistry Mechanism (CACM; Griffin et al., 2003, 2005; Chen et al., 2006). The former includes 84 species and 249 reactions, and the latter 300 species and 630 gas-phase reactions with partitioning to aerosol via the Model to Predict the Multiphase Partitioning of Organics (MPMPO; Chen et al., 2006; Ashworth et al., 2015).

Vertical mixing in and above the canopy are based on Baldocchi (1988) and Gao et al. (1993) respectively, following first-order K-theory (Blackadar, 1963). Eddy diffusivity is constrained by friction velocity measurements made close to but just above the top of the canopy as K-theory breaks down in the highly turbulent canopy sub-layer (Bryan et al., 2012).

Deposition onto vegetated surfaces and stomatal uptake is a major sink for tropospheric ozone (Royal Society, 2008). Ozone taken up through stomata is known to diminish plant growth and health leading to a decrease in productivity rates and causing billions of dollars in crop losses annually (Ainsworth et al., 2012, Avnery et al., 2011). Stomatal conductance is a key factor controlling ozone deposition velocity and deposition rates, and therefore the extent and severity of damage. However, estimates of stomatal conductance are sensitive to model formulation and the choice of model parameters used in vegetation models leading to uncertainty in estimated impacts of O_3 on vegetation (Damour et al., 2010). Here, we describe how FORCAsT1.0 estimates deposition velocity and subsequently investigate how the choice of model formulation and parameters affect these estimates.

The rate of dry deposition to the soil and foliage is calculated for all gas-phase compounds for each model layer in the canopy following the parameterisations of Wesely (1989) and Gao et al. (1993), and is described in full in Bryan et al. (2012). Deposition is assumed to occur at a rate dependent on a species-specific Henry's law coefficient,

diffusivity relative to water vapour and a nominal reactivity factor accounting for enhanced uptake of some species due to reactions occurring within plant cells following uptake. Of importance here is the method of calculating the deposition velocity within the foliar layers, based on four resistances: the quasi-laminar boundary layer at the leaf surface (R_b), stomatal (R_s), mesophyll (R_m), and cuticular (R_c) resistances, such that for each trace gas (i), the deposition velocity (v_d) at each level is:

$$v_{d,i}(z) = \frac{1}{R_{b,i}(z) + R_s(z) \frac{D_{H_2O}}{D_i} + R_{m,i}(z)} + \frac{2}{R_{b,i}(z) + R_{c,i}(z)} \quad 4.3$$

where z is the height of the midpoint of the model level, and D_{H_2O}/D_i ($=1.6$) is the ratio of the molecular diffusivities of water to ozone (Gao et al., 1993). Resistances depend on factors such as LAI, leaf length and the reactivity factor of the trace gas and are calculated on-line in the model. Stomatal resistance, R_s , is deduced as the inverse of stomatal conductance (Ashworth et al., 2015).

Ozone deposition rate, D_r , is then calculated as:

$$D_r = v_d \times [O_3] \quad 4.4$$

where $[O_3]$ is the average concentration of ozone in the canopy layers.

In FORCAST1.0, stomatal conductance was calculated using the Jarvis multiplicative model. Here we extend the Jarvis approach to include photosynthesis and incorporate two coupled stomatal conductance-photosynthesis models into FORCAST-gs, allowing the user to select between three different approaches to calculating photosynthesis and stomatal conductance (see Section 2.2). In all other respects, dry deposition remains unchanged (Bryan et al., 2012; Ashworth et al., 2015).

4.2.2 Physiology: coupled stomatal conductance-photosynthesis models

There are currently three distinct approaches to modelling stomatal conductance and net photosynthesis: empirical multiplicative models that estimate stomatal conductance and thence photosynthesis rate (e.g. Jarvis, 1976); coupled stomatal conductance-photosynthesis models that simultaneously solve for both (e.g. Ball et al., 1987); and optimisation models that simultaneously maximise carbon assimilation while minimising water loss (e.g. Medlyn

et al., 2011). We describe below the key aspects of the three that we incorporated into FORCAsT-gs. A more detailed description of the mathematical formulations for each model is presented in the supplementary information.

The Jarvis model (Jarvis, 1976) assumes stomatal aperture is downregulated from a theoretical maximum by the effects of environmental conditions such as temperature, PAR, and leaf age. The scale of each down-regulation is based on experimental observations and g_s is then calculated as:

$$g_s = g_{max} \times f_{phen} \times f_{light} \times \max\{f_{min}, (f_{temp} \times f_{VPD} \times f_{SWC})\} \quad 4.5$$

where g_s ($\text{mol m}^{-2} \text{s}^{-1}$) is stomatal conductance at each model level and g_{max} ($\text{mol m}^{-2} \text{s}^{-1}$) is the plant species-specific maximum value of canopy stomatal conductance for H_2O . The scaling functions, f_{phen} , f_{light} , f_{temp} , f_{VPD} , and f_{SWC} have values between 0 and 1 and account for the reduction in stomatal conductance due to leaf age (phenology), photosynthetic photon flux density (PPFD, $\mu\text{mol m}^{-2} \text{s}^{-1}$; defined as the intensity of PAR reaching each square meter of the canopy per second), temperature (T , $^{\circ}\text{C}$), vapour pressure deficit (VPD, kPa), and volumetric soil water content (SWC, $\text{m}^3 \text{m}^{-3}$), respectively. f_{min} is the minimum stomatal conductance during daylight. Details of the calculations of each of the functions are given in S1.1.

Net photosynthesis rate, A_n , is then assumed to be directly proportional to the conductance, g_s , such that:

$$A_n = g_s \times C_i \quad 4.6$$

where C_i is the ratio of ambient to internal concentrations of CO_2 and is normally taken as 0.7. Parameter values for each site were determined from field measurements, lab-based experiments or taken from literature for the nearest equivalent and are shown in Table 4.2.

The Ball-Berry coupled stomatal conductance-photosynthesis model assumes that stomatal conductance is regulated directly by the instantaneous rate of photosynthesis to balance CO_2 concentrations inside the leaf with ambient levels. Photosynthesis rate (A ; $\mu\text{mol m}^{-2} \text{s}^{-1}$) at each level in the canopy is calculated following the formulations of Farquhar et al. (1980), Harley et al. (1992) and Baldocchi (1994):

$$A = V_c - 0.5V_o - R_d \quad 4.7$$

where V_c is the carboxylation rate, V_o the oxygenation rate, R_d the dark respiration rate and

$$V_c - 0.5V_o = \min[A_c, A_j] \times (1 - \Gamma/C_i) \quad 4.8$$

i.e. assuming that photosynthesis rate is limited by either Ribulose bisphosphate saturation during carboxylation (A_c) or by the rate of electron transport for Ribulose bisphosphate regeneration during oxygenation (A_j). Γ is the CO₂ compensation point (the CO₂ concentration at which net CO₂ fixation is zero at a given O₂ level and temperature (Moss et al., 1969)) in the absence of dark respiration, and C_i is the intercellular CO₂ concentration (Farquhar and von Caemmerer, 1982).

The internal CO₂ concentration of the leaf, C_i is:

$$C_i = C_s - \frac{A}{g_s} \quad 4.9$$

where g_s is stomatal conductance and C_s is the CO₂ concentration at the leaf surface. Here, g_s was calculated following Ball et al. (1987) as:

$$g_s = g_o + m \frac{A * RH}{C_s} \quad 4.10$$

where g_o is the residual stomatal conductance as A tends to zero, m is a species-specific coefficient expressing the sensitivity of g_s to changes in A , and RH is the relative humidity at the leaf surface.

Medlyn et al. (2011) also assume that photosynthesis rate at each level in the canopy is the minimum of carboxylation and electron transport rate. The version incorporated into FORCAST-gs is based on the parameterisations of Farquhar et al. (1980) for photosynthesis rate (A ; $\mu\text{mol m}^{-2} \text{s}^{-1}$) in C3 plants such that:

$$A = \min(A_j, A_c) - R_d \quad 4.11$$

where R_d ($\text{mol m}^{-2} \text{s}^{-1}$) is the leaf dark respiration.

Stomatal conductance (g_s) is then modelled following optimisation theory (Medlyn et al., 2011) in which stomatal aperture is regulated to maximise carbon gain while simultaneously minimising water loss:

$$g_s \approx g_o + \left(1 + \frac{g_1}{\sqrt{D}}\right) \frac{A}{C_s} \quad 4.12$$

where g_o ($\text{mol m}^{-2} \text{s}^{-1}$) is the residual stomatal conductance as A approaches zero and g_1 is the slope of the sensitivity of g_s to changes in A . D (kPa) is the vapour pressure deficit and C_s ($\mu\text{mol mol}^{-1}$) the CO_2 concentration at the leaf surface as before. The values of g_o and g_1 are determined at the species- or PFT-level from experimental data, and in this study were obtained from Lin et al. (2015) and De Kauwe et al. (2015). Values for each site are listed in Table 4.3.

The Jarvis model includes soil moisture stress as one of the factors limiting stomatal conductance. The relationship between SWC and g_s is modelled following B ker et al. (2015):

$$f_{swc} = \begin{cases} 1 & \text{for } PAW_t \leq PAW \leq 1 \\ (1 - f_{min}) \frac{PAW}{PAW_t} + f_{min} & \text{for } 0 < PAW < PAW_t \end{cases} \quad 4.13$$

where PAW is plant available water and is given by:

$$PAW = \frac{\theta - \theta_w}{\theta_f - \theta_w} \quad 4.14$$

where θ is the volumetric soil water content (SWC, $\text{m}^3 \text{m}^{-3}$), θ_f and θ_w are the SWC at field capacity and wilting point respectively, and PAW_t is a site-specific threshold of the fraction of water in the soil that is available to the plant estimated from site soil characteristics.

For both the Ball-Berry and Medlyn models, we assumed the effect of water stress on photosynthesis to be the result of biochemical limitations as demonstrated in previous studies (e.g. see Egea et al., 2011). A soil moisture stress function (β) was therefore applied

to the maximum rate of RuBP carboxylation (V_{cmax}) and the maximum rate of electron transport (J_{max}) to reflect the impact of soil moisture deficit on plant gas exchange.

β ranges between 1 (in the absence of water stress) to 0 (at wilting point) and is calculated based on soil water content following Porporato et al. (2001); Keenan et al. (2009); Keenan et al. (2010):

$$\beta = \begin{cases} 1 & \text{for } \theta \geq \theta_c \\ \left[\frac{(\theta - \theta_w)}{(\theta_c - \theta_w)} \right]^q & \text{for } \theta_w < \theta < \theta_c \\ 0 & \text{for } \theta < \theta_w \end{cases} \quad 4.15$$

where θ ($\text{m}^3 \text{m}^{-3}$) is the volumetric soil moisture, θ_w is the wilting point ($\text{m}^3 \text{m}^{-3}$), and θ_c is a critical soil moisture content above which water stress is found not to affect plant-atmosphere CO_2 and water vapour exchange (Egea et al., 2011). q is a site-specific empirical factor describing the non-linearity of the effects of soil water stress on tree physiological processes, and here, was derived from observations at each site.

Photosynthesis and stomatal conductance are then estimated using the water-stressed values V_{cmax*} and J_{max*} :

$$V_{cmax*} = V_{cmax} \times \beta \quad 4.16a$$

$$J_{max*} = J_{max} \times \beta \quad 4.16b$$

The Medlyn model further assumes direct limitation to stomatal conductance due to water stress following De Kauwe et al. (2015), such that, stomatal conductance becomes:

$$g_s \approx g_o + \left(1 + \frac{g_1 \beta}{\sqrt{D}} \right) \frac{A}{c_s} \quad 4.17$$

These soil moisture stress functions are applied in all of the simulations conducted here.

4.2.3 FLUXNET sites

An overview of the five sites is given below with further information provided in Table 4.1 and Figure 4.6. The sites are included in the FLUXNET2015 dataset which categorises each location by IGBP ecosystem type (Loveland et al., 2000). “Forests” indicates >60% of landcover is woody vegetation at least 2 m in height. “Evergreen Forests”

retain green foliage throughout the year, while “Deciduous Forests” exhibit a seasonal cycle in which there are periods with foliage on the trees and other periods when there is no foliage.

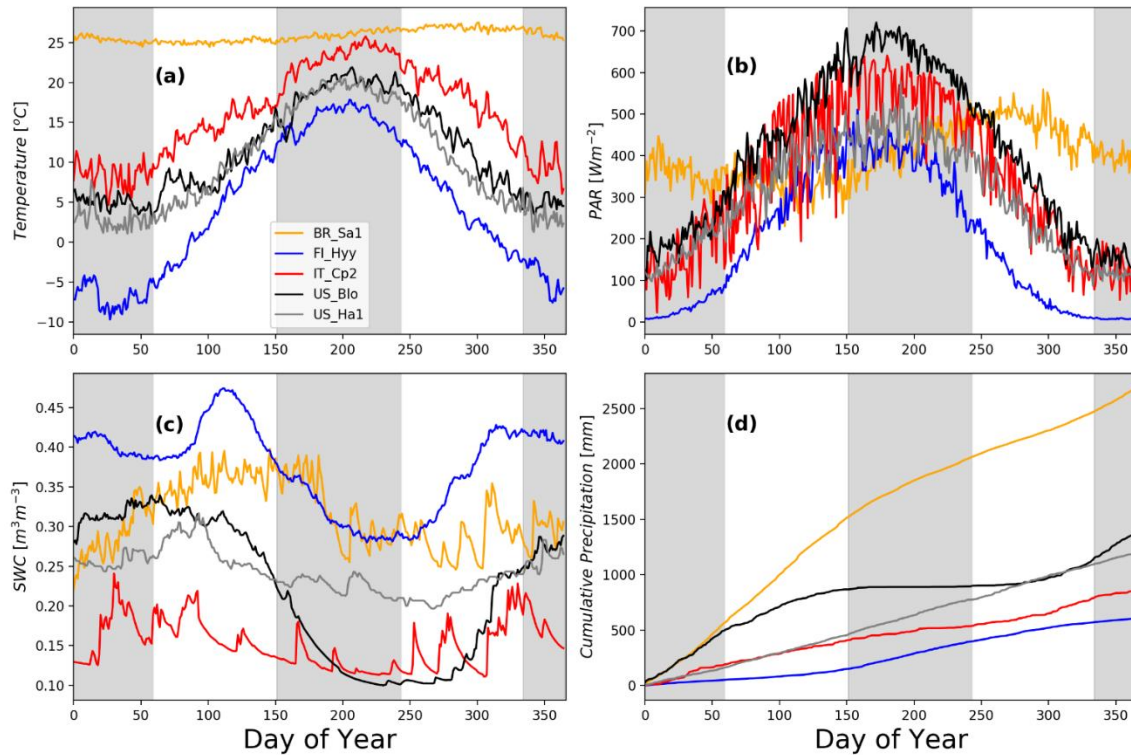


Figure 4.1: Site conditions and meteorology showing (a) soil moisture (volumetric soil water content, SWC; $m^3 m^{-3}$); (b) cumulative precipitation (mm); (c) 2-m air temperature ($^{\circ}C$) and (d) photosynthetically active radiation (PAR) at the top of the canopy ($W m^{-2}$) for an average year at BR_Sa1 (yellow), FI_Hyy (blue), IT_Cp2 (red), US_Blo (black) and US_Ha1 (grey)

4.2.3.1 Santarém-Km67-Primary Forest (BR_Sa1)

BR_Sa1 is in Amazonian Brazil and consists of primary forest comprising a wide range of tree species of varied ages, epiphytes, and high numbers of decaying logs. A flux tower, which was established in 2000 for the Large-scale Biosphere-Atmosphere (LBA) experiment (Rice et al., 2004) is sited on a large level plateau with forest cover stretching 5-40 km in all directions (Goulden et al., 2004). There is closed-canopy forest to an average height of 40 m within the footprint of the flux tower, with numerous emergent trees up to 55m in height (Rice et al., 2004).

Figure 4.1 shows volumetric soil moisture and meteorological data from BR_Sa1 (yellow line) for an average annual profile. The site is categorised as Tropical Evergreen Forest and has a hot humid tropical environment with average rainfall of 1920 mm y^{-1} and relative humidity of 85% (Parotta et al., 1995). Although a number of intense precipitation

events occur during the dry season (Aug-Dec each year), the majority of the rainfall occurs during the wet season (Dec-Jul) with maximum intensity between 13h00-16h00 local time (da Rocha et al., 2004). Annual average temperature is $\sim 25^{\circ}\text{C}$, with little diurnal or seasonal variability (Rice et al., 2004). Daily maximum temperatures range between $24\text{-}32^{\circ}\text{C}$ and minimum $20\text{-}25^{\circ}\text{C}$. The wet season is $\sim 1\text{-}3^{\circ}\text{C}$ cooler than the dry, with incoming solar radiation substantially lower due to cloud cover (da Rocha et al., 2004).

The clay soil has little organic content and retains water well. Soil moisture is not routinely measured at BR_Sa1 and we use data from a nearby site (BR_Sa3 at the 83 km marker) located in the same area of forest. A selective logging experiment commenced at BR_Sa3 shortly after the main LBA campaign and has continued to this day. Less than 5% of aboveground biomass is removed each time, leaving only small gaps between areas of closed-canopy forest (Goulden et al., 2004). Soil moisture at 5 cm depth at BR_Sa3 responds quickly to precipitation, ranging between $\sim 0.30\text{-}0.47\text{ m}^3\text{ m}^{-3}$. At a depth of 250 cm, there is little variation with soil moisture relatively constant at $\sim 0.46\text{ m}^3\text{ m}^{-3}$ during the wet season, declining gradually to $\sim 0.42\text{ m}^3\text{ m}^{-3}$ by the end of the dry season (Rice et al., 2004).

4.2.3.2 Hyytiälä (FI_Hyy)

FI_Hyy is located in the sub-boreal climate zone at the SMEAR II (Station for Measuring Ecosystem-Atmosphere Relation) boreal forest research station at Hyytiälä, $\sim 220\text{ km}$ NW of Helsinki (Hari and Kulmala, 2005; Rinne et al., 2007). The 73-m flux tower is situated on relatively level ground, surrounded by predominantly uniform age ($\sim 60\text{-year-old}$) Scots pine (*Pinus sylvestris*) with an average canopy height of 14 m (Hari and Kulmala, 2005; Suni et al., 2003).

Figure 4.1 shows volumetric soil moisture and meteorological data from FI_Hyy (blue line) for an average year. The site is categorised as Boreal Evergreen Forest with climatological (1959-2014) average annual temperature of 3.5°C and precipitation of 693 mm y^{-1} falling predominantly as snow during the winter months (Suni et al., 2003; SMEARII, 2021). Average monthly temperatures range between -7.7°C in February, and 16°C in July (SMEARII, 2021). Prevailing winds are SSW and are generally moderate, with average annual windspeed of $\sim 2.8\text{ m s}^{-1}$ and maximum of 14 m s^{-1} (SMEARII, 2021). The soil comprises sandy and coarse silty glacial till (Suni et al., 2003). Soil moisture peaks at $>0.45\text{ m}^3\text{ m}^{-3}$ after snow melt and drops to $\sim 0.30\text{ m}^3\text{ m}^{-3}$ or lower during occasional summer droughts.

4.2.3.3 Castelporziano (IT_Cp2)

IT_Cp2 is located at “Grotta di Piastra” within the Presidential Estate at Castelporziano, on the Tyrrhenian coast ~25 km SW of Rome. The 6000 ha Estate has been used for environmental research since 1951 with a flux tower first installed in 1996. The current tower is ~20 m tall and surrounded almost exclusively by even-aged Holm oak (*Quercus ilex*) of average ~14 m height (Fares et al., 2019). This is a typical macchia species, well-adapted to an environment characterised by hot dry summers and nutrient-poor sandy soils (Fares et al., 2009).

Figure 4.1 shows volumetric soil moisture and meteorological data from IT_Cp2 (red line) for an average year. The site is categorised as Temperate Evergreen Forest and has a Mediterranean environment with an average rainfall of 745 mm y⁻¹ of which <100 mm y⁻¹ falls in the summer months (May-early September). Between 1996-2011, mean monthly temperatures ranged between 8.4-24.7°C, with a maximum temperature of 30.3 °C and minimum of 5.0 °C recorded in August and February respectively (Fusaro et al., 2015).

The soil is sandy and freely draining. Soil moisture is thus highly variable and tightly coupled to precipitation events. Soil moisture averaged over a depth of 10-50 cm ranges from ~5% at the end of the summer drought period to ~32% during the winter (Fares et al., 2019).

4.2.3.4 Blodgett Forest (US_Blo)

US_Blo is located in a uniform-age Ponderosa pine plantation in the Sierra Nevada mountain range on the western coast of the continental USA. The plantation was established in 1990 and a 15-m flux tower, which has been the site of long-term monitoring and numerous intensive field campaigns, erected in 1997 (Goldstein, 2000). The average height of the canopy is ~9 m (Park et al., 2014).

Figure 4.1 shows volumetric soil moisture and meteorological data from US_Blo (black line) for an average year. The site is categorised as Temperate Evergreen Forest with a Mediterranean climate. Annual average precipitation is ~1630 mm y⁻¹ with little rain during the summer months (May-early September). Average daily temperatures range between 17-24 °C in the summer, and 0-9 °C in the winter (Goldstein, 2000).

The soil is predominantly free draining loam, and soil moisture tracks precipitation (Goldstein, 2000). Average soil moisture at a depth of 10-20 cm ranges from ~0.10 m³ m⁻³ during summer droughts to just below 0.35 m³ m⁻³ in the winter.

4.2.3.5 Harvard Forest (US_Ha1)

US_Ha1 is located within a ~1600 ha area of old-growth (75+ years) mixed forest in NE USA that has been the site of long-term ecological and environmental monitoring since 1907. A 30-m flux tower was erected in 1990 and has been used for continuous measurements and summer field campaigns since (Goldstein et al., 1998; McKinney et al., 2011). The average height of the canopy is ~24 m (Clifton et al., 2019)

Figure 4.1 shows volumetric soil moisture and meteorological data from US_Ha1 (grey line) for an average year. The site is categorised as Temperate Deciduous Forest with the footprint of the tower dominated by red oak (*Quercus rubra*) and red maple (*Acer rubrum*), although there are a number of red and white pines (*Pinus resinosa* and *P. strobus*) to the NW of the tower (Clifton et al., 2019).

The site has been shown to be relatively homogeneous in all directions from the tower with energy budget closure achieved to within 20% (Goldstein et al., 1998). Annual average precipitation is ~1000 mm y⁻¹ and is relatively evenly distributed through the year. Average daily temperatures range between ~20 °C in the summer, and ~1 °C in the winter.

The soil around the flux tower is a sandy loam (Allen, 1995). Soil moisture typically ranges from ~0.25-0.55 m³ g⁻³, but can drop below 0.20 m³ m⁻³ during (infrequent) drought years (Clifton et al., 2019).

4.2.4 Simulations

Stomatal conductance, photosynthesis rate (instantaneous fluxes of CO₂) and deposition velocity are calculated for each leaf angle class (9 sunlit and 1 shaded) for each foliage-containing level within the canopy in FORCAsT-gs using each of the three physiological approaches outlined in Section 2.2. These are then weighted by leaf angle fraction and leaf area distribution at each level and summed over all model layers to obtain canopy-scale conductance, photosynthesis rates (canopy-top fluxes of CO₂) and deposition velocity. FLUXNET2015 sites report the total rate of photosynthesis throughout the canopy as Gross Primary Productivity (GPP), deduced from the Penrose-Monteith physiology model. We therefore evaluate model performance via comparison of modelled canopy CO₂ fluxes to measured GPP.

During preliminary model configuration at each site, site-specific phenological and canopy structure were set to best fit modelled to observed GPP. However, the physiological

parameters used in each of the three coupled stomatal conductance-photosynthesis algorithms were set to average values reported from previous studies in-situ at similar ecosystems or in controlled environments. These semi-optimised configurations provided our baseline simulations at each site (hereafter referred to as BASE).

To determine the sensitivity of the model to perturbations in the physiological parameters, which are mostly derived from controlled environment experiments, and to provide uncertainty bounds for our estimates of GPP and ozone deposition rates, we conducted a series of sensitivity tests. Only parameters with a direct relationship to stomatal conductance were used in these sensitivity tests to ensure consistency in approach.

In the Jarvis multiplicative model, stomatal conductance is estimated by scaling the maximum conductance observed in saturating light conditions (g_{max} ; Equation 4.5) according to environmental and phenological limitations. Average values of g_{max} for specific plant functional types are generally used, but Hoshika et al. (2018) found variations of up to 70 % between the upper and lower bounds of g_{max} and the mean for different PFTs. Here, we use the mean values for different forest ecosystems for baseline simulations (JV) and the upper and lower bounds as JV+ and JV- respectively (Table 4.1).

For the Ball-Berry coupled stomatal conductance-photosynthesis model, the coefficient m (Equation 4.10) describing the relationship between stomatal conductance and photosynthesis typically ranges between 9 and 12. We use these as our lower (BB-) and upper (BB+) bounds, with the baseline (BB) set to a value of 10. See Table 4.3 for further details of parameter settings.

The equivalent coefficient, g_l (Equation 4.12), is tested in the Medlyn optimisation model. We take the upper (MD+) and lower (MD-) bounds of g_l as reported by De Kauwe et al. (2015) and Lin et al (2015) for different forest ecosystems with error margins of 2-10%. Our baseline simulations (MD) use the average value for each site. Further details of parameter settings are given in Table 4.3.

Simulations for each site were driven with observed half-hourly meteorological and environmental conditions for as many years as the site has been active (see Table 4.1). At the end of the simulation period, average annual and diel profiles of total canopy photosynthesis were calculated and compared with observed GPP. To assess the relative performance of each model at each of the five sites, we define a single summary statistic, that reduces the three individual Taylor model performance indicators to a single value. This summary statistic is the product of the difference between modelled and observed Taylor statistics calculated as:

$$Summary = cRMSE \times (1.0 - r^2) \times |normSD - 1.0| \quad 4.18$$

where r^2 is Pearson's correlation coefficient, normSD the normalised standard deviation and cRMSE the centred root mean square error. The closer this value is to zero, the closer the model fit to observations.

4.3 Results

4.3.1 BASE

We first evaluate the skill of each of the three stomatal conductance-photosynthesis models to reproduce the average diel and annual profiles of GPP at each site for the time periods shown in Table 4.1. The BASE simulations presented here use the parameter values given in Table 4.2.

4.3.1.1 Jarvis (JV)

As shown by the orange lines on Figure 4.2, the multiplicative stomatal conductance model (JV) reproduces the seasonal variation in GPP at all sites except for BR_Sa1, although it substantially overestimates seasonal GPP at the three broadleaf forests (BR_Sa1, IT_Cp2 and US_Ha1) and underestimates at the Boreal needleleaf forest (FI_Hyy). At BR_Sa1, JV overestimates GPP by a factor of 1.5-2. At IT_Cp2 and US_Ha1, however, while JV overestimates GPP by 50-100% in spring and summer it performs well in the rest of the year. For FI_Hyy, JV consistently underestimates productivity from summer through to early autumn, by a factor of 2. However, the model reproduces GPP at US_Blo, which is also a needleleaf forest, to within 20% of the observations at all times of the year. This suggests that the phenology of Boreal ecosystems is not well-captured.

The diel profiles of modelled GPP using JV follows a similar inter-site pattern to that of the seasonal profile with overestimation of diurnal GPP at BR_SA1, IT_Cp2 and US_Ha1 by 5-200%, and underestimation of ~75% at FI_Hyy.

Of the three, JV is the poorest performer across all the sites. The summary statistics shown in Table 4.4 ranges from 0.02 at US_Blo where JV performed well at reproducing observed GPP to 28.86 at BR_Sa1 where it overestimates both seasonal and diurnal profile of GPP. Seasonal cRMSE ranging between 1.24-10.64, normSD between 0.40-3.72 and r^2 as low as 0.01 at BR_Sa1, further confirms the relatively poor performance of this model.

4.3.1.2 Ball Berry (BB)

The coupled stomatal conductance-photosynthesis model (BB) reproduces the observed seasonality and magnitude of GPP within 10-50% at all but the tropical BR_Sa1 ecosystem as shown by the brown lines on the first column of Figure 4.2. BB underestimates summer GPP at FI_Hyy by 30% but overestimates GPP at IT_Cp2 by a similar margin in the summer when seasonal drought occurs. It closely matches observed GPP throughout the season at US_Blo and US_Ha1 with <10% variation between model estimates and observations. Although BB overestimates GPP by as much as 50% at BR_Sa1 throughout the year, it outperforms both JV and MD at this site.

The diurnal profile of GPP estimated by BB confirms its superior performance at the tropical site BR_Sa1, with modelled GPP closely matching the observations during the day. The diurnal profile at the other sites shows that BB underestimates GPP by ~5% in the early hours of the day at FI_Hyy and IT_Cp2 but tends to overestimate GPP by ~20% in the later afternoons.

As shown by the Summary statistic in Table 4.4, which ranges between 0.01 and 0.99, BB outperforms JV at all sites. As summarised by the Taylor diagram in Figure 4.3, BB's performance is better than that of JV, with cRMSE of 1.07 - 2.47, r^2 of 0.85-0.97 (excluding BR_Sa1) and normSD of 0.80-1.82.

4.3.1.3 Medlyn (MD)

Output from the Medlyn model (MD) is shown in blue in Figure 4.2. While MD follows the seasonal fluctuation of GPP at BR_Sa1, estimated fluxes are a factor of ~1.5 higher than observations throughout the year. This overestimation of GPP at the tropical site is also apparent in the profile over the course of an average day. By contrast, at the two Mediterranean sites, MD reproduces both the observed seasonal and diurnal profile of GPP and is within 20% of the observed values at any time during the year or day. MD also shows excellent agreement with both the magnitude and timing of observed GPP throughout the year at FI_Hyy but overestimates the average diurnal profile of GPP by ~20%. MD performs best at the temperate deciduous forest site, US_Ha1, where there is <5% between model estimates and observations across both the year and day.

The superior performance of MD across sites is confirmed by the Taylor diagrams in Figure 4.3 and the summary statistics in Table 4.4. MD exhibits high correlation (0.56-0.98),

and low deviations (1.01-1.92) and error (0.90-3.03). Summary statistics ranging between 0.0003 and 1.25 confirm it as the best performing model overall.

These results show that MD provides the best estimates of GPP at four of the five forest sites used in this study (FI_Hyy, IT_Cp2, US_Blo and US_Ha1) while BB was the overall best performer at BR_Sa1. JV was the least skilful of the three models, substantially overestimating GPP at BR_Sa1, IT_Cp2, US_Ha1 and underestimating at FI_Hyy. All three BASE models were most successful in reproducing observed GPP at the temperate deciduous forest, US_Ha1, and poorest at the tropical forest, BR_Sa1.

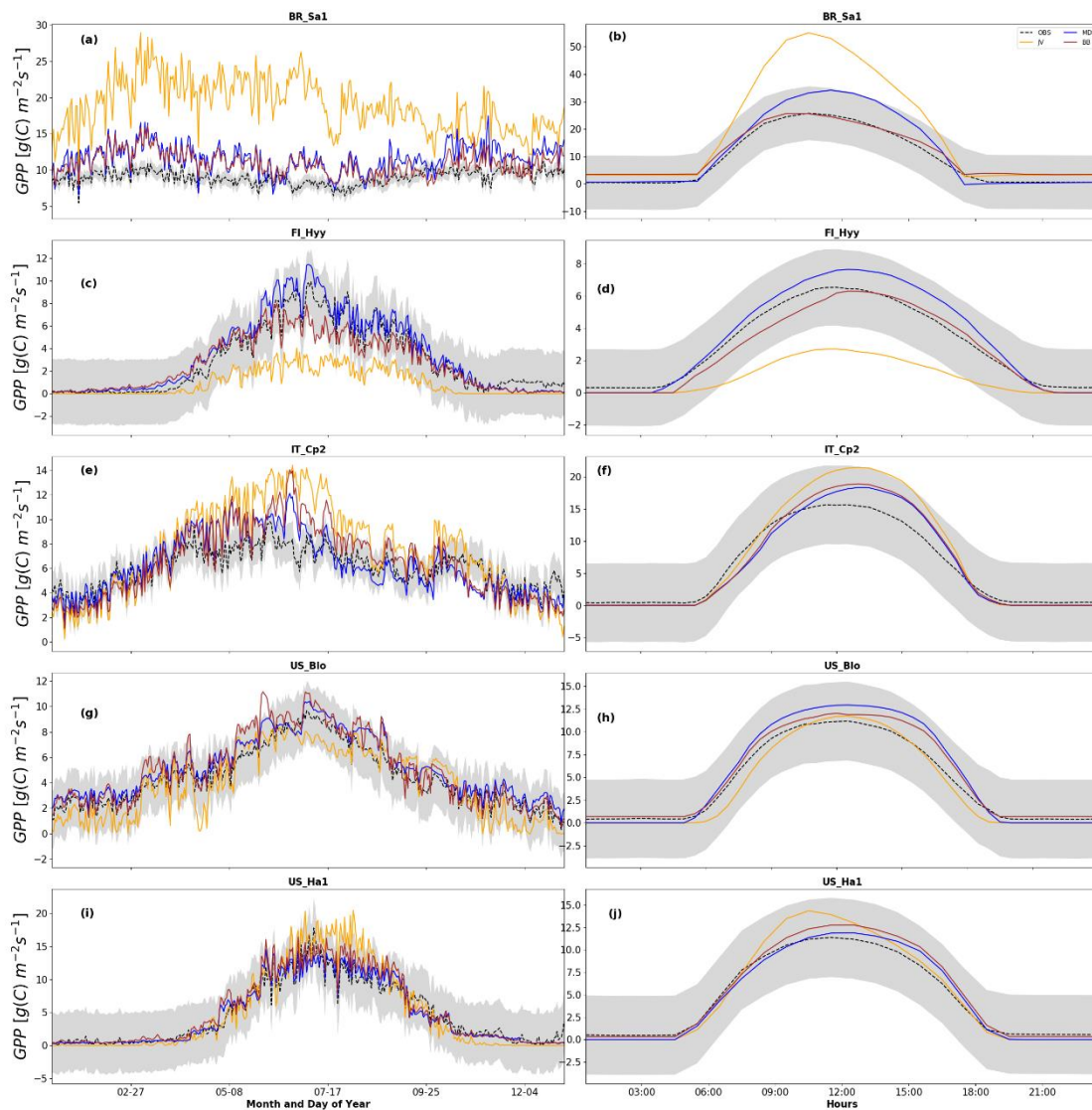


Figure 4.2: Net photosynthesis for an average year at each of the five FLUXNET sites, from top to bottom: BR_Sa1, FI_Hyy, IT_Cp2, US_Blo, US_Ha1. The first column shows average annual and the second average diel profiles of Gross Primary Productivity (GPP, a measure of photosynthesis rate) estimated from the Jarvis multiplicative (gold), Ball-Berry coupled (red) and Medlyn stomatal optimisation coupled (blue) stomatal conductance-photosynthesis models. The black dashed lines show observed GPP.

4.3.2 Sensitivity of stomatal conductance to model parameters

The BASE simulations used mid-range values for species-specific parameters g_{max} (JV; Equation 4.5), m (BB; Equation 4.10), and g_l (MD; Equation 4.12). As described in Section 2.4, we carried out sensitivity tests using lower and upper bound estimates for these parameters. Here we analyse the effect that those parameter changes have on estimated photosynthesis rates for each of the three models, identifying similarities and differences in responses between sites and providing an estimate of uncertainty bounds for GPP and stomatal conductance in each case.

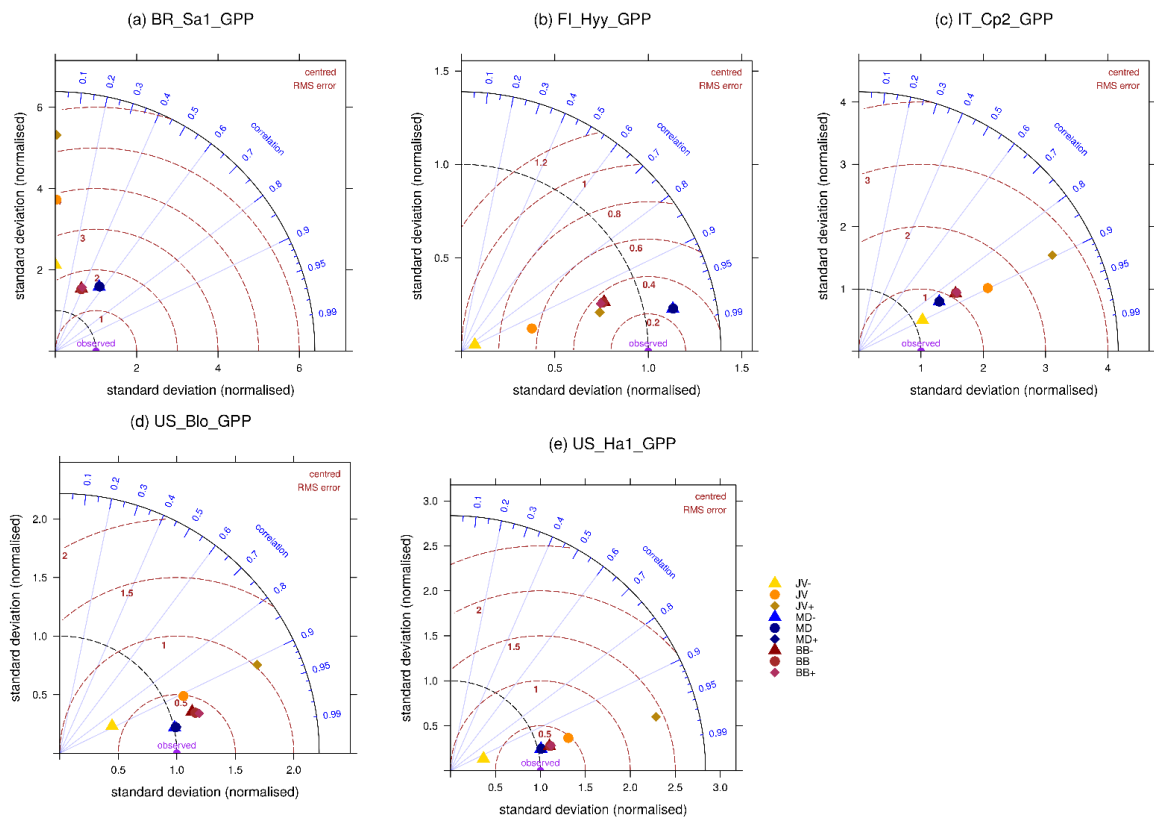


Figure 4.3: Taylor Diagram summarising model output statistics from FORCAsT sensitivity tests. Observed GPP has $SD=1.0$, $RMSE=0.0$ and $r=1.0$ (purple circle). Black and brown dashed curves and blue lines show normalised standard deviation (SD), centred root mean squared error (RMSE) and correlation coefficients (r) respectively against observations for each model on each diagram. The summary statistics for each JV simulation are shown by gold symbols, BB by red, MD simulation by blue. BASE simulations are denoted by circles, lower bounds (TEST-) by triangles, and upper bounds (TEST+) by diamonds. Note that JV, MD and BB in these plots are the BASE simulations described in sections 2.5.1 and 3.1, and Figure 4.2.

4.3.2.1 JV

The plant species-specific theoretical maximum value of canopy stomatal conductance for H₂O (g_{max} ; Equation 4.5) is central to the performance of the JV model in reproducing observed plant gas exchange. Changes in g_{max} lead to proportional changes in both stomatal conductance (Figure 4.9) and GPP (Figure 4.4) at all sites. In general, decreasing g_{max} to its lower limit decreases GPP by between ~75-120% depending on the site, while an increase to the upper bound increases GPP by similar magnitudes.

At the tropical and temperate forests (BR_Sa1, IT_Cp2, US_Blo and US_Ha1) where JV over-estimated GPP, using instead the lower limit of g_{max} (JV-) provided the best model-observation fit in both seasonal and diel cycles at BR_Sa1, but substantially underestimated GPP at IT_Cp2, US_Blo and US_Ha1. By contrast, at FI_Hyy, where JV underestimated GPP, the use of the upper bound of g_{max} (JV+) reduced, but did not completely overcome, model underestimation through the seasons or over the course of an average day. JV+ modelled GPP was around half to two-thirds of observed fluxes, a substantial improvement on the factor of 2 underestimations in JV.

As shown by the Taylor plots presented in Figure 4.3, and Table 4.4, both normalised SD and centred RMSE are substantially increased in JV-. While this is a major improvement in overall model performance at BR_Sa1 (with cRMSE reduced from 10.6 in JV to 2.36 in JV-), JV- substantially worsens model fit at all the other sites. JV+ exacerbates the tendency to over-estimation across all sites, with Summary statistics increasing to 0.22-87.40. The correlation coefficient between modelled and measured GPP is unchanged as it essentially summarises the temporal fit.

4.3.2.2 BB

For both the BB and MD parameterisations, stomatal conductance and net photosynthesis rate are explicitly linked and solved simultaneously. Variations in species-specific response parameters therefore directly affect both g_s and GPP. Similarly to JV, the upper bound increased and lower bound reduced flux estimates compared to the baseline.

In BB, increasing m , i.e. the change in photosynthesis rate for a given change in stomatal conductance, results in proportionally larger increases in GPP than the decreases resulting from reducing m . GPP was slightly over-estimated by BB at all sites (except during the summer months at FI_Hyy where modelled fluxes were lower than observed). BB- therefore provides a better fit to observed GPP across all sites except FI_Hyy where BB+ performed better. It should be noted however, that changes in GPP (0.5-1.0%) are

considerably smaller than those observed for JV between the upper and lower bound simulations.

This is further corroborated by the Taylor diagrams (Figure 4.3) summarising the average, upper and lower bound simulations. Across all sites, there was little change in correlation between estimated and observed GPP, reflecting the minor changes in temporal profile. NormSD also remained virtually unchanged between simulations for GPP fluxes (~1.0 at US_Blo and US_Ha1, ~0.8 at FI_Hyy and ~2.0 at IT_Cp2). cRMSE is consistently low for all simulations at the extra-tropical sites (~1.0-1.2 for GPP at US_Blo and FI_Hyy, and 1.4-1.8 at IT_Cp2 and US_Ha1), indicating the relatively good match to absolute values. By contrast, cRMSE remained high (>2.5) at the tropical rainforest site, BR_Sa1, where a high normSD and low correlation coefficient also confirm the poor performance of the model at capturing both the magnitude and temporal variations in GPP at this ecosystem. The BASE simulation BB proved the closest fit to observed GPP at BR_Sa1.

4.3.2.3 MD

Similarly to BB, changes in g_l in MD result in very small changes in estimated GPP. At the two Mediterranean sites (IT_Cp2 and US_Blo) where GPP was over-estimated by the baseline (MD) simulations, MD- provides a closer fit to observations (Figure 4.3) although the change is only ~1%. Changes in g_l have a negligible effect on GPP at BR_Sa1, FI_Hyy or US_Ha1 (Figure 4.3), where droughts are rare and there is less need for plants to conserve water, i.e. where there is less conflict between maximising photosynthesis and minimising transpiration.

As shown by the Taylor diagrams (Figure 4.3), increasing the value of g_l from the average (10.0) to the upper bound (12.0) improves the correlation between estimated and observed GPP at US_Blo, while decreasing the value improves the fit slightly at IT_Cp2. As suggested by the temporal profiles, there is no noticeable change in correlation at BR_Sa1, FI_Hyy or US_Ha1. The normSD for GPP are very close to 1.0 (i.e. a perfect fit to observations) and centred RMSE <0.5 at FI_Hyy, US_Ha1 and US_Blo but near 2.0 and 1.0 respectively at IT_Cp2, again likely a result of the severity of droughts at Castelporziano, where water conservation is a key driver of stomatal conductance. All three statistics remain poor at BR_Sa1, where r^2 remains virtually unchanged at ~0.6, normSD at 2.0, and cRMSE at ~1.8 for all values of g_l . Considering the relatively small changes observed in GPP in response to changes in g_l , we conclude that the mean values of g_l are sufficient for estimating stomatal conductance and GPP using the Medlyn model at these sites.

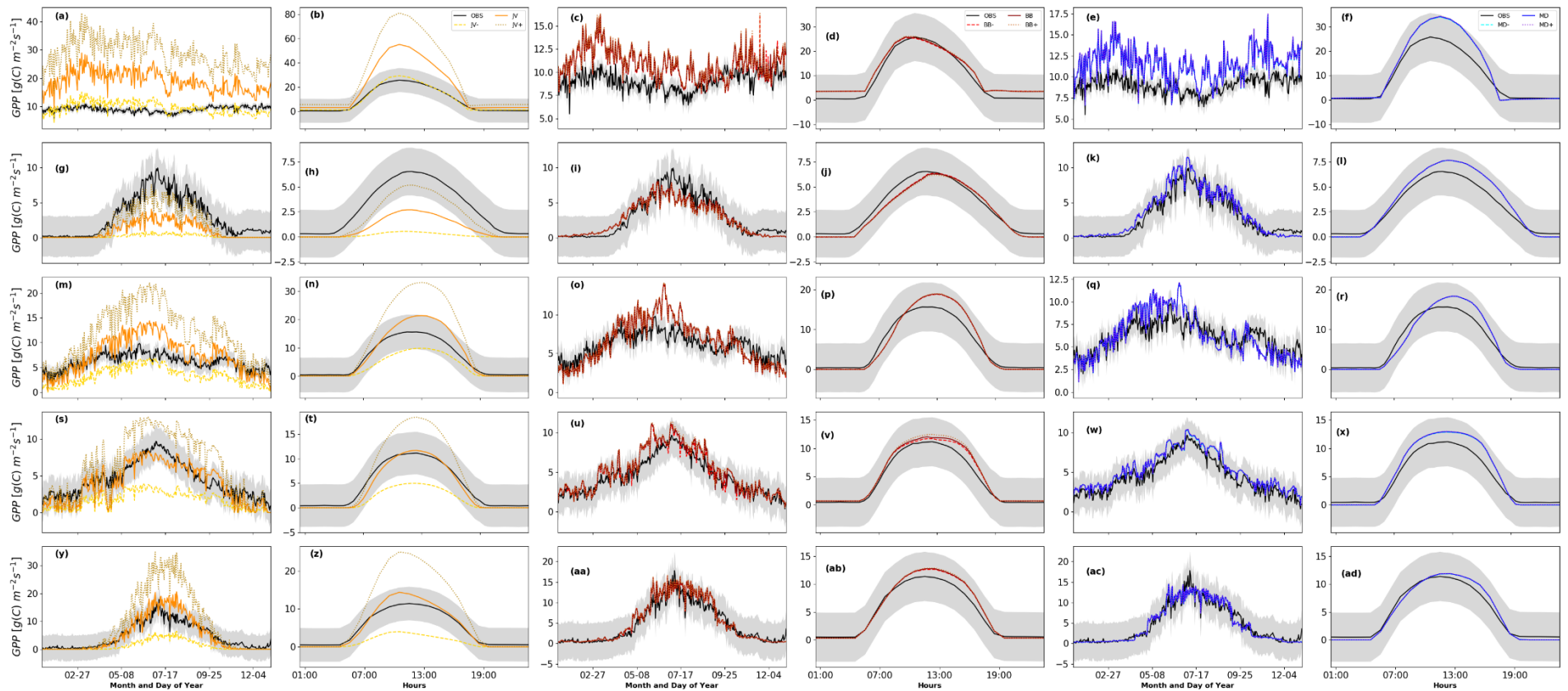


Figure 4.4: Gas exchange for an average year at each of the five FLUXNET sites, from top to bottom: BR_Sa1, FI_Hyy, IT_Cp2, US_Blo, US_Ha1, for, from left to right, the Jarvis, Ball-Berry and Medlyn stomatal conductance model sensitivity tests. Solid lines denote the unperturbed (BASE) simulation as shown in Figure 4.2 for each model, with dashed paler line for TEST- and dashed darker line for TEST+ simulations respectively. The black dashed lines show observed GPP at each site.

4.3.2.4 Summary of sensitivity tests

As shown by Figures 3 and 4, and Table 4.4, GPP estimates in JV were more sensitive to variations in g_{max} than BB and MD estimates were to m and g_l , respectively. However, modelled GPP does not vary by the same magnitude as the variation in model parameters. For instance, modelled GPP values in JV- and JV differed from BASE (JV) estimates by as much as 100% in response to up to 60% variation in g_{max} causing substantial differences in model output statistics (Figure 4.3 and Table 4.4). GPP estimates using upper and lower bounds of m (BB) and g_l (MD) only differed by 1-5% in response to a 10-20% change in the model parameterisation. It must be noted that these sensitivity tests only focused on stomatal conductance parameters in all three models. Tests conducted on photosynthetic parameters such as V_{cmax} and J_{max} have shown a greater difference in estimated GPP compared to what we find here (e.g. see Fares et al., 2019) but do not have an equivalent in JV.

4.3.3 Stomatal conductance

As the three physiology models in FORCAsT-gs explicitly couple photosynthesis and stomatal conductance, we now assume that the parameterisation that best represents GPP (as a proxy for photosynthesis) at each of the sites also best captures fluctuations in stomatal aperture. Figure 4.5 presents the performance of the models at each site relative to the stomatal conductance or ozone deposition rate simulated by the best-performing model.

The first and second columns of Figure 4.5 show the average seasonal and diurnal profiles of stomatal conductance at each site with that estimated by the best performing model shown as a black line (i.e. assumed as “truth”). The grey shading indicates the full range of stomatal conductance estimated by the various model configurations.

At the tropical site, BR_Sa1, the BB model, which best captured GPP, is taken to represent observed stomatal conductance. Stomatal conductance estimated with the model that had the lowest GPP estimates (JV-) is ~75% lower while the configuration with the greatest overestimation of GPP (JV+) is ~25% higher. The difference between the models remains almost constant throughout the year at this tropical site. The divergences in stomatal conductance at FI_Hyy, IT_Cp2, US_Blo and US_Ha1 are seasonal. For these sites, MD- was used to represent observed g_s due to its lower summary statistics shown in Table 4.4. The difference between the models that over or underestimated GPP were <30% in the

winter and spring increasing rapidly to >100% at IT_Cp2 and US_Blo in the summer, and >200% at FI_Hyy and US_Ha1.

The diel profile of stomatal conductance between the best and worst performing models is similar to the seasonal profile observed at each site. As shown by the second columns of Figure 4.5, BR_Sa1, IT_Cp2 and US_Blo show the widest variation in modelled stomatal conductance between the different model configurations during peak periods of the day. There is about 10% overestimation of peak daytime stomatal conductance values at FI_Hyy and US_Ha1 between the best and overestimating model configurations. On the contrary, the models that underestimated GPP at these sites (JV-) also underestimated stomatal conductance by and >50%.

4.3.4 Ozone deposition

The differences in simulated stomatal conductance between configurations of FORCAsT-gs affects estimated ozone deposition velocity and hence the rate at which ozone is lost to this key sink. Figure 4.11 shows the seasonal and diel profiles of variations in ozone deposition velocity between the models. The tropical site, BR_Sa1, and the temperate broadleaf forest, US_Ha1, have the highest estimated ozone deposition velocities as expected from their higher g_s compared to the other sites. This higher g_s and hence ozone deposition velocities are likely due to the fact that plants in these forests also have bigger leaf sizes and higher leaf area index – highlighting the role of forest structure and characteristics in plant physiological processes (Meyers & Baldocchi, 1988; Padro, 1996).

The deposition velocity is however dependent on several resistances as shown in Equation 4.3, including the stomatal resistance (the inverse of g_s). As a result, the models that overestimated GPP and g_s do not necessarily overestimate seasonal deposition velocity when compared to the best performing model across all sites. However, the model configurations that underestimated GPP and g_s do underestimate seasonal ozone deposition velocity, although to a lesser extent. For example, JV- underestimated GPP and g_s by >100% during the peak growing season but only underestimated deposition velocity by ~15%, with an average value of 0.36 cm s^{-1} compared with 0.42 cm s^{-1} estimated with the best performing model (MD). Similarly, at the tropical site, the average deposition velocity in the optimal model configuration (BB) was 0.88 cm s^{-1} . This value was 13% higher than the average deposition velocity in JV- which underestimated GPP and 6% lower than that of JV+ which overestimated GPP by a factor of 2.

The variation between modelled deposition velocities at FI_Hyy, IT_Cp2 and US_Blo between the model configurations is similar to those described for BR_Sa1 and US_Ha1 although the absolute values are smaller. The only exception here is at IT_Cp2 where JV+ overestimates deposition velocity in the summer just as it did for GPP and g_s . The model divergence in diel profile of ozone deposition velocity exhibits similar variability to that of the seasonal profile.

The seasonal changes in deposition velocity are also very different to that of g_s at their respective sites. Ozone deposition velocities at BR_Sa1, IT_Cp2 and US_Ha1, show the greatest variations, ranging between <5% and ~30% for model configurations that over or underestimated GPP respectively, relative to the model configuration that produces the best summary statistics for each site, as defined by Equation 4.18 and summarised in Table 4.4. The two needleleaf forests, FI_Hyy and US_Blo show the least variation in seasonal deposition velocities of <10%.

As shown in Equation 4.4, ozone deposition rates depend on ozone concentration as well as deposition velocity. Hence, while the differences estimated in deposition velocity would be expected to produce changes in ozone deposition rates at the study sites, they will not be directly proportional.

Figure 4.12 shows average ozone concentrations for each study site for the relevant simulation time periods. As ozone is produced through photochemical processes concentrations at all sites peak during the spring and summer and decline steadily in the autumn and winter.

Figure 4.5 shows that the seasonal variation in ozone deposition rate closely follows the seasonal variation in ozone concentration at all sites. On the contrary, the diel profile of ozone deposition differs from that of the concentration. While ozone concentrations at all sites peak in the late afternoon or early evening, deposition rates are highest just after midday when g_s and deposition velocity are at a maximum. This clearly indicates that deposition velocity, and hence stomatal conductance, is the key determinant of deposition rates on shorter timescales, while atmospheric ozone concentrations drive longer temporal trends. The greatest variations in seasonal and diurnal deposition rates between different model configurations, indicated by the grey shaded areas on Figure 4.5, were observed at FI_Hyy and US_Ha1, as for the deposition velocities.

The diel profile of ozone deposition rates, and their variations due to changes in stomatal conductance parameterisations, are similar to those of the deposition velocities (Figure 4.11). Variations in deposition rates estimated by JV+ which overestimated GPP and

stomatal conductance, and the best-fit models averaged 0.10% - 10% across sites. A 7-13% difference was also seen in the deposition rates calculated using the best fit and maximal underestimating model configurations.

However, the seasonal variations observed in deposition rates are much lower than the variations in either stomatal conductance or deposition velocity across all sites. There was only ~1% variation between seasonal ozone deposition rates in model configurations which overestimated GPP and the best performing model across sites, apart from IT_Cp2 where deposition rate varied by ~5% in the summer. Similarly, seasonal deposition rates estimated by model configurations with the lowest GPP were 7-13% lower than those estimated with the best performing model configurations (Figure 4.5). By contrast, modelled stomatal conductance and deposition velocities varied by up to 100% and up to 30% respectively for these same model configurations (Figure 4.5), confirming the modulating effect of ozone concentrations.

The role of ozone concentrations in determining ozone deposition rates is exemplified at BR_Sa1. Average g_s and deposition velocity were a factor of 2 higher at this site than US_Ha1 which had the next highest values. However, the average ozone deposition rates at BR_Sa1 were approximately the same as those at US_Ha1 ($0.18 \text{ ppb cm s}^{-1}$). This is due to lower canopy-level average ozone concentration at BR_Sa1 (20 ppb) compared to US_Ha1 (43 ppb) as shown in Figure 4.12s.

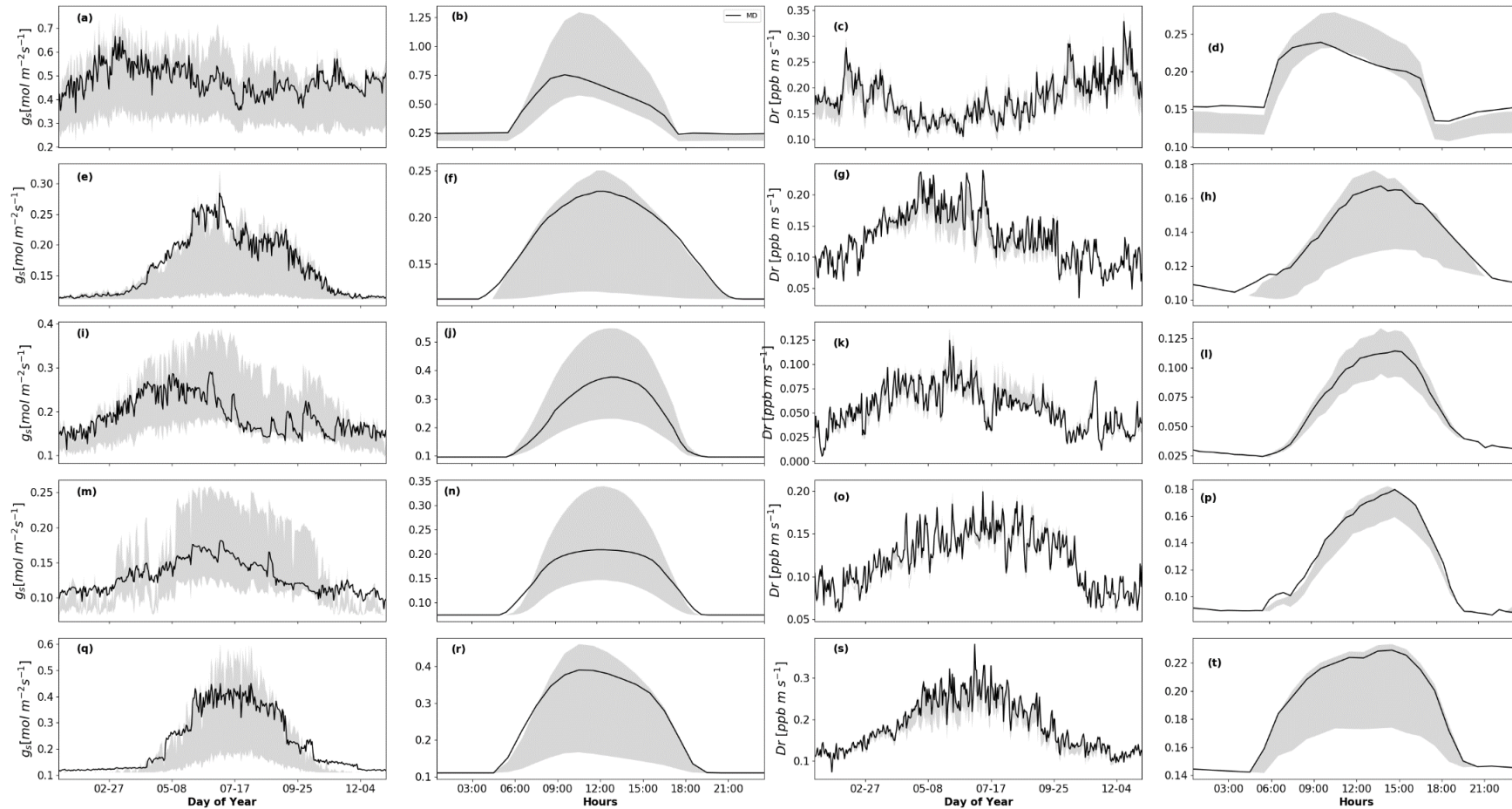


Figure 4.5: Stomatal conductance and ozone deposition rates for an average year and day at each of the five FLUXNET sites, from top to bottom: BR_Sa1, FI_Hyy, IT_Cp2, US_Blo, and US_Ha1. Solid lines black lines denote the output from the model that best reproduced GPP at each site as shown in Figure 4.3 and 4. The shaded regions indicate the spread in stomatal conductance and deposition rates across all the model sensitivity tests.

4.4 Discussion and Conclusion

We have found that ozone deposition rates estimated using stomatal conductance simulated by three of the most widely used stomatal conductance-photosynthesis models can vary by as much as 10% depending on ecosystem, season and time of day. As dry deposition is the primary sink for tropospheric ozone, this has potentially significant implications for estimated ozone budgets across space and time.

By introducing the Jarvis, Ball-Berry and Medlyn parameterisations of stomatal conductance and photosynthesis into FORCAsT1.0, a 1-D column model of trace gas exchange between a forest canopy and the atmosphere (Ashworth et al. 2015; Otu-Larbi et al., 2020a, 2020b), we were able to evaluate the performance of the three physiological models via comparison of simulated photosynthesis with long-term measurements of gross primary productivity (GPP) taken from the FLUXNET2015 dataset (Pastorello et al., 2020). We find that all three models reproduce the seasonal and diel variations in GPP well at a range of forest types, Boreal evergreen (FI_Hyy), Temperate deciduous (US_Ha1), and Mediterranean evergreen (IT_Cp2 and US_Blo), but struggle to capture seasonality at a Tropical broadleaf evergreen site (BR_Sa1).

As shown by Figures 2 and 4, the Medlyn stomatal optimisation model provides the best overall performance at four of the five FLUXNET sites used in this study (FI_Hyy, IT_Cp2, US_Blo and US_Ha1), with estimates of GPP within 20%, but is out-performed by the Ball-Berry coupled stomatal conductance-photosynthesis model at BR_Sa1. The Ball-Berry model also successfully captures GPP across all sites, with divergence from observation mostly <10% except for the drought-prone Mediterranean IT_Cp2 site, at which modelled GPP is 15-20% higher than observed GPP during the middle of the day. The superior performance of MD compared to BB at this site could be expected as MD was specifically developed as an improvement on BB to optimise carbon gain while limiting water loss (Medlyn et al., 2011). Except for US_Blo, where JV reproduced the observed annual and diel profiles of GPP to within 20%, the Jarvis multiplicative model either substantially overestimated or underestimated GPP, by as much as a factor of 2. The relatively poor performance of JV in reproducing observed GPP is perhaps not surprising since photosynthesis estimates are based on a simple assumption of a linear relationship between stomatal conductance and carbon assimilation (Equation 4.6).

The superior performance of the Medlyn optimisation model in the two Mediterranean climates could also be due to the fact that vegetation response to soil moisture stress is better accounted for through a combination of stomatal and biochemical limitations (e.g. see De Kauwe et al., 2015; Lin et al., 2015; Otu-Larbi et al., 2020). BB, by comparison, assumes that drought stress directly downregulates photosynthesis rates or is the result of biochemical limitation only (e.g. see Best et al., 2011; Clark et al., 2011; Fares et al., 2019). This finding is supported by previous work which shows that the choice of drought stress parameterisation is an important factor that determines model performance in a water stressed environment (Egea et al., 2011; Keenan et al., 2010).

The poor performance of the models at the tropical evergreen site (BR_Sa1) is likely due to the assumption of a uniform forest structure for this evergreen forest site throughout the year as it is an evergreen forest. Subsequently, f_{phen} in JV (Equation 4.5) is set to a value of 1 and constant LAI is used in estimating photosynthetic capacity in BB and MD models. A modelling study by Flack-Prain et al. (2019) indicates that changes in LAI could account for up to 33% of observed variations in Amazonian forest GPP. This suggests the need for an improved understanding of changes in forest structure and phenology in tropical ecosystems to obtain more accurate model estimation of GPP at this and other tropical sites (Rödig et al., 2018). In addition, photosynthetic rates and stomatal conductance are controlled by solar radiation and temperature and limited by stress factors like drought and air pollutants including ozone (Nemani et al., 2003). For BR_Sa1, both temperature and PAR (Figure 4.1a and b; orange lines) remain fairly constant throughout the year which would lead to higher modelled photosynthetic capacity in BB and MD since modelled V_{cmax} and J_{max} are reliant on temperature. Seasonal variations in V_{cmax} and J_{max} are reported to be a major source of uncertainty in GPP estimates in Amazonian forests (Flack-Prain et al., 2019). It is worth noting that US_Blo and IT_Cp2 which are also evergreen forest were treated similarly, but as shown in Figures 2 and 4, the models performed better at this site, perhaps due to a compensating error in modelling drought stress.

Results from sensitivity tests conducted on key stomatal conductance parameters in JV, BB and MD models revealed that modelled GPP and stomatal conductance values are highly sensitive to the choice of conductance parameters. Variations of ~5-75% from base model estimates were observed in modelled GPP and stomatal conductance in response to ~10-60% variation in model parameters. Such wide differences could reduce the reliability of estimated reductions in crop or plant productivity due to air pollutants such as ozone.

The findings from this study make it imperative that more measurements of these key conductance parameters are made to improve understanding and model representation of dry deposition. The Jarvis model showed greater sensitivity to choice of parameter value than either Ball-Berry or Medlyn. It must be noted that the Jarvis parameter g_{max} is typically measured in sunlit leaves at the top of the canopy. Leaves below the canopy often differ in their shape and leaf angle classes from those at the top of the canopy (Niinemets, 2010). The JV model as implemented in FORCAsT and elsewhere assumes the same g_{max} for all angle classes and model levels. More work is needed to improve the parameterisation of variations in g_{max} for different levels in the canopy and leaf angle classes.

We conclude that the Medlyn coupled stomatal conductance-photosynthesis model would be the best default selection. However, our model simulations also point to the need for improved stomatal conductance-photosynthesis model parameterisations for tropical ecosystems where seasonality is driven by contrasts in precipitation rather than temperature and solar radiation.

We tested the response of ozone deposition rate at different ecosystems to changes in stomatal conductance parameterisations while keeping model calculations of other resistances unchanged. The choice of stomatal conductance model parameters was found to be a very important factor in determining ozone deposition rates across all sites. Seasonal and daily deposition rates to the forest canopy changed by as much as 13% with implications for air quality modelling and assessment of ozone damage to crops and plants. Most models used in assessing air quality at global, regional, and local levels consider dry deposition using variants of the same Wesely deposition scheme used in FORCAsT-gs (Hardacre et al., 2015). Many international assessments of ozone damage to crops and forests are based on dose-response parameters developed using the JV model (e.g. see Emberson et al., 2000, Hayes et al., 2007; Mills et al., 2011; Buker et al., 2015). Like air quality models, dose-response relationships rely on ozone deposition rates and their accuracy and reliability could be severely diminished if the appropriate model parameterisations are not used. Large uncertainty in modelled deposition rates due to the choice of model parameters, as found in this study, could therefore affect modelled surface ozone concentrations with negative implications for air quality monitoring as well as assessments of plant productivity losses from ozone damage. This is especially true for models that rely on the Jarvis multiplicative model to estimate stomatal conductance. Our results highlight the need for models to carefully consider the choice of model parameters as this will ultimately determine model performance.

Similar to other studies, we found the highest stomatal conductance and ozone deposition velocities at tropical and broadleaf forest site compared to needleleaf and coniferous forests (e.g. see Emberson et al., 2001; Fowler et al., 2001; 2011; Kumar et al., 2011; Silva & Heald, 2018). The larger LAI at the broadleaf forests (BR_Sa1 and US_Ha1), leads to greater canopy conductance, lower stomatal resistance, and subsequently higher deposition velocity as these are important for estimating total canopy and leaf boundary resistance (Meyers & Baldocchi, 1988; Padro, 1996). Ozone deposition velocities at BR_Sa1 were up to a factor of three higher than those at IT_Cp2, US_Blo and FI_Hyy. However, the difference in ozone deposition rates were much lower (<30%) due to lower ozone concentrations at this remote forest site.

Our findings of the sensitivity of stomatal conductance estimates to parameter and algorithm choice could also have important implications in modelling biogenic volatile organic compound (BVOC) emissions. Current BVOC emission models rely on leaf temperature and solar radiation to drive emission rates and are known to reproduce observations for a range of forest ecosystems and climates within a factor of two (e.g. see Guenther et al., 1993; 1995; 2006). However, such models have been shown to struggle to reproduce diurnal emission patterns of short-chained carboxylic acids and aldehydes, leading to suggestions that the failure to include stomatal conductance in such models could be a limiting factor in model performance (Kesselmeier et al., 1997; Martin et al., 1999; Staudt et al., 2000; Niinemets and Reichstein, 2003). Including stomatal control of emission rates in land-atmosphere models would need to account for the sensitivity of simulated stomatal conductance to the choice of physiological model.

4.5 Supplementary material for Chapter 4

4.5.1 Text S1 Jarvis Model

The response of stomatal conductance to phenology (f_{phen}) is described as follows:

$$f_{phen} = \begin{cases} \left((1 - f_{phen,c}) \left(\frac{(DOY - A_{start})}{f_{phen,a}} \right) + f_{phen,c} \right) & \text{for } A_{start} \leq DOY \leq (A_{start} + f_{phen,b}) \\ 1 & \text{for } (A_{start} + f_{phen,a}) \leq DOY \leq (A_{start} - f_{phen,b}) \\ \left((1 - f_{phen,c}) \left(\frac{(DOY - A_{start})}{f_{phen,a}} \right) + f_{phen,c} \right) & \text{for } (A_{end} - f_{phen,b}) \leq DOY \leq A_{end} \end{cases} \quad 4.19$$

where DOY is the day of the year, A_{start} and A_{end} are the DOY for the start and end of the growing season, respectively. $f_{phen,a}$ represents the number of days from A_{start} required for f_{phen} to reach its maximum value (canopy maturity) while $f_{phen,b}$ is the number of days during the decline of f_{phen} to its minimum value at the end of the season. In between these days, the canopy is assumed mature, i.e. that phenology does not limit stomatal conductance, and f_{phen} is set to unity. The parameters $f_{phen,c}$ and $f_{phen,d}$ represent the maximum fraction of f_{phen} at A_{start} and A_{end} , respectively, and are species-specific. For evergreen sites with green foliage present all year, f_{phen} is set to unity.

The response of stomatal conductance to PPFD (f_{light}) is specified as:

$$f_{light} = 1 - \exp(a \cdot \text{PPFD}) \quad 4.20$$

where a is a species-specific parameter defining the shape of the exponential relationship between PPFD and g_s .

The stomatal response to leaf temperature (f_{temp}) is described by the parabolic function:

$$f_{temp} = \left(\frac{T - T_{min}}{T_{opt} - T_{min}} \right) \left\{ \left(\frac{T_{max} - T}{T_{max} - T_{opt}} \right)^{\left(\frac{T_{max} - T_{opt}}{T_{opt} - T_{min}} \right)} \right\} \quad 4.21$$

where T_{opt} , T_{min} , and T_{max} respectively denote the optimal, minimum, and maximum temperature for stomatal conductance.

The response of stomatal conductance to vapor pressure deficit (f_{VPD}) is given as follows:

$$f_{VPD} = \begin{cases} 1 & \text{for } VPD \geq VPD_{max} \\ \frac{(1 - f_{min})(VPD_{min} - VPD)}{VPD_{min} - VPD_{max}} & \text{for } VPD_{min} \leq VPD < VPD_{max} \\ f_{min} & \text{for } VPD < VPD_{min} \end{cases} \quad 4.22$$

where VPD_{min} and VPD_{max} denote the threshold of VPD (kPa) for attaining minimum and full stomatal aperture, respectively.

4.5.2 Text S2 Ball-Berry (BB) Model

The value of A_c is calculated as:

$$A_c = \frac{V_{cmax}(C_i - \Gamma)}{C_i + K_c(1 + [O_2]/K_o)} \quad 4.23$$

where V_{cmax} is the maximum carboxylation rate when RuBP is saturated and K_o and K_c are the Michaelis-Menten coefficients for O_2 and CO_2 , respectively.

A_j is defined as:

$$A_j = \frac{J(C_i - \Gamma)}{4C_i + 8\Gamma} \quad 4.24$$

Where J is the potential rate of electron transport and is a function of incident photosynthetic photon flux density (I), the quantum yield (α), and the maximum rate of electron transport (J_{max}):

$$J = \frac{\alpha I}{\sqrt{1 + \alpha^2 I^2 / J_{max}}} \quad 4.25$$

The internal CO_2 concentration of the leaf, C_i is:

$$C_i = C_s - \frac{A}{g_s} \quad 4.26$$

where g_s is stomatal conductance and C_s is the CO_2 concentration at the leaf (surface) level and is calculated as:

$$C_s = C_a - A * (R_a + R_{bcO_2}) \quad 4.27$$

where C_a is the ambient CO_2 concentration, which is supplied to the model from observations as an input parameter.

4.5.3 Text S3 Medlyn (MD) Model

The limiting rates, A_j (electron transport) and A_c (carboxylation) are:

$$A_j = \frac{J(C_i - \Gamma)}{4(C_i + 2\Gamma)} \quad 4.28$$

where J ($\mu\text{mol m}^{-2} \text{s}^{-1}$) is the rate of electron transport, Γ is the CO_2 compensation point in the absence of dark respiration and C_i (ppm) is the leaf internal CO_2 concentration. J is estimated from:

$$J = \frac{\alpha L + J_{max} - \sqrt{(\alpha L + J_{max})^2 - 4\alpha\delta L J_{max}}}{2\delta} \quad 4.29$$

where α is the initial quantum yield, L ($\mu\text{mol m}^{-2} \text{s}^{-1}$) PPFD, J_{max} ($\mu\text{mol m}^{-2} \text{s}^{-1}$) the maximum electron transport rate, δ the curvature of the light response curve and

$$A_c = V_{cmax} \frac{C_i - \Gamma}{C_i + K_m} \quad 4.30$$

where V_{cmax} ($\mu\text{mol m}^{-2} \text{s}^{-1}$) is the maximum rate of Rubisco activity and K_m is the Michaelis–Menten coefficient for Rubisco kinetics, such that:

$$K_m = K_c \left(1 + \frac{O_i}{K_o}\right) \quad 4.31$$

where K_c (Pa) and K_o (Pa) are the Michaelis–Menten parameters for CO_2 and O_2 respectively as before and O_i (ppm) is the leaf internal oxygen concentration, assumed to be equal to the oxygen concentration of the external air.

Table 4.1: : Summary of the five FLUXNET2015 datasets used to evaluate modelled canopy-top CO₂ and latent heat fluxes. IGBP ecosystems are described as: EBF – Evergreen Broadleaf Forests, ENF – Evergreen Needleleaf Forests, DBF - Deciduous Broadleaf Forests according to dominant vegetation type, canopy height and time of foliage cover.

Site ID	BR-Sa1	IT-Cp2	FI-Hyy	US-Blo	US-Ha1
Site Name	Santarem- Km67- Primary Forest	Castelporzia no	Hyytiälä	Blodgett Forest	Harvard Forest EMS Tower (HFR1)
Latitude	-2.85667	41.70427	61.84741	38.8953	42.5378
Longitude	-54.95889	12.35729	24.29477	-120.6328	-72.1715
Elevation (m)	88	19	181	1315	340
LAI (m ² m ⁻²)	5.50	3.20	2.80	2.50	3.70
Years	2002-2003	2013-2014	1996-2014	2003-2004	2008-2010
Avg. Temp(°C)	26.13	15.2	3.8	11.09	6.62
Avg. Rainfall (mm)	2074.79	805	709	1226	1071
IGBP Ecosystem	EBF	EBF	ENF	ENF	DBF
FLUXNET20 15 data doi:	10.18140/FL X /1440032	10.18140/FL X /1440233	10.18140/FL X /1440158	10.18140/FL X /1440068	10.18140/F LX/144007 1

Table 4.2: Summary of the site- and species-specific parameter values used in model parameterisation at the five sites. N/A denotes not applicable. Where applicable, references for each value are indicated by superscripts and listed below.

Paramet	Units	BR-Sa1	FI-Hyy	IT-Cp2	US-Blo	US-Ha1
G_{\max}	mmol H ₂ O m ⁻² s ⁻¹	230 ¹	190 ²	200 ³	180 ¹	290 ¹
A	μmol photons m ⁻²	0.004 ¹	0.006 ²	0.009 ³	0.004 ¹	0.005 ¹
A _{start}	-	1	90 ²	1	1	90 ¹
A _{end}	-	365	300 ²	365	365	304 ¹
f _{phen_a}	Days	N/A	40 ²	N/A	N/A	90 ¹
f _{phen_b}	Days	N/A	40 ²	N/A	N/A	90 ¹
f _{phen_c}	-	N/A	0.8 ²	N/A	N/A	0.3 ¹
f _{phen_d}	-	N/A	0.8 ²	N/A	N/A	0.3 ¹
T _{max}	°C	45 ¹	36 ²	39 ³	45 ¹	45 ¹
T _{opt}	°C	30 ¹	20 ²	23 ³	22 ¹	24 ¹
T _{min}	°C	10 ¹	0 ²	1 ³	5 ¹	5 ¹
VPD _{max}	kPa	2.8 ¹	2.8 ²	7.4 ³	7.4 ¹	2.8 ²
VPD _{min}	kPa	0.6 ¹	0.6 ²	0.8 ³	0.8 ¹	0.6 ²
PAW _t	-	0.90 [*]	0.32 [*]	0.32 [*]	0.32 [*]	0.32 [*]
θ _f	m ³ m ⁻³	0.40 [*]	0.30 ⁴	0.15 [*]	0.14 [*]	0.30 [*]
θ _w	m ³ m ⁻³	0.10 [*]	0.08 ⁴	0.04 [*]	0.04 [*]	0.08 [*]
f _{min}	-	0.03 ⁵	0.04 ⁵	0.03 ⁵	0.03 ⁵	0.03 ⁵
V _{cmax}	μmol m ⁻² s ⁻¹	80 ⁶	50 ⁷	78 ⁸	75 ⁹	60 ¹⁰
g ₀	mol m ⁻² s ⁻¹	0.03 ⁵	0.04 ⁵	0.03 ⁵	0.03 ⁵	0.03 ⁵

¹Hoshika et al. (2018), ²Büker et al. (2015), ³Fares et al. (2013), ⁴Gao et al. (2016), ⁵De Kauwe et al. (2015), ⁶Fares et al. (2019), ⁷Kolari et al. (2014), ⁸Fares et al. (2019), ⁹Keenan et al. (2010), ¹⁰Williams et al., 1996, ^{*}This study.

Table 4.3: Perturbed parameter values for each model simulation at each of the five FLUXNET2015 data sites. The first column indicates the stomatal conductance or coupled conductance-photosynthesis model applied, with – denoting lower bound and + upper. Those with no symbol represent the baseline simulation for each model. The values used in baseline simulations are highlighted in bold fonts.

Simulation	Altered parameter	BR_Sa1	FI_Hyy	IT_Cp2	US_Blo	US_Ha1
JV-	g_{max}	0.22	0.07	0.10	0.10	0.13
JV	(Eqn.7)	0.36	0.12	0.17	0.17	0.31
JV+	values from Hoshika et al. (2018)	0.50	0.17	0.24	0.24	0.49
MD-	g_l (Eqn. 28); values from De	4.09	2.1	4.03	2.1	4.09
MD		4.45	2.35	4.12	2.35	4.45
MD+	Kauwe et al. (2015)	4.81	2.6	4.21	2.6	4.81
BB-		9	9	9	9	9
BB	m (Eqn. 22)	10	10	10	10	10
BB+		12	12	12	12	12

Table 4.4: Summary statistics for an average year at each site for each test, showing number of data (n), centred Root Mean Square Error ($cRMSE$), coefficient of correlation (r^2), normalised standard deviation (relative to the observations; $normSD$) used to create the Taylor plots (Fig. 6). The summary for GPP for each model at each site shows the product of $cRMSE$, $1-r^2$ and the absolute value of $normSD-1$.

Site	Model	N	cRMSE	r	SD	Summary
BR-Sa1	JV-	365	2.35614	-0.00028	2.12653	2.65499
	JV	365	10.64232	0.00598	3.72807	28.85946
	JV+	365	20.36928	0.00648	5.31898	87.40478
	MD-	365	2.97886	0.56191	1.91724	1.19702
	MD	365	3.02963	0.56338	1.92702	1.22625
	MD+	365	3.07469	0.56470	1.93561	1.25223
	BB-	365	2.43166	0.38323	1.67004	1.00491
	BB	365	2.47790	0.38682	1.65285	0.99194
BB+	365	2.63425	0.38845	1.70265	1.13196	
FI_Hyy	JV-	365	3.87634	0.90176	0.07923	0.35065
	JV	365	2.72495	0.95140	0.39591	0.08001
	JV+	365	1.42572	0.96258	0.76913	0.01232
	MD-	365	0.89782	0.98026	1.15444	0.00274
	MD	365	0.90152	0.98032	1.15614	0.00277
	MD+	365	0.90382	0.98037	1.15729	0.00279

	BB-	365	1.06230	0.94481	0.80824	0.01124
	BB	365	1.07289	0.94525	0.80182	0.01164
	BB+	365	1.09752	0.94628	0.78780	0.01251
IT_Cp2	JV-	365	2.86646	0.89779	1.13942	0.04085
	JV	365	2.70923	0.89810	2.30640	0.36065
	JV+	365	6.98750	0.89587	3.47059	1.79764
	MD-	365	1.35806	0.85102	1.51782	0.10477
	MD	365	1.36133	0.85114	1.51987	0.10535
	MD+	365	1.36452	0.85127	1.52185	0.10591
	BB-	365	1.76773	0.85856	1.81089	0.20275
	BB	365	1.78949	0.85785	1.82088	0.20881
	BB+	365	1.82104	0.85684	1.83548	0.21782
US_Blo	JV-	365	3.14114	0.88712	0.50372	0.17597
	JV	365	1.24427	0.90790	1.16417	0.01881
	JV+	365	2.96151	0.91269	1.84766	0.21918
	MD-	365	0.90553	0.97601	1.00507	0.00011
	MD	365	0.92641	0.97590	1.01455	0.00032
	MD+	365	0.94517	0.97579	1.02286	0.00052
	BB-	365	1.04399	0.95413	1.18512	0.00886
	BB	365	1.10892	0.95836	1.20853	0.00963
	BB+	365	1.22281	0.96167	1.23914	0.01121
US_Ha1	JV-	365	4.52995	0.93818	0.39115	0.17051
	JV	365	2.20948	0.96334	1.36000	0.02916
	JV+	365	7.78592	0.96737	2.36357	0.34639
	MD-	365	1.11499	0.97184	1.03552	0.00112
	MD	365	1.11749	0.97191	1.03882	0.00122
	MD+	365	1.11988	0.97198	1.04166	0.00131
	BB-	365	1.40901	0.97037	1.13401	0.00559
	BB	365	1.43638	0.97043	1.14174	0.00602
	BB+	365	1.49135	0.97033	1.15537	0.00687

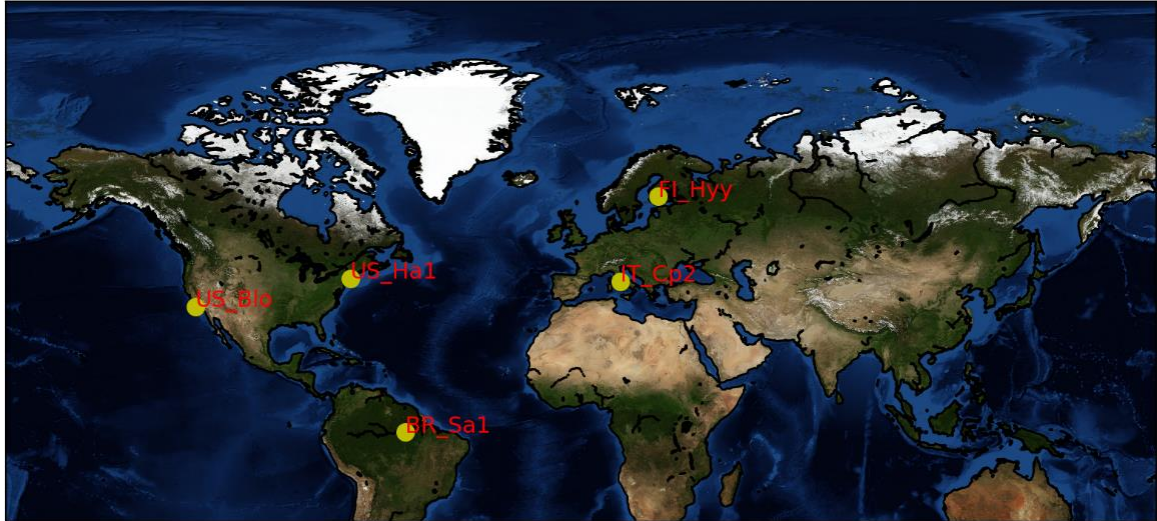


Figure 4.6: Locations of forest sites used in this study.

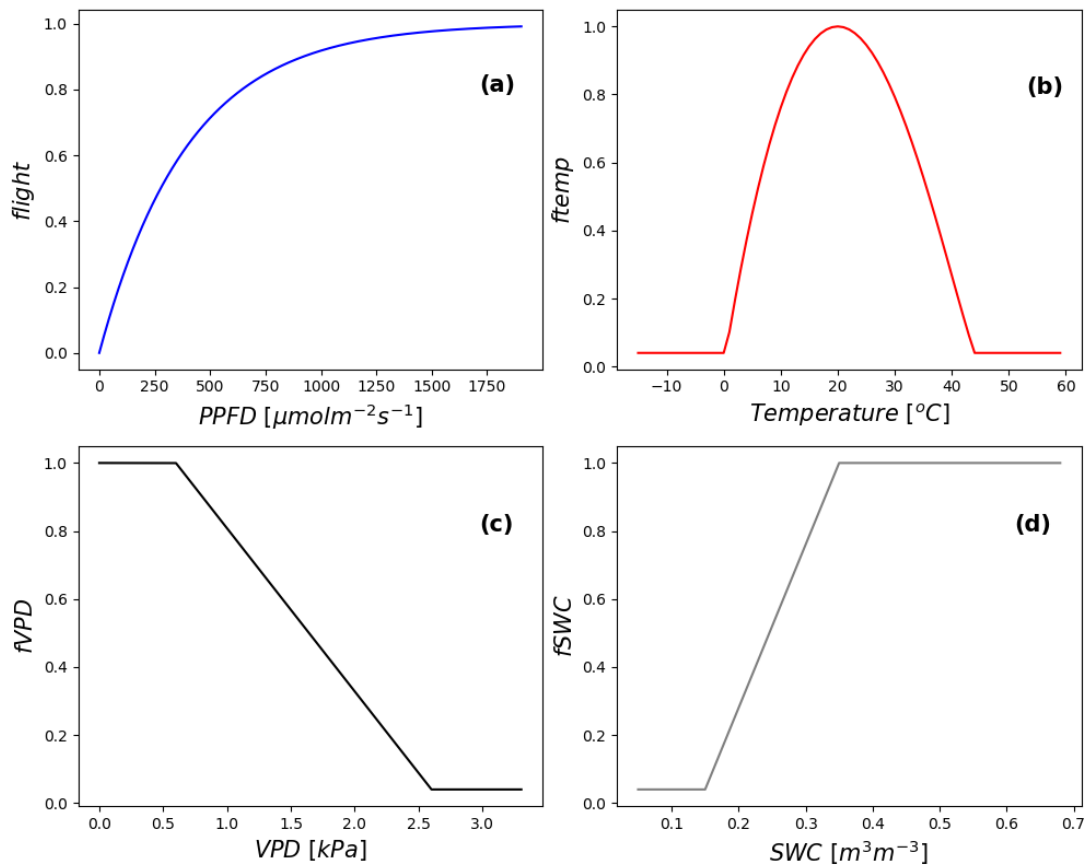


Figure 4.7: Graphs showing the response of stomatal conductance in the Jarvis model to (a) photosynthetic flux density (f_{light}), (b) Temperature (f_{temp}) (c) vapour pressure deficit (f_{VPD}) and (d) soil water content (f_{swc})

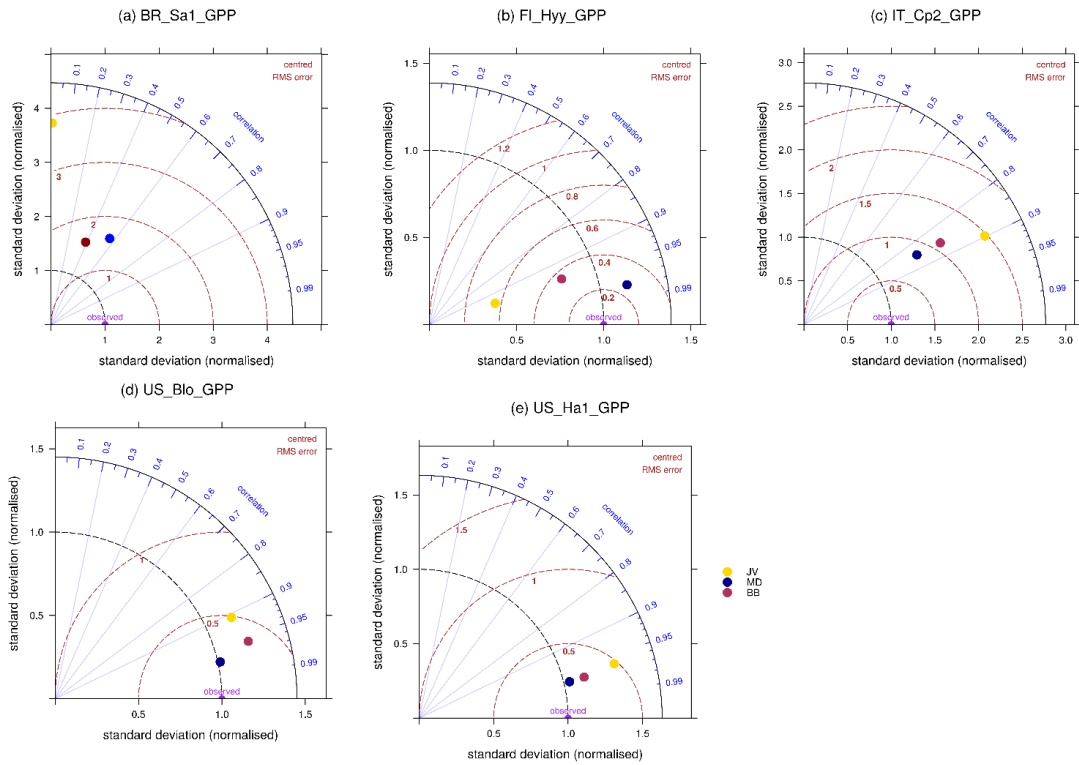


Figure 4.8: Taylor Diagram summarising model output statistics from FORCAsT BASE model configurations. The black and brown dashed curves and blue lines show normalised standard deviation (SD), centred root mean squared error (RMSE) and correlation coefficients (r) respectively against observations for each model on each diagram. The summary statistics for each JV simulation are shown by gold circles, BB by red, MD simulation by blue.

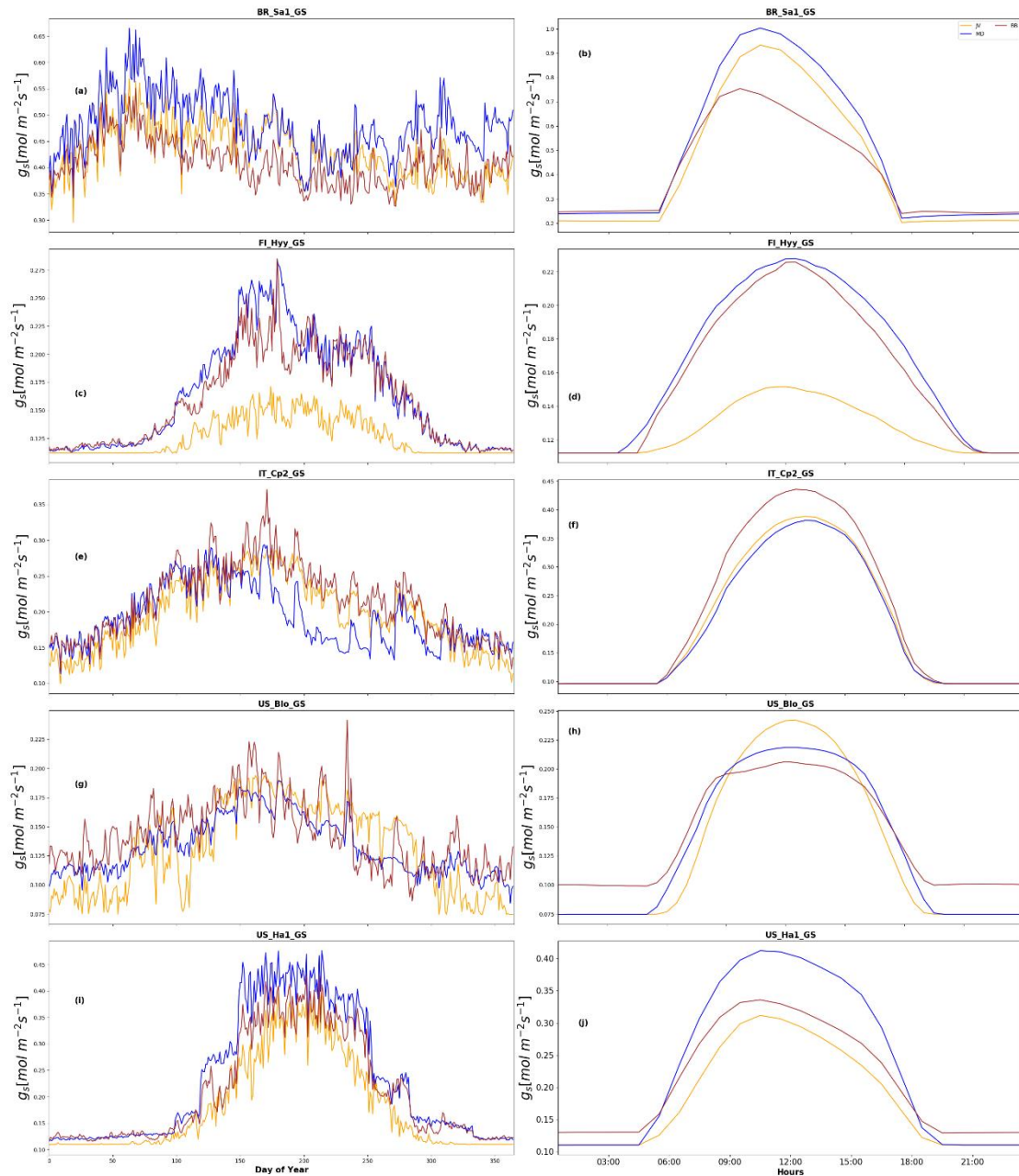


Figure 4.9: Stomatal conductance for an average year at each of the five FLUXNET sites, from top to bottom: BR-Sa1, FI-Hyy, IT-Cp2, US-Blo, US-Ha1. The first column shows average annual and the second average diel profiles of stomatal conductance estimated from the Jarvis multiplicative (gold), Ball-Berry coupled (red) and Medlyn stomatal optimisation coupled (blue) stomatal conductance-photosynthesis models.

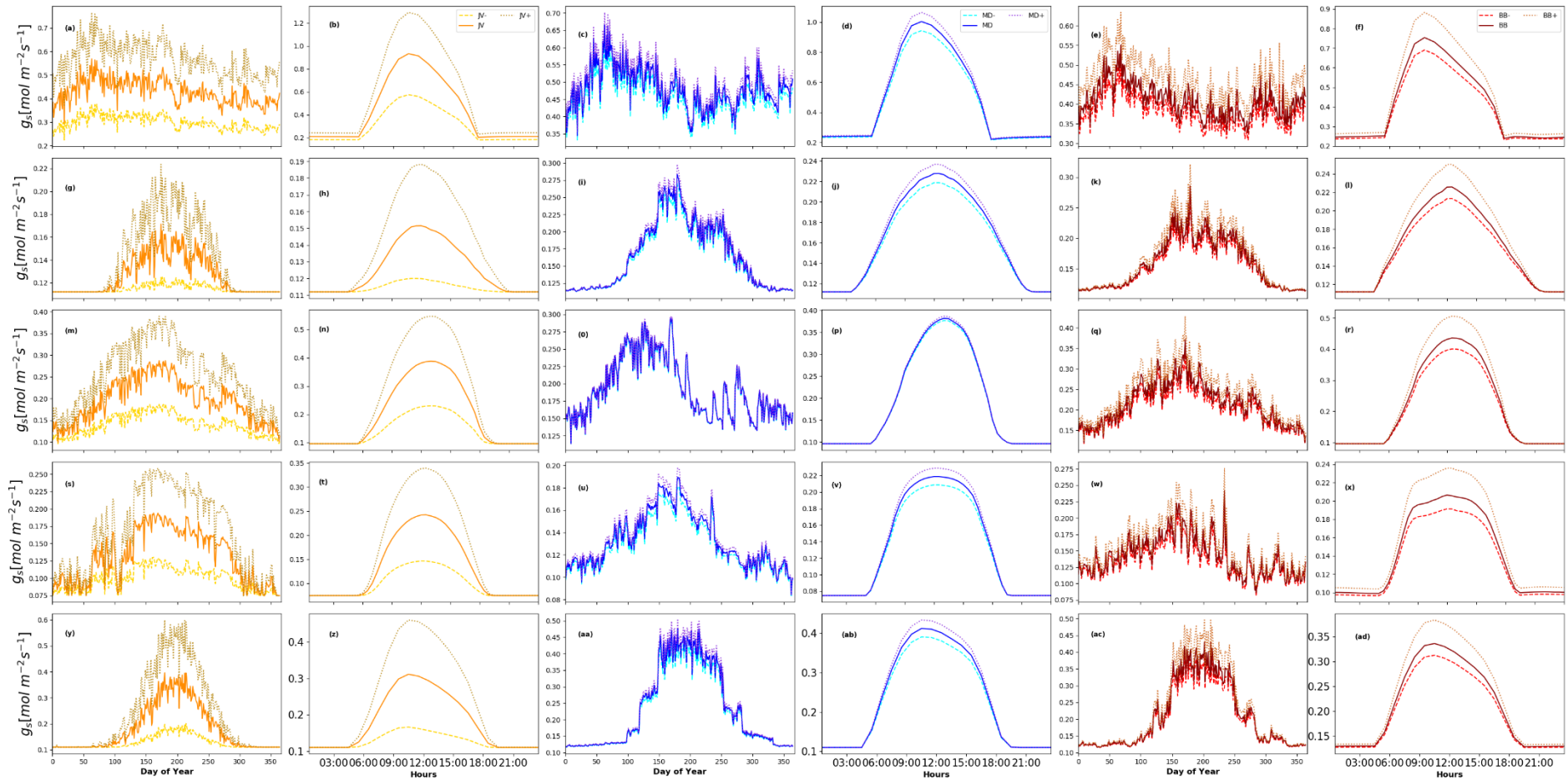


Figure 4.10: Stomatal conductance for an average year at each of the five FLUXNET sites, from top to bottom: BR-Sa1, FI-Hyy, IT-Cp2, US-Blo, US-Ha1, for, from left to right, the Jarvis, Ball-Berry and Medlyn stomatal conductance model sensitivity tests. Solid lines denote the unperturbed (BASE) simulation for each model, with dashed paler line for TEST- and dashed darker line for TEST+ simulations respectively.

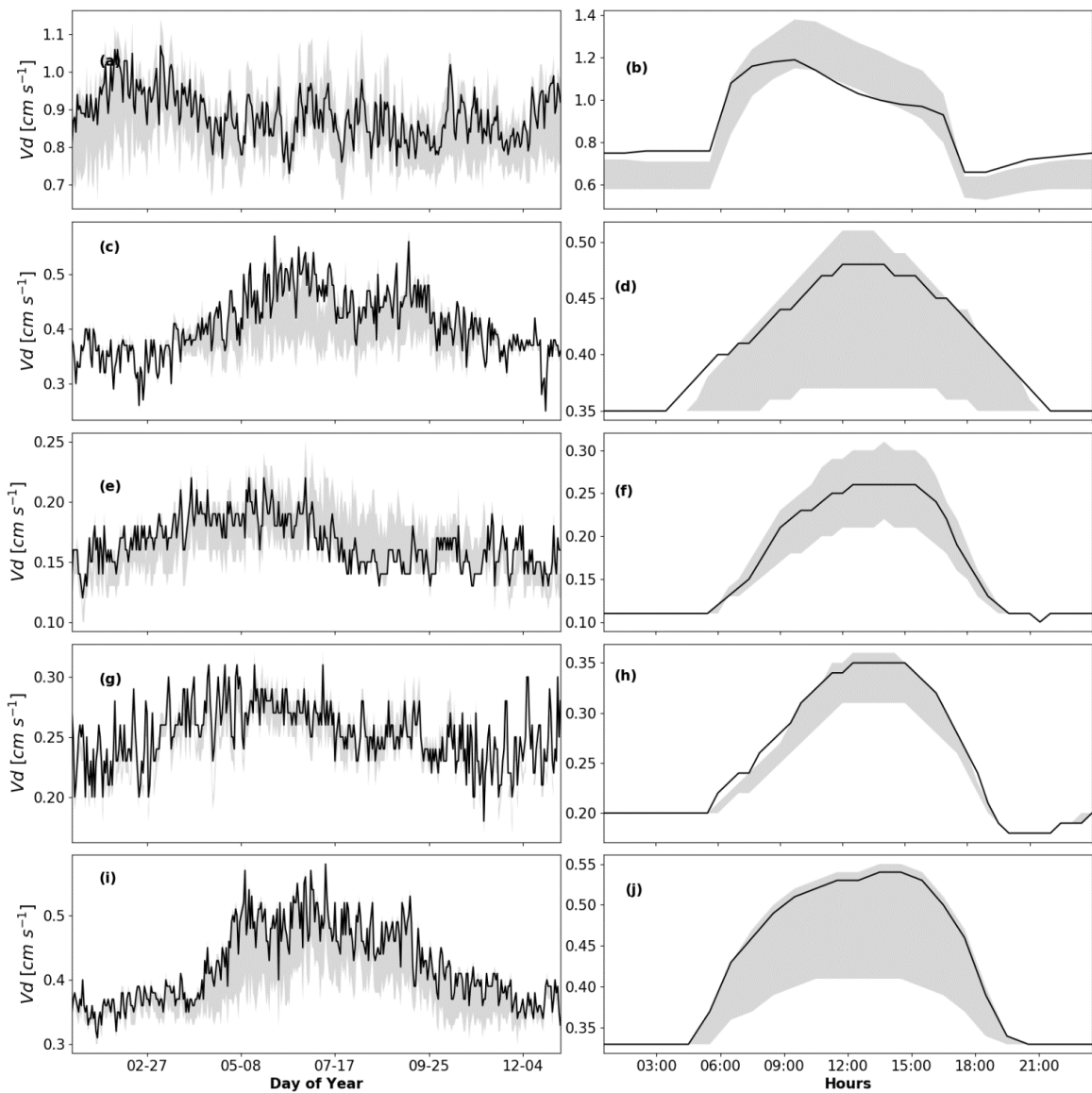


Figure 4.11: Ozone deposition velocity for an average year and day at each of the five FLUXNET sites, from top to bottom: BR-Sa1, FI-Hyy, IT-Cp2, US-Blo, and US-Ha1. Solid lines black lines denote the output from the model that best reproduced GPP at each site. The shaded regions indicate the spread in stomatal conductance and deposition rates across all of the model sensitivity tests.

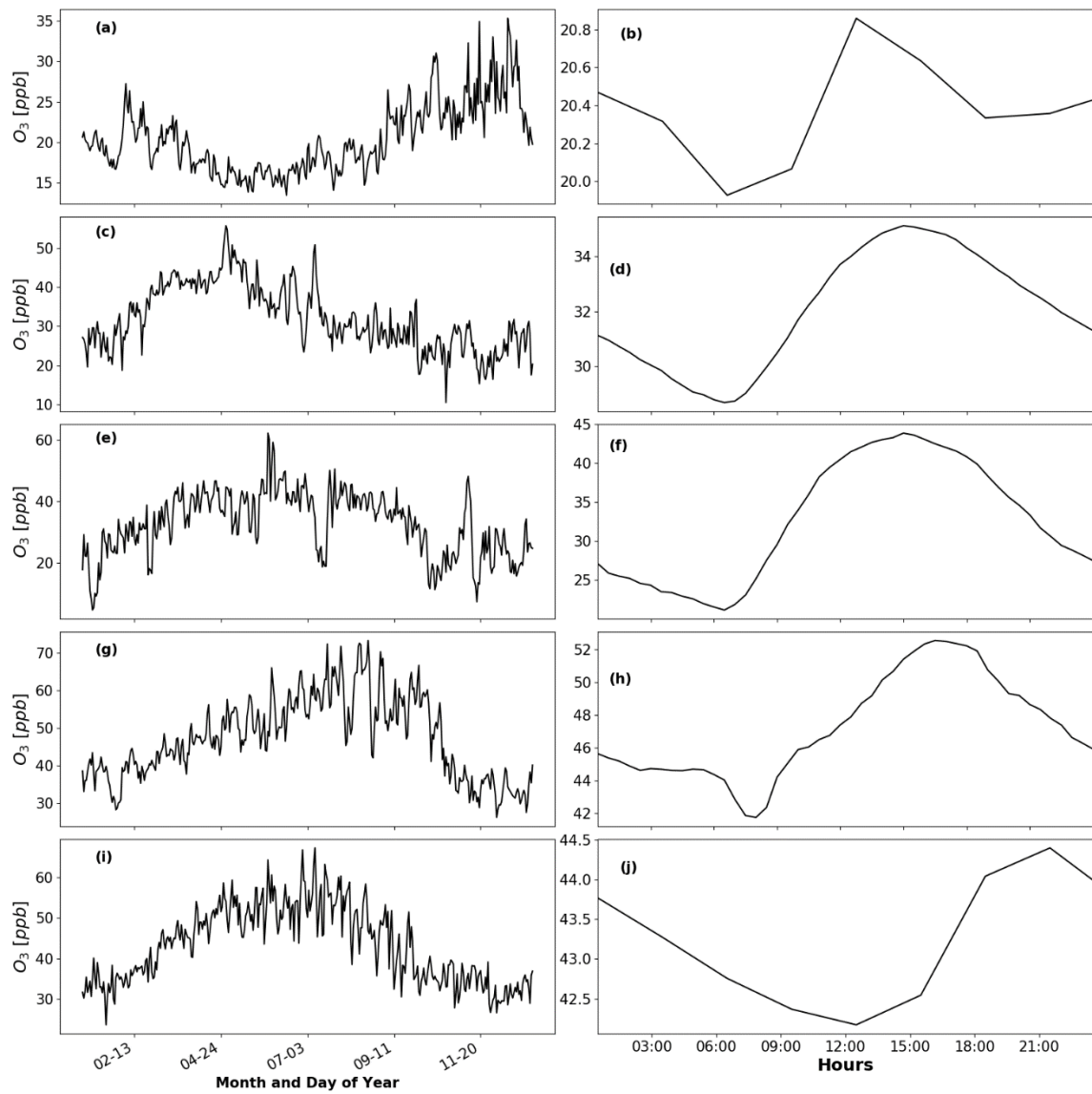


Figure 4.12: Concentration of ozone for an average year and day at each of the five FLUXNET sites, from top to bottom: BR-Sa1, FI-Hyy, IT-Cp2, US-Blo, and US-Ha1.

Chapter 5: Current and future impacts of drought and ozone stress on Northern Hemisphere forests.

This chapter presents the results of a modelling study looking at the role of drought and ozone stress in regulating gas exchange at three forest ecosystems. As global climate changes, droughts are expected to increase in frequency and severity by 50%–200% (Zhao and Dai, 2017). Similarly, ozone concentrations are increasing in the Northern Hemisphere with the increase projected to be as much as 18% by the end of this century (Gaudel et al., 2020; Young et al., 2013). Drought and ozone are both known to reduce plant productivity and increases in both could reduce the carbon sequestration capacity of forests, further exacerbating climate change.

While there are studies focusing on the impacts of drought or ozone as separate stress factors for plants, there are very few that focus on the combined effects of the two. Consequently, the relative contribution of drought and ozone stress to the reduction in plant productivity and gas exchange remains uncertain. Additional uncertainty arises from the fact that the impacts of drought stress and ozone damage on forests depend on the frequency and severity of occurrence as well as a plant's adaptation to a particular stress factor.

This raises questions such as a) what is the relative contribution of drought and ozone stress in reducing GPP and LE fluxes in forests presently? b) how will the impacts of drought stress and ozone damage on forest gas exchange change in future climates? c) do these stress factors act independently or counteract each other? d) is ozone stress tolerated or avoided at the sites under study?

Here, we conduct model experiments based on both avoidance and tolerance approaches to ozone damage, and empirical parameterizations of drought stress in an optimal stomatal conductance-photosynthesis model. We investigate the effects of drought and ozone stress acting independently and in combination on present day observations of GPP and LE fluxes. Subsequently, we apply the understanding obtained from present day experiments to investigate future changes in GPP and LE fluxes at these sites and the roles of drought and ozone stress in future climates using CMIP5 (5th Phase of the Coupled Model Intercomparison Project) and RCP8.5 (representative concentration pathway) climate data. We show that in both present-day and future climates, the impacts of drought stress outweigh the impacts of ozone stress, but *under current conditions* the best model performance was obtained when both stresses were considered.

This work has been published in Global Change Biology, 26(11) on 13 December 2019 (citation: Otu-Larbi et al., 2020; <https://doi.org/10.1111/gcb.15339>). The authors and their contributions are listed below

Frederick Otu-Larbi: Designed research methodology, performed model simulations with FORCAsT, processed model output and performed model-observation comparison. Interpreted results and compiled manuscript together with co-authors.

Adriano Conte: Supplied and processed model input and evaluation datasets, participated in research conceptualisation and interpretation of results, and helped in compilation of manuscript.

Silvano Fares: Designed and conducted observations, supplied observed data for model parameterisations and evaluation, participated in research conceptualisation and interpretation of results, and helped in compilation of manuscript.

Oliver Wild: Participated in research conceptualisation and design, interpretation of results and compilation of manuscript.

Kirsti Ashworth: Designed research methodology, provided guidelines on FORCAsT simulations, interpreted results and compiled manuscripts.

Abstract

Rising ozone (O₃) concentrations, coupled with an increase in drought frequency due to climate change, pose a threat to plant growth and productivity which could negatively affect carbon sequestration capacity of Northern Hemisphere (NH) forests. Using long-term observations of O₃ mixing ratios and soil water content (SWC), we implemented empirical drought and O₃ stress parameterizations in a coupled stomatal conductance–photosynthesis model to assess their impacts on plant gas exchange at three FLUXNET sites: Castelporziano, Blodgett and Hyytiälä. Model performance was evaluated by comparing model estimates of gross primary productivity (GPP) and latent heat fluxes (LE) against present-day observations. CMIP5 GCM model output data were then used to investigate the potential impact of the two stressors on forests by the middle (2041–2050) and end (2091–2100) of the 21st century. We found drought stress was the more significant as it reduced model overestimation of GPP and LE by ~11%–25% compared to 1%–11% from O₃ stress. However, the best model fit to observations at all the study sites was obtained with O₃ and drought stress combined, such that the two stressors counteract the impact of each other. With the inclusion of drought and O₃ stress, GPP at CPZ, BLO and HYY is projected to increase by 7%, 5% and 8%, respectively, by mid-century and by 14%, 11% and 14% by 2091–2100 as atmospheric CO₂ increases. Estimates were up to 21% and 4% higher when drought and O₃ stress were neglected respectively. Drought stress will have a substantial impact on plant gas exchange and productivity, off-setting and possibly negating CO₂ fertilization gains in future, suggesting projected increases in the frequency and severity of droughts in the NH will play a significant role in forest productivity and carbon budgets in future

5.1 Introduction

Tropospheric ozone (O_3) concentrations have doubled in the Northern Hemisphere (NH) since the pre-industrial period (Yeung et al., 2019) and are currently increasing at a rate of 0.5%–2% per year due to changes in the release of precursor compounds from industrial activities (Gaudel et al., 2018; Hartmann et al., 2013). By the end of this century, NH tropospheric O_3 could increase by as much as 18% (Young et al., 2013) and drought frequency by 50%–200% (Zhao and Dai, 2017). Surface O_3 is a powerful phytotoxin (Ainsworth et al., 2012; Ashmore, 2005). It enters leaves through the stomata and damages cell membranes, proteins and DNA through oxidation reactions (Leisner and Ainsworth, 2012; Omasa and Takayama, 2002). O_3 damages the photosynthetic apparatus affecting leaf gas exchange, leading to reductions in plant productivity, growth and biomass accumulation (Ainsworth et al., 2012; Paoletti, 2009).

Plants can respond to O_3 -induced oxidative stress by closing stomata (an avoidance strategy), thus limiting water loss and stomatal O_3 flux, and by synthesizing antioxidants (a tolerance strategy) to regulate reactive oxygen species levels (Andersen, 2003; Pellegrini et al., 2019). Both tolerance and avoidance can be parameterized in vegetation models. The former assumes that plants can detoxify limited doses of O_3 , thus reducing the oxidative stress. Such a pathway has been extensively described by several authors in the phytotoxic O_3 dose PODy metric (De Marco et al., 2016; Emberson et al., 2007; Mills, Hayes, et al., 2011; Mills, Pleijel, et al., 2011). In broad terms, the PODy represents the cumulative quota of O_3 that a plant is not able to detoxify, and that is consequently harmful to the plant's ecophysiological processes. This approach has been shown to perform well across a variety of ecosystems in modelling studies (Clark et al., 2011; Sitch et al., 2007). The latter strategy assumes that plants regulate stomata by directly reducing the exposure of internal plant tissues to O_3 . It has been observed in many experiments that plants fumigated to high concentration of O_3 exhibit a general decrease in stomatal conductance (Wittig et al., 2007). Hoshika, Watanabe, Inada, and Koike (2013) recently hypothesized that plants can optimize their stomatal behaviour to minimize O_3 influx and transpiration while maximizing carbon assimilation, and they reparameterized the optimal stomatal behaviour model developed by Medlyn et al. (2011). This optimal stomatal behaviour theory has also been shown to improve model estimates of photosynthesis and stomatal conductance on different seedling species in field experiments (Hoshika et al., 2013) but has not been widely applied.

Although light and temperature are the main controls on instantaneous photosynthesis rates, drought stress is the limiting environmental factor for global plant photosynthesis and productivity (Nemani et al., 2003) and mortality, diminished growth and reduced productivity have all been observed in plants exposed to drought stress (Basu et al., 2016; Farooq et al., 2009). In response to drought stress, plants avoid oxidative and dehydrative damage to their cells by reducing their stomatal conductance to conserve water (Wilkinson and Davies, 2010), at the cost of reduced photosynthesis (Bréda et al., 1993; Clenciala et al., 1998; Granier et al., 2007).

Both O₃ (Ainsworth et al., 2012; Leisner and Ainsworth, 2012) and drought stress (Nemani et al., 2003; Osakabe et al., 2014) reduce plant growth and productivity thereby reducing the carbon uptake of NH forests. While many studies have focused on the effects of either drought (Egea et al., 2011; Keenan et al., 2010) or O₃ (Ashmore, 2005; Büker et al., 2015; Emberson et al., 2000) stress on forest productivity and gas exchange, few have looked at how these two stressors interact (e.g. Grüters et al., 1995; Hoshika et al., 2013). As drought induces stomatal closure, it is generally thought to minimize O₃ damage since reduced stomatal conductance would reduce stomatal O₃ deposition and uptake (Panek and Goldstein, 2001). However, the interaction between drought stress and O₃ exposure is complex and while some studies show no significant interaction between the two stressors (Wittig et al., 2009), others have shown additive effects with O₃-induced loss of stomatal regulation increasing drought stress impact (Paoletti and Grulke, 2010).

The complexity of modelling O₃ and drought stress impacts on vegetation is compounded by the differing levels of sensitivity of different ecosystems. Mediterranean climates are characterized by high temperature, strong insolation and prolonged drought during the summer, conditions which promote photochemical tropospheric O₃ formation (Millán et al., 2000; Paoletti, 2006). These conditions are expected to increase in frequency and intensity in future (IPCC, 2013). Vegetation in this region has developed adaptations to such stresses, for example, leaf morphology, water conservation by reduced transpiration and the synthesis and emission of biogenic volatile organic compounds including powerful antioxidants and compatible solutes (Calfapietra et al., 2009; Nali et al., 2004; Paoletti, 2006), and may therefore be better able to tolerate such stressors. By contrast, Boreal climates have mild wet summers and cold winters, leading to generally low O₃ concentrations and infrequent droughts. Hence, Boreal forests have not developed strategies to avoid or tolerate either stress and may be more vulnerable to damage than Mediterranean forest ecosystems. These contrasting characteristics make Mediterranean and

Boreal ecosystems ideal for testing the effect of droughts and O₃ on NH forests. As they also make up 9.4% (M'Hirit, 1999) and 17% (Kasischke, 2000) of the Earth's land surface area, respectively, changes in their productivity could have major implications for the global carbon cycle.

Vegetation models play an important role in predicting likely impacts of climate change on forest productivity, but confidence in future projections is dependent on their performance when evaluated against present-day observations. We test the skill of a one-dimensional canopy-exchange model (FORest Canopy-Atmosphere Transfer [FORCAsT]; Ashworth et al., 2015) to reproduce observed carbon assimilation via gross primary productivity (GPP) and water loss via latent heat fluxes (LE) at sites in two Mediterranean and one Boreal evergreen forests.

Here, we investigate the implications of increasing O₃ and drought events for carbon sequestration by the middle (2041–2050) and end (2091–2100) of the 21st century under Representative Concentration Pathway RCP8.5. Our objectives are to determine: (a) defensive strategies used against O₃ stress in Mediterranean and Boreal forests under present-day conditions, (b) the relative contributions and possible interactions of drought and O₃ stress to changes in plant gas exchange, and (c) the potential impacts of future changes in SWC and O₃ concentrations on gas exchange and hence productivity.

5.2 Methods

5.2.1 FORCAsT model

FORCAsT is a 1D model of biosphere–atmosphere chemical exchange which has previously been used to study canopy structure and mixing (Bryan et al., 2012, 2015), stomatal regulation and atmospheric chemistry within and above forest canopies (Ashworth et al., 2015, 2016) and the impact of drought stress on biogenic volatile organic compound emissions and forest gas exchange (Otu-Larbi et al., 2020a). A full description of the FORCAsT model can be found in Ashworth et al. (2015). Three different coupled photosynthesis-stomatal conductance ($A-g_s$) models have since been incorporated into FORCAsT giving users the flexibility to select the most appropriate for the ecosystem of interest and the meteorological and physiological observations available (see Otu-Larbi et al., 2020b for full details).

Here, we describe the parameterizations of drought and O₃ stress used in this study. We apply the Medlyn et al. (2011) optimal stomatal behaviour modification of the

Farquhar, Von Caemmerer, and Berry (1980) photosynthesis model in which photosynthesis rate (A ; $\mu\text{mol m}^{-2} \text{s}^{-1}$) is the minimum of two limiting factors: electron transport and carboxylation rate. Stomatal conductance (g_s) is modelled assuming that stomatal aperture is regulated to maximize carbon gain while simultaneously minimizing water loss (Medlyn et al., 2011):

$$g_s \approx g_o + \left(1 + \frac{g_1}{\sqrt{D}}\right) \frac{A}{C_s} \quad 5.1$$

where g_o ($\text{mol m}^{-2} \text{s}^{-1}$) is the residual stomatal conductance when A approaches zero and g_1 is a fitted parameter representing the sensitivity of g_s to A . The values of g_o and g_1 are determined at the species- or plant functional type (PFT)-specific level from experimental data. Here, we use values obtained from Lin et al. (2015) and De-Kauwe et al. (2015), respectively, as indicated in Table 5.2. D (kPa) is the vapour pressure deficit calculated by FORCAsT and C_s ($\mu\text{mol/mol}$) is the CO_2 concentration at the leaf surface.

LE (W/m^2) is estimated following Lhomme et al. (1998) as:

$$\left(\frac{\rho C_p}{\gamma}\right) g e_v (e_s - e_a) \quad 5.2$$

where ρ (kg/m^3) is the air density, C_p ($\text{J kg}^{-1} \text{K}^{-1}$) is the specific heat capacity of air at constant pressure, γ (kPa/K) is the psychrometric constant (the ratio of C_p to latent heat of vaporization of water), e_s and e_a (kPa) are the saturated vapour pressure at leaf temperature and the air water vapour pressure, respectively, and $g e_v$ (m/s) is an equivalent conductance for horizontal vapour transfer estimated as:

$$g e_v = 2LAI_i \left(\frac{g_{bw} g_{sw}}{g_{bw} + g_{sw}}\right) \quad 5.3$$

where LAI_i (m^2/m^2) is the leaf area index at model layer i , g_{bw} ($\text{mol m}^{-2} \text{s}^{-1}$) and g_{sw} ($\text{mol m}^{-2} \text{s}^{-1}$) are the leaf boundary layer and stomatal conductance to water respectively.

5.2.2 Soil moisture stress

Accounting for drought stress impacts on plants in vegetation models is challenging. The response depends on soil characteristics, climatic conditions and PFT. Metrics based on SWC, soil water potential and predawn leaf water potential have all been developed to assess plant water status (e.g. see Keenan et al., 2010; Zhou et al., 2014). Predawn leaf water potential provides the best measure of plant water status, but the lack of long-term observations makes these metrics difficult to apply in modelling studies. In contrast, SWC, while not as robust, is measured at most forest sites and can also be derived from satellite data making it easier to use in model parameterizations and simulations.

In this study, the effect drought stress on A and g_s is assumed to be the result of biochemical and stomatal limitations as demonstrated in previous studies (e.g. see Egea et al., 2011). A soil moisture stress function was incorporated into the photosynthesis module in FORCAsT as described by Otu-Larbi, Conte, et al. (2020). The stress function, β , ranges between 1 (in the absence of drought stress) and 0 (at wilting point) and is calculated from:

$$\beta = \begin{cases} 1 & \text{for } \theta \geq \theta_c \\ \left[\frac{(\theta - \theta_w)}{(\theta_c - \theta_w)} \right]^q & \text{for } \theta_w < \theta < \theta_c \\ 0 & \text{for } \theta < \theta_w \end{cases} \quad 5.4$$

where θ (m^3/m^3) is the volumetric soil moisture, θ_w is the wilting point (m^3/m^3) and θ_c is a critical soil moisture content above which drought stress is found not to affect plant–atmosphere gas exchange (Egea et al., 2011; Keenan et al., 2010). q is a site-specific empirical factor describing the non-linearity of the effects of soil drought stress on tree physiological processes. θ_c , θ_w and q were calculated from soil texture data (i.e. sand, clay and silt fractions) or calibrated using long-term soil moisture observations at each site as detailed in Otu-Larbi, Conte, et al., 2020 and provided in Table 5.2.

The water-stressed values of carboxylation (V_{cmax*}) and electron transport (J_{max*}) rate are then calculated from the maximum rates (V_{cmax} and J_{max}) as:

$$V_{cmax*} = V_{cmax} \times \beta \quad 5.5a$$

$$J_{max}^* = J_{max} \times \beta \quad 5.5b$$

and these values are applied to calculate the impact of soil moisture deficit on photosynthesis. The stomatal conductance then becomes:

$$g_s \approx g_o + \left(1 + \frac{g_1\beta}{\sqrt{D}}\right) \frac{A}{C_s} \quad 5.6$$

5.2.3 Incorporating O₃ damage

The reduction in photosynthesis and plant productivity due to O₃ cellular damage is incorporated into FORCAsT following two assumed strategies.

5.2.3.1 O₃ avoidance (AVD)

O₃ avoidance (stomatal closure) follows Hoshika, Watanabe, et al. (2013). The details of the mathematical formulation are provided in Medlyn et al. (2011) and Hoshika, Watanabe, et al. (2013) and only a short summary is given here. The O₃ flux through the stomata (F_{st} : mol m⁻² s⁻¹) is given by:

$$F_{ST} = \frac{g_s}{1.6} ([O_3]_{air} - [O_3]_{leaf}) \quad 5.7$$

where $[O_3]_{air}$ is the ambient O₃ concentration (ppbv) and $[O_3]_{leaf}$ is the O₃ concentration inside the leaf, usually assumed negligible (e.g. Laisk et al., 1989). 1.6 is the ratio of the diffusion coefficients of water vapour and O₃.

In the optimal stomatal behaviour theory, the control of leaf gas exchange may be considered optimal when it maximizes carbon gain while simultaneously minimizing water loss. Assuming stomata act to minimize O₃ damage in a similar manner, then the optimal stomatal conductance can be found from a modification of Equation (5.6):

$$g_s \approx g_o + \left(1 + \frac{g_1\beta}{\sqrt{D+(k/1.6)[O_3]_{air}}}\right) \frac{A}{C_a} \quad 5.8$$

where k (mol H₂O/mol O₃) is the ratio of the marginal water cost of plant carbon gain to the marginal O₃ damage of plant carbon gain and is calculated as:

$$0.1 \frac{1.6D}{[O_3]_{air}} < k < \frac{1.6D}{[O_3]_{air}} \quad 5.9$$

where D and $[O_3]_{air}$ are the long-term mean VPD (kPa) and $[O_3]_{air}$ respectively. The value of k for each site is provided in Table 5.2.

5.2.3.2 O₃ tolerance (TLR)

Plants' strategy to tolerate O₃ consists of enzymatic processes and chemical reactions to detoxify photooxidants. O₃-tolerant trees (e.g. *Pinus strobus*) have been shown to have higher glutathione reductase and ascorbate peroxidase than O₃-sensitive species (Chevone, 1991). This prevents oxidative damage to the photosystem, enabling plants to maintain photosynthesis at higher doses of O₃. Here, we assume that the instantaneous uptake of O₃ by plants only leads to an immediate suppression of leaf photosynthesis above a critical stomatal O₃ flux threshold. The decrease in leaf photosynthesis from its potential maximum is therefore proportional to the flux above that critical flux. The reduction factor, F , is calculated following Pleijel et al. (2004) as:

$$F = 1 - \alpha \cdot \max[F_{O_3} - Y, 0] \quad 5.10$$

where F_{O_3} (nmol m⁻² s⁻¹) is the instantaneous flux of O₃ into the leaf, α (mmol⁻¹ m⁻²) is a PFT-specific parameter indicating the fractional reduction of photosynthesis with O₃ uptake by leaves and Y is the PFT-specific O₃ flux threshold above which O₃ damage occurs. In this study, we use α values of 0.04 and 0.02 for broadleaf and needleleaf trees respectively (Clark et al., 2011) and a threshold of 1 nmol m⁻² s⁻¹ for forest trees as recommended by Mills et al. (2011a) and Mills et al. (2011b). F_{O_3} is calculated as:

$$F_{O_3} = \frac{[O_3]_{air}}{r_a + kO_3/g_s} \quad 5.11$$

where $[O_3]_{air}$ is the ambient O₃ concentration (ppbv), r_a (s/m) is the combined aerodynamic and boundary layer resistance of the leaf surface, kO_3 (1.67) is the ratio of the leaf resistance for O₃ to water vapour (Sitch et al., 2007) and g_s (m/s) is the leaf conductance for H₂O.

The O₃-affected values of photosynthesis rate (A^*) and stomatal conductance (g_s^*) are estimated as:

$$A^* = A \times F \quad 5.12a$$

$$g_s^* = g_s \times F \quad 5.12b$$

where A and g_s are the (potential) photosynthesis rate and stomatal conductance in the absence of O₃.

5.2.4 Scaling up to the canopy

GPP is estimated as:

$$GPP = A_n + R_d \quad 5.13$$

where A_n ($\mu\text{mol m}^{-2} \text{s}^{-1}$) is the net photosynthesis (including the effects of drought and O₃ stress) and R_d ($\mu\text{mol m}^{-2} \text{s}^{-1}$) is the canopy dark respiration which is estimated by the model. Leaf-level A_n , GPP and LE in each layer of the canopy (i) were scaled by LAI at each model level (LAI_i) and summed over all model layers (n) to obtain canopy-scale (c) estimates of A , GPP and LE.

$$A_c = \sum_{i=1}^n A_i \times LAI_i \quad 5.14a$$

$$GPP_c = \sum_{i=1}^n GPP_i \times LAI_i \quad 5.14b$$

$$LE_c = \sum_{i=1}^n LE_i \times LAI_i \quad 5.14c$$

5.2.5 Study sites and data

Three evergreen NH forest sites with long-term continuous measurements of meteorology, O₃ concentrations, GPP and LE fluxes were used in this study: a Holm oak forest at Castelporziano (CPZ; Fares, Alivernini, Conte, and Maggi, 2019), a Boreal pine forest at Hyytiälä (HYY; Hari et al., 2013) and a Ponderosa pine forest at Blodgett (BLO;

Sorooshian, Li, Hsu, and Gao, 2012). These sites are part of the FLUXNET network (Pastorello et al., 2017). Full details of the sites, and the data and model parameters used are provided in Table 5.2

Observations of photosynthetically active radiation (PAR; $\mu\text{mol m}^{-2} \text{s}^{-1}$), air temperature (K), CO_2 concentration (ppm), volumetric SWC (m^3/m^3), wind speed (m/s) and direction (degrees clockwise from North), relative humidity (RH; %) and atmospheric pressure (Pa) were obtained for each site from the FLUXNET-2015 data set at a temporal resolution of 30 min. O_3 data were obtained directly from site lead investigators. The number of years for which data are available at each site is given in Table 5.2.

The Castelporziano Estate ($41^\circ42'\text{N}$, $12^\circ21'\text{E}$) is located 25 km SW of Rome, Italy, and 1.5 km from the Mediterranean coast. The forest is dominated by evergreen Holm oak (*Quercus ilex*), and the average LAI and mean tree height are $3.69 \text{ m}^2/\text{m}^2$ and 16 m respectively (Fares et al., 2019). The climate at CPZ is classified as Csa (Mediterranean: mild with dry, hot summer) according to the Köppen climate classification (Köppen, 1923). Precipitation mainly occurs in autumn and winter with little or none in the summer, resulting in annual droughts. Average soil moisture (Figure 5.1) drops from $0.20 \text{ m}^3/\text{m}^3$ in the winter and spring to $\sim 0.10 \text{ m}^3/\text{m}^3$ during the summer. The long-term (1997–2009) annual average precipitation is 780 mm and the mean temperature is 15.6°C . As shown in Figure 5.1, O_3 mixing ratios in this ecosystem exhibit strong seasonality with higher concentrations observed during the warm, dry summer months (up to 50 ppb) than the winter (as low as 20 ppb). Similarly, PAR has higher values in the summer ($\sim 600 \text{ W}/\text{m}^2$) than winter ($\sim 100 \text{ W}/\text{m}^2$).

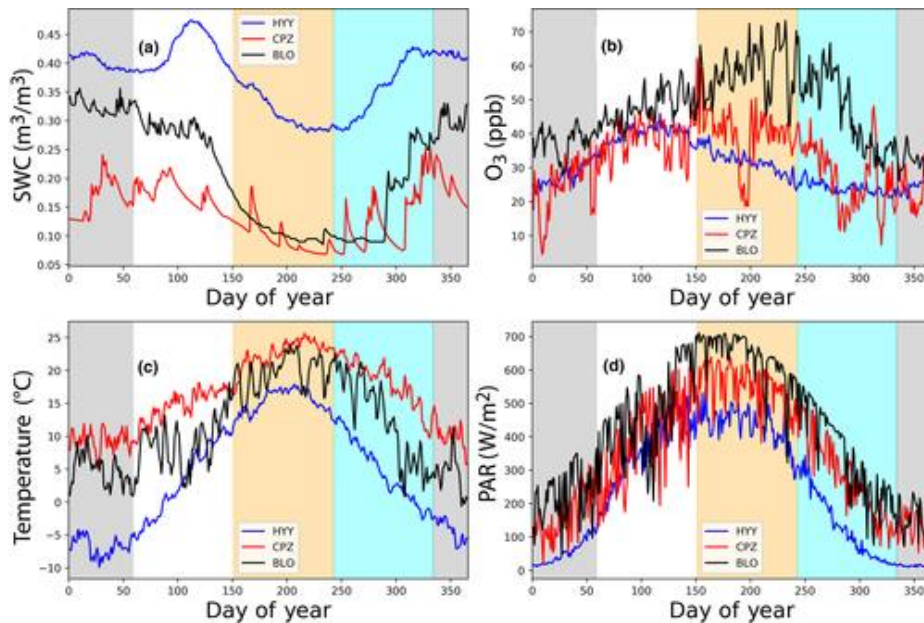


Figure 5.1: Average annual profiles of observed (a) volumetric soil water content (SWC), (b) O₃ mixing ratios, (c) air temperature and (d) photosynthetically active radiation at: Castelporziano (CPZ; red lines), Hyytiälä (HYT; blue lines) and Blodgett (BLO; black lines). The coloured backgrounds denote meteorological seasons: winter (grey), spring (white), summer (orange) and autumn (cyan)

BLO Forest (38°53'N 120°37'W) is located at 1,315 m a.s.l. in the Sierra Nevada Mountains of California, United States. Ponderosa pine (*Pinus ponderosa* L.) dominates with average LAI and tree height of 3.20 m²/m² and 6 m (Law and Gower, 2001) respectively. This site also has a Koppen climate classification of Csa; the summers are dry with rainfall only occurring in the winter and spring (except during 2003 and 2004 when 38 and 22 mm of summer rain fell respectively). Data from 1997 to 2007 show an annual mean precipitation and temperature of 1,230 mm and 11.1°C respectively. Summer drought is a yearly occurrence. Figure 5.1 shows that soil moisture content follows the precipitation pattern with a peak of ~0.30 m³/m³ in the winter–spring and a summer low of ~0.10 m³/m³. The seasonal pattern of PAR, temperature and O₃ concentrations is similar with highest values in the summer and lowest in winter.

The Station to Measure Ecosystem–Atmosphere Relations (SMEAR II) located in HYT, Finland (61°51'N, 24°17'E; 181 m a.s.l.; Hari and Kulmala, 2005), is a Boreal coniferous forest with a Koppen climate classification of Dfc (Continental subarctic climate). Seventy-five percent of this forest constitutes Scots pine (*Pinus sylvestris*) with Norway Spruce (*Picea abies*) and deciduous trees making up the remainder (Zhou et al., 2017). Average LAI is ~2.7 m²/m² and the canopy height is ~23 m. Average annual

mean air temperature and precipitation are 3.8°C and 709 mm, respectively, for the period 1996–2014. Droughts are infrequent but occurred here during 2003 (Ciais et al., 2005) and 2006 (Gao et al., 2016). Temperature and PAR peak in the summer. O₃ mixing ratios are lowest in the winter (25 ppb) and reach a peak of 40 ppb during spring. Soil moisture is highest in spring (~0.45 m³/m³) and lowest in summer (~0.30 m³/m³). Further details of the canopy and site characteristics can be found in Hari and Kulmala (2005) and Hari et al. (2013).

5.2.6 Impact of future changes in SWC and O₃ concentrations

We investigate the potential impacts of climate change on GPP and LE fluxes in the middle (2041–2050) and end (2091–2100) of the 21st century. Monthly mean data for surface O₃ mixing ratios, SWC, solar radiation, RH, wind speed, Pa, temperature and carbon dioxide (CO₂) were obtained from general circulation models (GCMs) participating in the 5th Phase of the Coupled Model Intercomparison Project (CMIP5; Taylor et al., 2012) and Atmospheric Chemistry and Climate Model Intercomparison Project. Output from different participating models differs in space and time (Taylor et al., 2012; see <https://portal.enes.org/data/enes-model-data/cmip5/resolution> for a list of models and their characteristics). Only the seven models (from five modelling centres) that provide both O₃ mixing ratios and SWC were selected. Details of these are provided in Table 5.3.

Variables were obtained from historical GCM simulations for 1850–2005 and GCM future simulations for 2006–2100 following RCP8.5, a scenario in which emissions of CO₂ follow an exponential growth trajectory throughout the century (Riahi et al., 2011), with concentrations increasing to 936 pspm and nominal anthropogenic forcing to 8.5 W/m² by 2100 (IPCC, 2014).

Comparing historical model output and observations shows systematic (but differing) biases in all seven models (see Figure 5.7). We used historical data for 1996–2005 (corresponding to our observations) to bias-correct each model for 2006–2100, before applying it to drive FORCAsT simulations. We calculated monthly averages for each variable at each site from both observations and GCM data for the 1996–2005 period. Monthly relative bias correction factors were calculated for each variable and month as follows:

$$RBF_i = \frac{OBS_i}{HMOD_i} \quad 5.15$$

where RBF_i , OBS_i and $HMOD_i$ represent the relative bias factor, observed values and historical model output value of a variable for each month, i .

Future GCM model output for 2041–2050 and 2091–2100 was then bias corrected assuming that historical and future model biases are similar:

$$BC_i = FMOD_i \times RBF_i \quad 5.16$$

where BC_i is the bias-corrected data, $FMOD_i$ is the original GCM future projection and RBF_i is the relative bias correction factor for month of the year, i . The bias-corrected data for each site are shown in Figure 5.8- Figure 5.10.

5.2.7 Model configurations and experiments

We evaluate FORCAsT performance and determine the most suitable O_3 -stress response strategy at each site from present-day simulations, driven with site observation data. FORCAsT simulations driven by future climate are used to investigate potential changes in forest productivity due to future changes in drought and O_3 stress. Six model simulations were performed for each site. An initial control (CTR) simulation was run without either O_3 or drought stress and modelled GPP and LE were compared against observations. We then tested the effect of drought stress only (CTR + Dr) and each of the O_3 -stress responses (TLR and AVD), comparing the results of each simulation against CTR as well as observations. Finally, we tested the impact of combining O_3 and drought stress (AVD + Dr and TLR + Dr). Although observations at HYY span the period from 1997 to 2014, we use data for only 2 years for consistency with CPZ and BLO. We select 2005–2006 for the analysis because 2006 was a drought year (Gao et al., 2016) and therefore allows for assessment of drought impact. An evaluation of FORCAsT performance at HYY for the entire 1997–2014 period is shown in Figure 5.11.

Four simulations were conducted using bias-corrected future meteorological data from each GCM model at each site to test the impact of drought and O_3 on GPP and LE fluxes. These simulations tested the effects of (a) not accounting for either O_3 or drought stress in the model (FUT), (b) including only drought stress (FUT + Dr), (c) including only O_3 stress (FUT + O_3) and (d) including both (FUT + Dr O_3). The O_3 impacts were modelled using the strategy that provided the best present-day model-observation fit.

5.3 Results

Droughts occur almost annually at BLO and CPZ but rarely at HYY, as shown in Figure 5.1. O₃ concentrations are also higher at the Mediterranean sites. We present the impacts of drought and O₃ stress on modelled GPP and LE under present-day conditions in Section 3.1. Model performance is evaluated against observed GPP and LE fluxes for the three sites from the FLUXNET-2015 data set. We determine the relative magnitude of the impacts of drought and O₃ on modelled GPP and LE and assess which defensive mechanism (tolerance [TLR] or avoidance [AVD]) is most appropriate for each ecosystem. Section 3.2 focuses on the potential impacts of drought and O₃ stress on future GPP and LE and the implications for future carbon sink.

5.3.1 Current impacts of drought and O₃ on GPP and LE

Table 5.1 and Figure 5.2 show the annual average observed and simulated GPP and LE for each site calculated for each 2-year simulation period. Under present-day conditions, CPZ and BLO are more productive than HYY; observed GPP at HYY was about half of that observed at CPZ and ~70% of that at BLO. LE at BLO was approximately 35% and 60% higher than the observed values at CPZ and HYY respectively.

Table 5.1: Summary of observed and modelled annual cumulative gross primary productivity (GPP) and latent heat fluxes (LE) in present-day simulations. Observations (OBS) and best-fit model simulations are highlighted in bold

SITE	Cumulative GPP (g (C) m ⁻² year ⁻¹)			Cumulative LE (W m ⁻² year ⁻¹)		
	CPZ	BLO	HYY	CPZ	BLO	HYY
OBS	2120	1629	1084	305	465	196
CTR	2774	2191	s1382	402	604	231
CTR+Dr	2306	1900	1244	324	535	210
AVD	2749	2093	1377	380	552	220
AVD+Dr	2291	1818	1239	311	495	201
TLR	2543	2020	1347	372	569	226
TLR+Dr	2171	1772	1217	308	510	207

In general, FORCAsT overestimated GPP and LE across all three sites in CTR simulations when the effects of stress were excluded. Model overestimation was higher when drought stress was excluded (CTR) than O₃ stress irrespective of whether TLR or AVD was assumed. Drought stress has a greater impact on model estimates of GPP and LE at CPZ and BLO than at HYY due to the lower SWC and frequent drought at these sites. At CPZ and BLO, the inclusion of drought stress alone in FORCAsT (CTR + Dr) led to a 20% average reduction in model overestimation of GPP and LE but only a 10% reduction at HYY.

The impact of including O₃ stress differed between individual sites and the choice of O₃ stress parameterization adopted but generally improved the model fit to observations for both GPP and LE compared to CTR simulations. O₃ stress alone produced better agreement between modelled and observed GPP at all sites when tolerance rather than avoidance was assumed. For example, while TLR led to 11% reduction in model overestimation of GPP at CPZ, AVD only led to a 1% reduction. Like drought stress, O₃ stress alone has greater impacts on plant productivity at the Mediterranean forests than the Boreal forest.

Inclusion of drought and O₃ stress in the model (AVD + Dr and TLR + Dr) produced the lowest deviations and hence the best fit to observations at all study sites for both GPP and LE. For GPP, TLR + Dr simulations, shown in grey bars, fitted the observations better at all sites. LE estimates from AVD + Dr provided lower deviations from observations at BLO and HYY while TLR + Dr was the closest to observed values at CPZ. The combined effect of the two stresses was less than the sum of the individual stresses at all sites. For example, while CTR + Dr and TLR led to 22% and 11% reductions in GPP, respectively, their combined effect (TLR + Dr) was ~5% less (a 28% reduction). Similar results were obtained for all sites for both TLR and AVD parameterizations.

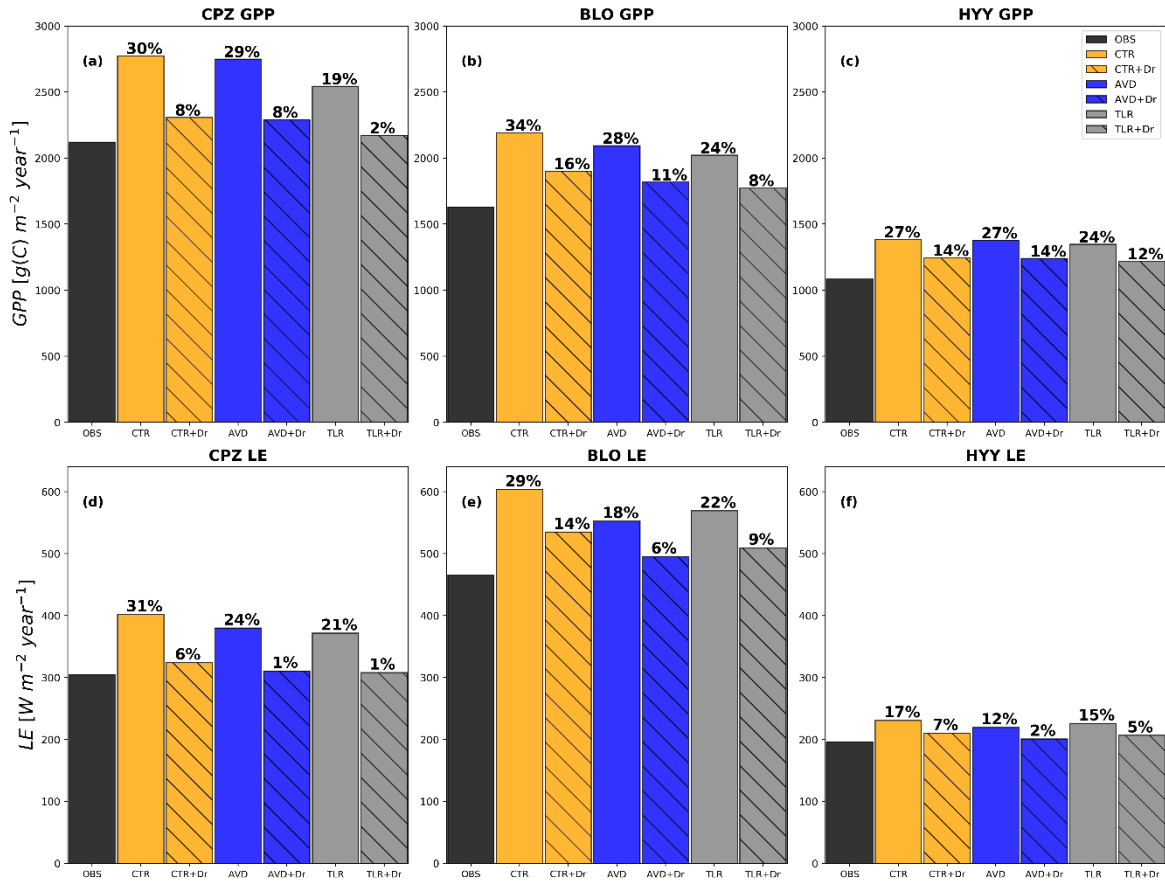


Figure 5.2: Annual mean gross primary productivity (GPP) (a–c) and latent heat flux (LE) (d–f) for Castelporziano (CPZ), Blodgett (BLO) and Hyttiälä (HYY). Observed (OBS) values are shown with black bars while model results are coloured as follows: orange (CTR and CTR + Dr), blue (AVD and AVD + Dr) and grey (TLR and TLR + Dr), with striped bars indicating drought stress. The percentage difference between modelled and observed values for each simulation is shown at the top of the bars. Positive values indicate model overestimation

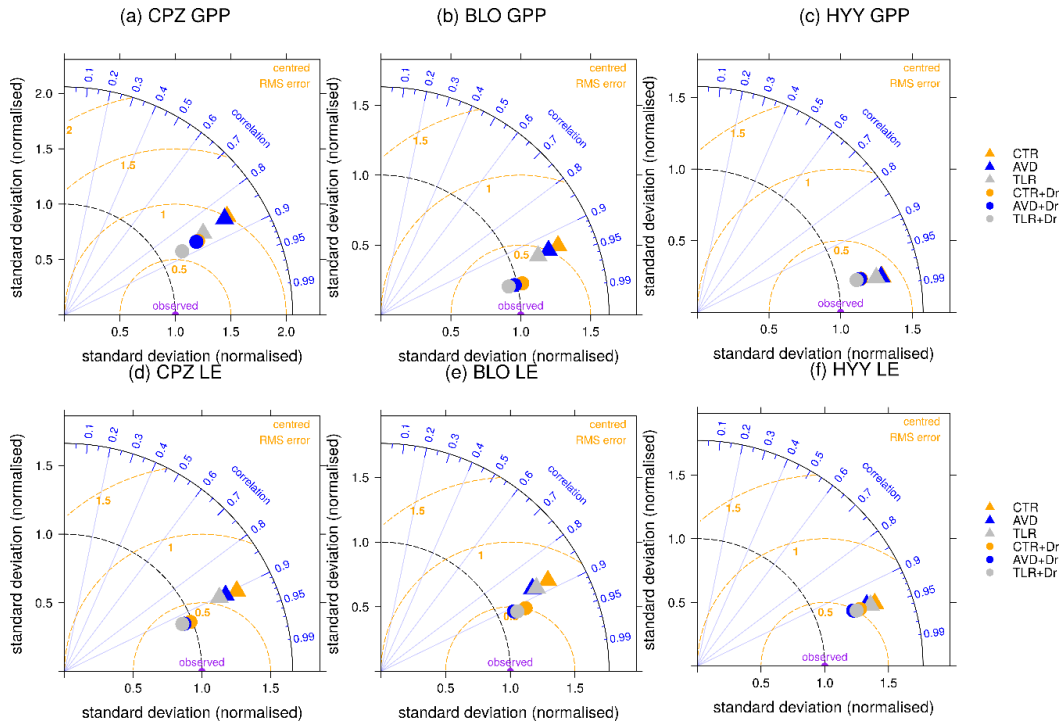


Figure 5.3: Taylor diagram showing model output statistics from FORCAsT simulations. Panels a, b and c show output statistics for gross primary productivity (GPP) at CPZ, BLO and HYY respectively while panels d, e and f show output statistics for latent heat flux (LE) at the same sites. Black and orange dashed curves and blue lines show normalized standard deviation (SD), centred root mean squared error (RMSE) and correlation coefficients (r) respectively against observations. Observed GPP and LE have $SD = 1.0$, $RMSE = 0.0$ and $r = 1.0$ (purple circle). The summary statistics for each model simulation are shown by orange (CTR and CTR + Dr), blue (AVD and AVD + Dr), and grey (TLR and TLR + Dr). Triangles represent simulations without drought stress and circles those with. Note the difference in scale of standard deviation on panel (a)

The Taylor diagrams (Taylor, 2001) presented in Figure 5.3 show three model performance statistics: correlation coefficient (r : blue lines), normalized standard deviation (SD : black dashed lines) and centred root-mean-square error (RMSE; orange dashed lines). A model simulation which exactly reproduces observations would lie on top of the observations (indicated by a purple dot on Figure 5.3). Therefore, the closer a model's performance statistics are to that of the observations on the Taylor diagram, the better its performance. Figure 5.3 shows high correlation coefficients for all model simulations for both GPP (0.85–0.98) and LE (0.88–0.95) indicating that FORCAsT reproduces the observed seasonal cycles for all sites. At CPZ, FORCAsT simulations showed better correlation with observations for LE than GPP (Figure 5.3a,d) whereas the reverse was true at both BLO and HYY. SD and RMSE were lower for both GPP and LE across all sites when drought stress was included (i.e. CTR + Dr, AVD + Dr and TLR + Dr), further confirming

the results shown in Figure 5.2. As seen from Figure 5.2 and Figure 5.3 and Table 5.1, TLR + Dr simulations had the lowest deviations between model and observations in addition to high correlation coefficients and lower RMSE suggesting that this is the best model parameterization for estimating GPP. For LE, TLR + Dr performed better at CPZ than any other model configuration while AVD + Dr provided the best model-observation fit at BLO and HYY. Considering all the model statistics, TLR + Dr was found to be the parameterization that best simulated observed GPP and LE and was therefore chosen to study the impacts of future changes in SWC and O₃ on plant productivity and gas exchange.

5.3.2 Future impacts of drought and O₃ stress

To assess how closely FORCAsT was able to reproduce observed GPP and LE driven by meteorological and O₃ data from each GCM, a test simulation was conducted for each site using bias-corrected ‘historical’ data for the period 1996–2005 (Figure 5.8). Figure 5.4 shows that although there were differences in the GPP and LE estimated from each individual GCM, the ensemble means closely matched estimates made using observed meteorology. The good performance of the historical GCM driving data relative to the observed driving data is further confirmed by low RMSEs, high correlation coefficients and low *SDs* (see Taylor diagrams in Figure 5.12), lending confidence in our use of ensemble mean driving data for future simulations.

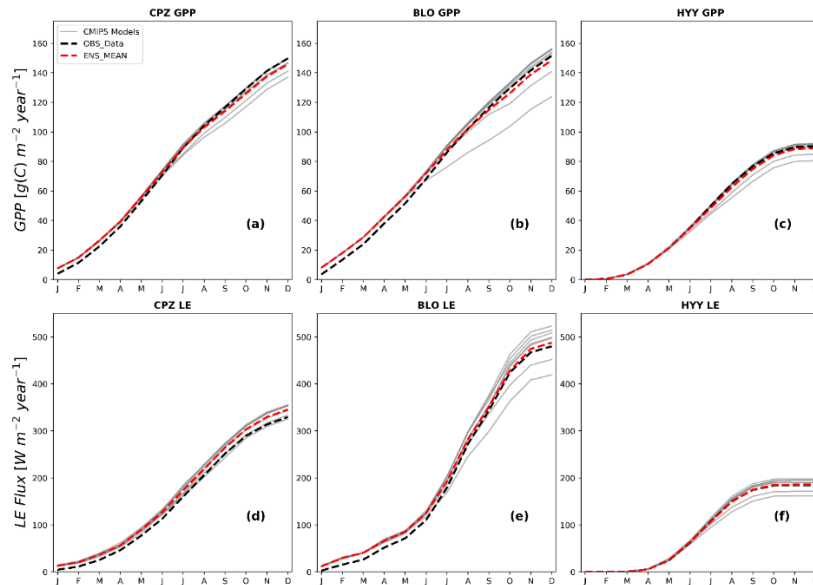


Figure 5.4: Estimates of gross primary productivity (GPP; a–f) and latent heat flux (LE; d–e) at CPZ, BLO and HYY respectively using bias-corrected historical (1996–2005) general circulation model (GCM) output data compared with estimates from observed driving data. Ensemble mean is indicated by red dashed lines while present-day estimates are shown in black dashed lines. Individual GCM estimates are shown by grey lines

5.3.3 Changes in GPP and LE in future

Figure 5.5 shows ensemble means of modelled estimates of GPP and LE using bias-corrected GCM data and TLR + Dr (the best model configuration) at each site for 2041–2050 and 2091–2100 as well as present-day estimates based on historical GCM and observed driving data. GPP and LE estimates for individual ensemble members for 2041–2050 and 2091–2100 are presented in Figure 5.15 and Figure 5.16 and show that while there is general agreement about changes to mid-century, there is greater uncertainty towards the end of the century. They also show good agreement between ensemble members at the beginning of the year, but they begin to diverge during at the start of the growing season which also coincides with changes in SWC and O_3 .

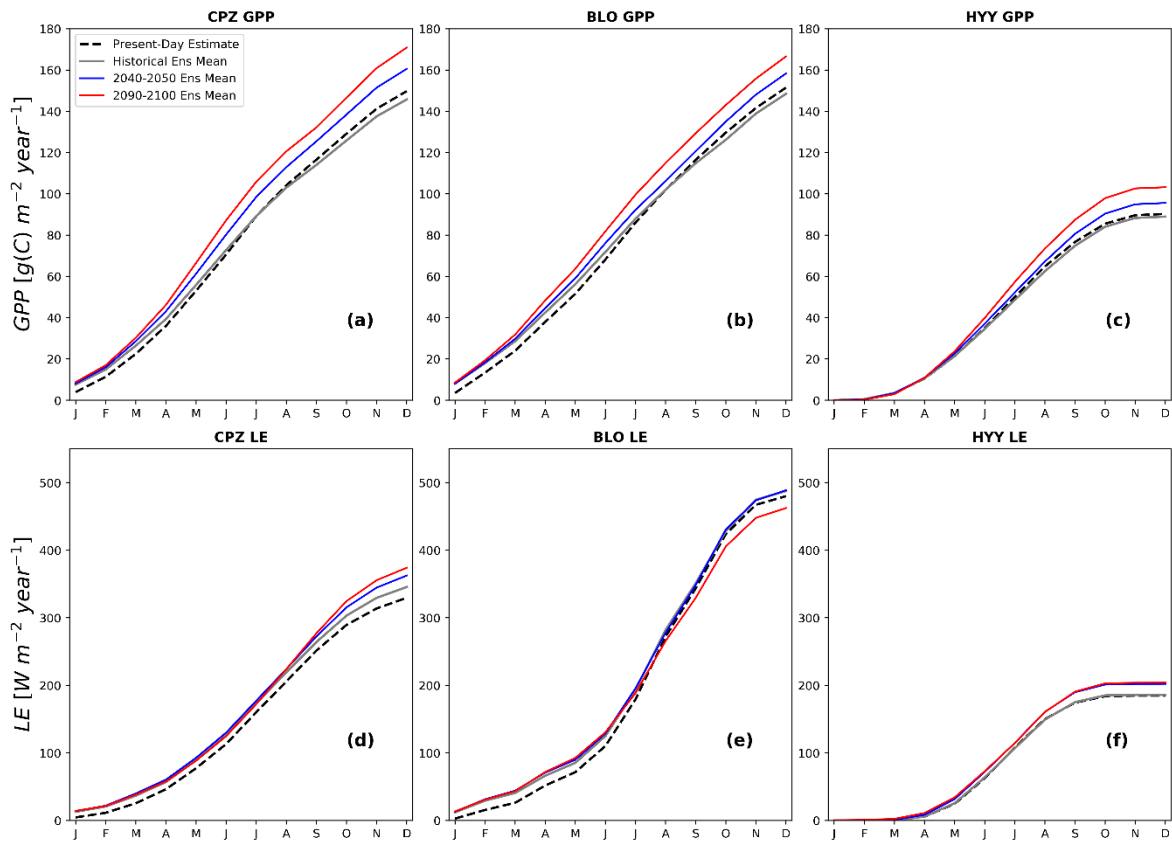


Figure 5.5: Ensemble mean estimates of average yearly gross primary productivity (GPP) (a–c) and latent heat flux (LE) (d–f) compared with present-day estimates using observed driving data for CPZ, BLO and HYY respectively. Ensemble means for 2041–2050 and 2091–2100 are indicated by blue and red lines respectively while present-day estimates are shown by grey lines (historical general circulation model driving data) and black dashed lines (observed driving data)

GPP is projected to increase by the middle and end of the 21st century at all three sites (Figure 5.5). Relative to present-day estimates, GPP could increase by 7% at CPZ (from 150 to 161 g C m⁻² year⁻¹), 5% at BLO (from 151 to 158 g C m⁻² year⁻¹) and 8% at HYY (from 90 to 96 g C m⁻² year⁻¹) by 2041–2050 while LE is projected to increase by 10%, 2% and 9% for the same period. By 2091–2100, GPP could increase by 14% at CPZ and HYY and 11% at BLO while LE increases at CPZ and HYY by 13% and 10% relative to present-day estimates but decreases by 4% at BLO. For CPZ and BLO, these projected increases in GPP and LE occur throughout the year, but at HYY, the increase starts in spring. However, as shown by Figure 5.15 and Figure 5.16, there is uncertainty about the projected GPP and LE fluxes in future as individual GCM ensemble members provide diverse estimates. The uncertainty is higher between 2091 and 2100 (Figure 5.16) than 2041–2050 (Figure 5.15). The projected decrease in ensemble mean LE at BLO is due to lower LE estimated by several individual GCM ensemble members as shown on Figure 5.15. HYY and CPZ are expected to experience higher percentage increases in productivity between the middle and end of the century than BLO although the overall productivity level at HYY will remain lower than those at CPZ and BLO. The higher productivity projected for CPZ and HYY could be due to bigger increase in projected winter and spring temperatures at the two sites (Figure 5.9 and Figure 5.10), which is likely to extend the length of the growing season at these sites.

5.3.4 Impacts of drought and O₃ through the 21st century

Figure 5.6 shows the impact of drought and O₃ stress on future GPP and LE fluxes by mid-century (2041–2050) and end of century (2091–2100). As for present-day simulations, modelled GPP and LE at all three sites were highest when neither the effects of drought or O₃ stress were included. Modelled GPP and LE were lowest when both were included (FUT + DrO₃), with the impact of drought stress (FUT + Dr) again far outweighing that of O₃ (FUT + O₃).

The impact of drought stress on modelled GPP and LE flux increases through the century. As shown in Figure 5.6, drought stress has a higher impact on estimated LE than GPP at all three sites between 2041 and 2050, but this is reversed towards the end of the century as drought stress leads to a greater reduction on GPP than LE at CPZ and BLO and has similar impacts on GPP and LE at HYY between 2091 and 2100. For both periods, drought stress is projected to have higher impacts at the Mediterranean forests than the Boreal forest. This is similar to present-day simulations and indicates that the relative

impacts of drought stress in different climatic regions are unlikely to change. For instance, drought stress causes a reduction of 21% and 19% in GPP and LE, respectively, at CPZ between 2091 and 2100 compared to 16% and 18% between 2041 and 2050. Similarly, at BLO, GPP and LE are reduced by 18% and 17%, respectively, in 2091–2100 compared to a projected decrease of 14% and 16% by mid-century. There is negligible difference between the impacts of drought stress on either GPP or LE at the end and middle of the century at HYY.

The addition of O₃ stress based on the tolerance parameterization (FUT + O₃) reduced estimated GPP and LE at all three sites compared to FUT, although the reduction was more pronounced at CPZ and BLO than at HYY and for 2041–2050 than 2091–2100. GPP could be reduced by 3%–4% due to O₃ damage by mid-century but only 2%–3% (1% less) by the end of the century, with similar impacts seen on LE across all sites.

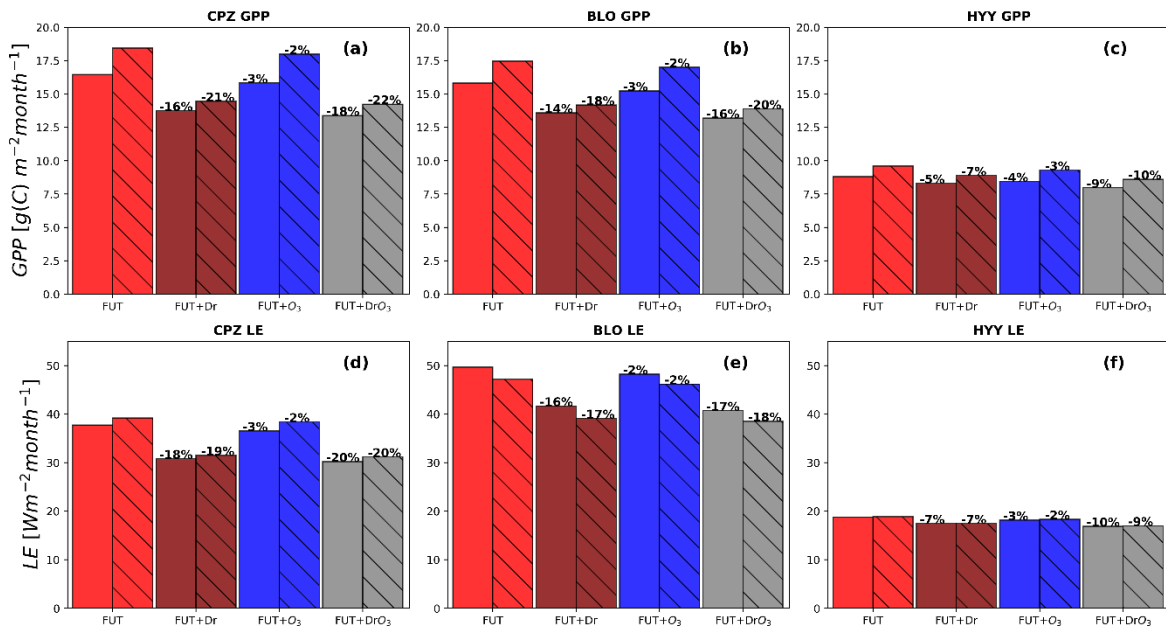


Figure 5.6: CMIP5 ensemble mean estimates of gross primary productivity (GPP) and latent heat flux (LE) for the period 2041–2050 (plain bars) and 2091–2100 (striped bars). Panels (a–c) show GPP and (d–f) LE for Castelporziano (CPZ), Blodgett (BLO) and Hyytiälä (HYY) respectively. Red, brown, blue and grey bars represent FUT, FUT + Dr, FUT + O₃ and FUT + DrO₃ model simulations respectively

Figure 5.6 shows that the combined effect of drought and O₃ stress leads to bigger decreases, but there are differences in the impacts at each site and during different periods. For example, the combined impact of drought and O₃ stress is higher at CPZ and BLO than HYY reflecting the projected changes in SWC and O₃ mixing ratios at these sites (shown in Figure 5.9 and Figure 5.10). By mid-century, drought and O₃ stress could lead to reductions

in GPP and LE at CPZ from 16 to 13 g C m⁻² month⁻¹ and 38–30 W m⁻² month⁻¹, decreases of 18% and 20% respectively. The combined impact of drought and O₃ stress on GPP increases to a reduction of ~22% by the end of the century, although their impact on LE remains unchanged. Reductions in GPP and LE are also projected for BLO and HYY as shown on Figure 5.6.

For the Mediterranean sites, there is a marginal difference (~1% lower) between the sum of drought and O₃ impacts on GPP and LE when applied separately than when the two stressors are applied together while no difference is observed at HYY. This is smaller than the 5% difference seen under present-day conditions, which suggested that the two stresses interact and could compensate for each other.

5.4 Discussion

We investigated the current and future impacts of drought and O₃ stress on gas exchange and forest productivity in three NH forests: Mediterranean forests at BLO and CPZ and a Boreal forest at HYY. We found that all three become more productive over time with GPP projected to increase by 7%, 5% and 8% at CPZ, BLO and HYY by 2041–2050 and by 14%, 11% and 14% by 2091–2100, in line with previous studies. For example, Madani et al. (2018) found a 31% increase in GPP for the NH under the RCP8.5 scenario by 2070, similar to the increases of 36%, 31% and 24% at CPZ, BLO and HYY, respectively, we see by 2100 in the absence of drought and O₃, though it must be noted that the increase estimated by Madani et al. (2018) is averaged over mid and high latitudes of the entire NH (>45°N), rather than for individual sites.

Under RCP8.5, CO₂ concentrations are projected to increase rapidly from current values of ~380 to 936 ppm by 2100, and average global temperature by 4.5°C with some areas experiencing even higher temperature increases as shown by Figure 5.9 and Figure 5.10. Warmer temperatures could lead to an earlier onset of the growing season (Menzel et al., 2006) leading to increased plant productivity early in the season (Keenan et al., 2014). Increased atmospheric CO₂ is also expected to provide additional atmospheric CO₂ for photosynthesis, and the resultant CO₂ fertilization (a phenomenon observed in FACE experiments; e.g. Norby et al., 2010) drives the modelled increase in productivity. The effect of both increased global temperatures and CO₂ fertilization has been accounted for in this study through the use of bias-corrected CMIP5 data to drive FORCAST.

We found increases in plant productivity at all study sites which could be explained by CO₂ fertilization effect and the impact of warmer global temperatures. Increased productivity suggests an increased carbon sequestration capability by these forests, but such an interpretation is limited by several factors. For instance, Jiang et al. (2020) and Norby et al. (2010) have shown that although mature trees can take up more CO₂ under elevated conditions, assimilation is ultimately limited by the availability of other nutrients with re-emission of the extra carbon back into the atmosphere observed. Nitrogen (Norby et al., 2010) and phosphorus (Cleveland et al., 2013) availability are particularly crucial to terrestrial carbon storage as they regulate plant productivity throughout the terrestrial biosphere (Cleveland et al., 2013). Wieder et al., (2015) have shown that accounting for nitrogen and nitrogen–phosphorus limitation could lower model-projected primary productivity substantially, highlighting the important role that these two nutrients could play in the ability of plants to sequester CO₂ in future. However, it is not currently understood how soil nutrient availability will change in future and we have not explicitly considered that here.

Plant response to increasing atmospheric CO₂ is also modulated by drought and temperature (Gray et al., 2016; Manderscheid et al., 2014), factors which could become even more relevant in the warmer drier climate projected under RCP8.5. Other factors that could limit the CO₂ fertilization effect in forests include tree species migration (Midgley et al., 2007; Scheller and Mladenoff, 2005) and forest management practices which could affect the structure, density and tree diversity in these forests, and hence the impacts estimated here. Therefore, our simulations are intended to investigate specific ecosystems (three managed forests) and do not attempt to predict responses for broad PFTs. By using driving data from a range of GCMs, the impact of future changes in drought and temperature and their associated uncertainties have been implicitly accounted for in our estimate of changes in GPP and LE. However, we have not explored the impacts of the availability of soil nutrients or tree age on future GPP and LE. This presents an uncertainty in the projected increases in plant productivity for middle and end of the century and the impact these will have on carbon uptake at the study sites.

Unique to this study, we have tested how plant responses to O₃ exposure (i.e. tolerance or avoidance) affect model estimates of GPP and LE at each site. We found that the assumption that plants tolerate O₃ stress by reducing the subsequent internal damage was better at explaining the observed GPP at all sites while avoidance of O₃ appeared better suited to LE. However, this difference likely arises from the parameterization approach taken

in each case. Under the tolerance approach following Sitch et al. (2007), we assumed that photosynthesis and stomatal conductance (g_s) are downregulated equally in response to increasing stomatal O_3 flux. However, our results suggest that O_3 stress affects A and g_s with different intensity, inducing a decoupling effect between the two processes as described by Lombardozzi et al. (2015). Therefore, the application of a correction factor derived from the response of A to O_3 uptake (as in Equation 5.10) led to an underestimation of the impact of O_3 on g_s and consequently LE. The avoidance method (Hoshika, Watanabe, et al., 2013) assumes that only g_s is directly affected as stomatal O_3 flux increases, with only an indirect impact on photosynthetic rate. Plant transpiration rates, and hence LE, however, are controlled only by g_s , resulting in a greater impact on LE.

When comparing the O_3 stress strategies alone (when drought stress function β was set to 1), we observed that the best performances were provided by applying the tolerance strategy in the study sites characterized by a Mediterranean climate. We hypothesize that in these sites, drought-induced stomatal control dominates over the O_3 -induced stomatal control protecting plants from both the stressors (L w et al., 2006) and that their characteristic O_3 -induced antioxidants production (Nali et al., 2004; Paoletti, 2006) was best accounted for by the tolerance strategy. Conversely in Hyytiala, where drought stress is less pronounced, the O_3 -induced stomatal control could be more relevant, explaining the better performance of the avoidance strategy at this site.

Our findings that the assumption of tolerance provided a better model-observation fit for GPP while avoidance appeared more appropriate for LE suggests that stomatal and stomatal limitations to plant productivity and gas exchange under O_3 exposure are similar to that found under drought stress (e.g. De Kauwe et al., 2015; Egea et al., 2011; Keenan et al., 2010). However, as demonstrated in this study, such limitations are dependent on climatic conditions and tree or crop species. Future modelling and laboratory studies are required, focused on developing parameterization schemes to enable estimation of the combined effect of stomatal and non-stomatal O_3 damage and to improve the quantification of O_3 uptake by plants and its impact on plant and crop productivity.

Unsurprisingly, our simulations suggest that O_3 stress will become less important between the middle and end of the century at all the study sites. There could be several possible explanations for the decreasing impacts of O_3 in future. First, the RCP8.5 scenario assumes an increase in atmospheric CO_2 concentration from ~390 to 936 ppm by 2100 (IPCC, 2014), which would reduce stomatal conductance (e.g. Mills, Hayes, et al., 2011; Mills, Pleijel, et al., 2011), the key determinant of stomatal O_3 flux (Emberson et al., 2018).

Elevated CO₂ has been observed to significantly decrease O₃ damage in several plant species (Fiscus et al., 1997; Harmens et al., 2007; Mills, Hayes, et al., 2011; Mills, Pleijel, et al., 2011). Our results show a decrease in stomatal conductance in future relative to the present day which is likely to reduce stomatal O₃ flux and hence its impact. Second, the decreasing impact of O₃ on plants could also be due to the interactive effects of drought and O₃ stress on plants as drought stress reduces stomatal conductance (e.g. Basu et al., 2016; Farooq et al., 2009). In FORCAST, as most coupled stomatal conductance–photosynthesis models, drought stress directly downregulates both stomatal conductance and photosynthesis rates (e.g. Clark et al., 2011; De Kauwe et al., 2015; Egea et al., 2011; Keenan et al., 2010). In present-day simulations, we found that the combined effects of the two stresses were up to 5% lower than the sum of the impacts of the two stresses acting individually. A similar but less pronounced interaction between the two stresses is also seen in future simulations (Figure 5.6). We therefore conclude that the decreasing impacts of O₃ stress in future climates are partly due to the decrease in stomatal conductance as a result of increasing frequency and severity in drought stress projected for future climates (Dai, 2011; IPCC, 2014). This conclusion is supported by recent findings that future stomatal O₃ uptake in plants will decrease under drought stress (e.g. see Fuhrer, 2009; Lin et al., 2020).

We found that drought stress had a greater effect on estimated GPP and LE than O₃ stress at all sites across all time periods and was more pronounced at the Mediterranean sites (CPZ and BLO). We hypothesized that when water availability is limited, Mediterranean vegetation is more responsive to drought stress than to O₃ exposure (L w et al., 2006), so stomatal regulation induced by drought stress indirectly acts as O₃ response, by reducing the O₃ stomatal flux together with the water loss, explaining also the reduced predictive ability of the model when both stressors are combined (Figure 5.6). Although a general rapid reduction of stomatal aperture in response to short-term exposure to O₃ was observed (Wittig et al., 2007), the chronic exposure to O₃ may induce a phenomenon known as ‘stomatal sluggishness’, that is, a reduction of plant's ability to regulate stomata (Carriero et al., 2015; Emberson et al., 2009; Hoshika et al., 2015, 2016, 2018). This is a serious problem for plants, since it can lead to plants inability to regulate the loss of water (Paoletti, 2005; Sun et al., 2012) further exacerbating the impacts of other stresses such as drought. O₃-induced stomatal sluggishness could therefore magnify the higher impact of drought on GPP and LE at the sites with Mediterranean climate, where O₃ concentrations are high relative to the Boreal site (HYY). However, there is not previous clear scientific evidence of sluggishness on sclerophyll leaves (i.e. *Q. ilex*) or Pine needles (i.e. *P.*

ponderosa), and we did not explicitly account for sluggishness in this study. We believe that long-term O₃ fumigation experiments are needed to identify species-specific response of *A* and *g_s* to O₃ including sluggishness effects.

In present-day simulations, the inclusion of drought stress alone led to ~20% decrease in estimated GPP and LE at CPZ and BLO, but at HYY, the reduction was only 13% for GPP and 10% for LE. This is a surprising result considering that drought is an annual occurrence at CPZ and BLO, and accounting for drought stress has been shown to improve model fit to observations of photosynthesis in Mediterranean ecosystems (Fares et al., 2019; Keenan et al., 2010). This indicates that although plants in Mediterranean ecosystems have adapted to drought stress (Calfapietra et al., 2009; Paoletti, 2006), their growth and productivity is still likely to be negatively impacted by any further decrease in SWC. The results for HYY over the 1997–2014 period (Figure 5.11 and 2005–2006 (Figure 5.2 and Figure 5.3), and observed effects in Boreal forests in Canada (Kljun et al., 2007; Krishnan, 2006), Finland (Gao et al., 2016) and across Europe (Ciais et al., 2005) show that even for a well-watered forest, anomalous drought events can have a big impact on plant productivity. The Boreal region, extending across North America, Europe and Asia, constitutes the second largest forested biome after tropical forests (Landsberg and Gower, 1997) and therefore plays an important role in the global carbon cycle (Keeling et al., 1996). As global climate changes, productivity in Boreal ecosystems will be at a risk from drought stress although this effect could be mitigated by longer growing seasons which would potentially increase productivity as has been seen in other regions (e.g. Dragoni et al., 2011; White, Running, and Thornton, 1999).

One of the main challenges hindering accurate quantification of drought and O₃ stress impacts is the lack of long-term measurements at an appropriate spatial and temporal resolution for model parameterization, calibration and evaluation (see review by Emberson et al., 2018). In this study, we use half-hourly measurements of SWC and O₃ and empirical equations that relate these stresses to plant productivity and gas exchange. Present-day simulations show that incorporating both drought and O₃ stress gives the best model fit to observed GPP and LE, and that these two stresses counteract each other. Productivity increases in our Mediterranean and Boreal forest sites, with GPP (and potentially carbon sequestration) increasing by between 11% and 14%. Although we have not investigated future changes for other ecosystems, if our results were scaled to the regional level, the projected increase in GPP could be significant for the global carbon budget.

S

5.5 Supplementary Information for Chapter 5

5.5.1 Summary of supplementary figures.

Figure 5.7 shows a comparison between historical CMIP5 GCM data for the period 1996-2005 and observations at each site for years shown in Table 5.2. CMIP5 Model names have been shortened as follows GFDL = GFDL-ESM2M, GFDL2 = GFDL-ESM2G, GISS = GISS-E2-R, IPSL = IPSL-CM5B, IPSL2 = IPSL-CM5A, CSIRO = CSIRO-MK3, BNU = BNU-ESM. This figure reveals that although several of the GCMs reproduce the observed seasonal cycle at the study sites there are biases in magnitude. For example, IPSL2, IPSL show a consistent dry bias in soil moisture but reproduce the seasonality of soil moisture reasonably well. O₃ mixing ratios in GISS are ~100% higher than those observed. These biases are corrected using historical model output from 1996-2005 and shown in Figure 5.8. Since the same period was used to estimate the relative biases in each variable, the bias corrected data now matches the observed data exactly with no deviations. The relative biases estimated between individual GCMs and for each variable was then applied to correct the biases in the future model projections based on the assumptions that the biases in historical and future estimates are identical. We acknowledge that this may not be the case, as tipping points may be reached, model parameterisations suitable for current conditions may not accurately reflect future conditions, and processes either not included or not well parameterised may increase in importance in the future.

Figure 5.9 and Figure 5.10 show the bias-corrected data for 2041-2050 and 2091-2100 respectively. These plots show similarities as well as differences expected between these two decades in the future. For example, PAR remains similar between the middle and end of the century and between models since solar radiation is not expected to change substantially in the future. Under RCP8.5, temperature is expected to increase as atmospheric CO₂ increases exponentially. Figure 5.9 shows that all GCMs project higher temperatures for 2041-2050 compared to present-day observations and Figure 5.10 shows that the sites will be even warmer in 2091-2100 than it will be 2041-2050. For CPZ, GCMs are projecting an increase in mean temperature from 16.3 °C in present-day observations to 17.9 °C by 2041-2050 and 20.0 °C by the end of the century. BLO sees 1.7 °C and 3.9 °C increase in temperature by middle and end of the century respectively over the present-day observed value of 11.4 °C. The highest increase in temperature is projected for HYY where average

annual temperature could rise by 2.8 °C and 5.6 °C to 7.1 °C and 9.9°C by 2041-2050 and 2091-2100 respectively, from 4.3 °C currently.

Figure 5.11 shows that the inclusion of drought and O₃ stress has mixed impacts on GPP and LE in model simulations for the 1997-2014 period at HYY. FORCAsT shows a tendency to overestimate GPP and therefore the inclusion of drought or O₃ stress always improves model performance. However, FORCAsT underestimates LE over the entire year and the further reductions under drought and O₃ stress worsens model performance. Model underestimations of LE at HYY was likely due to the presence of snow on the ground in the winter months as previously been observed by (Launiainen et al., 2019).

To test the suitability of CMIP5 data for driving FORCAsT, a test simulation was conducted using historical (1996-2005) GCM output data. Model performance statistics for this test run compared to a similar simulation using observed driving data is presented in Figure 5.12. The high correlation coefficients (blue lines), low root mean squared errors (orange dashed lines) and low standard deviations (black dashed lines) indicate that the GCM data was performing as well as the observed data when used to drive FORCAsT. Ensemble mean indicated by the red circles show that GCM driving data better matched the “observed” LE than GPP at all sites with less variability between models. GPP estimated with the historical datasets at HYY were closer to those from observations and less variable than at BLO and CPZ.

Figure 5.13 and Figure 5.14 show GPP (top panels) and LE (bottom panels) estimated using individual GCM driving data for 2041-2050 and 2091-2100 respectively. These plots highlight the impact of driving data on model performance. For example, IPSL and IPSL2 estimates of GPP and LE are both strongly affected by drought stress because projected soil moisture content is low in these models. FORCAsT estimates of GPP at each site showed little variability for all GCM driving data in the absence of drought or O₃ stress as shown by the orange bars on GPP plots but the variability increased as drought and O₃ stress were included. This is because the models are generally in good agreement for meteorological variables but considerably less so for O₃ and SWC. On the contrary, there was large variability in estimates of LE without any stress, an indication that LE flux is more sensitive to input data than GPP. The differences in model estimates of GPP and LE attributable to model driving data was more pronounced at the Mediterranean forests than at the Boreal forest.

Figure 5.15 and Figure 5.16 show cumulative GPP and LE estimated by FORCAsT driven with data from each GCM. These plots represent model best estimates since both

drought and O₃ stress has been accounted for in these simulations. The ensemble means (red dashed lines) show an increase in GPP for all sites for both 2041-2050 and 2091-2100 from present-day estimates (black dashed lines). Similarly, LE is projected to increase at all sites across both time periods, except for BLO where a decline is expected toward the end of the 21st century. The range of GPP and LE is small for 2041-2051, an indication that of good model agreement out to mid-century. The range increases towards the end of the century as GCM meteorological variables begin to diverge from one another leading to greater uncertainty. GPP and LE showed the highest variability at BLO and lowest at HYY presumably a reflection of the differences in model estimates of meteorological variables as well as O₃ and SWC between 2091-2100 as shown by Figure 5.10. Due to their dry bias (Figure 5.7,5.9 and 5.10), IPSL and IPSL2 project the lowest future GPP.

Table 5.2: Details of study sites and parameter values used in estimating drought and ozone stress. References for each value are indicated by superscripts and listed below

FLUXNET Site ID	Units	IT-CP2 (CPZ)	US-Blo (BLO)	FI-Hyy (HYY)
Lat, Lon	Degrees	41°70'N, 12°35"E	38°53'N, 120°37'W	61°51'N, 24°17'E
Data used in study	N/A	2013-2014	2003-2004	1997-2014
Dominant Vegetation	N/A	Holm oak (<i>Q. ilex</i>)	Ponderosa pine (<i>P. ponderosa</i>)	Scots Pine (<i>P. Sylvestris</i>)
PFT	N/A	Evergreen Broadleaf	Evergreen Needleleaf	Evergreen Needleleaf
Canopy Height	m	16	7	18
Max. leaf area index (LAI)	m ² m ⁻²	3.69	2.9	2.50
Climate (Koppen Classification)	N/A	Mediterranean (Csa)	Mediterranean (Csa)	Boreal (Dfc)
Mean Temperature	°C	15	12	3.0
Annual Precipitation	mm	805	1226	709
Frequency of Droughts	N/A	Annually	Annually	Rarely
Vcmax	μmolm ⁻² s ⁻¹	78 ^[1]	75 ^[2]	50 ^[3]
g ₁	kPa ^{0.5}	2.21 ^[4]	2.35 ^[5]	2.35 ^[5]
K	molH ₂ Omol ⁻¹ O ₃	200000	140000	290000
Depth of SWC measurement	m	1.0	1.0	0.75
θ _c ,	m ³ m ⁻³	0.15 ^[6]	0.14 ^[6]	0.30 ^[6]
θ _w	m ³ m ⁻³	0.04 ^[6]	0.04 ^[6]	0.08 ^[6]
.q	N/A	0.60 ^[6]	0.60 ^[6]	0.80 ^[6]
FLUXNET2015 doi:	N/A	10.18140/FLX /1440233	10.18140/FLX /1440068	10.18140/FLX /1440158

^[1]Fares et al., (2019) , ^[2]Keenan et al., (2010), ^[3]Kolari et al.,(2014), ^[4]Lin et al., (2015),
^[5]De Kauwe et al., (2015), ^[6]Otu-Larbi et al., 2020

Table 5.3: Details of general circulation models (GCMs) used in future impact studies

Model	Atmospheric Spacing	Grid	Modelling Centre and Country	References
	Latitude	Longitude		
BNU-ESM (BNU)	2.7906	2.8125	(BNU, China)	Ji et al. 2014
CSIRO-Mk3.6.0 (CSIRO)	1.8653	1.875	(CSIRO, Australia)	Gordon et al., 2002
GFDL-ESM2G (GFDL)	2.0225	2	(NOAA, USA)	Dunne et al. 2012
GFDL-ESM2M (GFDL2)	2.0225	2.5	(NOAA, USA)	Dunne et al. 2012
GISS-E2-R (GISS)	2	2.5	(NASA, USA)	Shindell et al., 2013
IPSL-CM5A-MR (IPSL2)	1.2676	2.5	(IPSL, France)	Dufresne et al. 2013
IPSL-CM5B-LR (IPSL)	1.8947	3.75	(IPSL, France)	Dufresne et al. 2013

Table 5.4a: Model performance statistics for FORCAsT compared to observation at CPZ. Bold numbers indicate the best performing model configuration in each category.

	Model Performance Statistics for CPZ					
	GPP			LE		
	RMSE	r	Normalised SD	RMSE	R	Normalised SD
CTR	2.53	0.85	1.67	0.46	0.91	1.38
CTR+Dr	1.33	0.87	0.81	0.22	0.93	0.71
AVD	2.44	0.86	1.22	0.40	0.90	1.31
AVD+Dr	1.29	0.87	0.81	0.22	0.93	0.73
TLR	1.80	0.86	1.07	0.37	0.90	1.32
TLR+Dr	1.02	0.88	0.83	0.22	0.93	0.74

Table 5.4b: Model performance statistics for FORCAsT compared to observation at BLO. Bold numbers indicate the best performing model configuration in each category.

Model Performance Statistics for BLO						
	GPP			LE		
	RMSE	r	Normalised SD	RMSE	R	Normalised SD
CTR	2.01	0.93	1.36	0.75	0.88	1.47
CTR+Dr	0.91	0.98	0.76	0.47	0.92	0.83
AVD	1.72	0.93	1.24	0.62	0.88	1.09
AVD+Dr	0.72	0.98	0.76	0.41	0.91	0.84
TLR	1.47	0.94	1.22	0.65	0.88	1.21
TLR+Dr	0.64	0.98	0.78	0.42	0.92	0.84

Table 5.4c: Model performance statistics for FORCAsT compared to observation at HYY. Bold numbers indicate the best performing model configuration in each category.

Model Performance Statistics for HYY						
	GPP			LE		
	RMSE	r	Normalised SD	RMSE	R	Normalised SD
CTR	1.31	0.98	1.29	0.24	0.95	1.26
CTR+Dr	0.85	0.98	0.88	0.21	0.95	0.89
AVD	1.27	0.98	1.12	0.23	0.94	1.06
AVD+Dr	0.83	0.98	0.89	0.21	0.95	0.89
TLR	1.24	0.98	1.12	0.33	0.94	1.35
TLR+Dr	0.81	0.98	0.89	0.27	0.94	0.92

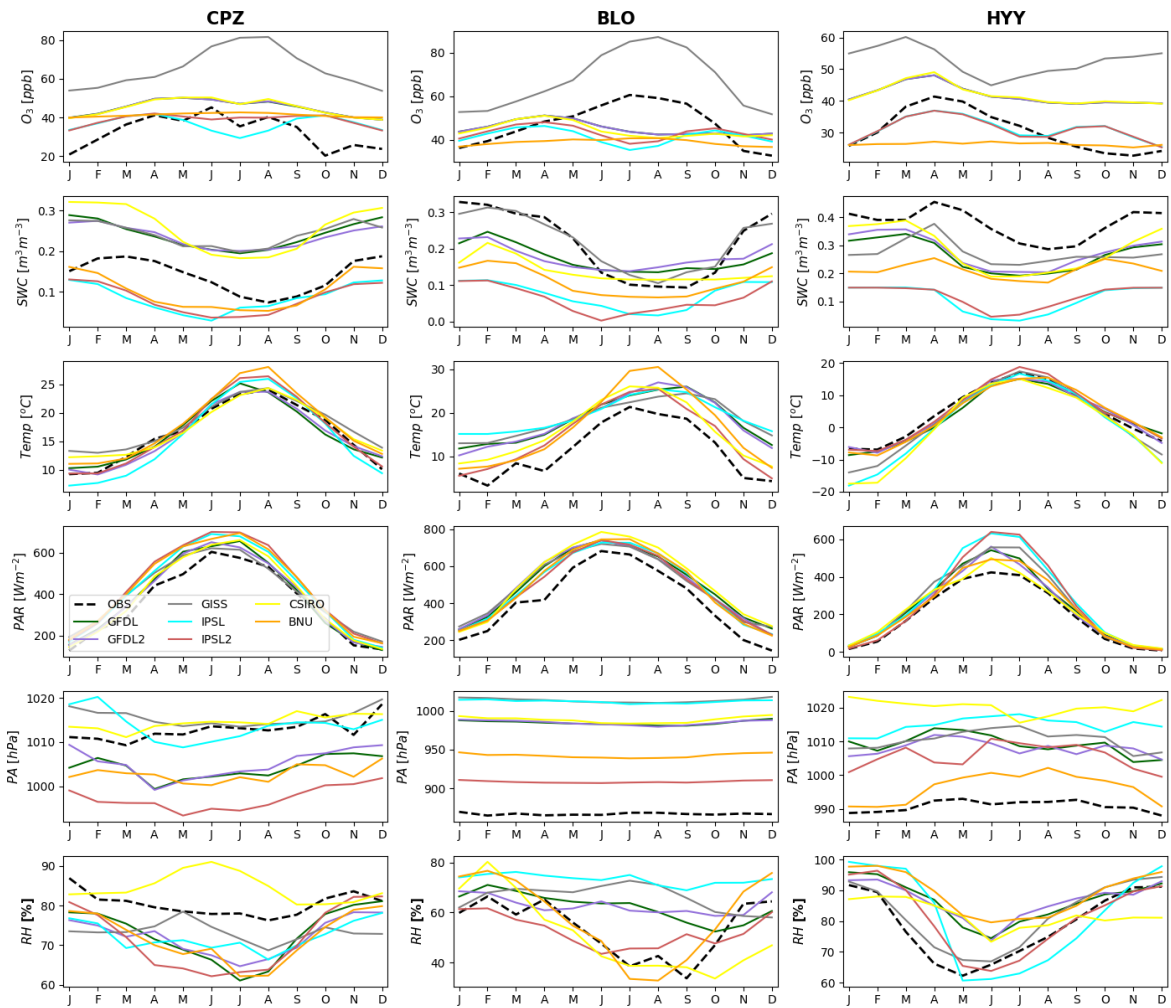


Figure 5.7: Comparison between non bias-corrected historical (1996-2005) CMIP5 model outputs and observations (black dashed lines) at CPZ (left column), BLO (middle column) and HYY (right column). Model output are shown in green (GFDL), violet (GFDL2), grey (GISS), cyan (IPSL), red (IPSL2), yellow (CSIRO) and orange (BNU) while observed (OBS) values are shown in black dashed lines.

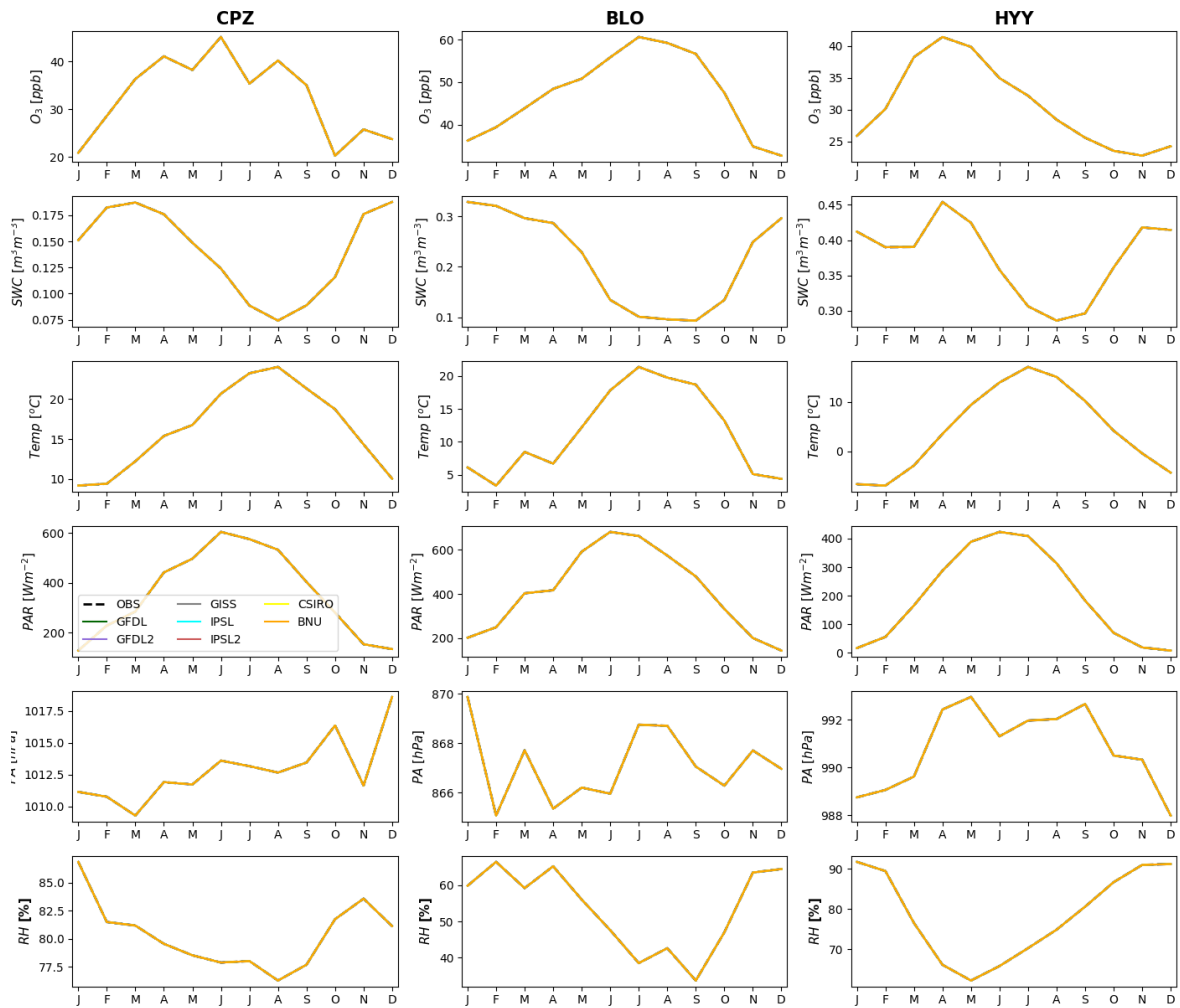


Figure 5.8: Annual profile of bias-corrected historical (1996-2005) CMIP5 GCM data at CPZ (left column), BLO (middle column) and HYY (right column). Model output are shown in green (GFDL), violet (GFDL2), grey (GISS), cyan (IPSL), red (IPSL2), yellow (CSIRO) and orange (BNU) while observed (OBS) values are shown in black dashed lines.

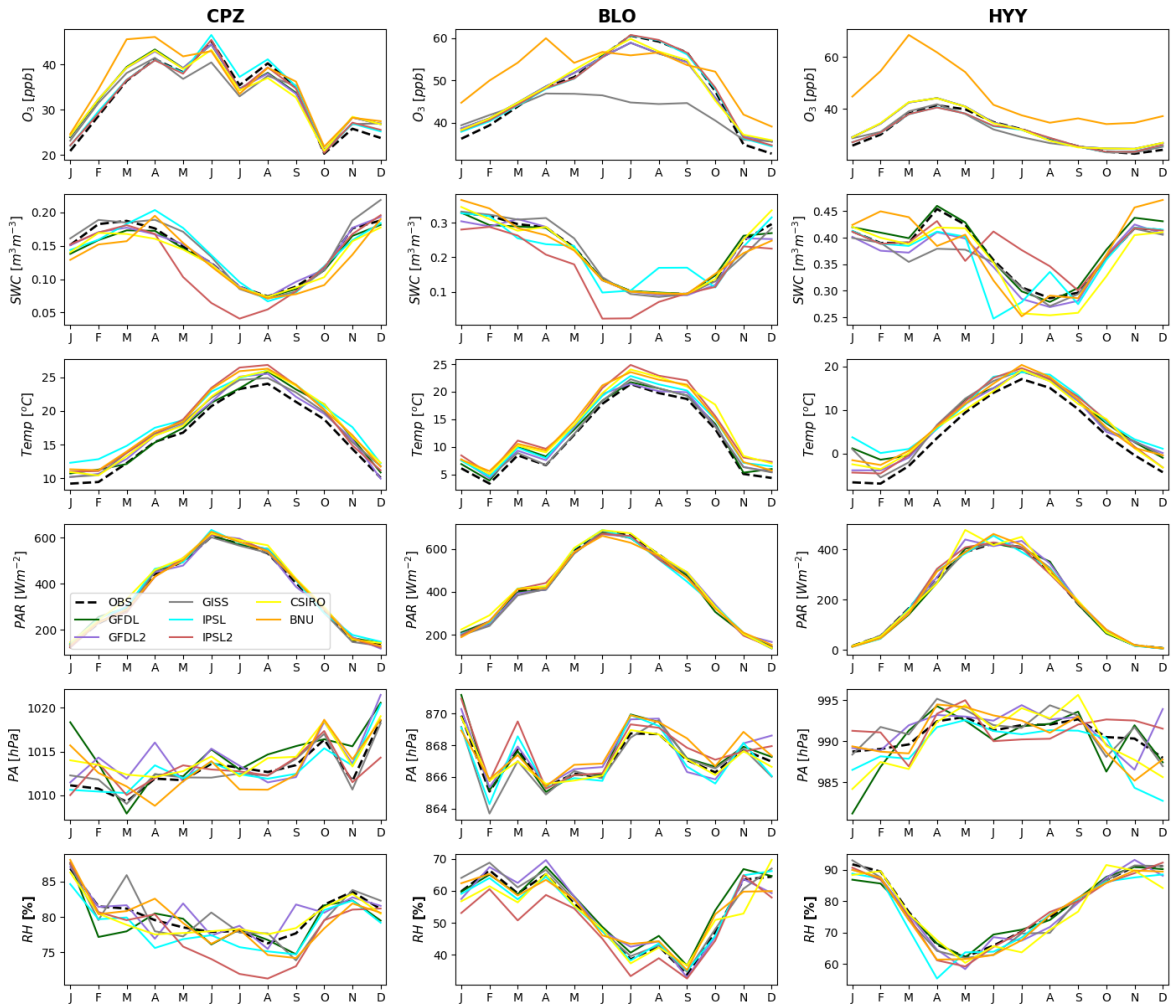


Figure 5.9: Annual profile of bias-corrected mid-century (2041-2050) CMIP5 GCM data at CPZ (left column), BLO (middle column) and HYY (right column). Model output are shown in green (GFDL), violet (GFDL2), grey (GISS), cyan (IPSL), red (IPSL2), yellow (CSIRO) and orange (BNU) while observed (OBS) values are shown in black dashed lines.

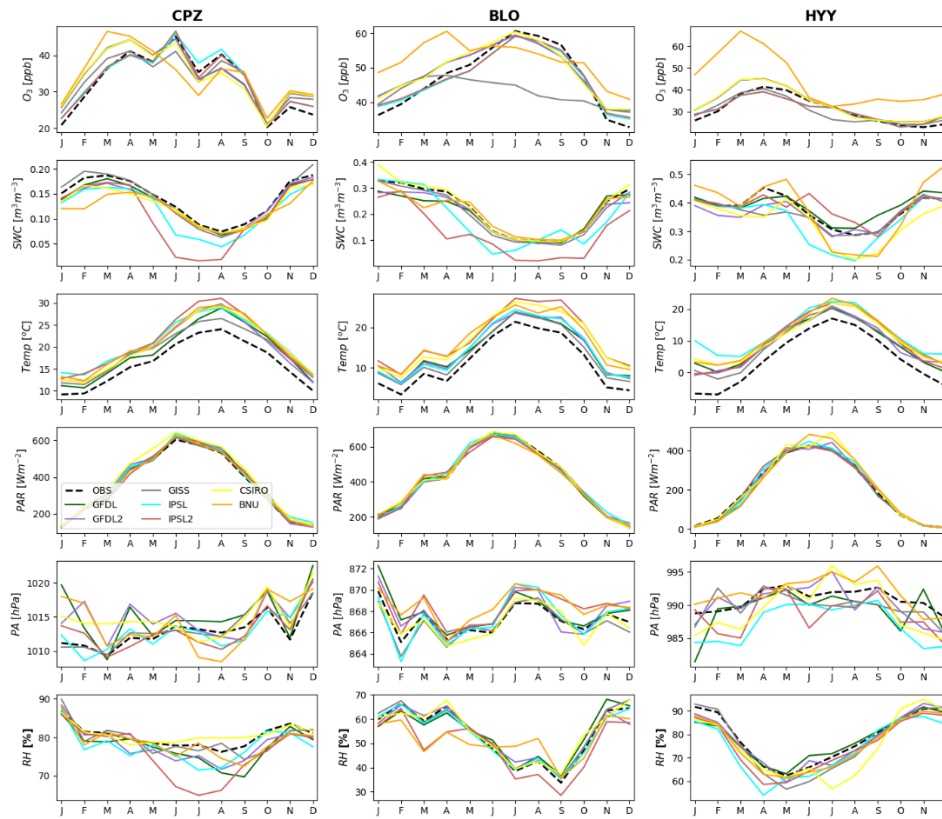


Figure 5.10: Annual profile of bias-corrected end of century (2091-2100) GCM data at CPZ (left column), BLO (middle column) and HYY (right column). Model output are shown in green (GFDL), violet (GFDL2), grey (GISS), cyan (IPSL), red (IPSL2), yellow (CSIRO) and orange (BNU) while observed (OBS) values are shown in black dashed lines.

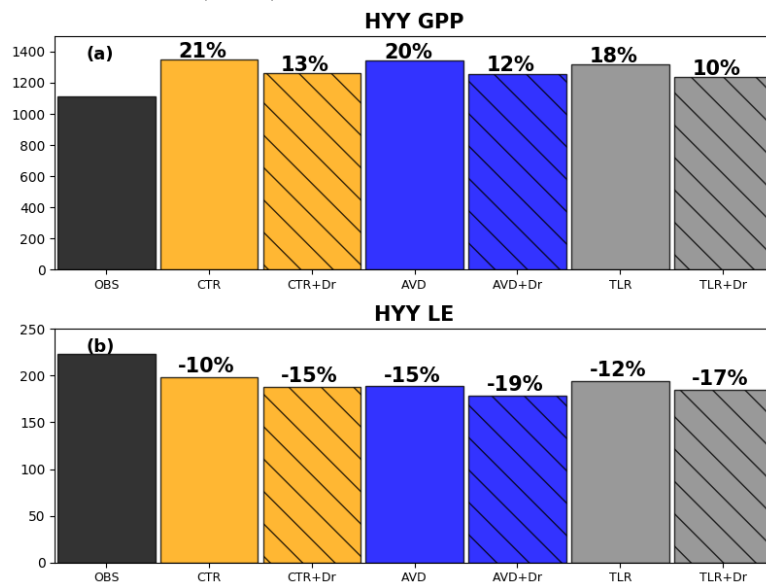


Figure 5.11: 1997-2014 annual average GPP (top) and LE flux (bottom) for HYY. Observed (OBS) values are shown by black bars while model output are: orange (CTR and CTR+Dr), blue (AVD and AVD+Dr), grey (TLR and TLR+Dr) with striped bars indicating drought stress. Percentage differences between modelled and observed values are shown at the top of the bars. Positive values indicate model overestimation while negative values indicate model underestimation.

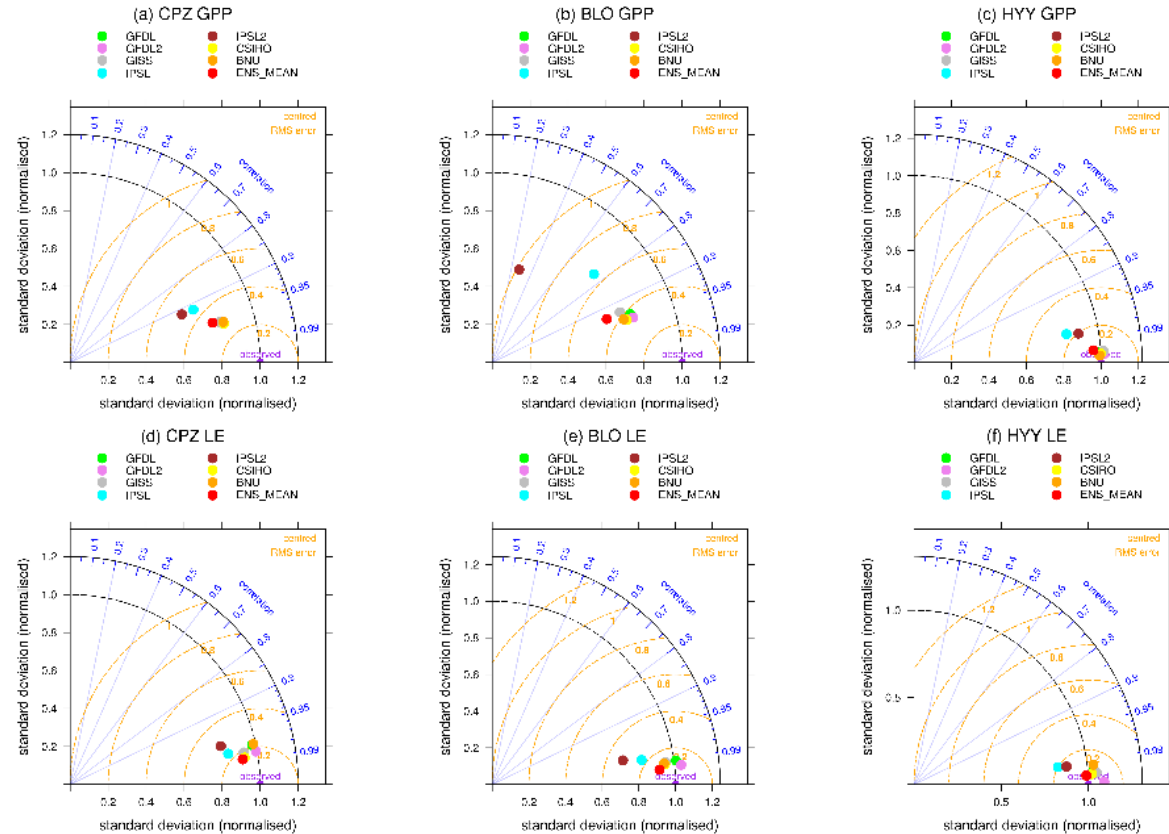


Figure 5.12: Taylor Diagram showing model output statistics from FORCAsT simulations using historical GCM driving data. Black and orange dashed curves and blue lines show normalised standard deviation (SD), centred root mean squared error (RMSE) and correlation coefficients (r) respectively against model estimates made with observed driving data. Observed GPP and LE are summarised by the purple circle with $SD=1.0$, $RMSE=0.0$ and $r=1.0$. The summary statistics for ensemble mean (ENS MEAN) is shown by red circles, while individual GCMs are shown by green (GFDL), violet (GFDL2), grey (GISS), cyan (IPSL), pink ((IPSL2), yellow (CSIRO), and orange (BNU). Note the change in scale on panel (f).

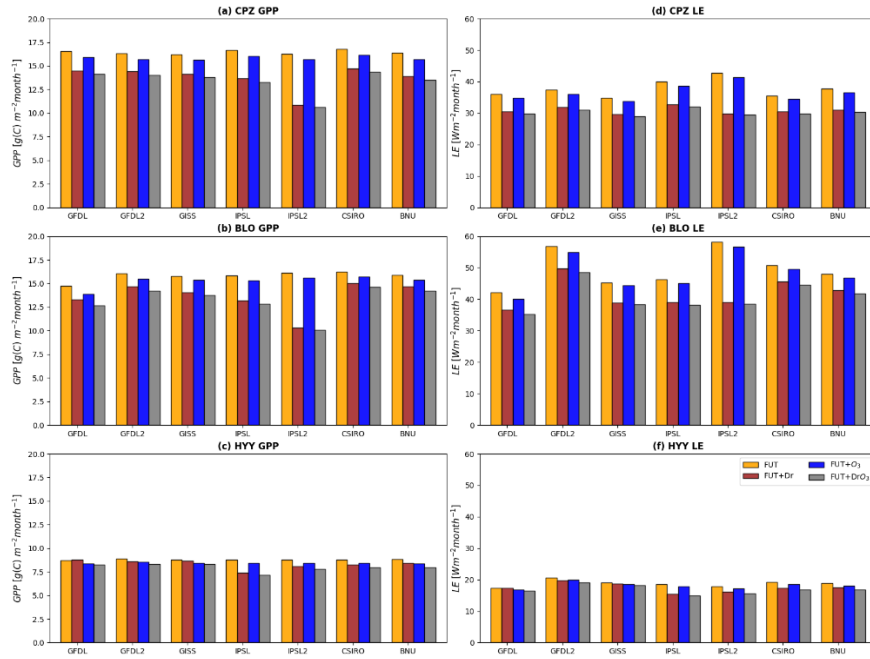


Figure 5.13: Estimate GPP and LE for 2041-2050 grouped by CMIP5 GCM ensemble member. Panels a- c show GPP while d-f show LE at CPZ, BLO and HYY respectively. Orange, brown, blue and grey bars represent FUT, FUT+Dr, FUT+O₃ and FUT+DrO₃ model configurations respectively.

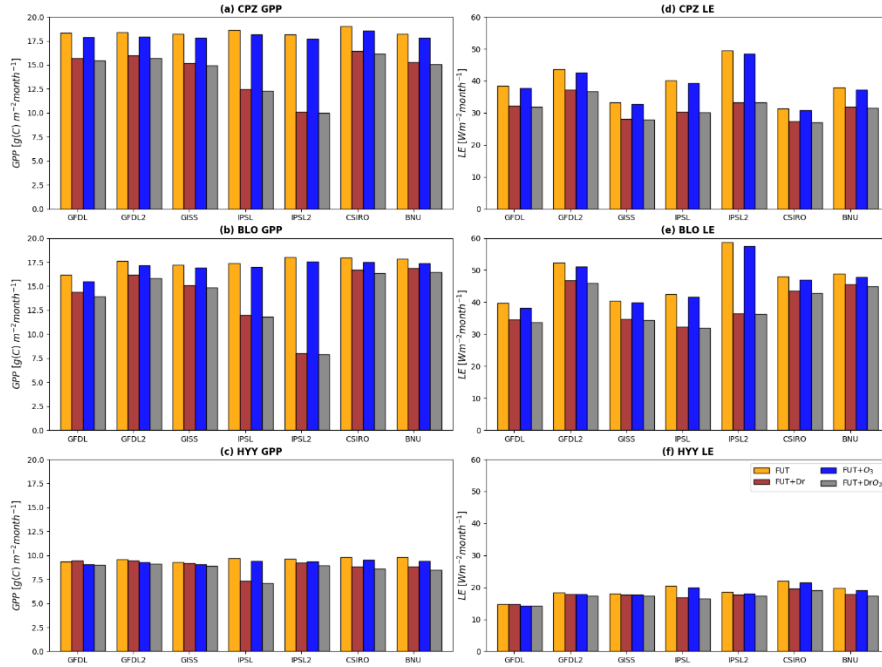


Figure 5.14: Estimate GPP and LE for 2091-2100 grouped by CMIP5 GCM ensemble member. Panels a-c show GPP while d-f show LE for CPZ, BLO and HYY respectively. Orange, brown, blue and grey bars represent FUT, FUT+Dr, FUT+O₃ and FUT+DrO₃ model configurations respectively.

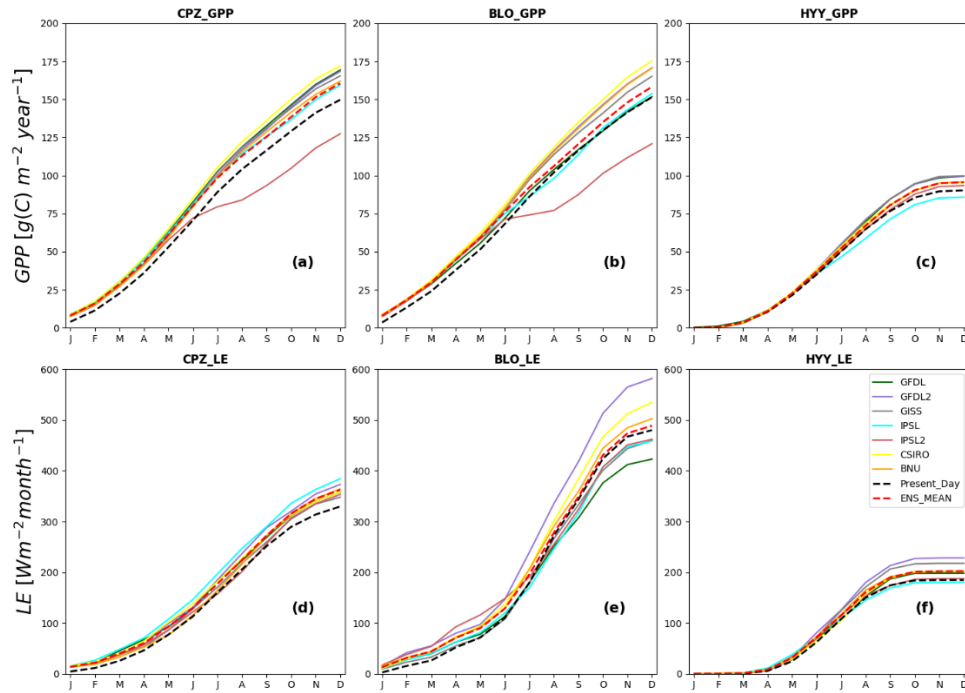


Figure 5.15: Best estimates of GPP and LE based on using different GCM model output data to drive FORCAsT for the period 2041-2050 compared with present-day estimates using observed driving data. Ensemble mean is indicated by red dashed lines and present-day estimates by black dashed lines. Estimates for each GCM are shown by green (GFDL), violet (GFDL2), grey (GISS), cyan (IPSL), pink (IPSL2), yellow (CSIRO), and orange (BNU).

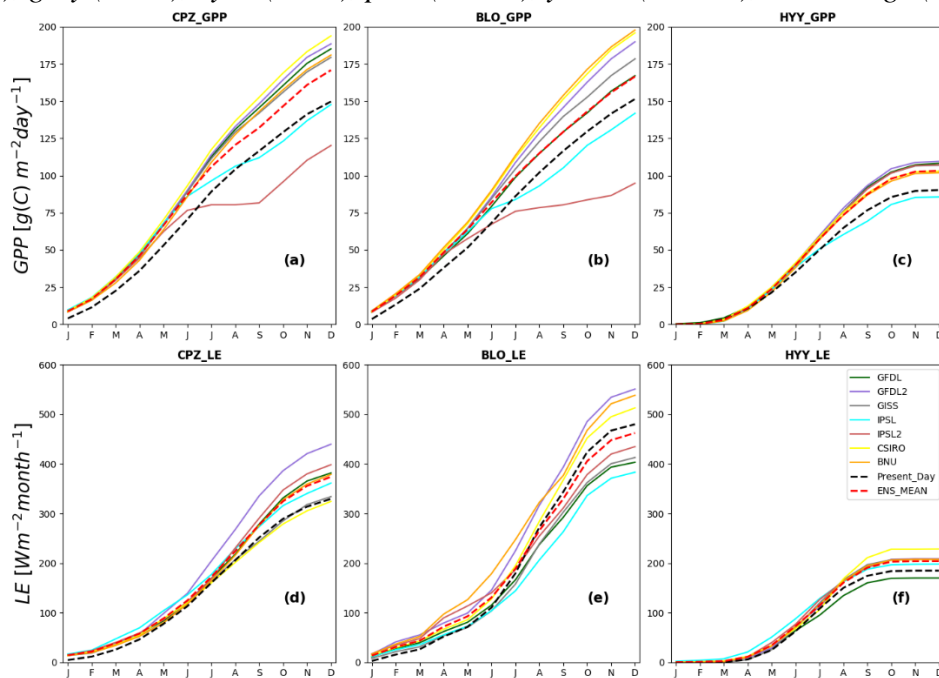


Figure 5.16: Best estimates of GPP and LE based on using different GCM model out to drive FORCAsT for the period 2091-2100 compared with present-day estimates using observed driving data. Ensemble mean is indicated by red dashed lines and present-day by black dashed lines. Estimates for each GCM are shown by green (GFDL), violet (GFDL2), grey (GISS), cyan (IPSL), pink (IPSL2), yellow (CSIRO), and orange (BNU).

Chapter 6: Process-based approach to modelling isoprene fluxes during drought

This work is yet to be finalized and submitted to a journal.

Summary

This study applies the process-based isoprene emission scheme within the JULES LSM to investigate how drought severity affects isoprene emission rates and how this alters the proportion of assimilated carbon that is re-emitted as isoprene. Model estimates are compared to continuous isoprene measurements made while two temperate deciduous broadleaf forests were experiencing drought of varying severity. We find that JULES reproduces observations to within 14-20% before and after drought events but underestimate isoprene fluxes by 58-72% during heatwave-drought events. Model performance was improved when new parameterisations for modelling isoprene emissions under moderate drought conditions were added to JULES leading to a reduction in model underestimation to between 6 and 20%. The percentage of assimilated carbon that is re-emitted as isoprene was found to increase by more than 100% at both forest sites during heatwave-drought episodes, affecting estimates of the forest carbon sink capacity.

6.1 Introduction

Terrestrial ecosystems assimilate carbon dioxide (CO₂) by photosynthesis, thus acting as a sink for atmospheric CO₂. An estimated 861 Pg C is stored in forests alone (Pan et al., 2011), higher than in either the atmosphere (760 Pg C) or oceans (800 Pg C) (NASA, 2020). Gross primary productivity (GPP) is used as a measure of the overall carbon fixed by vegetation through photosynthesis and is estimated at 120 Pg C yr⁻¹ globally (Kesselmeier et al., 2002). Of this, about half is lost through respiration and a further 50 Pg C yr⁻¹ returns to the atmosphere via decomposition of plant matter and soils (Intergovernmental Panel on Climate Change (IPCC), 2001). Deforestation is estimated to cause the release of 4.9 Pg of CO₂ into the atmosphere globally. However, plants also emit substantial amounts of carbon into the atmosphere in the form of biogenic volatile organic compounds (BVOCs) (Guenther et al., 1997; Guenther, 2002) which are themselves eventually oxidized into CO₂. BVOCs emitted from vegetation are estimated to produce >1 Pg C yr⁻¹ as CO₂ (Guenther, 2002) – equivalent to ~20% of the emissions attributable to deforestation. Although they constitute a relatively small percentage of the global carbon budget, BVOCs react with other atmospheric gases and can affect climate at local, regional, and global scales. However, the production and release of organic carbon through BVOC emissions are generally disregarded in carbon budget calculations.

Isoprene (C₅H₈) constitutes the greater part (~50%) of all BVOCs emitted by terrestrial vegetation. About 450-600 Tg C yr⁻¹ of isoprene is emitted globally (Arneth et al., 2008; Guenther et al., 2006; 2012) which is comparable to the magnitude of methane emissions. Isoprene emissions are directly linked to photosynthesis but emission rates are sensitive to environmental factors such as temperature, photosynthetically active radiation (PAR), soil water content (SWC) and CO₂ concentrations (Arneth et al., 2008; Monson et al., 1992; Pegoraro et al., 2004). While the effect of some of these factors, like temperature and PAR, on emission rates are relatively well understood and parametrised in land surface models, others, particularly the impacts of drought (low SWC) on isoprene emissions rates are not. Experimental and observational studies suggest that, while severe drought causes a decrease in isoprene emission rates as plant photosynthetic capacity falls, moderate drought leads to an increase in isoprene emissions due to stimulation of leaf temperature and decrease in leaf internal carbon dioxide concentrations (Brilli et al., 2007; Niinemets, 2010; Pegoraro et al., 2004; Potosnak et al., 2014; Rosenstiel et al., 2003).

Land Surface Models (LSMs) estimate isoprene emissions following one of two conceptualisations both of which are based on observed relationship between photosynthesis and isoprene emissions: a process-based approach which links isoprene production to photosynthetic processes and carbon assimilation, and empirical models which account for the effect of individual environmental factors on a baseline emission rate based on observed relationships (e.g. see Arneth et al., 2007a; 2007b; Guenther et al., 1995; Niinemets et al., 1999). The most widely used isoprene emission model (often referred to as G95) is an empirical parameterisation developed by Guenther et al. (1995). This approach assumes isoprene emissions from specific plants are intrinsically dependent on solar radiation (specifically PAR) and temperature. G95 has been further developed into the Model of Emissions of Gases and Aerosols from Nature (MEGAN: Guenther et al., 2006; 2012) in which emissions under standard conditions are modified by the observed response of isoprene emissions to changing atmospheric CO₂ concentrations, soil moisture and leaf age (Guenther et al., 2012; Jiang et al., 2018). MEGAN has been incorporated into most of the commonly-used global coupled land–atmosphere models to estimate global isoprene emissions for present and future climates and has been shown to reproduce observed isoprene fluxes and mixing ratios within a factor of 2 for most sites (e.g. Guenther et al., 2006). However, insights from recent modelling studies suggest that the impact of mild or moderate drought on isoprene emissions is not properly accounted for in the G95 and MEGAN model (e.g. Jiang et al., 2018; Otu-Larbi et al., 2020; Potosnak et al., 2014).

The second approach to estimating isoprene emissions is process-based, i.e. models that directly couple isoprene emission rates to specific processes within the mechanism of photosynthesis (e.g. see Martin et al., 2000; Niinemets et al., 1999; Zimmer et al., 2000). The Joint UK Land Environment Simulator (JULES), the land surface model incorporated in the UK Met Office suite of climate and Earth system models, takes this approach and estimates isoprene emissions using the methods proposed by Niinemets et al. (1999).

Like the G95 model, one major challenge for the photosynthesis-based emissions scheme is incorporating the impact of drought stress on GPP and hence isoprene emissions. Yet estimates of the emissions of isoprene have implications for the global carbon budget, atmospheric chemistry, and secondary aerosol formation which in turn affects atmospheric oxidative capacity and the concentrations of climate forcers such as methane and ozone (Kaplan et al., 2006; Laothawornkitkul et al., 2009; Pike & Young, 2009).

Although light and temperature are the main drivers controlling rates of photosynthesis, drought stress is the primary limiting environmental factor to global plant

productivity and C assimilation (Nemani et al., 2003; Zeppel et al., 2014). Reductions in photosynthesis resulting from drought stress could be expected to lead to a decrease in global isoprene emissions as the two are directly coupled under normal conditions. However, this proportionality between photosynthesis and isoprene emissions is known to break down during periods of moderate drought stress as isoprene emissions and photosynthesis become decoupled, implying that process-based models may also struggle to replicate isoprene emission rates during periods of soil moisture stress (Niinemets, 2010).

Long-term continuous measurements of isoprene mixing ratios and fluxes have been rare, especially in natural forest environments. However, recent measurement campaigns during heatwave and drought periods have produced valuable, albeit often short-duration, datasets that now allow for an exploration of the role of drought stress on GPP and isoprene emissions and provide an opportunity to better understand the effect of such stresses at the ecosystem-scale, and in particular the implications for the global carbon budget. In this study we use continuous isoprene and meteorological measurement from two temperate deciduous broadleaf forests to investigate how drought severity affects isoprene emission rates and how this may alter the proportion of assimilated carbon that is re-emitted as isoprene.

Our objectives are to determine: (i) how the severity of drought affects estimated isoprene emissions; (ii) the percentage of assimilated carbon that is re-emitted as isoprene during unstressed and water-stressed periods

Our main goal is to understand how changes in isoprene emissions during periods of drought stress affect the carbon uptake capacity of forests and the potential impacts this will have on the global carbon sink.

6.2 Materials and methods

6.2.1 JULES land surface model (LSM)

The Joint UK Land Environment Simulator (JULES) model is the land surface component of the UK Met Office (UKMO) Unified Model (UM), simulating the exchange of momentum and mass between the surface and the atmosphere, as well as processes occurring in the sub-surface soil and on the land surface (Best et al., 2011; Clark et al., 2011). Plant species with similar ecosystem functions and characteristics are grouped into Plant Functional Types (PFTs), which together with four non-vegetation types, make up the land surfaces represented in JULES, as described fully in Harper et al. (2016). JULES has been

shown to successfully reproduce observed plant processes GPP (Byrne et al., 2018; Slevin et al., 2017), isoprene emissions (Pacifico et al., 2011), surface energy fluxes (Blyth et al., 2010), and stomatal conductance at global, regional and point scales across different PFTs. A full description of the physiological and morphological processes incorporated in JULES has been provided in Clark et al. (2011) and Best et al. (2011). Here, we confine ourselves to a brief overview of the photosynthesis and isoprene emissions schemes within the model.

Photosynthesis rates (A_p) in JULES are simulated as the minimum of three limiting conditions (Collatz et al., 1991): (i) Rubisco-limited (W_C), (ii) light-limited (W_L) and (iii) transport of photosynthetic products-limited (W_E), i.e.:

$$A_p = \min(W_C, W_L, W_E) \quad 6.1$$

where

$$W_C = \begin{cases} V_{cmax} \left(\frac{C_i - \Gamma}{C_i + K_c \left(1 + \frac{O_i}{K_o}\right)} \right) & \text{for C3 plants} \\ V_{cmax} & \text{for C4 plants} \end{cases} \quad 6.2$$

where V_{cmax} ($\text{mol CO}_2 \text{ m}^{-2} \text{ s}^{-1}$) is the maximum rate of carboxylation of Rubisco, C_i (Pa) is the leaf internal CO_2 partial pressure, Γ (Pa) is the CO_2 compensation point in the absence of mitochondrial respiration, O_i (Pa) is the partial pressure of atmospheric oxygen, and K_c and K_o (Pa) are Michaelis-Menten parameters for CO_2 and O_2 , respectively.

$$W_L = \begin{cases} \alpha(1 - \omega)I_{par} \left(\frac{C_i - \Gamma}{C_i + 2\Gamma} \right) & \text{for C3 plants} \\ \alpha(1 - \omega)I_{par} & \text{for C4 plants} \end{cases} \quad 6.3$$

where α ($\text{mol CO}_2 \text{ mol}^{-1} \text{ PAR}$) is the quantum efficiency of photosynthesis, ω is the leaf scattering coefficient for PAR and I_{par} (PAR, $\text{mol m}^{-2} \text{ s}^{-1}$) is the incident photosynthetically active radiation.

$$W_E = \begin{cases} 0.5V_{cmax} & \text{for C3 plants} \\ 2 \times 10^4 V_{cmax} \frac{C_i}{P_*} & \text{for C4 Plants} \end{cases} \quad 6.4$$

where P_* is the surface air pressure.

In JULES, isoprene emission is linked to the electron requirement for isoprene synthesis (Pacifico et al., 2009). It is assumed that all isoprene emitted from plant leaves is synthesized in the chloroplasts and that a certain proportion of electrons released by PSII (Photosystem II) is used in isoprene synthesis (Arneth et al., 2007; Pacifico et al., 2011). The proportion of electrons released through this process is calculated from the estimated energy and redox equivalents requirements to reduce isoprene from the initial steps of carbon assimilation, considering the requirements of 6 moles assimilated CO₂ for one mole of isoprene produced (Pacifico et al., 2011). The effects of environmental factors like atmospheric CO₂ concentration, temperature and light in isoprene synthesis and emission are thus explicitly accounted for in process-based models due to the coupling with photosynthetic activity.

Leaf-level isoprene emission rates (ER) are modelled following Pacifico et al. (2011):

$$ER = IEF \frac{A+R_D}{A_{Jst}+R_{Dst}} f_t \cdot f_{CO_2} \quad 6.5$$

where *IEF* is a PFT-specific isoprene emission factor at standard conditions (i.e. at a temperature of 30 °C, photosynthetically active radiation of 1000 μmol m⁻² s⁻¹ and CO₂ atmospheric concentration of 370 ppm, see e.g. Guenther et al., 1995; Arneth et al., 2007b). *A* is leaf-level net photosynthesis when rubisco (RuBP) is limiting; *R_D* is leaf-level dark respiration. The subscript ‘*st*’ indicates that the variable was measured at standard conditions. *f_t* accounts for the dependence of isoprene emission on temperature, and *f_{CO₂}*, represents the inhibition of isoprene emission with increasing atmospheric CO₂ concentration, such that:

$$f_t = \min[e^{\alpha_T(T-T_{st})}; 2.3] \quad 6.6$$

where α_T is an empirical factor (currently set to 0.1 K) accounting for the higher temperature optimum of isoprene synthesis compared to that of the electron transport rate, *T* is air temperature and *T_{st}* is air temperature at standard conditions (30°C).

$$f_{CO_2} = \frac{C_{ist}}{C_i} \quad 6.7$$

where C_i is leaf internal CO_2 concentration, as before.

JULES has four soil layers, currently set at depths of 0.1, 0.35, 1 and 3 m. In each soil layer, k , soil moisture stress (β_k) is estimated based on volumetric soil water content (SWC) in that layer (θ_k ; $\text{m}^3 \text{m}^{-3}$) as:

$$\beta_k = \begin{cases} 1 & \theta_k \geq \theta_{c,k} \\ \frac{\theta_k - \theta_{w,k}}{\theta_{c,k} - \theta_{w,k}} & \theta_{w,k} \leq \theta_k \leq \theta_{c,k} \\ 0 & \theta_k \leq \theta_{w,k} \end{cases} \quad 6.8$$

where θ_w ($\text{m}^3 \text{m}^{-3}$) is the SWC at the wilting point. θ_c ($\text{m}^3 \text{m}^{-3}$), the SWC threshold at which the plant becomes water stressed, is estimated as:

$$\theta_c = \theta_w + (\theta_{crit} - \theta_w)(1 - p_0) \quad 6.9$$

where θ_{crit} is the critical SWC (usually defined as the field capacity) and p_0 is a PFT-dependent parameter that reduces the soil moisture at which a vegetation type first starts to experience water stress and is usually set to 0. θ_w and θ_{crit} are the SWC corresponding to matric water potentials of -1.5 MPa and -0.033 MPa, respectively, and are determined based on soil texture at a given site (Harper et al., 2020).

The accumulated soil moisture stress (β) experienced by plants in any grid box is then calculated based on the fraction of root mass (r_k) and soil moisture stress (β_k) in each soil layer:

$$\beta = \sum_k^{n_{soil}} r_k \beta_k \quad 6.10$$

The water-limited net leaf photosynthesis (A) in each grid cell is estimated by down-regulating the unstressed photosynthesis rate (A_p) by the stress factor β :

$$A = A_p \times \beta \quad 6.11$$

Stomatal conductance (g_s) can then be determined from the net photosynthesis rate, via the atmospheric and intercellular CO_2 concentrations, c_a and c_i respectively:

$$g_s = -1.6A \frac{RT_*}{c_i - c_a} \quad 6.12$$

where the factor of 1.6 represents the ratio of the internal diffusivities of CO₂ and water.

We define the severity of drought stress experienced as a measure of the soil water available to plants relative to the maximum available soil water (Betts, 2004; Granier et al., 2007; Seneviratne et al., 2010; Gao et al., 2017). We follow the classification proposed by Gao et al. (2017), using the grid cell accumulated soil moisture stress (Eqn. 8) to define 4 levels of drought severity as shown in Table 6.1 below.

Table 6.1: Drought severity defined using soil moisture stress (β)

Drought Severity	Extreme	Severe	Mild/Moderate	No drought
β range	$\beta \leq 0.20$	$0.20 < \beta \leq 0.40$	$0.40 < \beta \leq 0.60$	$\beta > 0.60$

Drought is believed to reduce photosynthesis due to decreased photosynthetic enzyme activity (Limousin et al., 2010; Martin-St Paul et al., 2012; Zhou et al., 2014). This assumption regarding enzyme activity was used to parameterise the response of isoprene emissions to water stress in the MEGAN3 model (Jiang et al; 2018) leading to improvements in model skill at reproducing observed isoprene emission rates under water-limited conditions. We adopt a similar approach here, modifying the unstressed isoprene emission rate according to drought stress severity:

$$ER^* = \begin{cases} ER & \text{for } \beta < 0.40 \text{ or } \beta > 0.60 \\ ER \times \left(\frac{V_{cmax}}{\alpha}\right) & \text{for } 0.40 \leq \beta \leq 0.60 \\ 0 & \text{for } \beta \leq 0 \end{cases} \quad 6.13$$

where ER^* is isoprene emission rate under drought stress, ER the unstressed emission rate estimated from Eqn. 10 and α a site-specific constant of proportionality determined from observation.

6.2.2 Study Sites and Data

Two comparable temperate forest sites have been used in this study: Wytham Woods, a deciduous woodland in Oxfordshire, UK (UK_Wyt: Kirby et al., 2014) and a mixed broadleaf forest in the Missouri Ozarks, US (US_Moz: Seco et al., 2015). At both sites, long-term continuous measurements of isoprene fluxes and/or mixing ratios, meteorology and soil

water content were made both during and outside of periods of drought over two-year periods. Observations of air temperature (K), net radiation (Wm^{-2}), downward shortwave radiation (Wm^{-2}), atmospheric pressure (Pa), specific humidity (kg kg^{-1}), rainfall (kg kg^{-1}), wind speed (ms^{-1}) and volumetric soil water content ($\text{m}^3 \text{m}^{-3}$) were obtained for each site and used to drive JULES. Hourly ERA5 datasets were used to fill gaps in in-situ measurements. The sites, data used, and their sources are summarised in Table 6.2; a fuller description of each follows.

Wytham Woods ($51^{\circ}46'23.3''\text{N}$ $1^{\circ}20'19.0''\text{W}$, 160 m.a.s.l) is located ~5km NW of Oxford in SW England. It is a deciduous broadleaf forest (DBF) dominated by European Ash (*Fraxinus excelsior* - 26%), Sycamore (*Acer pseudoplatanus* - 18%), European Beech (*Fagus sylvatica* - 11%) and English Oak (*Quercus robur* - 7%) (Kirby et al., 2014). The understory of the forest comprises other broadleaf trees and shrubs. Average leaf area index during peak growth season is estimated at $3.6 \text{ m}^2 \text{ m}^{-2}$ (Herbst et al., 2008) and the average canopy height is 18m. The isoprene budget is dominated by emissions from two species: *Q. robur* (~95%) and *A. pseudoplatanus* (~5%) (Bolas, 2020). The ages of mature trees range between 40 and 150 years (Morecroft et al., 2008; Thomas et al., 2011) and the forest consists of patches of ancient semi-natural woodland, secondary woodland, and modern plantations. The climate can be classified as warm temperate based on the Koppen climate classification. Rainfall occurs all year round with a climatological (1981-2010) average of ~600-700 mm y^{-1} . For the same period, average summer temperature ranges between 18-20 $^{\circ}\text{C}$ and declines to ~2 $^{\circ}\text{C}$ in the winter (UKMO, 2021).

The Missouri Ozarks site ($38^{\circ} 44' 38.76''\text{N}$ latitude, $92^{\circ} 12' 0''\text{W}$ longitude, 219 m.a.s.l) is an oak-dominated deciduous broadleaf forest (DBF). White (*Quercus alba*) and red (*Quercus rubra*) oak make up 63% of the forested area and constitute the main isoprene emitting species in the forest. The rest of the forest is comprised of sugar maple (*Acer saccharum* Marsh.), hickory (*Carya spp.* Nutt.), ash (*Fraxinus spp.* L.), and juniper (*Juniperus spp.* L.). The average peak growth leaf area index (LAI) during the period of this study was $3.7 \text{ m}^2 \text{ m}^{-2}$. Rainfall occurs throughout the year with no dry season. Annual average precipitation for the 2004-2017 period was 986 mm and the average temperature was ~12 $^{\circ}\text{C}$. Water stress is a recurring problem affecting photosynthesis and plant gas exchange at this site (Bahari et al., 1985; Potosnak et al., 2014) as the trees are unable to access deep soil moisture during periods of drought due to shallow water table (Gu et al., 2006). The site's characteristics are described in detail by Gu et al. (2006).

Table 6.2: Summary of site characteristics and datasets used in parameterising and driving JULES. Abbreviations are explained below the table.

Site ID	UK_Wyt	US-Moz
Site Name	Wytham Woods	Missouri Ozarks
Latitude	51.77	38.74
Longitude	-1.34	-92.20
Elevation (m)	160	220
Canopy height (m)	18	22
LAI (m ² m ⁻²)	3.6	3.7
Years	2018-2019	2011-2012
Temporal resolution of data	Hourly	Hourly
Mean annual temperature (°C)	18.0	12.1
Mean annual rainfall (mm)	700	986
PFT	DBF	DBF
Data from site PI / website	T, NR, SW, P, WS, SWC, PA	T, NR, SW, P, WS, SWC, PA
ERA 5 data used	Q, PA, SWC	Q, SWC
A	13	13
FLUXNET2015 data doi:	-	10.17190/AMF/1246081

where DBF=Deciduous broadleaf, T=Air Temperature, NR=Net Radiation, SW=Downward shortwave Radiation, P=Precipitation, WS=Wind Speed, SWC=Soil Water Content, PA=Air Pressure, Q=Specific Humidity.

6.2.3 Model experiments

Two simulations were conducted to explore the divergence between isoprene emissions estimates when drought stress is and is not explicitly accounted for. The aim of this study was to quantify the change in percentage of assimilated carbon re-emitted as isoprene under drought, and hence gain an understanding of the implications for the carbon budget. An initial simulation using the default isoprene emission scheme described in Eqns. 6.5-6.10 was carried out, hereafter referred to as CTR simulation, representing the emissions expected from the assumption that they remain coupled to photosynthesis under water stress.

The second incorporated the explicit representation of drought stress described by Eqn 6.13. We conducted a series of sensitivity tests in which the value of α (Eqn. 6.13) was modified to determine how to best replicate isoprene observations at each site during periods classified as mild/moderate drought. The optimal value of α for each site was then applied

in a simulation where isoprene emissions under water stress were modelled following Eqn. 6.13, i.e. assuming a decoupling of isoprene emission rate from photosynthesis under mild/moderate drought, hereafter referred to as CTR+Dr.

6.3 Results and discussion

The meteorological conditions observed during the WisDOM campaign and at the MOFLUX site have been extensively discussed elsewhere (e.g. see Ferracci et al., 2020, Jiang et al., 2018; Potosnak et al., 2014; Seco et al., 2015). A brief summary those of primary interest to this study (air temperature, PAR, SWC and precipitation) is provided here and then focus on the observed isoprene fluxes and the role of soil moisture stress in accounting for variations in these fluxes. I first describe the relationship between observed isoprene fluxes and soil water content and air temperature, and then compare isoprene fluxes estimated with the default isoprene emission scheme in JULES (CTR simulation). I highlight periods of divergence between estimated and measured fluxes, and demonstrate how the introduction of the soil moisture stress parameterisation (CTR+Dr) reduces the discrepancies. Finally, the percentage of assimilated carbon that is re-emitted as isoprene in both CTR and CTR+Dr simulations is calculated and the implications for modelling the carbon cycle considered.

6.3.1 Observed meteorology and isoprene fluxes

Figure 6.1 shows daily average observations of SWC, P, T, PAR at UK_Wyt and US_Moz for 2018-2019 and 2011-2012 respectively. In general, SWC was higher in the first year than the second at both sites. However, at UK_Wyt the longest sustained period of low SWC, corresponding to mild/moderate drought, also occurred in 2018, with few instances of SWC below $0.19 \text{ m}^3 \text{ m}^{-3}$ recorded in 2019. Air temperature and PAR remained similar for both years at each site. Soil moisture at both sites was sensitive to precipitation with several spikes in SWC following rainfall events (Figure 6.1a and c) due to the relatively shallow depths at which soil moisture measurements were taken (0.2 m at UK_Wyt and 0.05 m at US_Moz). Both sites are temperate, but US_Moz experiences warmer temperatures and lower PAR than UK_Wyt (Figure 6.1b and d).

At UK_Wyt, unusually high precipitation at the beginning of 2018 increased soil moisture to $0.45 \text{ m}^3 \text{ m}^{-3}$, just below the field capacity of $0.46 \text{ m}^3 \text{ m}^{-3}$, but SWC declined to $0.16 \text{ m}^3 \text{ m}^{-3}$, close to the wilting point by mid-July due to lack of rainfall from late May to

the end of June. SWC then increased to between 0.30-0.40 m³ m⁻³ in September 2018 and stayed in that range until a drought period in July 2019 caused a decline to 0.19 m³ m⁻³. SWC at UK_Wyt increased to 0.41 m³ m⁻³ by the end of 2019 in response to increased rainfall rates from September to December 2019. PAR followed a typical annual profile with less than 50 W m⁻² in the winter and 350 W m⁻² in the summer for both years. Temperatures averaged 6 °C in the winter months and rose to ~18 °C in the summer months. Compared to the long term (1993-2015) average for this site, temperatures were 1.7 °C and 1 °C warmer in 2018 and 2019 respectively (Otu-Larbi et al., 2020; UKMO, 2021). Exceptionally warm temperatures of 30.7 °C and 34.3 °C were recorded in 2018 and 2019 respectively. These high temperatures occurred during a heatwave-drought period lasting from 22 June–8 August 2018 and shorter heatwave in late July 2019.

Similarly, SWC was high (~0.52 m³ m⁻³) at US_Moz at the beginning of 2011 but rapidly fell to 0.25 m³ m⁻³, just above the wilting point of 0.23 m³ m⁻³, due to a dry spell in May and June (Seco et al., 2015). Rainfall in the later part of 2011 and early 2012 increased SWC to >0.40 m³ m⁻³ but a lack of precipitation in July and August 2012 reduced SWC to <0.20 m³ m⁻³ resulting in severe drought at this Missouri woodland (Jiang et al., 2018; Seco et al., 2015). In 2011, temperature in the winter declined to < -10 °C but increased rapidly to 32 °C by the summer. Winter 2012 was slightly warmer (-5°C) with average summer temperatures similar to the previous year. The long-term (2004-2017) mean winter and summer temperatures at this site are ~1 °C and 25 °C respectively. Hence the winters of 2011 and 2012 were colder than the long-term average but the summers were ~7 °C warmer. The highest temperature (41.5 °C) was recorded in 2011, compared with 39.4 °C in 2012. PAR ranged from about 70 Wm⁻² in the winter to 300 Wm⁻² in the summer, a smaller range than UK_Wyt. These values are comparable to the long-term values in the winter (65 W m⁻²) and summer (290 W m⁻²)

Figure 6.2 shows scatter plots of observed top-of-canopy isoprene fluxes against SWC (Figure 6.2a-d) and air temperature (Figure 6.2e-f) for both years at each site. At UK_Wyt, high isoprene fluxes of up to 8 mg m⁻² hr⁻¹ were observed at low soil water content (<0.20 m³ m⁻³) in 2018 (Figure 6.2a and e). Average temperatures during the heatwave-drought period in 2018 were about 3 °C above the long term mean for this site but appeared to have little impact on the observed increase in isoprene emissions during this period (Ferracci et al., 2020; Otu-Larbi et al., 2020a). However, in 2019 there was no observable relationship between soil moisture content and isoprene fluxes, which peaked at 6 mg m⁻²

hr⁻¹. The highest isoprene fluxes corresponded to anomalously high temperatures (>30°C) rather than the lowest SWC.

Isoprene fluxes also increase with decreasing SWC at US_Moz (Fig 2c and d) with a stronger relationship in 2012 than in 2011. The highest isoprene fluxes of 40 mg m⁻² hr⁻¹ and 25 mg m⁻² hr⁻¹ for 2011 and 2012 respectively were measured at SWC of ≤0.25 m³ m⁻³. In general, high isoprene fluxes were observed at SWC below 0.35 m³ m⁻³ and 0.30 m³ m⁻³ for 2011 and 2012 respectively. Below these thresholds, isoprene fluxes show little correlation with SWC. Similar to UK_Wyt, high temperature plays a minor role in the unusually high isoprene fluxes at US_Moz (Potosnak et al., 2014; Seco et al., 2015).

As shown in Figure 6.1b and d, PAR did not change significantly between the years at either site and in keeping with previous studies (e.g. Ferracci et al., 2020) we found no significant relationship between observed increases in isoprene fluxes and PAR. These observations provide further evidence that SWC played a primary role in the observed isoprene fluxes with a critical threshold below which isoprene emissions are affected by SWC at both sites.

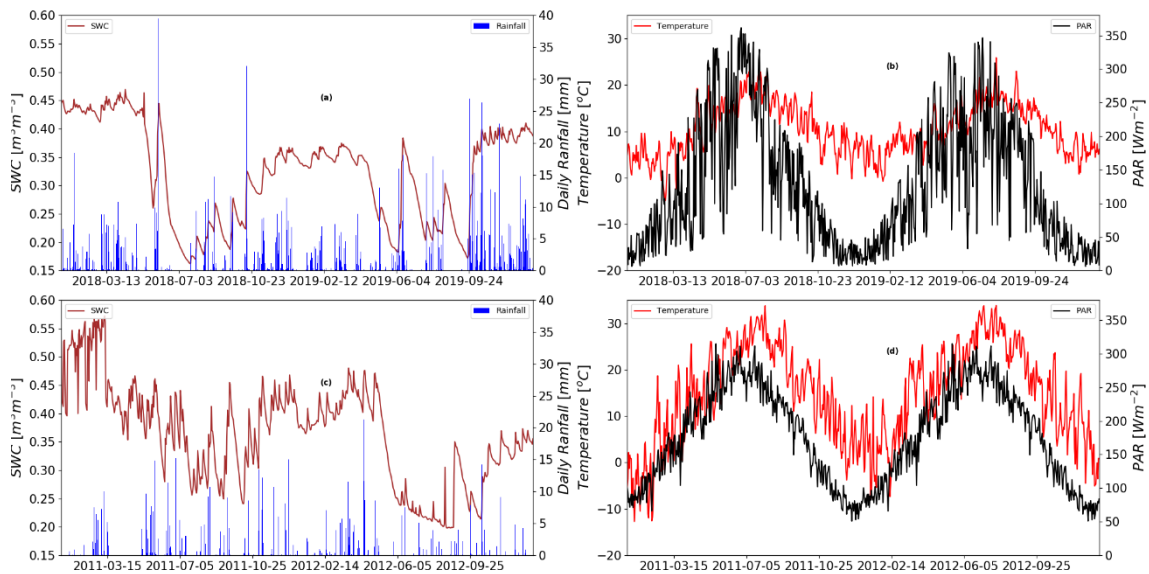


Figure 6.1: Observations of meteorology and soil conditions at each site. (a, c) SWC (brown) and rainfall (blue) and (b, d) Temperature (red) and PAR (black) at Wytham Woods (UK_Wyt) and MOFLUX site (US_Moz).

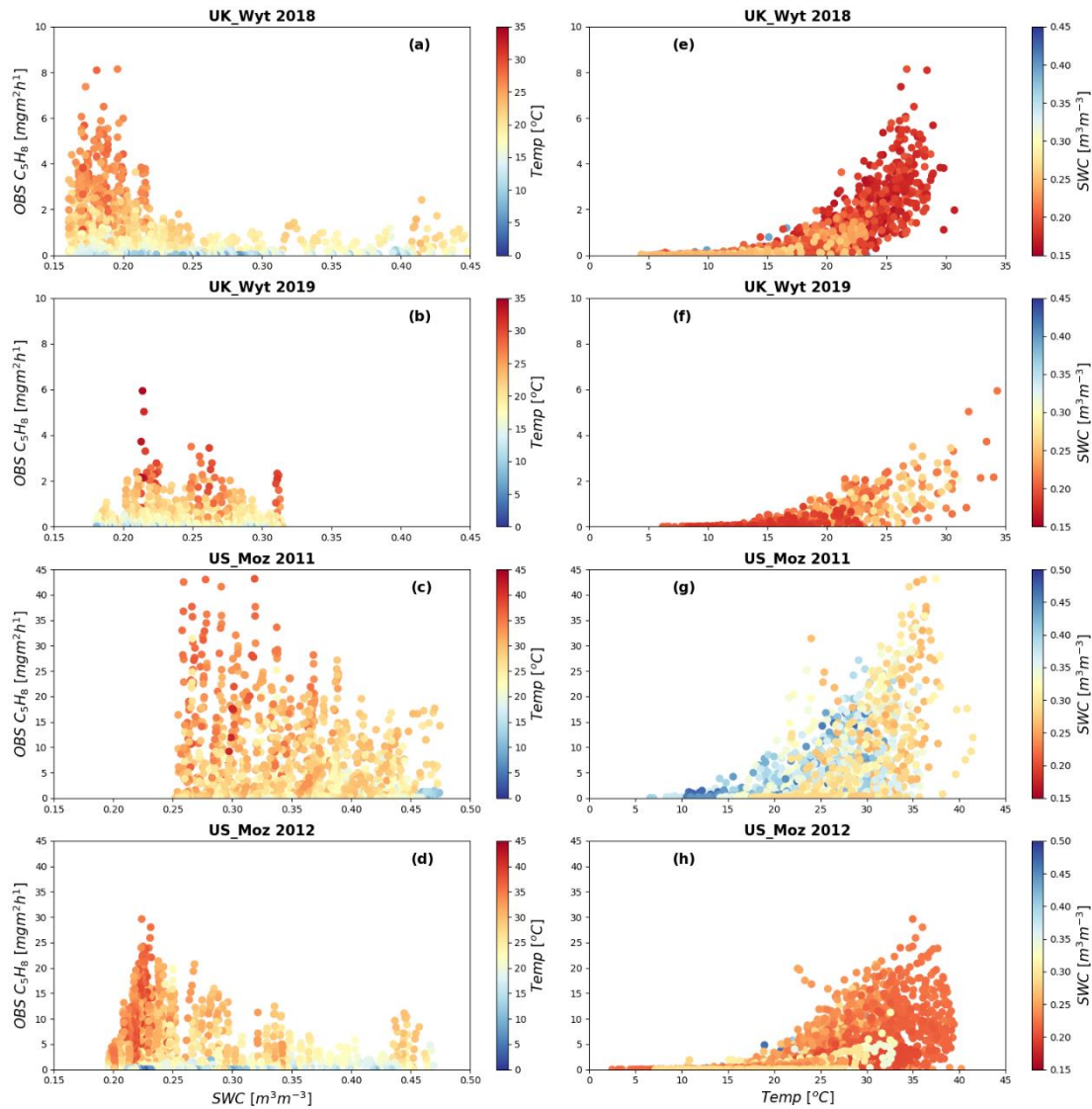


Figure 6.2: Scatter plots of isoprene fluxes against SWC coloured by temperature (left column) and temperature coloured by SWC (right column) at UK_Wyt and US_Moz. The top two rows present observations at UK_Wyt for 2018 and 2019 respectively. The bottom two US_Moz for 2011 and 2012 respectively. The isoprene vs SWC plots are coloured by temperature while the isoprene vs temperature plots are coloured by SWC.

6.3.2 CTR simulation

JULES estimates of isoprene fluxes from CTR, i.e. based on the assumption they are coupled with photosynthesis under all conditions as described in Section 2.1.2, are compared to observations at both UK_Wyt and US_Moz in Figure 6.3. Observations are shown in black while model estimates are shown in blue. The horizontal red dashed lines indicate the boundaries for moderate drought severity as defined in Section 2.1.4. Orange lines shows a time series of the dimensionless soil moisture availability factor, β , which gives an indication

of drought severity. Grey shaded areas indicate the period of moderate drought. A time series of isoprene fluxes for 2018 and 2019 at UK_Wyt are shown by Figure 6.3a and b respectively while average diurnal profiles for each year are shown in Figure 6.3c and d. Similarly, full time series for US_Moz are shown in Figure 6.3e and f, and average diurnal profiles in Figure 6.3g and h.

At UK_Wyt, CTR reproduced observed isoprene fluxes before and after the 2018 heatwave-drought period to within 14% but underestimated by 58% under moderate drought (Figure 6.3a). For 2019, CTR reproduces observation to within 5% throughout the season as soil moisture stress was limited to a brief period towards the end of the growing season. Isoprene fluxes are however overestimated towards the end of the growing season in both years possibly due to the inability of the model to accurately account for changes in phenology due to senescence. The average diurnal profile of observed and modelled isoprene fluxes (Figure 6.2c and d) further shows that CTR simulation underestimates peak daytime isoprene emissions by 50% in 2018, likely due to discrepancies during the heatwave-drought, but captures both the diurnal variations and peak isoprene fluxes in 2019 albeit with a slight overestimation in the early morning and late evening.

Model performance at US_Moz is similar to that of UK_Wyt. CTR reproduces observed isoprene emissions before the commencement of drought stress in 2011 and 2012 as well as during the severe phase of the drought in 2012 to within 30%. However, fluxes are underestimated by 68 and 72% during the moderate drought phase in 2011 and 2012 respectively. Unlike UK_Wyt, there is no overestimation of isoprene fluxes in the model at the end of the season but it should be noted that the measurements at US_Moz ended earlier (August in 2011 and early September in 2012) compared to measurements at UK_Wyt (late September in 2018 and early October in 2019), thereby avoiding potential issues around canopy senescence. The diurnal profile of isoprene shown in Figure 6.2g and h indicates that JULES not only underestimates peak daytime fluxes by >100%, but the timing of the peak also lags observations by about an hour. While average observed isoprene fluxes reach peak daytime values of $13 \text{ mg m}^{-2} \text{ hr}^{-1}$ in 2011, peak model estimates are a factor of three lower at $4 \text{ mg m}^{-2} \text{ hr}^{-1}$. A similar underestimation occurs for diurnal isoprene fluxes in 2012. JULES also underestimates peak daytime isoprene fluxes before and after the heatwave by about 35% at this site. A possible explanation is that the generic PFT emission factor for deciduous broadleaf trees in JULES is unrepresentative of the actual emission rates from this forest, which is dominated by strong isoprene emitters, causing the model to underestimate the diurnal and seasonal isoprene fluxes at this site.

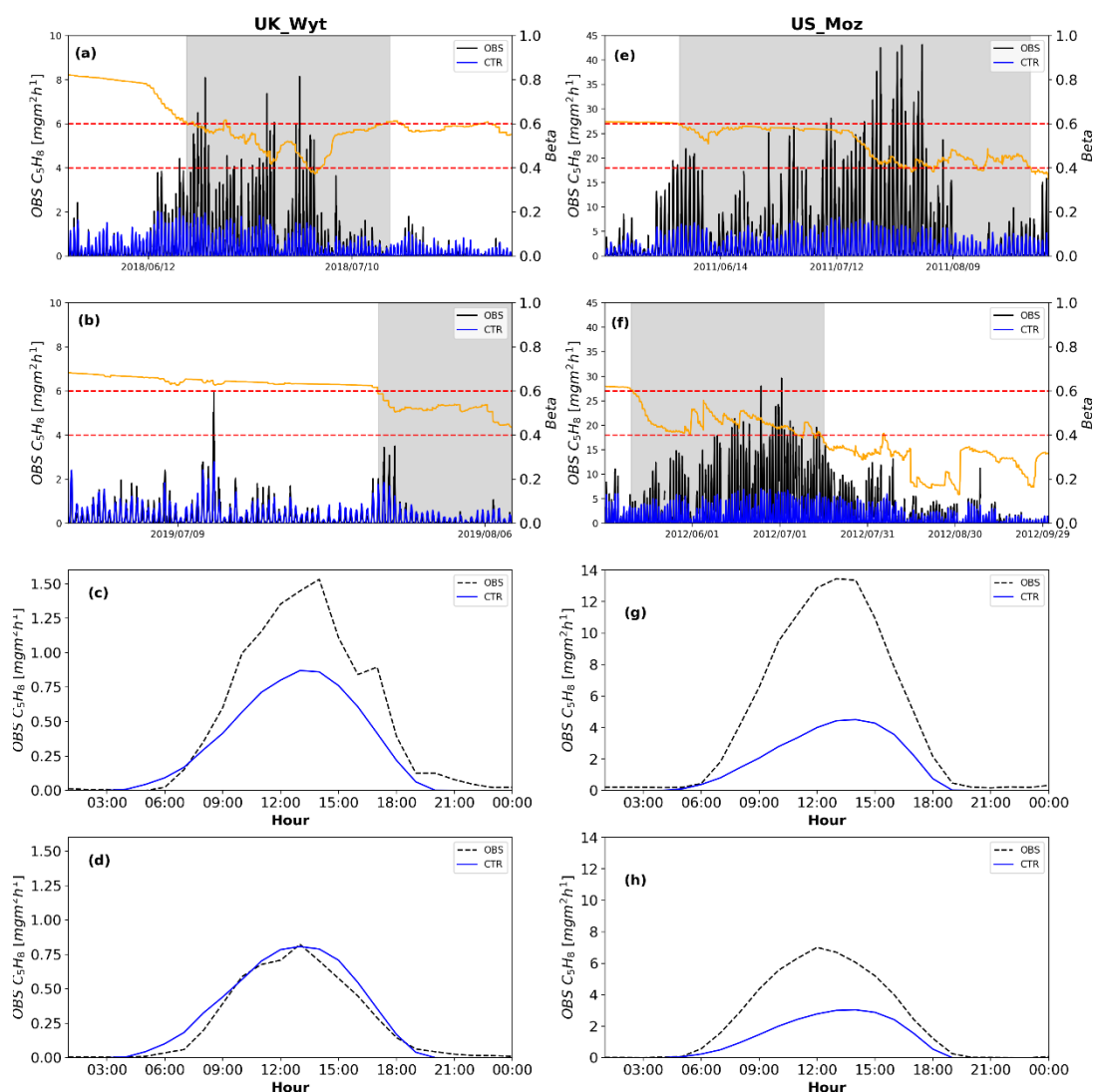


Figure 6.3: Timeseries of observed and modelled isoprene fluxes at UK_Wyt (a-d) and US_Moz (e-h). Observed isoprene is shown in black while model estimates (CTR) are shown in blue. Areas highlighted in grey are moderate drought periods as defined by Eqn. 8 and shown indicated by the orange lines. Dashed red lines indicate the upper and lower bounds of the moderate drought severity definition.

6.3.3 CTR+Dr Simulations

As described in Section 2.1.4 and Eqn. 13, isoprene emissions during periods of moderate drought are assumed to be enhanced proportionately to increases in plant photosynthetic activity (V_{max}), which is calculated online within JULES. The constant of proportionality (α) is site-specific with values of 13 and 20 found to provide the best model-observation fit at UK_Wyt and US_Moz respectively from our series of sensitivity tests. These values were used in CTR+Dr simulations for each site, in which isoprene emissions

and fluxes increase during mild/moderate drought as described in Section 2.1.4 (see Figure 6.3), but follow photosynthesis as per CTR outside of these periods.

At UK_Wyt model performance during the 2018 heatwave-drought period is improved substantially with underestimation falling from 58 to 6% in CTR+Dr. However, CTR+Dr still fails to reproduce isoprene fluxes during periods corresponding to soil rewetting following rainfall events as described in Otu-Larbi et al. (2020a), unsurprising given the model does not include parameterisations to account for this phenomenon. For 2019, CTR+Dr does not improve model skill during the main growth season as there were no periods of drought and worsens model overestimation at the end of the growing season when moderate drought did occur.

CTR+Dr improves model reproduction of observed isoprene fluxes at US_Moz during both years. Model underestimation of canopy-top isoprene fluxes is reduced from 68 to 12% and 72 to 20% for 2011 and 2012 respectively. However, the model fails to reproduce the extremely high isoprene fluxes observed during a period of moderate drought in late July 2011. These instances correspond with very high temperatures ($>35^{\circ}\text{C}$) observed at this site. Such high temperatures constitute heat stress to plants and may cause unexpectedly high increases in leaf temperature leading to additional increase in isoprene emissions. When drought becomes severe in 2012, CTR+Dr (Figure 6.4) fluxes return to those of CTR which successfully reproduced observed fluxes during this period, consistent with the assumption that under such conditions isoprene emissions are limited by lack of assimilated carbon and thus track photosynthesis. This together with model performance in the unstressed periods at both sites supports observations and the hypothesis that isoprene emissions are coupled to GPP when SWC is not a limiting factor and during severe droughts (e.g. see Brillì et al., 2007; Niinemets, 2010; Potosnak, 2014) but that isoprene emissions are decoupled from photosynthesis under moderate drought.

The improvements in CTR+Dr relative to CTR simulations are clearly seen in the average diurnal profile of isoprene fluxes at both sites. For UK_Wyt (Figure 6.4c-d), CTR+Dr reproduces the magnitude of isoprene fluxes to within $\sim 10\%$ in both years though underestimates in 2018 and overestimates in 2019. Peak daytime isoprene fluxes in CTR+Dr are $1.3 \text{ mg m}^{-2} \text{ hr}^{-1}$ in 2018, substantially closer to observation than the $0.8 \text{ mg m}^{-2} \text{ hr}^{-1}$ estimated in CTR. There is however a slight overestimation of isoprene fluxes in the early hours of the morning possibly due to leaves near the sample inlet being shaded at this time of the day.

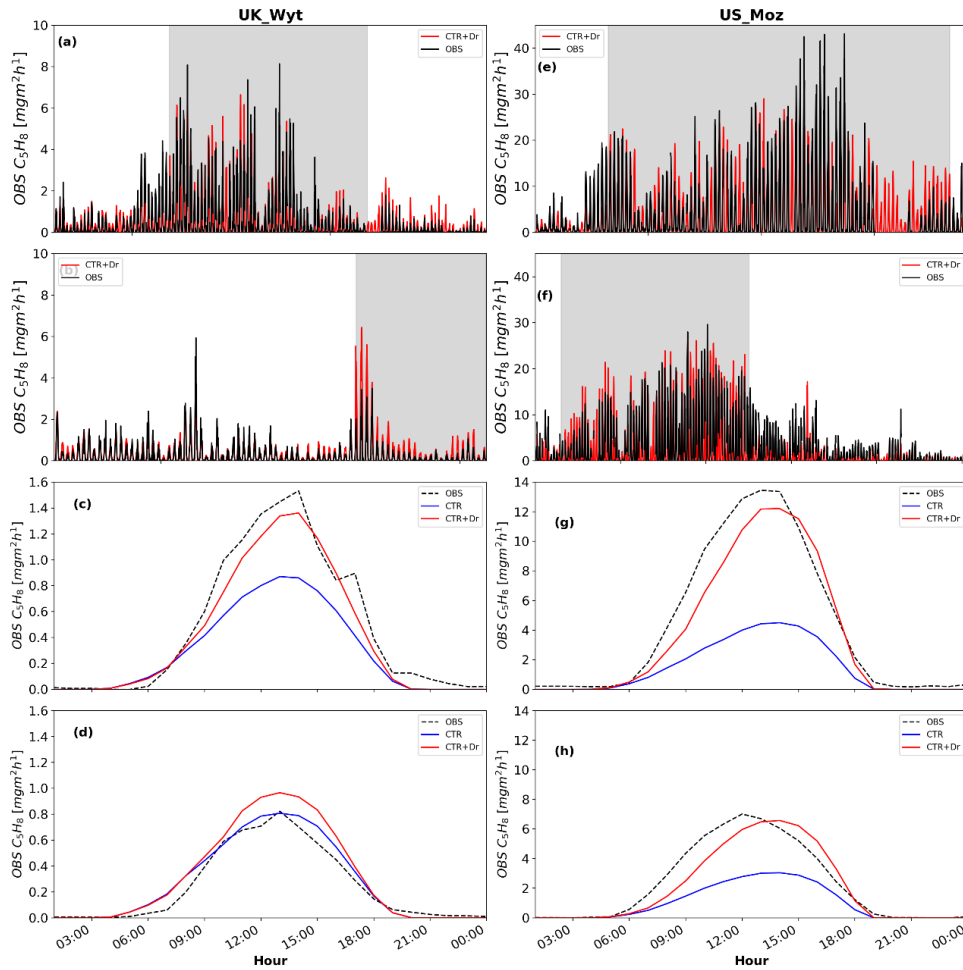


Figure 6.4: Timeseries of observed and modelled isoprene fluxes at UK_Wyt (a-c) and US_Moz (d-f). Observed isoprene is shown in black while model estimates are shown in blue (CTR) and red (CTR+Dr). Areas highlighted in grey are moderate drought periods as explained in Figure 6.3.

At US_Moz, CTR+Dr improves the diurnal profile of JULES isoprene fluxes compared to CTR for both years. For 2011, the underestimation of the daytime peak flux is reduced to ~10%, down from the factor of 3 underestimation in CTR, and the 2012, overestimation is reduced to ~5%. The 1-hour lag persists in both years. These results confirm that the effect of drought stress on isoprene emissions and fluxes over both long (seasonal) and short (daily) timescales is observable at the ecosystem scale. However, importantly, they also demonstrate the substantial impact on isoprene emissions and fluxes of moderate drought stress, conditions that are expected to increase in frequency and extent under global change. For both UK_Wyt and US_Moz, moderate drought stress caused an increase in emission rates and fluxes of up to 500%, a phenomena not currently incorporated in emissions or land surface models and with implications for net carbon assimilation by forest ecosystems.

6.3.4 Percentage of assimilated carbon emitted as isoprene

We now calculate the proportion of carbon estimated to be assimilated through photosynthesis in JULES that is re-emitted as isoprene under the assumption that (a) isoprene emissions always remain coupled to photosynthesis (CTR) and (b) isoprene emissions are decoupled from photosynthesis during periods of mild/moderate drought stress (CTR+Dr). Figure 6.5 shows modelled isoprene fluxes as a percentage of modelled GPP for both simulations at each site. On average, 0.3% and 2% of GPP is emitted as isoprene at UK_Wyt and US_Moz respectively when there is sufficient moisture, or severe drought, and isoprene emissions are coupled to GPP (CTR). These annual average values roughly double, to ~0.6% and ~5%, at the respective sites when the enhancement of isoprene emissions under moderate drought is accounted for (CTR+Dr). However, during the moderate phase of drought itself, the percentage of assimilated carbon re-emitted as isoprene increases to >1% at UK_Wyt and >10% at US_Moz. i.e. an increase of >100% at both sites.

These figures are comparable to those found elsewhere. Enclosure measurements have shown that Red Oak (*Quercus Rubra*), for example, re-emits ~1.4-7.2% of assimilated carbon as isoprene and monoterpenes (C₁₀H₁₆) (Loreto and Sharkey, 1990; Sharkey and Loreto 1993) although that percentage was lower for Holm oak (*Quercus ilex*) (0.7-3.0%; Kesselmeier et al., 1996; 1998). The 2-5% found here for US_Moz which is dominated by *Quercus Rubra* is of the same magnitude as that reported by Loreto and Sharkey (1990).

UK_Wyt and US_Moz cover total land areas of ~400 and ~353 hectares, respectively. Assuming a relatively homogenous distribution of tree species throughout each ecosystem, we can estimate the total carbon emitted into the atmosphere through isoprene from each forest. For UK_Wyt, average annual isoprene emissions in CTR would contribute ~1 g C m⁻² yr⁻¹ into the atmosphere, increasing to 1.3 g C m⁻² yr⁻¹ when the effect of moderate drought stress is factored in (CTR+Dr). For Wytham Woods as a whole, this translates to 3.88 and 5.37 Mt C yr⁻¹ with and without the impact of moderate drought respectively. For US_Moz, isoprene contributed 4.74 and 9.73 g C m⁻² yr⁻¹ into the atmosphere annually in CTR and CTR+Dr simulations, scaling to 15.35 Mt C yr⁻¹ for the entire forest in the absence of drought stress and 31.50 Mt C yr⁻¹ when moderate drought occurred.

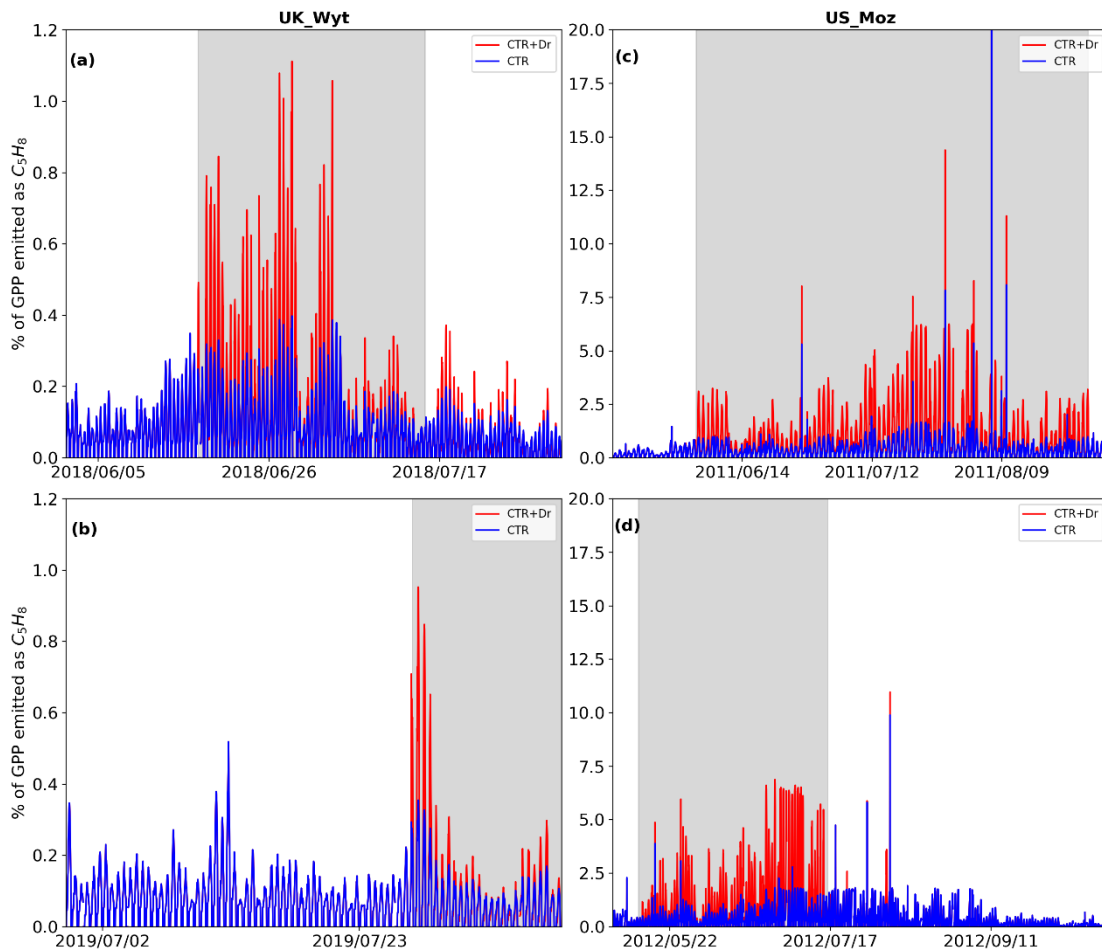


Figure 6.5: Percentage of assimilated carbon that is re-emitted as isoprene at UK_Wyt (a-b) and US_Moz (c-d). Areas highlighted in grey are moderate drought periods as explained in Figure 6.3.

Temperate forests constitute 16% of the world’s total forest cover and store an estimated 119 Pg C (14% of the total carbon in forests) (FAO, 2020; Pan et al., 2011). Based on the estimated 9.9 Pg C yr⁻¹ of GPP at temperate forests (Gough, 2011), our results indicate that between 0.005 and 0.05 Pg C yr⁻¹ of this assimilated carbon would be re-emitted as isoprene when there is sufficient soil moisture. However, these values increased to as much as 0.16 Pg C yr⁻¹, about a third of global isoprene emissions, for situations where relatively brief periods (~16 weeks per year at each site) of moderate drought occurred. Actual increases in the percentage of assimilated carbon that is re-emitted to the atmosphere as isoprene will however depend on the duration of drought stress and plants’ capacity to adapt to changing climatic conditions.

6.4 Conclusions

Much of central and northern Europe experienced prolonged periods of drought during the summers of 2018 and 2019 (Toreti et al., 2019). Wytham Woods in the UK was exposed to mild to moderate drought conditions during which soil moisture fell below $0.19 \text{ m}^3 \text{ m}^{-3}$ in both years, although only for a relatively short period in 2019. US_Moz similarly experienced a mild to moderate drought in the summer of 2011 which became severe in the late summer of 2012 due to continued absence of rainfall (Potosnak et al., 2014; Seco et al., 2015). Unusually high isoprene fluxes were observed in each of these deciduous broadleaf forests in the UK and US under these moderate drought events. The high temperatures and PAR that also occurred at these sites during the same periods were found insufficient to explain the observed increase in isoprene emissions and fluxes at either forest. Rather, isoprene fluxes were found to increase disproportionately during periods of mild to moderately low soil water content leading us to hypothesize that drought stress was the main factor driving the observed increased isoprene emissions. This hypothesis is supported by laboratory, field and modelling studies focusing on the role of drought stress in isoprene emissions (Bamberger et al., 2017; Genard-Zielinski et al., 2018; Pegoraro et al., 2004; Potosnak et al., 2014; Tattini et al., 2015) although the impact of drought stress on isoprene emissions from mature forest ecosystems is still uncertain due to a lack of observations in such environments. Our results support a growing body of literature that shows isoprene emission rates and fluxes from forests substantially increase during the onset of drought conditions (Ferracci et al., 2020; Seco et al., 2015).

The work presented here is the first attempt to include the effect of the observed decoupling of isoprene emissions from photosynthesis under moderate drought stress in a process-based model. The isoprene emission scheme, based on the electron transport theory proposed by Niinemets et al. (1999), in the JULES land surface model was used to investigate the role of drought stress in regulating isoprene fluxes measured over two temperate deciduous broadleaf forests over two growing seasons. We find that while this approach was able to reproduce observed isoprene fluxes during periods of no or severe drought, JULES underestimated observations at both sites during periods of mild or moderate drought in the same way as more widely-used empirical isoprene emission models (e.g. see Jiang et al., 2018; Potosnak et al., 2014; Otu-Larbi et al., 2020). This suggests the process-based emission model is unable to account for the decoupling that appears to occur between isoprene emissions and photosynthesis during mild and moderate drought stress.

We implemented a new soil moisture-based emission scheme that decouples isoprene emissions and GPP when soil moisture availability meets the criteria of mild or moderate drought stress in the JULES LSM. Model performance improved over both annual and diurnal time scales. We therefore conclude that this hypothesised decoupling is observable at the landscape scale, and that LSMs can successfully reproduce observed isoprene emissions across the full range of drought severities by incorporating this response.

We still found, however, that JULES was unable to reproduce high isoprene fluxes at either site associated with exceptionally high temperatures of as much as 12 °C and 10 °C above the climatological means at UK_Wyt and US_Moz respectively. This suggests that either the optimum temperature for isoprene emissions is set too low for the actual mix of species at each site or that leaf temperatures are enhanced beyond that expected. Further laboratory and field-based experiments and observations will be required to elucidate which, as well as the physiological and biochemical processes involved.

The forests used in this study represent temperate woodlands which make up 16% of global forest cover (FAO, 2020). As global climate changes, droughts are expected to increase in frequency due to changes in precipitation patterns (Zhao and Dai, 2017). Based on our findings, the ratio of assimilated carbon that is re-emitted as isoprene can be expected to increase in future climates. This will have implications for estimates of the terrestrial carbon sink and global climate change mitigation efforts as the world's forests will store less carbon than currently projected. We find that the percentage of assimilated carbon that is re-emitted as isoprene could increase by >100% under drought conditions based on our findings at the two sites used in this study. If these results are generalised over all temperate deciduous forests, future drought stress could lead to as much as a further 0.3 Pg C yr⁻¹ of additional isoprene re-emitted into the atmosphere from assimilated carbon over relatively short periods of moderate drought stress.

Tropical forests account for 40.8 Pg C yr¹ of global GPP, i.e. four times as much as temperate forests (Gough, 2011). Isoprene emissions from the tropics are also higher than those at other forest ecosystems but measurement campaigns in such environments are usually limited to short periods of weeks due to logistical and financial constraints, making it difficult to assess how tropical isoprene emissions may respond to drought stress over long time periods. This work highlights the need for more long-term ecosystem scale measurements of isoprene, especially in tropical forests, to enable a full assessment of the impacts of plant emissions on net carbon assimilation in an increasingly changing climate.

This work and other recent modelling studies show the need to account for increased isoprene emissions under moderate drought conditions in empirical and process-based emissions models to improve model performance (Jiang et al., 2018; Otu-Larbi et al., 2020a; Potosnak et al., 2014). Such improvements will have a cascading impact on modelling and understanding atmospheric composition and air quality as well as climate as isoprene chemistry is important in controlling concentrations of important trace gases like ozone and nitrogen oxides. However, future isoprene emission rates will also change in response to changing vegetation composition. Therefore, there is the need to fully couple LSMs with dynamic vegetation modules and atmospheric-chemistry models to understand the role of land cover as well as climatic change on isoprene emissions and hence atmospheric chemistry. This will improve understanding of the complex and competing feedbacks between isoprene emission and climate and enable better quantification of such feedbacks.

Chapter 7: Conclusions

This thesis was motivated by the need to improve our understanding of the effects of drought stress and ozone exposure on trace gas exchange between global forests and the atmosphere and how to account for such interactions in Land Surface Models (LSMs).

Long-term measurements of isoprene, gross primary productivity (GPP), latent heat fluxes (LE), meteorology and ozone concentrations were combined with vegetation models to understand how drought stress and ozone damage affect isoprene emissions and plant gas exchange. The ultimate aim of this research work was to improve how these processes are parameterised in models since models are fundamental to climate change mitigation efforts.

In Chapter 3, the empirical isoprene emission model of Guenther et al. (1995) was used within a 1-D canopy-atmosphere exchange model (FORCAsT) to investigate the effect of drought severity on estimates of isoprene emissions. The skill of the model to reproduce such impacts was evaluated. While FORCAsT reproduced observed isoprene mixing ratios before and after a period of moderate drought the model substantially underestimated during the drought by as much as 40%. This study revealed that current drought algorithms used in this popular isoprene emission scheme are inadequate to account for observed increases in isoprene emissions during moderate drought stress.

Three widely used coupled stomatal conductance-photosynthesis models were incorporated into the FORCAsT 1-D model in Chapter 4. The performance of each was assessed against measurements of Gross Primary Productivity (GPP), canopy-scale photosynthesis, at 5 forest sites representing a diverse range of ecosystems. The impact of variations in stomatal conductance parameters applied in each of the coupled models on plant productivity, ozone deposition velocity and deposition rates were explored to allow an estimation of the uncertainties associated with modelled stomatal conductance and, hence, ozone deposition rates.

Chapter 5 then explores the effect of ozone damage and soil water stress on canopy gas exchange, specifically CO₂ and water vapour fluxes, and how this may be affected by future climate change. Here, we found that drought stress had a greater impact on plant physiological processes than ozone but accounting for both stress factors provided better model-observation fit under current conditions.

In Chapter 6, the process-based isoprene emission scheme within the JULES LSM was used to investigate the relationship between gross primary productivity and isoprene emissions, and how the ratio between carbon assimilation and isoprene emissions changes

during periods of low soil water content. Similar to the FORCAsT model used in Chapter 3, we find that JULES reproduces observed isoprene fluxes in unstressed and severe drought conditions but underestimates fluxes during moderate drought stress. We also found that the percentage of assimilated carbon that is reemitted as isoprene increases by a factor of 2 during moderate drought stress, indicating the need for improved parameterisation of drought impacts on biogenic isoprene emissions especially as climate change increases the frequency of drought events.

This concluding chapter provides a synthesis of the main findings of the thesis and how they relate to the aims of the study (Section 7.1). Sources of uncertainty in the results presented in Chapters 3-6 and the future work required to constrain and reduce them are discussed in Section 7.2.

7.1 Summary of findings

Although not a direct regulator of plant physiology and growth, the lack of available water is the main limitation to plant productivity. Plants respond to low water availability in a variety of ways, including reductions in stomatal conductance, gas exchange and productivity. Although well-studied, the precise mechanisms driving these responses are still not fully elucidated.

In Chapter 4, we found that the Medlyn stomatal conductance-photosynthesis model outperformed the Ball-Berry model although both models are based on similar assumptions and methodology. The Medlyn model was found to best reproduce observed GPP with model estimates within 20% of observed values at Mediterranean, temperate and Boreal forest sites. It overestimated GPP at a tropical evergreen forest site however due to an inability to properly account for changes in forest structure and photosynthetic capacity throughout the year. We hypothesise that the optimisation theory approach, i.e. that plants optimise stomatal conductance to conserve water while best maintaining photosynthesis, on which the Medlyn model is based, better accounts for the physiological response to drought stress resulting in the superior performance of the Medlyn model especially in Mediterranean environments where droughts occur frequently and can be severe.

In Chapter 5, the assumption that drought stress imposes both stomatal and biochemical limitations on plant physiology proposed in previous studies by Egea et al. (2011) and Keenan et al. (2010) was used to study the impact of low soil moisture on plant productivity and latent heat fluxes. We found that neglecting the impact of drought stress

led to an overestimation of observed GPP by 27-34% and LE by 17-31% across two Mediterranean and one Boreal ecosystem. The effects of drought stress alone were sufficient to reduce present day GPP and LE estimates across the three sites by $150\text{-}400\text{ g C m}^{-2}\text{ yr}^{-1}$ and $20\text{-}80\text{ W m}^{-2}\text{ yr}^{-1}$ respectively depending on the duration and severity of the drought stress as well as a particular ecosystem's adaptation to drought stress. These reductions are ~15% of the annual mean GPP and LE observed at each site. Droughts were found to have a higher impact on GPP and LE in Mediterranean ecosystems but were also important in Boreal forests during the relatively infrequent drought episodes.

In general, the inclusion of a drought stress parameterisation in the model improved model-observation fit leading to better model output statistics under current conditions. The impact of drought stress on plant gas exchange was also demonstrated to progressively increase in future climate based on model simulations using seven CMIP5 models under the RCP8.5 scenario. Drought stress reduced estimated GPP and LE by 5-14% and 7-18% by the middle of the 20th century, and by as much as 21% and 19% respectively by the end of the century as changes in global precipitation patterns become more pronounced.

Drought stress is the main stress factor limiting plant growth and productivity (Nemani et al., 2003). It is therefore not surprising that the inclusion of drought stress parameterisation improved model reproduction of observations. We therefore conclude that drought stress will continue to have a major and increasing impact on terrestrial carbon sink which will affect global CO_2 levels and hence climate change. Assuming the impacts of drought stress on GPP found for the forests studied in Chapter 5 were global, lack of water could reduce the global carbon sink by 25 Pg C yr^{-1} , about 20% of current global GPP.

The data and results presented in Chapters 3 and 6 of this thesis show that increases in isoprene emission rates under mild or moderate drought stress are observable at the ecosystem-scale for mature forests. They also indicate that isoprene emission is decoupled from photosynthesis during mild or moderate drought as plants rely on older pools of stored carbon to synthesise and emit isoprene (e.g. Brillì et al., 2007). Thus, a reduction in stomatal conductance as a coping mechanism against drought stress does not directly affect isoprene emissions, although it leads to a decline in photosynthesis rates. Instead, under moderate drought reduced transpiration due to reduced stomatal conductance increases leaf temperature which in turn increases isoprene synthesis and emissions, which are known to ameliorate heat stress (e.g. Sharkey et al., 2001; Singsaas et al., 1997; Tattini et al., 2015).

The results from these modelling studies show that isoprene mixing ratios and fluxes increased substantially during the mild/moderate drought periods in response to large

increases in foliage emissions in both model formulations, driven by increases in air and, hence, leaf temperatures.. However, these increases were insufficient to account for the observed mixing ratios and fluxes of isoprene at either site during the onset of drought conditions. Modelled isoprene mixing ratios were 40% lower in FORCAsT than observations during the heatwave-drought period at Wytham Woods. The process-based isoprene emissions scheme in JULES also underestimated isoprene fluxes at Wytham Woods and Missouri Ozarks by ~60% and ~70% respectively during the mild/moderate phase of the droughts at both sites. Both models however performed well outside of these periods, reproducing observed isoprene fluxes, and mixing ratios to within 20%.

These results led us to conclude that the algorithms currently used in either of these two emissions models are unable to account for the actual increase in isoprene emission rate under mild to moderate drought stress. Previous studies have also shown that current soil moisture parameterisations fail to account for the observed response of isoprene emissions to soil moisture stress in cases of mild or moderate drought stress, although are effective in reproducing isoprene emissions under unstressed or severe drought scenarios (e.g. Guenther et al., 2006; Jiang et al., 2018, Potosnak et al., 2014).

This work proposes two methods for modelling the impacts of moderate drought stress on isoprene emissions. The first, presented in Chapter 3, allows for the combined effect of increased leaf temperature due to decreased plant respiration, and low soil moisture on isoprene emissions to be parameterized concurrently, based on the hypothesis of Niinemets (2010) and Potosnak et al. (2014). The mathematical formulations used here also account for the effect of soil rewetting following periods of drought on isoprene emissions. Soil rewetting has been observed in laboratory experiments to increase isoprene emissions, but this has not been previously tested in a model. The second method relies on plant photosynthetic activity, represented by V_{cmax} (the maximum rate of carboxylation of Rubisco) and the fraction of soil water available to plants (referred to as soil water availability factor, β). As described in Chapter 6, isoprene emissions are assumed to increase proportionally to changes in V_{cmax} during periods of mild/moderate drought, while remaining coupled to photosynthesis outside of these conditions.

This thesis has provided evidence of how moderate drought stress affects isoprene emissions, and hence fluxes and mixing ratios in mature forest environments. By taking these plant physiological processes into consideration, this work has provided a pathway by which both empirical and process-based isoprene emission models could be improved to realistically represent the observed response of isoprene emissions to drought stress. This is

important given the large volumes of isoprene emitted into the atmosphere, its role in regulating atmospheric oxidant levels, indirect climate forcing through formation of secondary aerosols, and the regulation of surface ozone and methane levels through its chemistry with nitrogen oxides. The methods described here are needed in a changing climate where droughts are expected to increase in frequency and geographical extent.

In Chapter 4, we showed that stomatal conductance estimated in a broad range of forest ecosystems using the Jarvis, Ball-Berry and Medlyn coupled stomatal conductance-photosynthesis models vary by up to 75% depending on the choice of model parameters used. Such large variations in modelled stomatal conductance led to a factor of 3 difference in model estimates of GPP between the best and worst performing model configurations at individual sites. The choice of stomatal conductance parameters within each of the three coupled stomatal conductance-photosynthesis models were also found to produce differences in seasonal and diel profiles of ozone deposition velocity of as much as 30% and deposition rate of up to 9%. The biggest variation in modelled ozone deposition rates were observed at Boreal and temperate forest ecosystems where changes in phenology caused stomatal conductance between model configurations to vary by more than a factor of 2. By contrast, modelled ozone deposition rates varied by <10% at evergreen forest sites. These results highlighted the importance of accurate model parameterisation of stomatal conductance on estimating ozone deposition rates, crucial for determining ozone fluxes and uptake, and hence the impacts on plant gas exchange.

Two methods for estimating the effect of ozone damage on forests based on the flux of ozone through the stomata (Pleijel et al., 2004; Sitch et al., 2007) and the hypothesis that plants close their stomata to avoid ozone damage (stomatal closure: Hoshika et al., 2013) were tested in this thesis. These methods are based on contrasting theories about how plants respond to ozone stress: the stomatal flux approach assumes that ozone stress is tolerated by plants while the stomatal closure approach assumes that plants avoid uptake and hence limit damage. Both assumptions rely on accurate estimates of stomatal conductance, the measure of stomatal aperture, to estimate the reduction in plant gas exchange due to ozone damage. In Chapter 5, we found that the assumption that plants tolerate ozone stress was better at explaining the observed GPP at Mediterranean and Boreal forest sites while avoidance of ozone by premature stomatal closure appeared better suited to LE. This is because the tolerance approach used downregulates photosynthesis directly in response to ozone damage. On the contrary, the avoidance method has only an indirect impact on photosynthesis rates but a direct effect on LE through its impact on stomatal conductance.

These findings suggest that ozone imposes both stomatal and non-stomatal limitations on plant productivity. Future modelling and laboratory studies are required, focused on understanding the relative contributions of stomatal and biochemical ozone damage on plants to enable better estimation of the impact of ozone damage on plant gas exchange. Future modelling studies should investigate the impact of applying ozone damage equations to photosynthetic capacity parameters, V_{cmax} and J_{max} , together with parameters describing the link between photosynthesis and stomatal conductance such as g_l and m in the Medlyn and Ball-Berry models (Ball et al., 1987; Medlyn et al., 2011).

This thesis has also demonstrated that the impact of ozone stress on vegetation would decrease in future relative to its present-day impacts. In future climates, high atmospheric CO_2 concentrations will cause a decrease in stomatal conductance hence decreasing stomatal ozone uptake. This causes a decline in the impact of ozone damage on forest productivity. GPP was reduced by as much 11% ($\sim 200 \text{ g C m}^{-2} \text{ yr}^{-1}$) in present day simulations but this effect declined to 3-4% by mid-century (2041-2050) and 2-3% by end of the century 2091-2100. While the impact of ozone damage on plant productivity is projected to decrease in future climates, it still constitutes an important control on global plant productivity currently estimated at 120 Pg C yr^{-1} (Kesselmeier et al., 2002). Assuming a uniform impact of ozone on forests, even a 2% reduction in global GPP due to ozone damage by the end of the 21st century could lead to a decline of about 2 Pg C yr^{-1} , about one-third of carbon emissions attributable to deforestation. However, as demonstrated in this thesis, such reductions will be dependent on climatic conditions and tree or crop species.

7.2 Limitations and Future Works

This thesis shows that abiotic stress factors play a significant role in driving biogenic isoprene emissions as well as productivity and gas exchange. However, there are multiple uncertainties associated with any model estimates. This is also true for the studies described in this thesis. Isoprene models for example have uncertainties associated with the choice of basal emission rates, forest structure such as leaf area index and meteorological forcing data.

Previous studies have shown that the source and temporal resolution of input meteorological data could affect modelled isoprene emission rates. For instance, Ashworth et al. (2010) report that global isoprene emissions were reduced from 766 Tg y^{-1} when using hourly input data to 746 Tg y^{-1} for daily average input data and 711 Tg y^{-1} for monthly average input meteorology. This represents up to 7% reduction based on the averaging

period of input data alone. The same study showed that such discrepancies can be even higher at a local scale. Here we have used half-hourly or hourly meteorological data to minimise the uncertainty associated input data.

A few studies have been conducted to estimate isoprene emission rates in future climates taking the combined effects of changes in soil moisture, carbon dioxide and temperature into account (e.g. Guenther et al., 2006; Heald et al., 2009). These studies show global isoprene emissions, estimated at 450-600 Tg C yr⁻¹ under current conditions, could increase by as much as ~190 Tg C y⁻¹ due to a temperature increase of 2.3 °C by 2100. However, the decrease in isoprene emissions due to increasing CO₂ concentrations could off-set this temperature effect almost entirely (Arneeth et al., 2008; Heald et al., 2009). Importantly though, the effect of drought stress on isoprene emissions was accounted for in these studies using the MEGAN SWC algorithm described in Chapter 2. As this thesis and other studies have shown, this algorithm fails to reflect the increase in emissions observed in cases of mild or moderate drought stress (e.g. Jiang et al., 2018; Potosnak et al., 2014). Future modelling should apply the approaches developed in this thesis to simulate global isoprene emissions as they have been shown to effectively account for the effects of drought stress of different severity across a wide range of forest ecosystems.

Impacts of ozone damage on plant productivity and gas exchange were modelled using PFT-specific thresholds above which ozone damage occurs following the approach of other studies (e.g. Mills et al., 2011; Sitch et al., 2007). A critical ozone flux threshold of 1 nmol m⁻² s⁻¹ was applied to forests throughout the growing season as recommended by Mills et al. (2011). However, a recent study Conte et al. (2021; under review) shows that this threshold did not remain constant through the year, but appeared dependent on the season, i.e. the phenology of the ecosystem. By applying a dynamic threshold that changed depending on time of the year to a linear dose-response function, model overestimation of GPP at a Mediterranean forest site was reduced by ~200 g C m⁻² yr⁻¹ leading to a better fit between model estimates and observation.

To enable a better estimation of the impact of ozone damage on plant productivity at ecosystem, regional and global levels, it is vital to consider predicted future changes in ozone. Interactions between ozone exposure and other environmental variables such as CO₂ should also be considered. Conducting such model experiments on a global basis may be difficult due to unavailability of routine measurements, especially in tropical regions. However, datasets like the Copernicus Atmosphere Monitoring Service reanalysis (CAMS; Inness et al., 2019) provides global atmospheric composition data that could be bias-

corrected and used in studying the ozone impacts on vegetation. Future work could use such datasets in conjunction with emerging concepts like the dynamic threshold approach to investigate ozone impacts on vegetation at local, regional and global levels.

Another source of uncertainty which is not tackled in this thesis is change in vegetation cover or species composition. Climate change is already modifying geographic distributions of species due to shifting of climate zones, incidence of extreme events and increases in biotic stresses, such as herbivory (Fitzpatrick et al., 2008). Global warming is expected to create optimal conditions for plant species in new parts of the world while simultaneously creating sub-optimal conditions elsewhere. For example, Boreal forests could be displaced by temperate forests and grassland while species native to Boreal ecosystems shift into tundra (Nielsen et al., 2005). Future climate scenarios indicate possible large losses in tropical forests although uncertainties exist around such projections (Neilson et al. 1998). Increasing temperatures and changes in precipitation as well as human activities such as forest clearing for agriculture, will lead to reduction in forest cover and possible desertification over some regions. These changes in vegetation cover will have impacts on global biogenic isoprene, and other BVOC, emissions, productivity, and water fluxes. Dynamic models that simultaneously account for changes in vegetation and plant physiological processes should be used in future studies to better account for global BVOC emissions and plant gas exchange following the methods shown here.

This thesis has shown two key abiotic stress factors - drought and ozone - affect isoprene emissions, gross primary productivity, and water fluxes. It has also highlighted some of the feedbacks that exist between the biosphere and atmosphere and how these feedbacks are controlled by these stressors. Decreased productivity under abiotic stress conditions reduces plant uptake of CO₂ leading to higher atmospheric CO₂ concentrations, a positive feedback on global warming. Additionally, CO₂ is known to affect isoprene emissions and rising levels of atmospheric CO₂ have been shown to potentially offset any increases in isoprene emissions due to increasing temperature (Heald et al., 2009). In model experiments where the combined impacts of drought stress and ozone damage on plant gas exchange was tested, we found that the impact of the two stressors acting together was less than the sum of the impacts of the individual stress factors. Plant tolerance to drought may be weakened if stomata are damaged by ozone exposure while stomatal closure under drought will also shield trees against ozone uptake and injury (Matyssek et al., 2008). Further laboratory, field-based and modelling studies are needed to explore ozone-drought interactions to better understand whether the effects are synergistic or antagonistic.

There are further implications for terrestrial ecosystem functioning due to the impacts of the abiotic stresses considered here, i.e. ozone pollution and drought-heatwave conditions, beyond the impacts on vegetation productivity and growth. There is therefore the need to continually make ecosystem scale and laboratory measurements of plant gas exchange and emissions under different CO₂, ozone and soil moisture conditions to enable a better understanding of the combined impacts of droughts and CO₂, or drought and ozone on plants. Long term measurements could be complemented with short intensive measurements of plant structure information like LAI and physiological parameters such as V_{cmax} and stomatal conductance to provide the needed information for process understanding and model parameterisation. Existing CO₂ and ozone free air concentration experiments could include routine soil moisture and isoprene measurements to achieve this purpose. Machine learning approaches could be adopted to explore and narrow the parameter space surrounding drought stress algorithms in LSMs. These actions will enable improved model parameterisations, better estimations of global carbon budget and ultimately better decision making about the role of terrestrial ecosystems, especially forests, in climate change mitigation efforts.

References

- Affek, H. P., & Yakir, D. (2002). Protection by isoprene against singlet oxygen in leaves. *Plant Physiology*, 129(1), 269-277. <https://doi.org/10.1104/pp.010909>
- Ainsworth, E. A., Yendrek, C. R., Sitch, S., Collins, W. J., & Emberson, L. D. (2012). The effects of tropospheric O₃ on net primary productivity and implications for climate change. *Annual Review of Plant Biology*, 63, 637– 661. <https://doi.org/10.1146/annurev-arplant-042110-103829>
- Albani, M., Medvigy, D., Hurtt, G. C., & Moorcroft, P. R. (2006). The contributions of land-use change, CO₂ fertilization, and climate variability to the Eastern US carbon sink. *Global change biology*, 12(12), 2370-2390. <https://doi.org/10.1111/j.1365-2486.2006.01254.x>
- Allen, A. (1995). Soil science and survey at Harvard Forest. *Soil survey horizons*, 36(4), 133-142. <https://doi.org/10.2136/sh1995.4.0133>
- Anav, A., Friedlingstein, P., Kidston, M., Bopp, L., Ciais, P., Cox, P., ... & Zhu, Z. (2013). Evaluating the land and ocean components of the global carbon cycle in the CMIP5 earth system models. *Journal of Climate*, 26(18), 6801-6843. <https://doi.org/10.1175/JCLI-D-12-00417.1>
- Anderegg, W. R., Schwalm, C., Biondi, F., Camarero, J. J., Koch, G., Litvak, M., ... & Pacala, S. (2015). Pervasive drought legacies in forest ecosystems and their implications for carbon cycle models. *Science*, 349(6247), 528-532. DOI: 10.1126/science.aab1833
- Andersen, C. P. (2003). Source–sink balance and carbon allocation below ground in plants exposed to O₃. *New Phytologist*, 157(2), 213– 228. <https://doi.org/10.1046/j.1469-8137.2003.00674.x>
- Anjum, S. A., Xie, X. Y., Wang, L. C., Saleem, M. F., Man, C., & Lei, W. (2011). Morphological, physiological and biochemical responses of plants to drought stress. *African journal of agricultural research*, 6(9), 2026-2032. <https://doi.org/10.5897/AJAR10.027>
- Arneth, A., Miller, P. A., Scholze, M., Hickler, T., Schurgers, G., Smith, B., & Prentice, I. C. (2007b). CO₂ inhibition of global terrestrial isoprene emissions: Potential implications for atmospheric chemistry. *Geophysical Research Letters*, 34(18). <https://doi.org/10.1029/2007GL030615>
- Arneth, A., Monson, R. K., Schurgers, G., Niinemets, Ü., & Palmer, P. I. (2008). Why are estimates of global terrestrial isoprene emissions so similar (and why is this not so for monoterpenes)? *Atmospheric Chemistry and Physics*, 8(16), 4605– 4620. <https://doi.org/10.5194/acp-8-4605-2008>
- Arneth, A., Niinemets, Ü., Pressley, S., Bäck, J., Hari, P., Karl, T., ... & Smith, B. (2007a). Process-based estimates of terrestrial ecosystem isoprene emissions: incorporating the effects of a direct CO₂-isoprene interaction. *Atmospheric Chemistry and Physics*, 7(1), 31-53. <https://doi.org/10.5194/acp-7-31-2007>
- Arneth, A., Schurgers, G., Lathiere, J., Duhl, T., Beerling, D. J., Hewitt, C. N., ... & Guenther, A. (2011). Global terrestrial isoprene emission models: sensitivity to variability in climate and vegetation. *Atmospheric Chemistry and Physics*, 11(15), 8037-8052. <https://doi.org/10.5194/acp-11-8037-2011>
- Arneth, A., Harrison, S. P., Zaehle, S., Tsigaridis, K., Menon, S., Bartlein, P. J., ... Vesala, T. (2010). Terrestrial biogeochemical feedbacks in the climate system. *Nature Geoscience*, 3(8), 525– 532. <https://doi.org/10.1038/ngeo905>
- Asensio, D., Peñuelas, J., Filella, I., & Llusà, J. (2007). On-line screening of soil VOCs exchange responses to moisture, temperature and root presence. *Plant and Soil*, 291(1), 249-261. <https://doi.org/10.1007/s11104-006-9190-4>
- Ashmore, M. R. (2005). Assessing the future global impacts of O₃ on vegetation. *Plant, Cell & Environment*, 28(8), 949– 964. <https://doi.org/10.1111/j.1365-3040.2005.01341.x>
- Ashmore, M., Emberson, L., Karlsson, P. E., & Pleijel, H. (2004). New directions: a new generation of ozone critical levels for the protection of vegetation in Europe. *Atmospheric environment* (1994), 38(15), 2213-2214. [doi.org/ 10.1016/j.atmosenv.2004.02.029](https://doi.org/10.1016/j.atmosenv.2004.02.029)

- Ashworth, K., Chung, S. H., Griffin, R. J., Chen, J., Forkel, R., Bryan, A. M., & Steiner, A. L. (2015). FORest Canopy Atmosphere Transfer (FORCAsT) 1.0: A 1-D model of biosphere–atmosphere chemical exchange. *Geoscientific Model Development*, 8(11), 3765–3784. <https://doi.org/10.5194/gmd-8-3765-2015>
- Ashworth, K., Wild, O., & Hewitt, C. N. (2010). Sensitivity of isoprene emissions estimated using MEGAN to the time resolution of input climate data. *Atmospheric Chemistry and Physics*, 10(3), 1193-1201. <https://doi.org/10.5194/acp-10-1193-2010>
- Ashworth, K., Chung, S. H., McKinney, K. A., Liu, Y., Munger, J. W., Martin, S. T., & Steiner, A. L. (2016). Modelling bidirectional fluxes of methanol and acetaldehyde with the FORCAsT canopy exchange model. *Atmospheric Chemistry and Physics*, 16(24), <https://doi.org/10.5194/acp-16-15461-2016>
- Atkinson, D. (1973). Seasonal changes in the length of white unsuberized root on raspberry plants grown under irrigated conditions. *Journal of Horticultural Science*, 48(4), 413-419. <https://doi.org/10.1080/00221589.1973.11514545>
- Atkinson, R., & Arey, J. (2003). Gas-phase tropospheric chemistry of biogenic volatile organic compounds: a review. *Atmospheric Environment*, 37, 197-219. [https://doi.org/10.1016/S1352-2310\(03\)00391-1](https://doi.org/10.1016/S1352-2310(03)00391-1)
- Avnery, S., Mauzerall, D. L., Liu, J., & Horowitz, L. W. (2011). Global crop yield reductions due to surface ozone exposure: 1. Year 2000 crop production losses and economic damage. *Atmospheric Environment*, 45(13), 2284-2296. <https://doi.org/10.1016/j.atmosenv.2010.11.045>
- Bäck, J., Hari, P., Hakola, H., Juurola, E., & Kulmala, M. (2005). Dynamics of monoterpene emissions in *Pinus sylvestris* during early spring. *Boreal Environment Research*, 10(5), 409-424.
- Bahari, Z. A., Pallardy, S. G., & Parker, W. C. (1985). Photosynthesis, water relations, and drought adaptation in six woody species of oak-hickory forests in central Missouri. *Forest Science*, 31(3), 557-569. <https://doi.org/10.1093/forestscience/31.3.557>
- Baldocchi D. (1988). A multi-layer model for estimating sulfur dioxide deposition to a deciduous oak forest canopy. *Atmospheric Environment* (1967), 22(5), 869–884. [https://doi.org/10.1016/0004-6981\(88\)90264-8](https://doi.org/10.1016/0004-6981(88)90264-8)
- Baldocchi, D. (1994). An analytical solution for coupled leaf photosynthesis and stomatal conductance models. *Tree physiology*, 14(7-8-9), 1069-1079. <https://doi.org/10.1093/treephys/14.7-8-9.1069>
- Baldwin, I. T. (2010). Plant volatiles. *Current Biology*, 20(9), R392-R397. <https://doi.org/10.1016/j.cub.2010.02.052>
- Ball, J. T., Woodrow, I. E., & Berry, J. A. (1987). A model predicting stomatal conductance and its contribution to the control of photosynthesis under different environmental conditions. In *Progress in photosynthesis research* (pp. 221-224). Springer, Dordrecht.
- Bamberger, I., Ruehr, N. K., Schmitt, M., Gast, A., Wohlfahrt, G., & Arneth, A. (2017). Isoprene emission and photosynthesis during heatwaves and drought in black locust. *Biogeosciences*, 14(15), 3649–3667. <https://doi.org/10.5194/bg-14-3649-2017>
- Basu, S., Ramegowda, V., Kumar, A., & Pereira, A. (2016). Plant adaptation to drought stress. *F1000Research*, 5. <https://doi.org/10.12688/f1000research.7678.1>
- Bernacchi, C. J., Leakey, A. D., Heady, L. E., Morgan, P. B., Dohleman, F. G., McGrath, J. M., ... & Ort, D. R. (2006). Hourly and seasonal variation in photosynthesis and stomatal conductance of soybean grown at future CO₂ and ozone concentrations for 3 years under fully open-air field conditions. *Plant, Cell & Environment*, 29(11), 2077-2090. <https://doi.org/10.1111/j.1365-3040.2006.01581.x>
- Best, M. J., Pryor, M., Clark, D. B., Rooney, G. G., Essery, R., Ménard, C. B., ... & Harding, R. J. (2011). The Joint UK Land Environment Simulator (JULES), model description–Part 1: energy and water fluxes. *Geoscientific Model Development*, 4(3), 677-699. <https://doi.org/10.5194/gmd-4-677-2011>

- Betts, A. K. (2004). Understanding hydrometeorology using global models. *Bulletin of the American Meteorological Society*, 85(11), 1673-1688. <https://doi.org/10.1175/BAMS-85-11-1673>
- Blackadar, A. K. (1962). The vertical distribution of wind and turbulent exchange in a neutral atmosphere. *Journal of Geophysical Research*, 67(8), 3095-3102. <https://doi.org/10.1029/JZ067i008p03095>
- Blackadar, A. K. (1979). High resolution models of the planetary boundary layer. In J. Pfafflin & E. Ziegler (Eds.), *Advances in environmental science and engineering* (Vol. 1, pp. 50– 85). New York, NY: Gordon and Breach.
- Blackman, C. J., Brodribb, T. J., & Jordan, G. J. (2009). Leaf hydraulics and drought stress: response, recovery and survivorship in four woody temperate plant species. *Plant, Cell & Environment*, 32(11), 1584-1595. <https://doi.org/10.1111/j.1365-3040.2009.02023.x>
- Blyth, E., Gash, J., Lloyd, A., Pryor, M., Weedon, G. P., & Shuttleworth, J. (2010). Evaluating the JULES land surface model energy fluxes using FLUXNET data. *Journal of Hydrometeorology*, 11(2), 509-519. <https://doi.org/10.1175/2009JHM1183.1>
- Bolas, C. G. (2020). Forest isoprene emissions: New insights from a novel field instrument (Doctoral dissertation). University of Cambridge.
- Bolas, C. G., Ferracci, V., Robinson, A. D., Mead, M. I., Nadzir, M. S. M., Pyle, J. A., et al. (2020). iDirac: A field-portable instrument for long-term autonomous measurements of isoprene and selected VOCs. *Atmospheric Measurement Techniques*, 1–21. <https://doi.org/10.5194/amt-2019-219>
- Bourtsoukidis, E., Behrendt, T., Yáñez-Serrano, A. M., Hellén, H., Diamantopoulos, E., Catão, E., ... & Williams, J. (2018). Strong sesquiterpene emissions from Amazonian soils. *Nature communications*, 9(1), 1-11. <https://doi.org/10.1038/s41467-018-04658-y>
- Bréda, N., Cochard, H., Dreyer, E., & Granier, A. (1993). Field comparison of transpiration, stomatal conductance and vulnerability to cavitation of *Quercus petraea* and *Quercus robur* under water stress. *Annales Des Sciences Forestières*, 50(6), 571– 582. <https://doi.org/10.1051/forest:19930606>
- Brilli, F., Barta, C., Fortunati, A., Lerda, M., Loreto, F., & Centritto, M. (2007). Response of isoprene emission and carbon metabolism to drought in white poplar (*Populus alba*) saplings. *New Phytologist*, 175(2), 244-254. <https://doi.org/10.1111/j.1469-8137.2007.02094.x>
- Brüggemann, N., & Schnitzler, J. P. (2002). Comparison of isoprene emission, intercellular isoprene concentration and photosynthetic performance in water-limited oak (*Quercus pubescens* Willd. and *Quercus robur* L.) saplings. *Plant Biology*, 4(04), 456– 463. <https://doi.org/10.1055/s-2002-34128>
- Bryan, A. M., Bertman, S. B., Carroll, M. A., Dusanter, S., Edwards, G. D., Forkel, R., ... & Steiner, A. L. (2012). In-canopy gas-phase chemistry during CABINEX 2009: sensitivity of a 1-D canopy model to vertical mixing and isoprene chemistry. *Atmospheric Chemistry and Physics*, 12(18), 8829-8849. <https://doi.org/10.5194/acp-12-8829-2012>
- Bryan, A. M., Cheng, S. J., Ashworth, K., Guenther, A. B., Hardiman, B. S., Bohrer, G., & Steiner, A. L. (2015). Forest-atmosphere BVOC exchange in diverse and structurally complex canopies: 1-D modeling of a mid-successional forest in northern Michigan. *Atmospheric Environment*, 120, 217-226. <https://doi.org/10.1016/j.atmosenv.2015.08.094>
- Büker, P., Feng, Z., Uddling, J., Briolat, A., Alonso, R., Braun, S., ... & Emberson, L. D. (2015). New flux based dose–response relationships for ozone for European forest tree species. *Environmental Pollution*, 206, 163-174. <https://doi.org/10.1016/j.envpol.2015.06.033>
- Burke, E. J., Brown, S. J., & Christidis, N. (2006). Modeling the recent evolution of global drought and projections for the twenty-first century with the Hadley Centre climate model. *Journal of Hydrometeorology*, 7(5), 1113-1125. <https://doi.org/10.1175/JHM544.1>
- Byrne, B., Wunch, D., Jones, D. B. A., Strong, K., Deng, F., Baker, I., ... & Roehl, C. M. (2018). Evaluating GPP and respiration estimates over northern midlatitude ecosystems using solar-induced

- fluorescence and atmospheric CO₂ measurements. *Journal of Geophysical Research: Biogeosciences*, 123(9), 2976-2997. <https://doi.org/10.1029/2018JG004472>
- Calfapietra, C., Fares, S., & Loreto, F. (2009). Volatile organic compounds from Italian vegetation and their interaction with O₃. *Environmental Pollution*, 157(5), 1478–1486. <https://doi.org/10.1016/j.envpol.2008.09.048>
- Calfapietra, C., Fares, S., Manes, F., Morani, A., Sgrigna, G., & Loreto, F. (2013). Role of Biogenic Volatile Organic Compounds (BVOC) emitted by urban trees on ozone concentration in cities: A review. *Environmental pollution*, 183, 71-80. <https://doi.org/10.1016/j.envpol.2013.03.012>
- Carlton, A. G., Wiedinmyer, C., & Kroll, J. H. (2009). A review of Secondary Organic Aerosol (SOA) formation from isoprene. *Atmospheric Chemistry and Physics*, 9(14), 4987-5005. <https://doi.org/10.5194/acp-9-4987-2009>
- Carriero, G., Emiliani, G., Giovannelli, A., Hoshika, Y., Manning, W. J., Traversi, M. L., & Paoletti, E. (2015). Effects of long-term ambient ozone exposure on biomass and wood traits in poplar treated with ethylenediurea (EDU). *Environmental Pollution*, 206, 575–581. <https://doi.org/10.1016/j.envpol.2015.08.014>
- Carslaw, K. S., Boucher, O., Spracklen, D. V., Mann, G. W., Rae, J. G. L., Woodward, S., & Kulmala, M. (2010). A review of natural aerosol interactions and feedbacks within the Earth system. *Atmospheric Chemistry and Physics*, 10(4), 1701–1737. <https://doi.org/10.5194/acp-10-1701-2010>
- Centritto, M., Brillì, F., Fodale, R., & Loreto, F. (2011). Different sensitivity of isoprene emission, respiration and photosynthesis to high growth temperature coupled with drought stress in black poplar (*Populus nigra*) saplings. *Tree Physiology*, 31(3), 275–286. <https://doi.org/10.1093/treephys/tpq1>
- Checa-Garcia, R., Hegglin, M. I., Kinnison, D., Plummer, D. A., & Shine, K. P. (2018). Historical tropospheric and stratospheric ozone radiative forcing using the CMIP6 database. *Geophysical Research Letters*, 45(7), 3264-3273. <https://doi.org/10.1002/2017GL076770>
- Chen, J., Mao, H., Talbot, R. W., & Griffin, R. J. (2006). Application of the CACM and MPMPO modules using the CMAQ model for the eastern United States. *Journal of Geophysical Research: Atmospheres*, 111(D23). <https://doi.org/10.1029/2006JD007603>
- Chevone, B. (1991). Seasonal changes in components of the antioxidant system in eastern white pine and ozone effects on antioxidant metabolism. *Air & Waste Management Association*, 91–142.
- Ciais, P. H., Reichstein, M., Viovy, N., Granier, A., Ogée, J., Allard, V., ... Valentini, R. (2005). Europe-wide reduction in primary productivity caused by the heat and drought in 2003. *Nature*, 437(7058), 529–533. <https://doi.org/10.1038/nature03972>
- Clark, D. B., Mercado, L. M., Sitch, S., Jones, C. D., Gedney, N., Best, M. J., ... Cox, P. M. (2011). The Joint UK Land Environment Simulator (JULES), model description – Part 2: Carbon fluxes and vegetation dynamics. *Geoscientific Model Development*, 4(3), 701–722. <https://doi.org/10.5194/gmd-4-701-2011>
- Clenciala, E., Kucera, J., Ryan, M. G., & Lindroth, A. (1998). Water flux in boreal forest during two hydrologically contrasting years; species specific regulation of canopy conductance and transpiration. In *Annales des Sciences Forestières* (Vol. 55, No. 1-2, pp. 47-61). EDP Sciences. <https://doi.org/10.1051/forest:19980104>
- Cleveland, C. C., Houlton, B. Z., Smith, W. K., Marklein, A. R., Reed, S. C., Parton, W., ... Running, S. W. (2013). Patterns of new versus recycled primary production in the terrestrial biosphere. *Proceedings of the National Academy of Sciences of the United States of America*, 110(31), 12733–12737. <https://doi.org/10.1073/pnas.1302768110>
- Clifton, O. E., Fiore, A. M., Munger, J. W., & Wehr, R. (2019). Spatiotemporal controls on observed daytime ozone deposition velocity over northeastern US forests during summer. *Journal of Geophysical Research: Atmospheres*, 124(10), 5612-5628. <https://doi.org/10.1029/2018JD029073>

- Collatz, G. J., Ball, J. T., Grivet, C., & Berry, J. A. (1991). Physiological and environmental regulation of stomatal conductance, photosynthesis and transpiration: a model that includes a laminar boundary layer. *Agricultural and Forest meteorology*, 54(2-4), 107-136. [https://doi.org/10.1016/0168-1923\(91\)90002-8](https://doi.org/10.1016/0168-1923(91)90002-8)
- Collatz, G. J., Ribas-Carbo, M., & Berry, J. A. (1992). Coupled photosynthesis-stomatal conductance model for leaves of C4 plants. *Functional Plant Biology*, 19(5), 519-538. <https://doi.org/10.1071/PP9920519>
- Conte A., Otu-Larbi F., Alivernini A., Hoshika Y., Paoletti E., Ashworth K., & Fares S. (2021) Exploring new strategies for ozone-risk assessment: a dynamic-threshold case study (Under Review: Environmental Pollution).
- Covariance, E. (2012). *A Practical Guide to Measurement and Data Analysis*. Series: Springer Atmospheric Sciences, edited by: Aubinet, M., Vesala, T., and Papale, D., XXII.
- Cowan, I. R., & GD, Farquhar, G.D. (1977). Stomatal function in relation to leaf metabolism and environment.
- Cox, P. M., Huntingford, C., & Harding, R. J. (1998). A canopy conductance and photosynthesis model for use in a GCM land surface scheme. *Journal of Hydrology*, 212, 79-94. [https://doi.org/10.1016/S0022-1694\(98\)00203-0](https://doi.org/10.1016/S0022-1694(98)00203-0)
- Crutzen, P. J., Delany, A. C., Greenberg, J., Haagenson, P., Heidt, L., Lueb, R., ... Zimmerman, P. (1985). Tropospheric chemical composition measurements in Brazil during the dry season. *Journal of Atmospheric Chemistry*, 2(3), 233–256. <https://doi.org/10.1007/BF00051075>
- Da Rocha, H. R., Goulden, M. L., Miller, S. D., Menton, M. C., Pinto, L. D., de Freitas, H. C., & e Silva Figueira, A. M. (2004). Seasonality of water and heat fluxes over a tropical forest in eastern Amazonia. *Ecological applications*, 14(sp4), 22-32. <https://doi.org/10.1890/02-6001>
- Dai, A. (2011). Drought under global warming: A review. *Wiley Interdisciplinary Reviews: Climate Change*, 2(1), 45– 65. <https://doi.org/10.1002/wcc.81>
- Damour, G., Simonneau, T., Cochard, H., & Urban, L. (2010). An overview of models of stomatal conductance at the leaf level. *Plant, cell & environment*, 33(9), 1419-1438. <https://doi.org/10.1111/j.1365-3040.2010.02181.x>
- De Kauwe, M. G., Kala, J., Lin, Y. S., Pitman, A. J., Medlyn, B. E., Duursma, R. A., ... & Miralles, D. G. (2015). A test of an optimal stomatal conductance scheme within the CABLE land surface model. *Geoscientific Model Development*, 8(2), 431-452. <https://doi.org/10.5194/gmd-8-431-2015>
- De Marco, A., Sicard, P., Fares, S., Tuovinen, J. P., Anav, A., & Paoletti, E. (2016). Assessing the role of soil water limitation in determining the Phytotoxic Ozone Dose (PODY) thresholds. *Atmospheric Environment*, 147, 88– 97. <https://doi.org/10.1016/j.atmosenv.2016.09.066>
- Deryng, D., Conway, D., Ramankutty, N., Price, J., & Warren, R. (2014). Global crop yield response to extreme heat stress under multiple climate change futures. *Environmental Research Letters*, 9(3), 034011.
- Dixon, R. K., & Turner, D. P. (1991). The global carbon cycle and climate change: responses and feedbacks from below-ground systems. *Environmental pollution*, 73(3-4), 245-262. [https://doi.org/10.1016/0269-7491\(91\)90052-X](https://doi.org/10.1016/0269-7491(91)90052-X)
- Dore, M. H. (2005). Climate change and changes in global precipitation patterns: what do we know?. *Environment international*, 31(8), 1167-1181. <https://doi.org/10.1016/j.envint.2005.03.004>
- Dragoni, D., Schmid, H. P., Wayson, C. A., Potter, H., Grimmond, C. S. B., & Randolph, J. C. (2011). Evidence of increased net ecosystem productivity associated with a longer vegetated season in a deciduous forest in south-central Indiana, USA. *Global Change Biology*, 17(2), 886– 897. <https://doi.org/10.1111/j.1365-2486.2010.02281.x>

- Egea, G., Verhoef, A., & Vidale, P. L. (2011). Towards an improved and more flexible representation of water stress in coupled photosynthesis–stomatal conductance models. *Agricultural and Forest Meteorology*, 151(10), 1370– 1384. <https://doi.org/10.1016/j.agrformet.2011.05.019>
- Emberson, L. D., Ashmore, M. R., Cambridge, H. M., Simpson, D., & Tuovinen, J. P. (2000). Modelling stomatal O₃ flux across Europe. *Environmental Pollution*, 109(3), 403– 413. [https://doi.org/10.1016/S0269-7491\(00\)00043-9](https://doi.org/10.1016/S0269-7491(00)00043-9)
- Emberson, L. D., Ashmore, M. R., Simpson, D., Tuovinen, J. P., & Cambridge, H. M. (2001). Modelling and mapping ozone deposition in Europe. *Water, Air, and Soil Pollution*, 130(1), 577–582. <https://doi.org/10.1023/A:1013851116524>
- Emberson, L. D., Büker, P., & Ashmore, M. R. (2007). Assessing the risk caused by ground level ozone to European forest trees: A case study in pine, beech and oak across different climate regions. *Environmental Pollution*, 147(3), 454– 466. <https://doi.org/10.1016/j.envpol.2006.10.026>
- Emberson, L. D., Büker, P., Ashmore, M. R., Mills, G., Jackson, L. S., Agrawal, M., ... Wahid, A. (2009). A comparison of North American and Asian exposure–response data for ozone effects on crop yields. *Atmospheric Environment*, 43(12), 1945– 1953. <https://doi.org/10.1016/j.atmosenv.2009.01.005>
- Emberson, L. D., Pleijel, H., Ainsworth, E. A., Van den Berg, M., Ren, W., Osborne, S., ... Ewert, F. (2018). O₃ effects on crops and consideration in crop models. *European Journal of Agronomy*, 100, 19– 34. <https://doi.org/10.1016/j.eja.2018.06.002>
- Emmerson, K. M., Palmer, P. I., Thatcher, M., Haverd, V., & Guenther, A. B. (2019). Sensitivity of isoprene emissions to drought over south-eastern Australia: Integrating models and satellite observations of soil moisture. *Atmospheric Environment*, 209, 112– 124. <https://doi.org/10.1016/j.atmosenv.2019.04.038>
- Essery, R. L. H., Best, M. J., Betts, R. A., Cox, P. M., & Taylor, C. M. (2003). Explicit representation of subgrid heterogeneity in a GCM land surface scheme. *Journal of Hydrometeorology*, 4(3), 530–543. [https://doi.org/10.1175/1525-7541\(2003\)004<0530:EROSHI>2.0.CO;2](https://doi.org/10.1175/1525-7541(2003)004<0530:EROSHI>2.0.CO;2)
- Fan, J., & Zhang, R. (2004). Atmospheric oxidation mechanism of isoprene. *Environmental Chemistry*, 1(3), 140–149. <https://doi.org/10.1071/EN04045>
- Fang, Y., Liao, K., Du, H., Xu, Y., Song, H., Li, X., & Xiong, L. (2015). A stress-responsive NAC transcription factor SNAC3 confers heat and drought tolerance through modulation of reactive oxygen species in rice. *Journal of experimental botany*, 66(21), 6803–6817. <https://doi.org/10.1093/jxb/erv386>.
- FAO. 2020. Global Forest Resources Assessment 2020 – Key findings. Rome. <https://doi.org/10.4060/ca8753en>
- Fares, S., Alivernini, A., Conte, A., & Maggi, F. (2019). O₃ and particle fluxes in a Mediterranean forest predicted by the AIRTREE model. *Science of the Total Environment*, 682, 494– 504. <https://doi.org/10.1016/j.scitotenv.2019.05.109>
- Fares, S., Matteucci, G., Mugnozza, G. S., Morani, A., Calfapietra, C., Salvatori, E., ... & Loreto, F. (2013). Testing of models of stomatal ozone fluxes with field measurements in a mixed Mediterranean forest. *Atmospheric environment*, 67, 242–251. <https://doi.org/10.1016/j.atmosenv.2012.11.007>
- Fares, S., Mereu, S., Scarascia Mugnozza, G., Vitale, M., Manes, F., Frattoni, M., ... & Loreto, F. (2009). The ACCENT-VOCBAS field campaign on biosphere-atmosphere interactions in a Mediterranean ecosystem of Castelporziano (Rome): site characteristics, climatic and meteorological conditions, and eco-physiology of vegetation. *Biogeosciences*, 6(6), 1043–1058. <https://doi.org/10.5194/bg-6-1043-2009>

- Farooq, M., Wahid, A., Kobayashi, N., Fujita, D. B. S. M. A., & Basra, S. M. A. (2009). Plant drought stress: Effects, mechanisms and management. *Sustainable agriculture* (pp. 153–188). Dordrecht: Springer. https://doi.org/10.1007/978-90-481-2666-8_12
- Farquhar, G. D., & Von Caemmerer, S. (1982). Modelling of photosynthetic response to environmental conditions. In *Physiological plant ecology II* (pp. 549-587). Springer, Berlin, Heidelberg.
- Farquhar, G. D., von Caemmerer, S. V., & Berry, J. A. (1980). A biochemical model of photosynthetic CO₂ assimilation in leaves of C₃ species. *Planta*, 149(1), 78-90. <https://doi.org/10.1007/BF00386231>
- Fatichi, S., Pappas, C., Zscheischler, J., & Leuzinger, S. (2019). Modelling carbon sources and sinks in terrestrial vegetation. *New Phytologist*, 221(2), 652-668. <https://doi.org/10.1111/nph.15451>
- Feeley, K. J., Joseph Wright, S., Nur Supardi, M. N., Kassim, A. R., & Davies, S. J. (2007). Decelerating growth in tropical forest trees. *Ecology letters*, 10(6), 461-469. <https://doi.org/10.1111/j.1461-0248.2007.01033.x>
- Fehsenfeld, F., Calvert, J., Fall, R., Goldan, P., Guenther, A. B., Hewitt, C. N., ... & Zimmerman, P. (1992). Emissions of volatile organic compounds from vegetation and the implications for atmospheric chemistry. *Global Biogeochemical Cycles*, 6(4), 389-430. <https://doi.org/10.1029/92GB02125>
- Feng, Z., Uddling, J., Tang, H., Zhu, J., & Kobayashi, K. (2018). Comparison of crop yield sensitivity to ozone between open-top chamber and free-air experiments. *Global change biology*, 24(6), 2231-2238. <https://doi.org/10.1111/gcb.14077>
- Ferracci, V., Bolas, C. G., Freshwater, R. A., Staniaszek, Z., King, T., Jaars, K., ... & Harris, N. R. (2020). Continuous isoprene measurements in a UK temperate forest for a whole growing season: effects of drought stress during the 2018 heatwave. *Geophysical Research Letters*, 47(15), e2020GL088885. <https://doi.org/10.1029/2020GL088885>
- Fiscus, E. L., Reid, C. D., Miller, J. E., & Heagle, A. S. (1997). Elevated CO₂ reduces O₃ flux and O₃-induced yield losses in soybeans: Possible implications for elevated CO₂ studies. *Journal of Experimental Botany*, 48(2), 307–313. <https://doi.org/10.1093/jxb/48.2.307>
- Fisher, J. I., & Mustard, J. F. (2007). Cross-scalar satellite phenology from ground, Landsat, and MODIS data. *Remote Sensing of Environment*, 109(3), 261-273. <https://doi.org/10.1016/j.rse.2007.01.004>
- Fitzpatrick, M. C., Gove, A. D., Sanders, N. J., & Dunn, R. R. (2008). Climate change, plant migration, and range collapse in a global biodiversity hotspot: the *Banksia* (Proteaceae) of Western Australia. *Global Change Biology*, 14(6), 1337-1352.
- Flack-Prain, S., Meir, P., Malhi, Y., Smallman, T. L., & Williams, M. (2019). The importance of physiological, structural and trait responses to drought stress in driving spatial and temporal variation in GPP across Amazon forests. *Biogeosciences*, 16(22), 4463-4484. <https://doi.org/10.5194/bg-16-4463-2019>
- Folberth, G. A., Hauglustaine, D. A., Lathière, J., & Brocheton, F. (2006). Interactive chemistry in the Laboratoire de Météorologie Dynamique general circulation model: model description and impact analysis of biogenic hydrocarbons on tropospheric chemistry. *Atmospheric Chemistry and Physics*, 6(8), 2273-2319.
- Forkel, R., Klemm, O., Graus, M., Rappenglück, B., Stockwell, W. R., Grabmer, W., ... & Steinbrecher, R. (2006). Trace gas exchange and gas phase chemistry in a Norway spruce forest: A study with a coupled 1-dimensional canopy atmospheric chemistry emission model. *Atmospheric environment*, 40, 28-42. <https://doi.org/10.1016/j.atmosenv.2005.11.070>
- Fowler, D., Flechard, C., Cape, J. N., Storeton-West, R. L., & Coyle, M. (2001). Measurements of ozone deposition to vegetation quantifying the flux, the stomatal and non-stomatal components. *Water, Air, and Soil Pollution*, 130(1), 63-74. <https://doi.org/10.1023/A:1012243317471>

- Fowler, D., Nemitz, E., Misztal, P., Di Marco, C., Skiba, U., Ryder, J., ... & Hewitt, C. N. (2011). Effects of land use on surface–atmosphere exchanges of trace gases and energy in Borneo: comparing fluxes over oil palm plantations and a rainforest. *Philosophical Transactions of the Royal Society B: Biological Sciences*, 366(1582), 3196-3209. <https://doi.org/10.1098/rstb.2011.0055>
- Fuentes, J. D., Lerdau, M., Atkinson, R., Baldocchi, D., Bottenheim, J. W., Ciccioli, P., ... Sharkey, T. D. (2000). Biogenic hydrocarbons in the atmospheric boundary layer: A review. *Bulletin of the American Meteorological Society*, 81(7), 1537– 1576. [https://doi.org/10.1175/1520-0477\(2000\)081%3C1537:BHITAB%3E2.3.CO;2](https://doi.org/10.1175/1520-0477(2000)081%3C1537:BHITAB%3E2.3.CO;2)
- Fuhrer, J. (2009). O₃ risk for crops and pastures in present and future climates. *Naturwissenschaften*, 96(2), 173– 194. <https://doi.org/10.1007/s00114-008-0468-7>
- Fuhrer, J., Skärby, L., & Ashmore, M. R. (1997). Critical levels for ozone effects on vegetation in Europe. *Environmental pollution*, 97(1-2), 91-106. [https://doi.org/10.1016/S0269-7491\(97\)00067-5](https://doi.org/10.1016/S0269-7491(97)00067-5)
- Fusaro, L., Salvatori, E., Mereu, S., Silli, V., Bernardini, A., Tinelli, A., & Manes, F. (2015). Researches in Castelporziano test site: ecophysiological studies on Mediterranean vegetation in a changing environment. *Rendiconti Lincei*, 26(3), 473-481. <https://doi.org/10.1007/s12210-014-0374-1>
- Ganzeveld, L., Eerdekens, G., Feig, G., Fischer, H., Harder, H., Königstedt, R., ... & Lelieveld, J. (2008). Surface and boundary layer exchanges of volatile organic compounds, nitrogen oxides and ozone during the GABRIEL campaign. *Atmospheric Chemistry and Physics*, 8(20), 6223-6243. <https://doi.org/10.5194/acp-8-6223-2008>
- Gao, W., Wesely, M. L., & Doskey, P. V. (1993). Numerical modeling of the turbulent diffusion and chemistry of NO_x, O₃, isoprene, and other reactive trace gases in and above a forest canopy. *Journal of Geophysical Research: Atmospheres*, 98(D10), 18339-18353. <https://doi.org/10.1029/93JD01862>
- Gao, Y., Markkanen, T., Aurela, M., Mammarella, I., Thum, T., Tsuruta, A., ... & Aalto, T. (2017). Response of water use efficiency to summer drought in a boreal Scots pine forest in Finland. *Biogeosciences*, 14(18), 4409-4422. <https://doi.org/10.5194/bg-14-4409-2017>
- Gao, Y., Markkanen, T., Thum, T., Aurela, M., Lohila, A., Mammarella, I., ... Aalto, T. (2016). Assessing various drought indicators in representing summer drought in boreal forests in Finland. *Hydrology and Earth System Sciences*, 20, 175– 191. <https://doi.org/10.5194/hess-20-175-2016>
- Gaudel, A., Cooper, R., Ancellet, G., Barret, B., Boynard, A., Burrows, J., ... Doniki, S. (2018). Tropospheric ozone assessment report: Present-day distribution and trends of tropospheric ozone relevant to climate and global atmospheric chemistry model evaluation. *Elementa: Science of the Anthropocene*, 6(1), art-39. <https://doi.org/10.1525/elementa.291>
- Geiger, H., Barnes, I., Bejan, I., Benter, T., & Spittler, M. (2003). The tropospheric degradation of isoprene: an updated module for the regional atmospheric chemistry mechanism. *Atmospheric Environment*, 37(11), 1503-1519. [https://doi.org/10.1016/S1352-2310\(02\)01047-6](https://doi.org/10.1016/S1352-2310(02)01047-6)
- Genard-Zielinski, A. C., Boissard, C., Ormeno, E., Lathiere, J., Reiter, I. M., Wortham, H., ... Fernandez, C. (2018). Seasonal variations of *Quercus pubescens* isoprene emissions from an in natura forest under drought stress and sensitivity to future climate change in the Mediterranean area. *Biogeosciences*, 15, 4711– 4730. <https://doi.org/10.5194/bg-15-4711-2018>
- Goldstein, A. H., & Galbally, I. E. (2007). Known and unexplored organic constituents in the earth's atmosphere. *Environmental science & technology*, 41(5), 1514-1521.
- Goldstein, A. H., & Schade, G. W. (2000). Quantifying biogenic and anthropogenic contributions to acetone mixing ratios in a rural environment. *Atmospheric Environment*, 34(29-30), 4997-5006. [https://doi.org/10.1016/S1352-2310\(00\)00321-6](https://doi.org/10.1016/S1352-2310(00)00321-6)
- Goldstein, A. H., Goulden, M. L., Munger, J. W., Wofsy, S. C., & Geron, C. D. (1998). Seasonal course of isoprene emissions from a midlatitude deciduous forest. *Journal of Geophysical Research: Atmospheres*, 103(D23), 31045-31056. <https://doi.org/10.1029/98JD02708>

- Goldstein, A. H., Hultman, N. E., Fracheboud, J. M., Bauer, M. R., Panek, J. A., Xu, M., ... & Baugh, W. (2000). Effects of climate variability on the carbon dioxide, water, and sensible heat fluxes above a ponderosa pine plantation in the Sierra Nevada (CA). *Agricultural and Forest Meteorology*, 101(2-3), 113-129. [https://doi.org/10.1016/S0168-1923\(99\)00168-9](https://doi.org/10.1016/S0168-1923(99)00168-9)
- Gough, C. M. (2011) Terrestrial Primary Production: Fuel for Life. *Nature Education Knowledge* 3(10):28
- Goulden, M. L., Miller, S. D., Da Rocha, H. R., Menton, M. C., de Freitas, H. C., e Silva Figueira, A. M., & de Sousa, C. A. D. (2004). Diel and seasonal patterns of tropical forest CO₂ exchange. *Ecological Applications*, 14(sp4), 42-54. <https://doi.org/10.1890/02-6008>
- Granier, A., Reichstein, M., Bréda, N., Janssens, I. A., Falge, E., Ciais, P., ... Wang, Q. (2007). Evidence for soil water control on carbon and water dynamics in European forests during the extremely dry year: 2003. *Agricultural and Forest Meteorology*, 143(1-2), 123-145. <https://doi.org/10.1016/j.agrformet.2006.12.004>
- Gray, S. B., Dermody, O., Klein, S. P., Locke, A. M., McGrath, J. M., Paul, R. E., ... Leakey, A. D. B. (2016). Intensifying drought eliminates the expected benefits of elevated carbon dioxide for soybean. *Nature Plants*, 2(9), 1-8. <https://doi.org/10.1038/nplants.2016.132>
- Griffin, R. J., Dabdub, D., & Seinfeld, J. H. (2005). Development and initial evaluation of a dynamic species-resolved model for gas phase chemistry and size-resolved gas/particle partitioning associated with secondary organic aerosol formation. *Journal of Geophysical Research: Atmospheres*, 110(D5). <https://doi.org/10.1029/2004JD005219>
- Griffin, R. J., Nguyen, K., Dabdub, D., & Seinfeld, J. H. (2003). A coupled hydrophobic-hydrophilic model for predicting secondary organic aerosol formation. *Journal of Atmospheric Chemistry*, 44(2), 171-190. <https://doi.org/10.1023/A:1022436813699>
- Grote, R., & Niinemets, Ü. (2007). Modeling volatile isoprenoid emissions—a story with split ends. *Plant biology*, 9(S 01), e42-e59. <https://doi.org/10.1055/s-2007-964975>
- Grüters, U., Fangmeier, A., & Jäger, H. J. (1995). Modelling stomatal responses of spring wheat (*Triticum aestivum* L. cv. Turbo) to O₃ and different levels of water supply. *Environmental Pollution*, 87(2), 141-149. [https://doi.org/10.1016/0269-7491\(94\)P2600-E](https://doi.org/10.1016/0269-7491(94)P2600-E)
- Gu, L., Meyers, T., Pallardy, S. G., Hanson, P. J., Yang, B., Heuer, M., ... & Wullschlegel, S. D. (2006). Direct and indirect effects of atmospheric conditions and soil moisture on surface energy partitioning revealed by a prolonged drought at a temperate forest site. *Journal of Geophysical Research: Atmospheres*, 111(D16). <https://doi.org/10.1029/2006JD007161>
- Guenther, A. (2002). The contribution of reactive carbon emissions from vegetation to the carbon balance of terrestrial ecosystems. *Chemosphere*, 49(8), 837-844. [https://doi.org/10.1016/S0045-6535\(02\)00384-3](https://doi.org/10.1016/S0045-6535(02)00384-3)
- Guenther, A. B., Jiang, X., Heald, C. L., Sakulyanontvittaya, T., Duhl, T., Emmons, L. K., & Wang, X. (2012). The model of emissions of gases and aerosols from nature version 2.1 (MEGAN2. 1): An extended and updated framework for modeling biogenic emissions. *Geoscientific Model Development*, 5(6), 1471-1492. <https://doi.org/10.5194/gmd-5-1471-2012>
- Guenther, A. B., Monson, R. K., & Fall, R. (1991). Isoprene and monoterpene emission rate variability: observations with eucalyptus and emission rate algorithm development. *Journal of Geophysical Research: Atmospheres*, 96(D6), 10799-10808. <https://doi.org/10.1029/91JD00960>
- Guenther, A., Hewitt, C. N., Erickson, D., Fall, R., Geron, C., Graedel, T., ... Pierce, T. (1995). A global model of natural volatile organic compound emissions. *Journal of Geophysical Research: Atmospheres*, 100(D5), 8873-8892. <https://doi.org/10.1029/94JD02950>
- Guenther, A., Karl, T., Harley, P., Wiedinmyer, C., Palmer, P. I., & Geron, C. (2006). Estimates of global terrestrial isoprene emissions using MEGAN (model of emissions of gases and aerosols from nature). *Atmospheric Chemistry and Physics*, 6(11), 3181-3210. <https://doi.org/10.5194/acpd-6-3181-2006>

- Guenther, A., Zimmerman, P. R., Harley, P. C., Monson, R. K., & Fall, R. (1993). Isoprene and monoterpene emission rate variability: Model evaluations and sensitivity analyses. *Journal of Geophysical Research*, 98(D7), 12609. <https://doi.org/10.1029/93JD00527>
- Hallquist, M., Wenger, J. C., Baltensperger, U., Rudich, Y., Simpson, D., Claeys, M., ... & Wildt, J. (2009). The formation, properties and impact of secondary organic aerosol: current and emerging issues. *Atmospheric chemistry and physics*, 9(14), 5155-5236. <https://doi.org/10.5194/acp-9-5155-2009>
- Hardacre, C., Wild, O., & Emberson, L. (2015). An evaluation of ozone dry deposition in global scale chemistry climate models. *Atmospheric Chemistry and Physics*, 15(11), 6419-6436. <https://doi.org/10.5194/acp-15-6419-2015>
- Hari, P., & Kulmala, M. (2005). Station for Measuring Ecosystem Atmosphere Relations (SMEAR II). *Boreal Environmental Research*, 10, 315– 322.
- Hari, P., Nikinmaa, E., Pohja, T., Siivola, E., Bäck, J., Vesala, T., & Kulmala, M. (2013). Station for measuring ecosystem-atmosphere relations: SMEAR. In P. Hari, K. Heliövaara, & L. Kulmala (Eds.), *Physical and physiological forest ecology*. Dordrecht: Springer. https://doi.org/10.1007/978-94-007-5603-8_9
- Harley, P. C., Litvak, M. E., Sharkey, T. D., & Monson, R. K. (1994). Isoprene emission from velvet bean leaves (interactions among nitrogen availability, growth photon flux density, and leaf development). *Plant Physiology*, 105(1), 279-285. <https://doi.org/10.1104/pp.105.1.279>
- Harley, P. C., Thomas, R. B., Reynolds, J. F., & Strain, B. R. (1992). Modelling photosynthesis of cotton grown in elevated CO₂. *Plant, Cell & Environment*, 15(3), 271-282. <https://doi.org/10.1111/j.1365-3040.1992.tb00974.x>
- Harmens, H., Mills, G., Emberson, L. D., & Ashmore, M. R. (2007). Implications of climate change for the stomatal flux of O₃: A case study for winter wheat. *Environmental Pollution*, 146(3), 763– 770. <https://doi.org/10.1016/j.envpol.2006.05.018>
- Harper, A. B., Cox, P. M., Friedlingstein, P., Wiltshire, A. J., Jones, C. D., Sitch, S., ... & Bodegom, P. V. (2016). Improved representation of plant functional types and physiology in the Joint UK Land Environment Simulator (JULES v4. 2) using plant trait information. *Geoscientific Model Development*, 9(7), 2415-2440. <https://doi.org/10.5194/gmd-9-2415-2016>
- Harper, A. B., Williams, K. E., McGuire, P. C., Duran Rojas, M. C., Hemming, D., Verhoef, A., ... & Wohlfahrt, G. (2020). Improvement of modelling plant responses to low soil moisture in JULESv4. 9 and evaluation against flux tower measurements. *Geoscientific Model Development Discussions*, 1-42. <https://doi.org/10.5194/gmd-2020-273>
- Hartmann, D. L., Tank, A. M. K., Rusticucci, M., Alexander, L. V., Brönnimann, S., Charabi, Y. A. R., ... Soden, B. J. (2013). Climate change 2013: Observations: Atmosphere and surface. In T. F. Stocker, D. Qin, G.-K. Plattner, M. Tignor, & S. K. Allen (Eds.), *Climate change 2013 the physical science basis: Working group I contribution to the fifth assessment report of the Intergovernmental Panel on Climate Change* (pp. 159– 254). Cambridge University Press. Retrieved from www.climatechange2013.org and www.ipcc.ch
- Hayes, F., Mills, G., Harmens, H., & Norris, D. (2007). Evidence of widespread ozone damage to vegetation in Europe (1990-2006). ICP Vegetation Programme Coordination Centre, CEH Bangor, UK.
- Heald, C. L., Wilkinson, M. J., Monson, R. K., Alo, C. A., Wang, G., & Guenther, A. (2009). Response of isoprene emission to ambient CO₂ changes and implications for global budgets. *Global Change Biology*, 15(5), 1127-1140. <https://doi.org/10.1111/j.1365-2486.2008.01802.x>
- Hellén, H., Hakola, H., Pystynen, K. H., Rinne, J., & Haapanala, S. (2006). C₂-C₁₀ hydrocarbon emissions from a boreal wetland and forest floor. *Biogeosciences*, 3(2), 167-174. <https://doi.org/10.5194/bg-3-167-2006>

- Herbst, M., Rosier, P. T. W., Morecroft, M. D., & Gowing, D. J. (2008). Comparative measurements of transpiration and canopy conductance in two mixed deciduous woodlands differing in structure and species composition. *Tree Physiology*, 28(6), 959–970. <https://doi.org/10.1093/treephys/28.6.959>
- Hetherington, A. M., & Woodward, F. I. (2003). The role of stomata in sensing and driving environmental change. *Nature*, 424(6951), 901–908. <https://doi.org/10.1038/nature01843>
- Holopainen, J. K. (2004). Multiple functions of inducible plant volatiles. *Trends in Plant Science*, 9(11), 529–533. <https://doi.org/10.1016/j.tplants.2004.09.006>
- Holtum, J. A., & Winter, K. (2010). Elevated [CO₂] and forest vegetation: more a water issue than a carbon issue?. *Functional Plant Biology*, 37(8), 694–702. <https://doi.org/10.1071/FP10001>
- Hoshika, Y., Katata, G., Deushi, M., Watanabe, M., Koike, T., & Paoletti, E. (2015). Ozone-induced stomatal sluggishness changes carbon and water balance of temperate deciduous forests. *Scientific Reports*, 5, 9871. <https://doi.org/10.1038/srep09871>
- Hoshika, Y., Omasa, K., & Paoletti, E. (2013). Both O₃ exposure and soil water stress are able to induce stomatal sluggishness. *Environmental and Experimental Botany*, 88, 19–23. <https://doi.org/10.1016/j.envexpbot.2011.12.004>
- Hoshika, Y., Osada, Y., De Marco, A., Penuelas, J., & Paoletti, E. (2018). Global diurnal and nocturnal parameters of stomatal conductance in woody plants and major crops. *Global Ecology and Biogeography*, 27(2), 257–275. <https://doi.org/10.1111/geb.12681>
- Hoshika, Y., Watanabe, M., Inada, N., & Koike, T. (2013). Model-based analysis of avoidance of O₃ stress by stomatal closure in Siebold's beech (*Fagus crenata*). *Annals of Botany*, 112(6), 1149–1158. <https://doi.org/10.1093/aob/mct166>
- Hoshika, Y., De Marco, A., Materassi, A., & Paoletti, E. (2016). Light intensity affects ozone-induced stomatal sluggishness in snapbean. *Water, Air, & Soil Pollution*, 227(11), 419. <https://doi.org/10.1007/s11270-016-3127-1>
- Hoshika, Y., Watanabe, M., Carrari, E., Paoletti, E., & Koike, T. (2018). Ozone-induced stomatal sluggishness changes stomatal parameters of Jarvis-type model in white birch and deciduous oak. *Plant Biology*, 20(1), 20–28. <https://doi.org/10.1111/plb.12632>
- Huntingford, C., Oliver, R. J., Mercado, L. M., & Sitch, S. (2018). A simple theoretical model framework to describe plant stomatal “sluggishness” in response to elevated ozone concentrations. *Biogeosciences*, 15(17), 5415–5422. <https://doi.org/10.5194/bg-15-5415-2018>
- Inness, A., Ades, M., Agusti-Panareda, A., Barré, J., Benedictow, A., Blechschmidt, A. M., ... & Suttie, M. (2019). The CAMS reanalysis of atmospheric composition. *Atmospheric Chemistry and Physics*, 19(6), 3515–3556. <https://doi.org/10.5194/acp-19-3515-2019>
- Intergovernmental Panel on Climate Change (IPCC) (2001). The carbon cycle and atmospheric carbon dioxide, in *Climate Change 2001: The scientific basis, Contribution of Working Group I to the Third Assessment Report of the Intergovernmental Panel on Climate Change*, edited by J. T. Houghton et al., pp. 183–237, Cambridge Univ. Press, New York.
- IPCC [Intergovernmental Panel on Climate Change]. (2013). Near-term climate change: Projections and predictability. T. F. Stocker, D. Qin, G. K. Plattner, M. Tignor, S. K. Allen, J. Boschung, A. Nauels, Y. Xia, V. Bex, & P. M. Midgley (Eds.), *Climate change 2013: The physical science basis. Contribution of working group I to the fifth assessment report of the Intergovernmental Panel on Climate Change* (pp. 978–980). Cambridge, UK and New York, NY: Cambridge University Press.
- IPCC [Intergovernmental Panel on Climate Change]. (2014). Summary for policymakers. *Climate change 2014: Impacts, adaptation and vulnerability – Contribution of working group II to fifth assessment report of the Intergovernmental Panel on Climate Change* (pp. 1–32). <https://doi.org/10.1016/j.renene.2009.11.012>

- Irvine, J., Perks, M. P., Magnani, F., & Grace, J. (1998). The response of *Pinus sylvestris* to drought: stomatal control of transpiration and hydraulic conductance. *Tree physiology*, 18(6), 393-402. <https://doi.org/10.1093/treephys/18.6.393>
- Jacobs, C. M. J. (1994). Direct impact of atmospheric CO₂ enrichment on regional transpiration. Ph.D Thesis, Wageningen Agricultural University.
- Jamieson, P. D., Francis, G. S., Wilson, D. R., & Martin, R. J. (1995). Effects of water deficits on evapotranspiration from barley. *Agricultural and Forest Meteorology*, 76(1), 41-58. [https://doi.org/10.1016/0168-1923\(94\)02214-5](https://doi.org/10.1016/0168-1923(94)02214-5)
- Jarvis, P. G. (1976). The interpretation of the variations in leaf water potential and stomatal conductance found in canopies in the field. *Philosophical Transactions of the Royal Society of London. B, Biological Sciences*, 273(927), 593-610. <https://doi.org/10.1098/rstb.1976.0035>
- Jiang, J., Aksoyoglu, S., Ciarelli, G., Oikonomakis, E., El-Haddad, I., Canonaco, F., ... Prévôt, A. S. (2019). Effects of two different biogenic emission models on modelled ozone and aerosol concentrations in Europe. *Atmospheric Chemistry and Physics*, 19(6), 3747–3768. <https://doi.org/10.5194/acp-19-3747-2019>
- Jiang, M., Medlyn, B. E., Drake, J. E., Duursma, R. A., Anderson, I. C., Barton, C. V. M., ... Ellsworth, D. S. (2020). The fate of carbon in a mature forest under carbon dioxide enrichment. *Nature*, 580(7802), 227–231. <https://doi.org/10.1038/s41586-020-2128-9>
- Jiang, X., Guenther, A., Potosnak, M., Geron, C., Seco, R., Karl, T., ... & Pallardy, S. (2018). Isoprene emission response to drought and the impact on global atmospheric chemistry. *Atmospheric Environment*, 183, 69-83. <https://doi.org/10.1016/j.atmosenv.2018.01.026>
- Jimenez, J. L., Canagaratna, M. R., Donahue, N. M., Prevot, A. S. H., Zhang, Q., Kroll, J. H., ... & Worsnop, D. R. (2009). Evolution of organic aerosols in the atmosphere. *Science*, 326(5959), 1525-1529. DOI: 10.1126/science.1180353
- Jones, H. G., & Corlett, J. E. (1992). Current topics in drought physiology. *The Journal of Agricultural Science*, 119(3), 291-296. <https://doi.org/10.1017/S0021859600012144>
- Jung, M., Maire, G. L., Zaehle, S., Luyssaert, S., Vetter, M., Churkina, G., ... & Reichstein, M. (2007). Assessing the ability of three land ecosystem models to simulate gross carbon uptake of forests from boreal to Mediterranean climate in Europe. *Biogeosciences*, 4(4), 647-656. <https://doi.org/10.5194/bg-4-647-2007>
- Kaplan, J. O., Folberth, G., & Hauglustaine, D. A. (2006). Role of methane and biogenic volatile organic compound sources in late glacial and Holocene fluctuations of atmospheric methane concentrations. *Global Biogeochemical Cycles*, 20(2). <https://doi.org/10.1029/2005GB002590>
- Karl, T., Guenther, A., Jordan, A., Fall, R., & Lindinger, W. (2001). Eddy covariance measurement of biogenic oxygenated VOC emissions from hay harvesting. *Atmospheric Environment*, 35(3), 491-495. [https://doi.org/10.1016/S1352-2310\(00\)00405-2](https://doi.org/10.1016/S1352-2310(00)00405-2)
- Karnosky, D. F., Zak, D. R., Pregitzer, K. S., Awmack, C. S., Bockheim, J. G., Dickson, R. E., ... & Isebrands, J. G. (2003). Tropospheric O₃ moderates responses of temperate hardwood forests to elevated CO₂: a synthesis of molecular to ecosystem results from the Aspen FACE project. *Functional Ecology*, 17(3), 289-304. <https://doi.org/10.1046/j.1365-2435.2003.00733.x>
- Kasischke, E. S. (2000). Boreal ecosystems in the global carbon cycle. In E. S. Kasischke & B. J. Stocks (Eds.), *Fire, climate change, and carbon cycling in the boreal forest* (pp. 19–30). New York, NY: Springer.
- Keeling, C. D., Chin, J. F. S., & Whorf, T. P. (1996). Increased activity of northern vegetation inferred from atmospheric CO₂ measurements. *Nature*, 382(6587), 146–149. <https://doi.org/10.1038/382146a0>

- Keenan, T. F., Gray, J., Friedl, M. A., Toomey, M., Bohrer, G., Hollinger, D. Y., ... Richardson, A. D. (2014). Net carbon uptake has increased through warming-induced changes in temperate forest phenology. *Nature Climate Change*, 4(7), 598–604. <https://doi.org/10.1038/nclimate2253>
- Keenan, T., García, R., Friend, A. D., Zaehle, S., Gracia, C., & Sabate, S. (2009). Improved understanding of drought controls on seasonal variation in Mediterranean forest canopy CO₂ and water fluxes through combined in situ measurements and ecosystem modelling. *Biogeosciences*, 6(8), 1423-1444. <https://doi.org/10.5194/bg-6-1423-2009>
- Keenan, T., Sabate, S., & Gracia, C. (2010). Soil water stress and coupled photosynthesis–conductance models: Bridging the gap between conflicting reports on the relative roles of stomatal, mesophyll conductance and biochemical limitations to photosynthesis. *Agricultural and Forest Meteorology*, 150(3), 443–453. <https://doi.org/10.1016/j.agrformet.2010.01.008>
- Kesselmeier, J., Bode, K., Gerlach, C., & Jork, E. M. (1998). Exchange of atmospheric formic and acetic acids with trees and crop plants under controlled chamber and purified air conditions. *Atmospheric Environment*, 32(10), 1765-1775. [https://doi.org/10.1016/S1352-2310\(97\)00465-2](https://doi.org/10.1016/S1352-2310(97)00465-2)
- Kesselmeier, J., Bode, K., Hofmann, U., Müller, H., Schäfer, L., Wolf, A., ... & Torres, L. (1997). Emission of short chained organic acids, aldehydes and monoterpenes from *Quercus ilex* L. and *Pinus pinea* L. in relation to physiological activities, carbon budget and emission algorithms. *Atmospheric Environment*, 31, 119-133. [https://doi.org/10.1016/S1352-2310\(97\)00079-4](https://doi.org/10.1016/S1352-2310(97)00079-4)
- Kesselmeier, J., Ciccioli, P., Kuhn, U., Stefani, P., Biesenthal, T., Rottenberger, S., ... & Andreae, M. O. (2002). Volatile organic compound emissions in relation to plant carbon fixation and the terrestrial carbon budget. *Global Biogeochemical Cycles*, 16(4), 73-1. <https://doi.org/10.1029/2001GB001813>
- Kesselmeier, J., Schäfer, L., Ciccioli, P., Brancaleoni, E., Cecinato, A., Frattoni, M., ... & Torres, L. (1996). Emission of monoterpenes and isoprene from a Mediterranean oak species *Quercus ilex* L. measured within the BEMA (Biogenic Emissions in the Mediterranean Area) project. *Atmospheric Environment*, 30(10-11), 1841-1850. [https://doi.org/10.1016/1352-2310\(95\)00376-2](https://doi.org/10.1016/1352-2310(95)00376-2)
- Kirby, K. J., Bazely, D. R., Goldberg, E. A., Hall, J. E., Isted, R., Perry, S. C., & Thomas, R. C. (2014). Changes in the tree and shrub layer of Wytham Woods (Southern England) 1974–2012: Local and national trends compared. *Forestry*, 87(5), 663–673. <https://doi.org/10.1093/forestry/cpu026>
- Kljun, N., Black, T. A., Griffis, T. J., Barr, A. G., Gaumont-Guay, D., Morgenstern, K., ... Nesic, Z. (2007). Response of net ecosystem productivity of three boreal forest stands to drought. *Ecosystems*, 10(6), 1039–1055. <https://doi.org/10.1007/s10021-007-9088-x>
- Knapp, A. K., & Smith, M. D. (2001). Variation among biomes in temporal dynamics of aboveground primary production. *Science*, 291(5503), 481-484. [10.1126/science.291.5503.481](https://doi.org/10.1126/science.291.5503.481)
- Kokhanovsky, A. (2004). Optical properties of terrestrial clouds. *Earth-Science Reviews*, 64(3-4), 189-241. [https://doi.org/10.1016/S0012-8252\(03\)00042-4](https://doi.org/10.1016/S0012-8252(03)00042-4)
- Kolari, P., Chan, T., Porcar-Castell, A., Bäck, J., Nikinmaa, E., & Juurola, E. (2014). Field and controlled environment measurements show strong seasonal acclimation in photosynthesis and respiration potential in boreal Scots pine. *Frontiers in plant science*, 5, 717. <https://doi.org/10.3389/fpls.2014.00717>
- Köppen, W. P. (1923). *Die klimate der erde: Grundriss der klimakunde*. Berlin, Germany: Walter de Gruyter GmbH & Co KG.
- Krishnan, P., Black, T. A., Grant, N. J., Barr, A. G., Hogg, E. T. H., Jassal, R. S., & Morgenstern, K. (2006). Impact of changing soil moisture distribution on net ecosystem productivity of a boreal aspen forest during and following drought. *Agricultural and Forest Meteorology*, 139(3–4), 208–223. <https://doi.org/10.1016/j.agrformet.2006.07.002>

- Kumar, A., Chen, F., Niyogi, D., Alfieri, J. G., Ek, M., & Mitchell, K. (2011). Evaluation of a photosynthesis-based canopy resistance formulation in the Noah land-surface model. *Boundary-layer meteorology*, 138(2), 263-284. <https://doi.org/10.1007/s10546-010-9559-z>
- Laisk, A., Kull, O., & Moldau, H. (1989). O₃ concentration in leaf intercellular air spaces is close to zero. *Plant Physiology*, 90(3), 1163– 1167. <https://doi.org/10.1104/pp.90.3.1163>
- Landsberg, J. J., & Gower, S. T. (1997). *Applications of physiological ecology to forest management*. San Diego, CA: Academic Press.
- Laothawornkitkul, J., Taylor, J. E., Paul, N. D., & Hewitt, C. N. (2009). Biogenic volatile organic compounds in the Earth system. *New Phytologist*, 183(1), 27-51. <https://doi.org/10.1111/j.1469-8137.2009.02859.x>
- Lavoit, A. V., Staudt, M., Schnitzler, J. P., Landais, D., Massol, F., Rocheteau, A., ... & Rambal, S. (2009). Drought reduced monoterpene emissions from the evergreen Mediterranean oak *Quercus ilex*: results from a throughfall displacement experiment. *Biogeosciences*, 6(7), 1167-1180. <https://doi.org/10.5194/bg-6-1167-2009>
- Law, B. E., Kelliher, F. M., Baldocchi, D. D., Anthoni, P. M., Irvine, J., Moore, D. V., & Van Tuyl, S. (2001). Spatial and temporal variation in respiration in a young ponderosa pine forest during a summer drought. *Agricultural and Forest Meteorology*, 110(1), 27– 43. [https://doi.org/10.1016/S0168-1923\(01\)00279-9](https://doi.org/10.1016/S0168-1923(01)00279-9)
- Leisner, C. P., & Ainsworth, E. A. (2012). Quantifying the effects of O₃ on plant reproductive growth and development. *Global Change Biology*, 18(2), 606– 616. <https://doi.org/10.1111/j.1365-2486.2011.02535.x>
- Lenton, T. M., & Huntingford, C. (2003). Global terrestrial carbon storage and uncertainties in its temperature sensitivity examined with a simple model. *Global Change Biology*, 9(10), 1333-1352. <https://doi.org/10.1046/j.1365-2486.2003.00674.x>
- Lerdau, M., & Keller, M. (1997). Controls on isoprene emission from trees in a subtropical dry forest. *Plant, Cell & Environment*, 20(5), 569– 578. <https://doi.org/10.1111/j.1365-3040.1997.00075.x>
- Levitt, J. (1980). *Responses of Plants to Environmental Stress, Volume 1: Chilling, Freezing, and High Temperature Stresses*. Academic Press.. pp.497
- Lewis, S. L., Malhi, Y., & Phillips, O. L. (2004). Fingerprinting the impacts of global change on tropical forests. *Philosophical Transactions of the Royal Society of London. Series B: Biological Sciences*, 359(1443), 437-462. <https://doi.org/10.1098/rstb.2003.1432>
- Lhomme, J. P., Elguero, E., Chehbouni, A., & Boulet, G. (1998). Stomatal control of transpiration: Examination of Monteith's formulation of canopy resistance. *Water Resources Research*, 34(9), 2301– 2308. <https://doi.org/10.1029/98WR01339>
- LIMOUSIN, J. M., Misson, L., LAVOIR, A. V., Martin, N. K., & Rambal, S. (2010). Do photosynthetic limitations of evergreen *Quercus ilex* leaves change with long-term increased drought severity?. *Plant, Cell & Environment*, 33(5), 863-875. <https://doi.org/10.1111/j.1365-3040.2009.02112.x>
- Lin, M., Horowitz, L. W., Xie, Y., Paulot, F., Malyshev, S., Shevliakova, E., ... Pilegaard, K. (2020). Vegetation feedbacks during drought exacerbate O₃ air pollution extremes in Europe. *Nature Climate Change*, 10(5), 444– 451. <https://doi.org/10.1038/s41558-020-0743-y>
- Lin, Y. S., Medlyn, B. E., Duursma, R. A., Prentice, I. C., Wang, H., Baig, S., ... & Wingate, L. (2015). Optimal stomatal behaviour around the world. *Nature Climate Change*, 5(5), 459-464. <https://doi.org/10.1038/nclimate2550>
- Litvak, M. E., Loreto, F., Harley, P. C., Sharkey, T. D., & Monson, R. K. (1996). The response of isoprene emission rate and photosynthetic rate to photon flux and nitrogen supply in aspen and white oak

trees. *Plant, Cell & Environment*, 19(5), 549-559. <https://doi.org/10.1111/j.1365-3040.1996.tb00388.x>

- Llusià, J., & Peñuelas, J. (1998). Changes in terpene content and emission in potted Mediterranean woody plants under severe drought. *Canadian Journal of Botany*, 76(8), 1366-1373. <https://doi.org/10.1139/b98-141>
- Llusia, J., Roahtyn, S., Yakir, D., Rotenberg, E., Seco, R., Guenther, A., & Penuelas, J. (2016). Photosynthesis, stomatal conductance and terpene emission response to water availability in dry and mesic Mediterranean forests. *Trees*, 30(3), 749–759. <https://doi.org/10.1007/s00468-015-1317-x>
- Lombardozzi, D., Levis, S., Bonan, G., Hess, P. G., & Sparks, J. P. (2015). The influence of chronic ozone exposure on global carbon and water cycles. *Journal of Climate*, 28(1), 292–305. <https://doi.org/10.1175/JCLI-D-14-00223.1>
- Lombardozzi, D., Sparks, J. P., Bonan, G., & Levis, S. (2012). Ozone exposure causes a decoupling of conductance and photosynthesis: implications for the Ball-Berry stomatal conductance model. *Oecologia*, 169(3), 651-659. <https://doi.org/10.1007/s00442-011-2242-3>
- Long, S. P., Ainsworth, E. A., Leakey, A. D., & Morgan, P. B. (2005). Global food insecurity. Treatment of major food crops with elevated carbon dioxide or ozone under large-scale fully open-air conditions suggests recent models may have overestimated future yields. *Philosophical Transactions of the Royal Society B: Biological Sciences*, 360(1463), 2011-2020. <https://doi.org/10.1098/rstb.2005.1749>
- Loreto, F., & Fares, S. (2007). Is ozone flux inside leaves only a damage indicator? Clues from volatile isoprenoid studies. *Plant Physiology*, 143(3), 1096-1100. <https://doi.org/10.1104/pp.106.091892>
- Loreto, F., & Schnitzler, J. P. (2010). Abiotic stresses and induced BVOCs. *Trends in plant science*, 15(3), 154-166. <https://doi.org/10.1016/j.tplants.2009.12.006>
- Loreto, F., & Sharkey, T. D. (1990). A gas-exchange study of photosynthesis and isoprene emission in *Quercus rubra* L. *Planta*, 182(4), 523-531. <https://doi.org/10.1007/BF02341027>
- Loreto, F., & Velikova, V. (2001). Isoprene produced by leaves protects the photosynthetic apparatus against ozone damage, quenches ozone products, and reduces lipid peroxidation of cellular membranes. *Plant Physiology*, (4), 1781–1787. <https://doi.org/10.1104/pp.010497>
- Loreto, F., Dicke, M., SCHNITZLER, J. P., & Turlings, T. C. (2014). Plant volatiles and the environment. *Plant, cell & environment*, 37(8), 1905-1908. <https://doi.org/10.1111/pce.12369>
- Loveland, T. R., Reed, B. C., Brown, J. F., Ohlen, D. O., Zhu, Z., Yang, L. W. M. J., & Merchant, J. W. (2000). Development of a global land cover characteristics database and IGBP DISCover from 1 km AVHRR data. *International Journal of Remote Sensing*, 21(6-7), 1303-1330. <https://doi.org/10.1080/014311600210191>
- Löw, M., Herbinger, K., Nunn, A. J., Häberle, K.-H., Leuchner, M., Heerdt, C., ... Matyssek, R. (2006). Extraordinary drought of 2003 overrules ozone impact on adult beech trees (*Fagus sylvatica*). *Trees*, 20(5), 539–548. <https://doi.org/10.1007/s00468-006-0069-z>
- Madani, N., Kimball, J. S., Ballantyne, A. P., Affleck, D. L. R., van Bodegom, P. M., Reich, P. B., ... Running, S. W. (2018). Future global productivity will be affected by plant trait response to climate. *Scientific Reports*, 8(1), 1–10. <https://doi.org/10.1038/s41598-018-21172-9>
- Makar, P. A., Staebler, R. M., Akingunola, A., Zhang, J., McLinden, C., Kharol, S. K., ... Zheng, Q. (2017). The effects of forest canopy shading and turbulence on boundary layer ozone. *Nature Communications*, 8, 15243. <https://doi.org/10.1038/ncomms15243>
- Manavalan, L. P., Guttikonda, S. K., Phan Tran, L. S., & Nguyen, H. T. (2009). Physiological and molecular approaches to improve drought resistance in soybean. *Plant and cell physiology*, 50(7), 1260-1276. <https://doi.org/10.1093/pcp/pcp082>

- Manderscheid, R., Erbs, M., & Weigel, H. J. (2014). Interactive effects of free-air CO₂ enrichment and drought stress on maize growth. *European Journal of Agronomy*, 52, 11–21. <https://doi.org/10.1016/j.eja.2011.12.007>
- Mao, J., Ren, X., Zhang, L., van Duin, D. M., Cohen, R. C., Park, J. H., Goldstein, A. H., Paulot, F., Beaver, M. R., Crouse, J. D., Wennberg, P. O., DiGangi, J. P., Henry, S. B., Keutsch, F. N., Park, C., Schade, G. W., Wolfe, G. M., Thornton, J. A., & Brune, W. H. (2012). Insights into hydroxyl measurements and atmospheric oxidation in a California forest. *Atmospheric Chemistry and Physics*, 12(17), 8009–8020. <https://doi.org/10.5194/acp-12-8009-2012>
- Martin, M. J., Stirling, C. M., Humphries, S. W., & Long, S. P. (2000). A process-based model to predict the effects of climatic change on leaf isoprene emission rates. *Ecological Modelling*, 131(2-3), 161–174. [https://doi.org/10.1016/S0304-3800\(00\)00258-1](https://doi.org/10.1016/S0304-3800(00)00258-1)
- Martin, R. S., Villanueva, I., Zhang, J., & Popp, C. J. (1999). Nonmethane hydrocarbon, monocarboxylic acid, and low molecular weight aldehyde and ketone emissions from vegetation in central New Mexico. *Environmental science & technology*, 33(13), 2186–2192. <https://doi.org/10.1021/es980468q>
- Martin-StPaul, N. K., Limousin, J. M., Rodríguez-Calcerrada, J., Ruffault, J., Rambal, S., Letts, M. G., & Misson, L. (2012). Photosynthetic sensitivity to drought varies among populations of *Quercus ilex* along a rainfall gradient. *Functional Plant Biology*, 39(1), 25–37. <https://doi.org/10.1071/FP11090>
- Matyssek, R., & Innes, J. L. (1999). Ozone—a risk factor for trees and forests in Europe?. *Water, Air, and Soil Pollution*, 116(1), 199–226. <https://doi.org/10.1023/A:1005267214560>
- Matyssek, R., Bytnerowicz, A., Karlsson, P. E., Paoletti, E., Sanz, M., Schaub, M., & Wieser, G. (2007). Promoting the O₃ flux concept for European forest trees. *Environmental pollution*, 146(3), 587–607. <https://doi.org/10.1016/j.envpol.2006.11.011>
- Matyssek, R., Günthardt-Goerg, M. S., Maurer, S., & Keller, T. (1995). Nighttime exposure to ozone reduces whole-plant production in *Betula pendula*. *Tree physiology*, 15(3), 159–165. <https://doi.org/10.1093/treephys/15.3.159>
- Matyssek, R., Sandermann, H., Wieser, G., Booker, F., Cieslik, S., Musselman, R., & Ernst, D. (2008). The challenge of making ozone risk assessment for forest trees more mechanistic. *Environmental Pollution*, 156(3), 567–582. <https://doi.org/10.1016/j.envpol.2008.04.017>
- Matyssek, R., Wieser, G., Ceulemans, R., Rennenberg, H., Pretzsch, H., Haberer, K., ... & Häberle, K. H. (2010). Enhanced ozone strongly reduces carbon sink strength of adult beech (*Fagus sylvatica*)—Resume from the free-air fumigation study at Kranzberg Forest. *Environmental Pollution*, 158(8), 2527–2532. <https://doi.org/10.1016/j.envpol.2010.05.009>
- McDowell, N. G. (2011). Mechanisms linking drought, hydraulics, carbon metabolism, and vegetation mortality. *Plant physiology*, 155(3), 1051–1059. <https://doi.org/10.1104/pp.110.170704>
- McKee, T. B., Doesken, N. J., & Kleist, J. (Eds.). (1993). The relationship of drought frequency and duration to time scales. In *Proceedings of the 8th conference on applied climatology* (Vol. 17, pp. 179–183). Boston, MA: American Meteorological Society.
- McKinney, K. A., Lee, B. H., Vasta, A., Pho, T. V., & Munger, J. W. (2011). Emissions of isoprenoids and oxygenated biogenic volatile organic compounds from a New England mixed forest. *Atmospheric Chemistry and Physics*, 11(10), 4807–4831. <https://doi.org/10.5194/acp-11-4807-2011>
- Medlyn, B. E., Duursma, R. A., Eamus, D., Ellsworth, D. S., Prentice, I. C., Barton, C. V., ... & Wingate, L. (2011). Reconciling the optimal and empirical approaches to modelling stomatal conductance. *Global Change Biology*, 17(6), 2134–2144. <https://doi.org/10.1111/j.1365-2486.2010.02375.x>
- Melillo, J. M., McGuire, A. D., Kicklighter, D. W., Moore, B., Vorosmarty, C. J., & Schloss, A. L. (1993). Global climate change and terrestrial net primary production. *Nature*, 363(6426), 234–240. <https://doi.org/10.1038/363234a0>

- Menzel, A., Sparks, T. H., Estrella, N., Koch, E., Aasa, A., Ahas, R., ... Zust, A. (2006). European phenological response to climate change matches the warming pattern. *Global Change Biology*, 12(10), 1969–1976. <https://doi.org/10.1111/j.1365-2486.2006.01193.x>
- Meyers, T. P., & Baldocchi, D. D. (1988). A comparison of models for deriving dry deposition fluxes of O₃ and SO₂ to a forest canopy. *Tellus B*, 40(4), 270-284. DOI: 10.3402/tellusb.v40i4.15916
- M'Hirit, O. (1999). Mediterranean forests: Ecological space and economic and community wealth. UNASYLVA, FAO, 3–15.
- Midgley, G. F., Thuiller, W., & Higgins, S. I. (2007). Plant species migration as a key uncertainty in predicting future impacts of climate change on ecosystems: Progress and challenges. *Terrestrial ecosystems in a changing world* (pp. 129–137). Berlin, Heidelberg: Springer. https://doi.org/10.1007/978-3-540-32730-1_11
- Mihók, B., Kenderes, K., Kirby, K. J., Paviour-Smith, K., & Elbourn, C. A. (2009). Forty-year changes in the canopy and the understorey in Wytham Woods. *Forestry*, 82(5), 515–527. <https://doi.org/10.1093/forestry/cpp021>
- Millán, M. M., Mantilla, E., Salvador, R., Carratalá, A., Sanz, M. J., Alonso, L., ... Navazo, M. (2000). O₃ cycles in the western Mediterranean basin: Interpretation of monitoring data in complex coastal terrain. *Journal of Applied Meteorology*, 39(4), 487–508. [https://doi.org/10.1175/1520-0450\(2000\)039<0487:OCITWM>2.0.CO;2](https://doi.org/10.1175/1520-0450(2000)039<0487:OCITWM>2.0.CO;2)
- Mills, G., Buse, A., Gimeno, B., Bermejo, V., Holland, M., Emberson, L., & Pleijel, H. (2007). A synthesis of AOT40-based response functions and critical levels of ozone for agricultural and horticultural crops. *Atmospheric Environment*, 41(12), 2630-2643. <https://doi.org/10.1016/j.atmosenv.2006.11.016>
- Mills, G., Hayes, F., Simpson, D., Emberson, L., Norris, D., Harmens, H., & Büker, P. (2011a). Evidence of widespread effects of O₃ on crops and (semi-) natural vegetation in Europe (1990–2006) in relation to AOT40-and flux-based risk maps. *Global Change Biology*, 17(1), 592–613.
- Mills, G., Pleijel, H., Braun, S., Büker, P., Bermejo, V., Calvo, E., ... & Simpson, D. (2011b). New stomatal flux-based critical levels for ozone effects on vegetation. *Atmospheric Environment*, 45(28), 5064-5068. <https://doi.org/10.1016/j.atmosenv.2011.06.009>
- Milly, P. C., Dunne, K. A., & Vecchia, A. V. (2005). Global pattern of trends in streamflow and water availability in a changing climate. *Nature*, 438(7066), 347–350. <https://doi.org/10.1038/nature04312>
- Mitchard, E. T. (2018). The tropical forest carbon cycle and climate change. *Nature*, 559(7715), 527-534. <https://doi.org/10.1038/s41586-018-0300-2>
- Monson, R. K., Harley, P. C., Litvak, M. E., Wildermuth, M., Guenther, A. B., Zimmerman, P. R., & Fall, R. (1994). Environmental and developmental controls over the seasonal pattern of isoprene emission from aspen leaves. *Oecologia*, 99(3), 260-270. <https://doi.org/10.1007/BF00627738>
- Monson, R. K., Jaeger, C. H., Adams, W. W., Driggers, E. M., Silver, G. M., & Fall, R. (1992). Relationships among isoprene emission rate, photosynthesis, and isoprene synthase activity as influenced by temperature. *Plant physiology*, 98(3), 1175-1180. <https://doi.org/10.1104/pp.98.3.1175>
- Monthly, seasonal and annual summaries 2018. (2019). UK Met Office website. Retrieved from <https://www.metoffice.gov.uk/research/climate/maps-and-data/summaries/index>
- Morales, P., Sykes, M. T., Prentice, I. C., Smith, P., Smith, B., Bugmann, H., ... & Ogee, J. (2005). Comparing and evaluating process-based ecosystem model predictions of carbon and water fluxes in major European forest biomes. *Global Change Biology*, 11(12), 2211-2233. <https://doi.org/10.1111/j.1365-2486.2005.01036.x>
- Morecroft, M. D., Stokes, V. J., Taylor, M. E., & Morison, J. I. (2008). Effects of climate and management history on the distribution and growth of sycamore (*Acer pseudoplatanus* L.) in a southern British

- woodland in comparison to native competitors. *Forestry*, 81(1), 59– 74. <https://doi.org/10.1093/forestry/cpm045>
- Morgan, J. M. (1984). Osmoregulation and water stress in higher plants. *Annual review of plant physiology*, 35, 299-319.
- Moss, D. N., Krenzer, E. G., & Brun, W. A. (1969). Carbon dioxide compensation points in related plant species. *Science*, 164(3876), 187-188. [10.1126/science.164.3876.187](https://doi.org/10.1126/science.164.3876.187)
- Musselman, R. C., Lefohn, A. S., Massman, W. J., & Heath, R. L. (2006). A critical review and analysis of the use of exposure-and flux-based ozone indices for predicting vegetation effects. *Atmospheric Environment*, 40(10), 1869-1888. <https://doi.org/10.1016/j.atmosenv.2005.10.064>
- Nali, C., Paoletti, E., Marabottini, R., Della Rocca, G., Lorenzini, G., Paolacci, A. R., ... Badiani, M. (2004). Ecophysiological and biochemical strategies of response to O₃ in Mediterranean evergreen broadleaf species. *Atmospheric Environment*, 38(15), 2247– 2257. <https://doi.org/10.1016/j.atmosenv.2003.11.043>
- NASA (2020): <https://www.earthobservatory.nasa.gov/features/CarbonCycle> (last accessed on 15/02/2021)
- Neill, S., Barros, R., Bright, J., Desikan, R., Hancock, J., Harrison, J., ... & Wilson, I. (2008). Nitric oxide, stomatal closure, and abiotic stress. *Journal of experimental botany*, 59(2), 165-176. <https://doi.org/10.1093/jxb/erm293>
- Neilson, R. P., Pitelka, L. F., Solomon, A. M., Nathan, R. A. N., Midgley, G. F., Fragoso, J. M., ... & Thompson, K. E. N. (2005). Forecasting regional to global plant migration in response to climate change. *Bioscience*, 55(9), 749-759.
- Neilson, R. P., Prentice, I. C., & Smith, B. (1998). Simulated changes in vegetation distribution under global warming. In *The regional impacts of climate change: an assessment of vulnerability* (pp. 439-456). Cambridge University Press. <http://hdl.handle.net/11858/00-001M-0000-000E-CB7D-9>
- Nemani, R. R., Keeling, C. D., Hashimoto, H., Jolly, W. M., Piper, S. C., Tucker, C. J., ... & Running, S. W. (2003). Climate-driven increases in global terrestrial net primary production from 1982 to 1999. *science*, 300(5625), 1560-1563. DOI: [10.1126/science.1082750](https://doi.org/10.1126/science.1082750)
- Niinemets, Ü. (2010). Mild versus severe stress and BVOCs: Thresholds, priming and consequences. *Trends in Plant Science*, 15(3), 145– 153. <https://doi.org/10.1016/j.tplants.2009.11.008>
- Niinemets, Ü., & Reichstein, M. (2003). Controls on the emission of plant volatiles through stomata: Differential sensitivity of emission rates to stomatal closure explained. *Journal of Geophysical Research: Atmospheres*, 108(D7). DOI: [10.1029/2002JD002626](https://doi.org/10.1029/2002JD002626)
- Niinemets, Ü., Tenhunen, J. D., Harley, P. C., & Steinbrecher, R. (1999). A model of isoprene emission based on energetic requirements for isoprene synthesis and leaf photosynthetic properties for *Liquidambar* and *Quercus*. *Plant, Cell & Environment*, 22(11), 1319-1335. <https://doi.org/10.1046/j.1365-3040.1999.00505.x>
- Norby, R. J., Warren, J. M., Iversen, C. M., Medlyn, B. E., & McMurtrie, R. E. (2010). CO₂ enhancement of forest productivity constrained by limited nitrogen availability. *Proceedings of the National Academy of Sciences of the United States of America*, 107(45), 19368– 19373. <https://doi.org/10.1073/pnas.1006463107>
- Omasa, K., & Takayama, K. (2002). Image instrumentation of chlorophyll a fluorescence for diagnosing photosynthetic injury. In *Air pollution and plant biotechnology* (pp. 287– 308). Tokyo: Springer. https://doi.org/10.1007/978-4-431-68388-9_15
- Osakabe, Y., Osakabe, K., Shinozaki, K., & Tran, L. S. P. (2014). Response of plants to water stress. *Frontiers in Plant Science*, 5, 86. <https://doi.org/10.3389/fpls.2014.00086>
- Otu-Larbi, F., Bolas, C. G., Ferracci, V., Staniaszek, Z., Jones, R. L., Malhi, Y., ... & Ashworth, K. (2020a). Modelling the effect of the 2018 summer heatwave and drought on isoprene emissions in a UK woodland. *Global change biology*, 26(4), 2320-2335. <https://doi.org/10.1111/gcb.14963>

- Otu-Larbi, F., Conte, A., Fares, S., Wild, O., & Ashworth, K. (2020b). Current and future impacts of drought and ozone stress on Northern Hemisphere forests. *Global Change Biology*, 26(11), 6218-6234. <https://doi.org/10.1111/gcb.15339>
- Pacifico, F., Harrison, S. P., Jones, C. D., & Sitch, S. (2009). Isoprene emissions and climate. *Atmospheric Environment*, 43(39), 6121– 6135. <https://doi.org/10.1016/j.atmosenv.2009.09.002>
- Pacifico, F., Harrison, S. P., Jones, C. D., Arneth, A., Sitch, S., Weedon, G. P., ... & Schurgers, G. (2011). Evaluation of a photosynthesis-based biogenic isoprene emission scheme in JULES and simulation of isoprene emissions under present-day climate conditions. *Atmospheric Chemistry and Physics*, 11(9), 4371-4389. <https://doi.org/10.5194/acp-11-4371-2011>
- Padro, J. (1996). Summary of ozone dry deposition velocity measurements and model estimates over vineyard, cotton, grass and deciduous forest in summer. *Atmospheric Environment*, 30(13), 2363-2369. [https://doi.org/10.1016/1352-2310\(95\)00352-5](https://doi.org/10.1016/1352-2310(95)00352-5)
- Pan, Y., Birdsey, R. A., Fang, J., Houghton, R., Kauppi, P. E., Kurz, W. A., ... & Hayes, D. (2011). A large and persistent carbon sink in the world's forests. *Science*, 333(6045), 988-993. DOI: 10.1126/science.1201609
- Panek, J. A., & Goldstein, A. H. (2001). Response of stomatal conductance to drought in ponderosa pine: Implications for carbon and O₃ uptake. *Tree Physiology*, 21(5), 337– 344. <https://doi.org/10.1093/treephys/21.5.337>
- Paoletti, E. (2006). Impact of O₃ on Mediterranean forests: A review. *Environmental Pollution*, 144(2), 463– 474. <https://doi.org/10.1016/j.envpol.2005.12.051>
- Paoletti, E. (2005). Ozone slows stomatal response to light and leaf wounding in a Mediterranean evergreen broadleaf, *Arbutus unedo*. *Environmental Pollution*, 134(3), 439– 445. <https://doi.org/10.1016/j.envpol.2004.09.011>
- Paoletti, E. (2009). O₃ and Mediterranean ecology: Plants, people, problems. *Environmental Pollution*, 157(5), 1397– 1525.
- Paoletti, E., & Manning, W. J. (2007). Toward a biologically significant and usable standard for ozone that will also protect plants. *Environmental Pollution*, 150(1), 85-95. <https://doi.org/10.1016/j.envpol.2007.06.037>
- Paoletti, E., & Grulke, N. E. (2010). O₃ exposure and stomatal sluggishness in different plant physiognomic classes. *Environmental Pollution*, 158(8), 2664– 2671. <https://doi.org/10.1016/j.envpol.2010.04.024>
- Park, J. H., Fares, S., Weber, R., & Goldstein, A. H. (2014). Biogenic volatile organic compound emissions during BEARPEX 2009 measured by eddy covariance and flux–gradient similarity methods. *Atmospheric Chemistry and Physics*, 14(1), 231-244. <https://doi.org/10.5194/acp-14-231-2014>
- Passioura, J. B. (2002). Soil conditions and plant growth. *Plant, Cell & Environment*, 25(2), 311-318. <https://doi.org/10.1046/j.0016-8025.2001.00802.x>
- Pastorello, G., Trotta, C., Canfora, E. et al. The FLUXNET2015 dataset and the ONEFlux processing pipeline for eddy covariance data. *Sci Data* 7, 225 (2020). <https://doi.org/10.1038/s41597-020-0534-3>
- Pastorello, G., Papale, D., Chu, H., Trotta, C., Agarwal, D., Canfora, E., ... Torn, M. (2017). A new data set to keep a sharper eye on land-air exchanges. *Eos, Transactions American Geophysical Union*, 98(8). <https://doi.org/10.1029/2017EO071597>
- Pegoraro, E., Potosnak, M. J., Monson, R. K., Rey, A., Barron-Gafford, G., & Osmond, C. B. (2007). The effect of elevated CO₂, soil and atmospheric water deficit and seasonal phenology on leaf and ecosystem isoprene emission. *Functional Plant Biology*, 34(9), 774-784. <https://doi.org/10.1071/FP07021>

- Pegoraro, E., Rey, A., Greenberg, J., Harley, P., Grace, J., Malhi, Y., & Guenther, A. (2004a). Effect of drought on isoprene emission rates from leaves of *Quercus virginiana* mill. *Atmospheric Environment*, 38(36), 6149– 6156. <https://doi.org/10.1016/j.atmosenv.2004.07.028>
- Pegoraro, E., Rey, A., Greenberg, J., Harley, P., Grace, J., Malhi, Y., & Guenther, A. (2004). Effect of drought on isoprene emission rates from leaves of *Quercus virginiana* Mill. *Atmospheric Environment*, 38(36), 6149-6156. <https://doi.org/10.1016/j.atmosenv.2004.07.028>
- Pegoraro, E., Abrell, L., Van Haren, J., Barron-Gafford, G., Grieve, K. A., Malhi, Y., ... Lin, G. (2005). The effect of elevated atmospheric CO₂ and drought on sources and sinks of isoprene in a temperate and tropical rainforest mesocosm. *Global Change Biology*, 11(8), 1234– 1246. <https://doi.org/10.1111/j.1365-2486.2005.00986.x>
- Pegoraro, E., Rey, A., Greenberg, J., Harley, P., Grace, J., Malhi, Y., & Guenther, A. (2004). Effect of drought on isoprene emission rates from leaves of *Quercus virginiana* Mill. *Atmospheric Environment*, 38(36), 6149– 6156. <https://doi.org/10.1016/j.atmosenv.2004.07.028>
- Pellegrini, E., Hoshika, Y., Dusart, N., Cotrozzi, L., Gérard, J., Nali, C., ... Paoletti, E. (2019). Antioxidative responses of three oak species under ozone and water stress conditions. *Science of the Total Environment*, 647, 390– 399. <https://doi.org/10.1016/j.scitotenv.2018.07.413>
- Pemadasa, M. A., & Lovell, P. H. (1974). The mineral nutrition of some dune annuals. *The Journal of Ecology*, 647-657. <https://doi.org/10.2307/2259004>
- Peñuelas, J., & Llusà, J. (2003). BVOCs: plant defense against climate warming?. *Trends in plant science*, 8(3), 105-109. [https://doi.org/10.1016/S1360-1385\(03\)00008-6](https://doi.org/10.1016/S1360-1385(03)00008-6)
- Peñuelas, J., & Llusà, J. (2002). Linking photorespiration, monoterpenes and thermotolerance in *Quercus*. *New Phytologist*, 155(2), 227– 237. <https://doi.org/10.1046/j.1469-8137.2002.00457.x>
- Peñuelas, J., Filella, I., Seco, R., & Llusia, J. (2009). Increase in isoprene and monoterpene emissions after re-watering of droughted *Quercus ilex* seedlings. *Biologia Plantarum*, 53(2), 351– 354. <https://doi.org/10.1007/s10535-009-0065-4>
- Perkins-Kirkpatrick, S. E., & Gibson, P. B. (2017). Changes in regional heatwave characteristics as a function of increasing global temperature. *Scientific Reports*, 7(1), 1-12. <https://doi.org/10.1038/s41598-017-12520-2>
- Piao, S., Sitch, S., Ciais, P., Friedlingstein, P., Peylin, P., Wang, X., ... & Zeng, N. (2013). Evaluation of terrestrial carbon cycle models for their response to climate variability and to CO₂ trends. *Global change biology*, 19(7), 2117-2132. <https://doi.org/10.1111/gcb.12187>
- Pike, R. C., & Young, P. J. (2009). How plants can influence tropospheric chemistry: the role of isoprene emissions from the biosphere. *Weather*, 64(12), 332-336. <https://doi.org/10.1002/wea.416>
- Pleijel, H., Danielsson, H., Karlsson, G. P., Gelang, J., Karlsson, P. E., & Selldén, G. (2000). An ozone flux–response relationship for wheat. *Environmental Pollution*, 109(3), 453-462. [https://doi.org/10.1016/S0269-7491\(00\)00048-8](https://doi.org/10.1016/S0269-7491(00)00048-8)
- Pleijel, H., Danielsson, H., Ojanperä, K., De Temmerman, L., Högy, P., Badiani, M., & Karlsson, P. E. (2004). Relationships between ozone exposure and yield loss in European wheat and potato—a comparison of concentration-and flux-based exposure indices. *Atmospheric Environment*, 38(15), 2259-2269. <https://doi.org/10.1016/j.atmosenv.2003.09.076>
- Porporato, A., Laio, F., Ridolfi, L., & Rodriguez-Iturbe, I. (2001). Plants in water-controlled ecosystems: active role in hydrologic processes and response to water stress: III. Vegetation water stress. *Advances in water resources*, 24(7), 725-744. [https://doi.org/10.1016/S0309-1708\(01\)00006-9](https://doi.org/10.1016/S0309-1708(01)00006-9)
- Possell, M., & Hewitt, C. N. (2011). Isoprene emissions from plants are mediated by atmospheric CO₂ concentrations. *Global Change Biology*, 17(4), 1595-1610. <https://doi.org/10.1111/j.1365-2486.2010.02306.x>

- Potosnak, M. J., LeSturgeon, L., Pallardy, S. G., Hosman, K. P., Gu, L., Karl, T., ... & Guenther, A. B. (2014). Observed and modeled ecosystem isoprene fluxes from an oak-dominated temperate forest and the influence of drought stress. *Atmospheric Environment*, 84, 314-322. <https://doi.org/10.1016/j.atmosenv.2013.11.055>
- Qaderi, M. M., Kurepin, L. V., & Reid, D. M. (2006). Growth and physiological responses of canola (*Brassica napus*) to three components of global climate change: temperature, carbon dioxide and drought. *Physiologia Plantarum*, 128(4), 710-721. <https://doi.org/10.1111/j.1399-3054.2006.00804.x>
- Raupach M. R. (1989). A practical Lagrangian method for relating scalar concentrations to source distributions in vegetation canopies. *Quarterly Journal of the Royal Meteorological Society*, 115(487), 609– 632. <https://doi.org/10.1002/qj.49711548710>
- Regional Values. (2019). UK Met Office website. Retrieved <https://www.metoffice.gov.uk/climate/uk/summaries/2018/summer/regional-values>
- Rennenberg, H., Loreto, F., Polle, A., Brill, F., Fares, S., Beniwal, R. S., & Gessler, A. (2006). Physiological responses of forest trees to heat and drought. *Plant Biology*, 8(05), 556– 571. <https://doi.org/10.1055/s-2006-924084>
- Riahi, K., Rao, S., Krey, V., Cho, C., Chirkov, V., Fischer, G., ... Rafaj, P. (2011). RCP 8.5 – A scenario of comparatively high greenhouse gas emissions. *Climatic Change*, 109(1–2), 33– 57. <https://doi.org/10.1007/s10584-011-0149-y>
- Rice, A. H., Pyle, E. H., Saleska, S. R., Hutyra, L., Palace, M., Keller, M., ... & Wofsy, S. C. (2004). Carbon balance and vegetation dynamics in an old-growth Amazonian forest. *Ecological applications*, 14(sp4), 55-71. <https://doi.org/10.1890/02-6006>
- Rinne, J., Taipale, R., Markkanen, T., Ruuskanen, T. M., Hellén, H., Kajos, M. K., ... & Kulmala, M. (2007). Hydrocarbon fluxes above a Scots pine forest canopy: measurements and modeling. *Atmospheric Chemistry and Physics*, 7(12), 3361-3372. <https://doi.org/10.5194/acp-7-3361-2007>
- Rödig, E., Cuntz, M., Rammig, A., Fischer, R., Taubert, F., & Huth, A. (2018). The importance of forest structure for carbon fluxes of the Amazon rainforest. *Environmental Research Letters*, 13(5), 054013. <https://doi.org/10.1088/1748-9326/aabc61>
- Rosenstiel, T. N., Potosnak, M. J., Griffin, K. L., Fall, R., & Monson, R. K. (2003). Increased CO₂ uncouples growth from isoprene emission in an agriforest ecosystem. *Nature*, 421(6920), 256-259. <https://doi.org/10.1038/nature01312>
- Royal Society (2008). Ground-level ozone in the 21st century: future trends, impacts and policy implications. Science Policy Report 15/08. The Royal Society, London.
- Sanderson, M. G., Jones, C. D., Collins, W. J., Johnson, C. E., & Derwent, R. G. (2003). Effect of climate change on isoprene emissions and surface ozone levels. *Geophysical Research Letters*, 30(18). <https://doi.org/10.1029/2003GL017642>
- Schade, G. W., & Goldstein, A. H. (2001). Fluxes of oxygenated volatile organic compounds from a ponderosa pine plantation. *Journal of Geophysical Research: Atmospheres*, 106(D3), 3111-3123. <https://doi.org/10.1029/2000JD900592>
- Schär, C., Vidale, P. L., Lüthi, D., Frei, C., Häberli, C., Liniger, M. A., & Appenzeller, C. (2004). The role of increasing temperature variability for European summer heat waves. *Nature*, 427, 332– 336. <https://doi.org/10.1038/nature02300>
- Scheller, R. M., & Mladenoff, D. J. (2005). A spatially interactive simulation of climate change, harvesting, wind, and tree species migration and projected changes to forest composition and biomass in northern Wisconsin, USA. *Global Change Biology*, 11(2), 307– 321. <https://doi.org/10.1111/j.1365-2486.2005.00906.x>

- Schnitzler, J. P., Graus, M., Kreuzwieser, J., Heizmann, U., Rennenberg, H., Wisthaler, A., & Hansel, A. (2004). Contribution of different carbon sources to isoprene biosynthesis in poplar leaves. *Plant Physiology*, 135(1), 152-160. <https://doi.org/10.1104/pp.103.037374>
- Seco, R., Karl, T., Guenther, A., Hosman, K. P., Pallardy, S. G., Gu, L., Geron, C., Harley, P., & Kim, S. (2015). Ecosystem-scale volatile organic compound fluxes during an extreme drought in a broadleaf temperate forest of the Missouri Ozarks (Central USA). *Global Change Biology*, 21(10), 3657– 3674. <https://doi.org/10.1111/gcb.12980>
- Seneviratne, S. I., Corti, T., Davin, E. L., Hirschi, M., Jaeger, E. B., Lehner, I., ... & Teuling, A. J. (2010). Investigating soil moisture–climate interactions in a changing climate: A review. *Earth-Science Reviews*, 99(3-4), 125-161. <https://doi.org/10.1016/j.earscirev.2010.02.004>
- Sharkey, T. D. (1996). Isoprene synthesis by plants and animals. *Endeavour*, 20(2), 74– 78. [https://doi.org/10.1016/0160-9327\(96\)10014-4](https://doi.org/10.1016/0160-9327(96)10014-4)
- Sharkey, T. D. (2000). Biogenic hydrocarbons in the atmospheric boundary layer: A review. *Bulletin of the American Meteorological Society*, 81(7), 1537– 1576. [https://doi.org/10.1175/1520-0477\(2000\)081%3C1537:BHITAB%3E2.3.CO;2](https://doi.org/10.1175/1520-0477(2000)081%3C1537:BHITAB%3E2.3.CO;2)
- Sharkey, T. D., & Loreto, F. (1993). Water-stress, temperature, and light effects on the capacity for isoprene emission and photosynthesis of kudzu leaves. *Oecologia*, 95(3), 328– 333. <https://doi.org/10.1007/BF00320984>
- Sharkey, T. D., Chen, X., & Yeh, S. (2001). Isoprene increases thermotolerance of fosmidomycin-fed leaves. *Plant Physiology*, 125(4).<https://doi.org/10.1104/pp.125.4.2001>
- Sharkey, T. D., Wiberley, A. E., & Donohue, A. R. (2008). Isoprene emission from plants: why and how. *Annals of botany*, 101(1), 5-18.<https://doi.org/10.1093/aob/mcm240>
- Shuttleworth, W. J., & Wallace, J. S. (1985). Evaporation from sparse crops-an energy combination theory. *Quarterly Journal of the Royal Meteorological Society*, 111(469), 839– 855. <https://doi.org/10.1002/qj.49711146910>
- Silva, S. J., & Heald, C. L. (2018). Investigating dry deposition of ozone to vegetation. *Journal of Geophysical Research: Atmospheres*, 123(1), 559-573. <https://doi.org/10.1002/2017JD027278>
- Sindelarova, K., Granier, C., Bouarar, I., Guenther, A., Tilmes, S., Stavrakou, T., ... Knorr, W. (2014). Global data set of biogenic VOC emissions calculated by the MEGAN model over the last 30 years. *Atmospheric Chemistry and Physics*, 14(17), 9317– 9341. <https://doi.org/10.5194/acp-14-9317-2014>
- Singsaas, E. L., Lerdau, M., Winter, K., & Sharkey, T. D. (1997). Isoprene increases thermotolerance of isoprene-emitting species. *Plant physiology*, 115(4), 1413-1420.<https://doi.org/10.1104/pp.115.4.1413>
- Sitch, S., Cox, P. M., Collins, W. J., & Huntingford, C. (2007). Indirect radiative forcing of climate change through O₃ effects on the land-carbon sink. *Nature*, 448(7155), 791– 794. <https://doi.org/10.1038/nature06059>
- Slemr, F., & Seiler, W. (1984). Field measurements of NO and NO₂ emissions from fertilized and unfertilized soils. *Journal of Atmospheric Chemistry*, 2(1), 1-24.
- Slevin, D., Tett, S. F., Exbrayat, J. F., Bloom, A. A., & Williams, M. (2017). Global evaluation of gross primary productivity in the JULES land surface model v3. 4.1. *Geoscientific Model Development*, 10(7), 2651-2670. <https://doi.org/10.5194/gmd-10-2651-2017>
- SMEAR II (2021). <https://eu-interact.org/field-sites/hyytiala-forestry-research-station-smear-ii/> last accessed 19/04/2021
- Sorooshian, S., Li, J., Hsu, K. L., & Gao, X. (2012). Influence of irrigation schemes used in regional climate models on evapotranspiration estimation: Results and comparative studies from California's Central Valley agricultural regions. *Journal of Geophysical Research: Atmospheres*, 117(D6). <https://doi.org/10.1029/2011JD016978>

- Staudt, M., Bertin, N., Hansen, U., Seufert, G., Cicciolij, P., Foster, P., ... & Fugit, J. L. (1997). Seasonal and diurnal patterns of monoterpene emissions from *Pinus pinea* (L.) under field conditions. *Atmospheric environment*, 31, 145-156. [https://doi.org/10.1016/S1352-2310\(97\)00081-2](https://doi.org/10.1016/S1352-2310(97)00081-2)
- Stavrakou, T., Peeters, J., & Müller, J. F. (2010). Improved global modelling of HO_x recycling in isoprene oxidation: evaluation against the GABRIEL and INTEX-A aircraft campaign measurements. *Atmospheric Chemistry and Physics*, 10(20), 9863-9878. <https://doi.org/10.5194/acp-10-9863-2010>
- Steinbrecher, R., Hauff, K., Hakola, H., & Rössler, J. (1999). A revised parameterisation for emission modelling of isoprenoids for boreal plants. Biogenic VOC emissions and photochemistry in the boreal regions of Europe: Biphorep, Final report, Contract No ENV4-CT95-0022, Air Pollution research report, (70), 29-44.
- Stockwell, W. R., Kirchner, F., Kuhn, M., & Seefeld, S. (1997). A new mechanism for regional atmospheric chemistry modeling. *Journal of Geophysical Research: Atmospheres*, 102(D22), 25847-25879. <https://doi.org/10.1029/97JD00849>
- Stroud, C., Makar, P., Karl, T., Guenther, A., Geron, C., Turnipseed, A., ... Fuentes, J. D. (2005). Role of canopy-scale photochemistry in modifying biogenic-atmosphere exchange of reactive terpene species: Results from the CELTIC field study. *Journal of Geophysical Research: Atmospheres*, 110(D17). <https://doi.org/10.1029/2005JD005775>
- Sun, G. E., McLaughlin, S. B., Porter, J. H., Uddling, J., Mulholland, P. J., Adams, M. B., & Pederson, N. (2012). Interactive influences of ozone and climate on streamflow of forested watersheds. *Global Change Biology*, 18(11), 3395-3409. <https://doi.org/10.1111/j.1365-2486.2012.02787.x>
- Suni, T., Rinne, J., Reissell, A., Altimir, N., Keronen, P., Rannik, U., ... & Vesala, T. (2003). Long-term measurements of surface fluxes above a Scots pine forest in Hyytiälä, southern Finland, 1996-2001. *Boreal Environment Research*, 8(4), 287-302.
- Surratt, J. D., Lewandowski, M., Offenberg, J. H., Jaoui, M., Kleindienst, T. E., Edney, E. O., & Seinfeld, J. H. (2007). Effect of acidity on secondary organic aerosol formation from isoprene. *Environmental science & technology*, 41(15), 5363-5369. <https://doi.org/10.1021/es0704176>
- Talhelm, A. F., Pregitzer, K. S., Kubiske, M. E., Zak, D. R., Company, C. E., Burton, A. J., ... & Karnosky, D. F. (2014). Elevated carbon dioxide and ozone alter productivity and ecosystem carbon content in northern temperate forests. *Global change biology*, 20(8), 2492-2504. <https://doi.org/10.1111/gcb.12564>
- Tang, J., Schurgers, G., & Rinnan, R. (2019). Process understanding of soil BVOC fluxes in natural ecosystems: A review. *Reviews of geophysics*, 57(3), 966-986. <https://doi.org/10.1029/2018RG000634>
- Tattini, M., Loreto, F., Fini, A., Guidi, L., Brunetti, C., Velikova, V., Gori, A., & Ferrini, F. (2015). Isoprenoids and phenylpropanoids are part of the antioxidant defense orchestrated daily by drought-stressed *Platanus × acerifolia* plants during Mediterranean summers. *New Phytologist*, 207(3), 613–626. <https://doi.org/10.1111/nph.13380>
- Taylor, K. E. (2001). Summarizing multiple aspects of model performance in a single diagram. *Journal of Geophysical Research: Atmospheres*, 106(D7), 7183–7192. <https://doi.org/10.1029/2000JD900719>
- Taylor, K. E., Stouffer, R. J., & Meehl, G. A. (2012). An overview of CMIP5 and the experiment design. *Bulletin of the American Meteorological Society*, 93(4), 485–498. <https://doi.org/10.1175/BAMS-D-11-00094.1>
- Thomas, M. V., Malhi, Y., Fenn, K. M., Fisher, J. B., Morecroft, M. D., Lloyd, C. R., ... McNeil, D. D. (2011). Carbon dioxide fluxes over an ancient broadleaved deciduous woodland in southern England. *Biogeosciences*, 8(6), 1595–1613. <https://doi.org/10.5194/bg-8-1595-2011>

- Thomas, M. V., Malhi, Y., Fenn, K. M., Fisher, J. B., Morecroft, M. D., Lloyd, C. R., ... McNeil, D. D. (2011). Carbon dioxide fluxes over an ancient broadleaved deciduous woodland in southern England. *Biogeosciences*, 8(6), 1595– 1613. <https://doi.org/10.5194/bg-8-1595-2011>
- Thornton, P. K., Ericksen, P. J., Herrero, M., & Challinor, A. J. (2014). Climate variability and vulnerability to climate change: A review. *Global Change Biology*, 20(11), 3313– 3328. <https://doi.org/10.1111/gcb.12581>
- Tingey, D. T., Evans, R., & Gumpertz, M. (1981). Effects of environmental conditions on isoprene emission from live oak. *Planta*, 152(6), 565– 570. <https://doi.org/10.1007/BF00380829>
- Toreti, A., Belward, A., Perez-Dominguez, I., Naumann, G., Luterbacher, J., Cronie, O., ... & Zampieri, M. (2019). The exceptional 2018 European water seesaw calls for action on adaptation. *Earth's Future*, 7(6), 652-663. <https://doi.org/10.1029/2019EF001170>
- Touchette, B. W., Iannacone, L. R., Turner, G. E., & Frank, A. R. (2007). Drought tolerance versus drought avoidance: a comparison of plant-water relations in herbaceous wetland plants subjected to water withdrawal and repletion. *Wetlands*, 27(3), 656-667. [https://doi.org/10.1672/0277-5212\(2007\)27\[656:DTVDA\]2.0.CO;2](https://doi.org/10.1672/0277-5212(2007)27[656:DTVDA]2.0.CO;2)
- Trenberth, K. E. (2011). Changes in precipitation with climate change. *Climate Research*, 47(1-2), 123-138. DOI: <https://doi.org/10.3354/cr00953>
- Uddling, J., Teclaw, R. M., Pregitzer, K. S., & Ellsworth, D. S. (2009). Leaf and canopy conductance in aspen and aspen-birch forests under free-air enrichment of carbon dioxide and ozone. *Tree physiology*, 29(11), 1367-1380. <https://doi.org/10.1093/treephys/tpp070>
- UK Extreme Events – Heatwaves. (2019). UK Met Office website. Retrieved from https://www.metoffice.gov.uk/research/climate/understanding-climate/uk-extreme-events_heatwaves
- UK Met Office. (2019a). Heatwave. Retrieved November 25, 2019, from <https://www.metoffice.gov.uk/weather/learn-about/weather/types-of-weather/temperature/heatwave>
- UK Met Office. (2019b). UK climate projections: Headline findings (Version 2). Retrieved April 6, 2020, from <https://www.metoffice.gov.uk/binaries/content/assets/metofficegovuk/pdf/research/ukcp/ukcp-headline-findings-v2.pdf>
- UKMO (2021). UK Met Office website. Retrieved <https://www.metoffice.gov.uk/climate/uk/summaries/2018/summer/regional-values>
- UNECE. (2004). Revised manual on methodologies and criteria for mapping critical levels/loads and geographical areas where they are exceeded., (Retrieved from www.icpmapping.org)
- Unger, N. (2014). On the role of plant volatiles in anthropogenic global climate change. *Geophysical Research Letters*, 41(23), 8563– 8569. <https://doi.org/10.1002/2014GL061616>
- VanderHeyden, D., Skelly, J., Innes, J., Hug, C., Zhang, J., Landolt, W., & Bleuler, P. (2001). Ozone exposure thresholds and foliar injury on forest plants in Switzerland. *Environmental Pollution*, 111(2), 321-331. [https://doi.org/10.1016/S0269-7491\(00\)00060-9](https://doi.org/10.1016/S0269-7491(00)00060-9)
- Velikova, V., & Loreto, F. (2005). On the relationship between isoprene emission and thermotolerance in *Phragmites australis* leaves exposed to high temperatures and during the recovery from a heat stress. *Plant, Cell & Environment*, 28(3), 318-327. <https://doi.org/10.1111/j.1365-3040.2004.01314.x>
- Velikova, V., Fares, S., & Loreto, F. (2008). Isoprene and nitric oxide reduce damages in leaves exposed to oxidative stress. *Plant, Cell & Environment*, 31(12), 1882-1894. <https://doi.org/10.1111/j.1365-3040.2008.01893.x>
- Verma, J. P., Yadav, J., Tiwari, K. N., & Kumar, A. (2013). Effect of indigenous Mesorhizobium spp. and plant growth promoting rhizobacteria on yields and nutrients uptake of chickpea (*Cicer arietinum* L.) under sustainable agriculture. *Ecological Engineering*, 51, 282-286. <https://doi.org/10.1016/j.ecoleng.2012.12.022>

- Vickers, C. E., Possell, M., Cojocariu, C. I., Velikova, V. B., Laothawornkitkul, J., Ryan, A., ... & Nicholas Hewitt, C. (2009). Isoprene synthesis protects transgenic tobacco plants from oxidative stress. *Plant, Cell & Environment*, 32(5), 520-531. <https://doi.org/10.1111/j.1365-3040.2009.01946.x>
- Vickers, C. E., Gershenson, J., Lerda, M. T., & Loreto, F. (2009). A unified mechanism of action for isoprenoids in plant abiotic stress. *Nature Chemical Biology*, 5, 283– 291. <https://doi.org/10.1038/nchembio.158>
- Vidale, P. L., Lüthi, D., Wegmann, R., & Schär, C. (2007). European summer climate variability in a heterogeneous multi-model ensemble. *Climatic Change*, 81(1), 209– 232. <https://doi.org/10.1007/s10584-006-9218-z>
- Visakorpi, K., Gripenberg, S., Malhi, Y., Bolas, C., Oliveras, I., Harris, N., ... Riutta, T. (2018). Small-scale indirect plant responses to insect herbivory could have major impacts on canopy photosynthesis and isoprene emission. *New Phytologist*, 220(3), 799– 810. <https://doi.org/10.1111/nph.15338>
- Vuichard, N., & Papale, D. (2015). Filling the gaps in meteorological continuous data measured at FLUXNET sites with ERA-Interim reanalysis. *Earth System Science Data*, 7(2), 157-171. doi:10.5194/essd-7-157-2015
- Wahid, A., Gelani, S., Ashraf, M., & Foolad, M. R. (2007). Heat tolerance in plants: an overview. *Environmental and experimental botany*, 61(3), 199-223. <https://doi.org/10.1016/j.envexpbot.2007.05.011>
- Warren, R., Yu, R., Osborn, T., & de la Nova Santos, S. (2009, February). Future European drought regimes under mitigated and un-mitigated climate change. In *IOP Conference Series: Earth and Environmental Science* (Vol. 6, No. 29, p. 292012). IOP Publishing. <https://doi.org/10.1088/1755-1307/6/29/292012>
- Wehner, G., Balko, C., Humbeck, K., Zyprian, E., & Ordon, F. (2016). Expression profiling of genes involved in drought stress and leaf senescence in juvenile barley. *BMC plant biology*, 16(1), 1-12. <https://doi.org/10.1186/s12870-015-0701-4>
- Wennberg, P. O., Bates, K. H., Crouse, J. D., Dodson, L. G., McVay, R. C., Mertens, L. A., ... & Seinfeld, J. H. (2018). Gas-phase reactions of isoprene and its major oxidation products. *Chemical reviews*, 118(7), 3337-3390. <https://doi.org/10.1021/acs.chemrev.7b00439>
- Wesely, M. L. (1989). Parameterization of surface resistances to gaseous dry deposition in regional-scale numerical models. *Atmospheric Environment*, 23 (1989), 1293-1304
- White, M. A., Running, S. W., & Thornton, P. E. (1999). The impact of growing-season length variability on carbon assimilation and evapotranspiration over 88 years in the eastern US deciduous forest. *International Journal of Biometeorology*, 42(3), 139– 145. <https://doi.org/10.1007/s004840050097>
- Wieder, W. R., Cleveland, C. C., Smith, W. K., & Todd-Brown, K. (2015). Future productivity and carbon storage limited by terrestrial nutrient availability. *Nature Geoscience*, 8(6), 441– 444. <https://doi.org/10.1038/ngeo2413>
- Wilkinson, S., & Davies, W. J. (2010). Drought, ozone, ABA and ethylene: new insights from cell to plant to community. *Plant, cell & environment*, 33(4), 510-525. <https://doi.org/10.1111/j.1365-3040.2009.02052.x>
- Williams, M., Rastetter, E. B., Fernandes, D. N., Goulden, M. L., Wofsy, S. C., Shaver, G. R., ... & Nadelhoffer, K. J. (1996). Modelling the soil-plant-atmosphere continuum in a *Quercus*–*Acer* stand at Harvard Forest: the regulation of stomatal conductance by light, nitrogen and soil/plant hydraulic properties. *Plant, Cell & Environment*, 19(8), 911-927. <https://doi.org/10.1111/j.1365-3040.1996.tb00456.x>
- Wittig, V. E., Ainsworth, E. A., Naidu, S. L., Karnosky, D. F., & Long, S. P. (2009). Quantifying the impact of current and future tropospheric ozone on tree biomass, growth, physiology and

- biochemistry: a quantitative meta-analysis. *Global change biology*, 15(2), 396-424. <https://doi.org/10.1111/j.1365-2486.2008.01774.x>
- Wittig, V. E., Ainsworth, E. A., & Long, S. P. (2007). To what extent do current and projected increases in surface ozone affect photosynthesis and stomatal conductance of trees? A meta-analytic review of the last 3 decades of experiments. *Plant, Cell & Environment*, 30(9), 1150–1162. <https://doi.org/10.1111/j.1365-3040.2007.01717.x>
- Wofsy, S. C. (2011). HIAPER Pole-to-Pole Observations (HIPPO): fine-grained, global-scale measurements of climatically important atmospheric gases and aerosols. *Philosophical Transactions of the Royal Society A: Mathematical, Physical and Engineering Sciences*, 369(1943), 2073-2086. <https://doi.org/10.1098/rsta.2010.0313>
- Wong, S. C., Cowan, I. R., & Farquhar, G. D. (1979). Stomatal conductance correlates with photosynthetic capacity. *Nature*, 282(5737), 424-426. <https://doi.org/10.1038/282424a0>
- Yeung, L. Y., Murray, L. T., Martinerie, P., Witrant, E., Hu, H., Banerjee, A., ... & Chappellaz, J. (2019). Isotopic constraint on the twentieth-century increase in tropospheric ozone. *Nature*, 570(7760), 224-227. <https://doi.org/10.1038/s41586-019-1277-1>
- Young, P. J., Archibald, A. T., Bowman, K. W., Lamarque, J. F., Naik, V., Stevenson, D. S., ... Zeng, G. (2013). Pre-industrial to end 21st century projections of tropospheric O₃ from the Atmospheric Chemistry and Climate Model Intercomparison Project (ACCMIP). *Atmospheric Chemistry and Physics*, 13, 2063–2090. <https://doi.org/10.5194/acp-13-2063-2013>
- Yu, Q., Zhang, Y., Liu, Y., & Shi, P. (2004). Simulation of the stomatal conductance of winter wheat in response to light, temperature and CO₂ changes. *Annals of Botany*, 93(4), 435-441. <https://doi.org/10.1093/aob>
- Yu, Z., Wang, J., Liu, S., Rentch, J. S., Sun, P., & Lu, C. (2017). Global gross primary productivity and water use efficiency changes under drought stress. *Environmental Research Letters*, 12(1), 014016. <https://doi.org/10.1088/1748-9326/aa5258>
- Zak, D. R., Pregitzer, K. S., Kubiske, M. E., & Burton, A. J. (2011). Forest productivity under elevated CO₂ and O₃: positive feedbacks to soil N cycling sustain decade-long net primary productivity enhancement by CO₂. *Ecology letters*, 14(12), 1220-1226. <https://doi.org/10.1111/j.1461-0248.2011.01692.x>
- Zandalinas, S. I., Mittler, R., Balfagón, D., Arbona, V., & Gómez-Cadenas, A. (2018). Plant adaptations to the combination of drought and high temperatures. *Physiologia Plantarum*, 162(1), 2–12. <https://doi.org/10.1111/ppl.12540>
- Zeppel, M. J. B., Wilks, J. V., & Lewis, J. D. (2014). Impacts of extreme precipitation and seasonal changes in precipitation on plants. *Biogeosciences*, 11(11), 3083-3093. <https://doi.org/10.5194/bg-11-3083-2014>
- Zhang, X., Wan, H., Zwiers, F. W., Hegerl, G. C., & Min, S. K. (2013). Attributing intensification of precipitation extremes to human influence. *Geophysical Research Letters*, 40(19), 5252-5257. <https://doi.org/10.1002/grl.51010>
- Zhao, T., & Dai, A. (2017). Uncertainties in historical changes and future projections of drought. Part II: Model-simulated historical and future drought changes. *Climatic Change*, 144(3), 535-548. <https://doi.org/10.1007/s10584-016-1742-x>
- Zhou, P., Ganzeveld, L., Rannik, Ü., Zhou, L., Gierens, R., Taipale, D., ... Boy, M. (2017). Simulating O₃ dry deposition at a boreal forest with a multi-layer canopy deposition model. *Atmospheric Chemistry & Physics*, 17(2). <https://doi.org/10.5194/acp-17-1361-2017>
- Zhou, S., Medlyn, B., Sabaté, S., Sperlich, D., & Prentice, I. C. (2014). Short-term water stress impacts on stomatal, mesophyll and biochemical limitations to photosynthesis differ consistently among tree species from contrasting climates. *Tree Physiology*, 34(10), 1035–1046. <https://doi.org/10.1093/treephys/tpu072>

- Zimmer, W., Brüggemann, N., Emeis, S., Giersch, C., Lehning, A., Steinbrecher, R., & Schnitzler, J. P. (2000). Process-based modelling of isoprene emission by oak leaves. *Plant, Cell & Environment*, 23(6), 585– 595. <https://doi.org/10.1046/j.1365-3040.2000.00578.x>
- Zimmer, W., Brüggemann, N., Emeis, S., Giersch, C., Lehning, A., Steinbrecher, R., & Schnitzler, J. P. (2000). Process-based modelling of isoprene emission by oak leaves. *Plant, Cell & Environment*, 23(6), 585– 595. <https://doi.org/10.1046/j.1365-3040.2000.00578.x>
- Zlatev, Z. S. (2005). Effects of water stress on leaf water relations of young bean plants. *Journal of Central European Agriculture* 6 (1), 5-14.